

Chapter 12: Long-term Climate Change: Projections, Commitments and Irreversibility

Coordinating Lead Authors: Matthew Collins (UK), Reto Knutti (Switzerland)

Lead Authors: Julie Arblaster (Australia), Ken Caldeira (USA), Jean-Louis Dufresne (France), Thierry Fichfet (Belgium), Pierre Friedlingstein (UK), Xuejie Gao (China), William Gutowski (USA), Tim Johns (UK), Gerhard Krinner (France), Mxolisi Shongwe (Swaziland), Claudia Tebaldi (USA), Andrew Weaver (Canada), Michael Wehner (USA)

Contributing Authors: Myles R. Allen, Tim Andrews, Cecilia Bitz, Claire Brutel, Mark Cane, Robin Chadwick, Ed Cook, Kerry H. Cook, Michael Eby, Veronika Eyring, Erich M. Fischer, Piers Forster, Peter Good, Hugues Goosse, Kevin I. Hodges, Marika Holland, Philippe Huybrechts, Manoj Joshi, Viatcheslav Kharin, Yochanan Kushnir, David Lawrence, Robert W. Lee, Spencer Liddicoat, Wolfgang Lucht, Damon Matthews, François Massonnet, Malte Meinshausen, Christina M. Patricola, Gwenaëlle Philippon, Prabhat, Stefan Rahmstorf, William J. Riley, Joeri Rogelj, Oleg Saenko, Richard Seager, Jan Sedlacek, Len Shaffrey, Jana Sillmann, Andrew Slater, Robert Webb, Giuseppe Zappa, Kirsten Zickfeld

Review Editors: Sylvie Joussaume (France), Abdalah Mokssit (Morocco), Karl Taylor (USA), Simon Tett (UK)

Date of Draft: 16 December 2011

Notes: TSU Compiled Version

Table of Contents

Executive Summary	3
12.1 Introduction	9
12.2 Sources of Uncertainty from Emissions to Projections	10
12.2.1 <i>General Concepts: Sources of Uncertainties</i>	10
12.2.2 <i>From Ensembles to Uncertainty Quantification</i>	12
12.2.3 <i>Joint Projections of Multiple Variables</i>	12
12.3 Projected Changes in Forcing Agents, including Emissions and Concentrations	13
12.3.1 <i>Description of Scenarios</i>	13
12.3.2 <i>Implementation of Forcings in CMIP5 Experiments</i>	15
12.3.3 <i>Projected Radiative Forcing for the 21st Century</i>	18
12.4 Projected Climate Change over the 21st Century	18
12.4.1 <i>Time-Evolving Global Quantities</i>	19
12.4.2 <i>Pattern Scaling</i>	21
12.4.3 <i>Changes in Temperature and Energy Budget</i>	23
12.4.4 <i>Changes in Atmospheric Circulation</i>	29
12.4.5 <i>Changes in the Water Cycle</i>	32
12.4.6 <i>Changes in Cryosphere</i>	38
12.4.7 <i>Changes in the Ocean</i>	41
12.4.8 <i>Consistency and Main Differences CMIP3/CMIP5 and SRES/RCPs</i>	43
12.4.9 <i>Changes Associated with Biogeochemical Feedbacks</i>	45
12.5 Long Term Climate Change, Commitment and Irreversibility	47
12.5.1 <i>RCP Extensions</i>	47
12.5.2 <i>Climate Change Commitment</i>	47
12.5.3 <i>Global Measures of Climate Sensitivity and Transient Response</i>	50
12.5.4 <i>Climate Stabilization and Long-term Climate Targets</i>	53
Box 12.1: Equilibrium Climate Sensitivity and Transient Climate Response	54
12.5.5 <i>Abrupt Change and Irreversibility</i>	57
FAQ 12.1: Why are so Many Models and Scenarios Used to Project Climate Change?	62
FAQ 12.2: How will the Earth’s Water Cycle Change?	64

1	FAQ 12.3: What would Happen to Future Climate if We Stopped Emissions Today?	65
2	References.....	67
3	Tables	87
4	Figures	90
5		

1 **Executive Summary**

3 **Uncertainties**

- 4 • Our understanding of the sources and means of characterizing uncertainties in long-term projections of
5 climate change has not changed significantly since AR4, but new experiments and studies have continued
6 to work towards an incrementally more complete and rigorous quantification. The three main sources of
7 uncertainty are model structural and parametric choices, future forcing scenarios and the internal
8 variability of the system (both the real system and its representation through models). For the long-term,
9 multi-decadal and large-scale projections addressed in this chapter, the prevalent sources are the first two,
10 but natural variability remains important for regionally detailed future changes, especially for variables
11 other than temperature and aspects of climate change other than changes in means (e.g., characterization
12 of changes in some extremes).
- 13 • Improved methods to quantify model robustness show lack of agreement across models on local trends is
14 often a result of natural variability, rather than models actually disagreeing on their forced response.
15 Model agreement depends on the variable and spatial and temporal averaging, with better agreement for
16 larger scales. Agreement and thus confidence in projections is higher for temperature related quantities
17 than for those related to the water cycle or circulation.

19 **Scenarios and Experiments**

- 20 • There are new scenarios, called Representative Concentration Pathways (RCPs) and new experiments run
21 with new models collected as part of phase 5 of the Coupled Model Intercomparison Project (CMIP5), for
22 this assessment. Many new models may be classed as Earth Systems Models (ESMs), broadly meaning
23 that they have an interactive carbon cycle component. Others, without such feedbacks included, are
24 described as Atmosphere-Ocean General Circulation Models (AOGCMs).
- 25 • There is a much more comprehensive experimental design in CMIP5 than CMIP3, permitting more
26 consistent diagnosis of model-dependent ranges in forcing, climate sensitivity and feedbacks. The number
27 of participating models is expected to be roughly double compared to CMIP3 although not all
28 experiments and models were available for the preparation of this draft. The CMIP5 co-ordinated
29 experiment sees a marked increase in the number of ESMs compared with CMIP3. There is also a general
30 increase in the number of forcing agents represented (in terms of types of aerosols and land use
31 particularly), and black carbon aerosol is now a commonly included forcing agent, although nitrate
32 aerosol is still not common.
- 33 • Both “concentrations-driven” projections (for both AOGCMs and ESMs) and “emissions-driven”
34 projections (for ESMs) are assessed from CMIP5, the former allowing projections from the two classes of
35 model to be combined on a more equal footing in assessing response uncertainties, and the latter (along
36 with additional experiments within CMIP5) allowing climate-carbon cycle interactions to be explored
37 more fully.
- 38 • New RCP scenarios, with internally consistent emissions and socioeconomic storylines, are used as the
39 basis for the forcing inputs to complex model projections. The closest correspondence between RCPs and
40 SRES for total Long Lived Greenhouse Gas (LLGHG) forcing is between SRES B1 and RCP4.5. RCP
41 scenarios explore a broader range of radiative forcing through the 21st century than the SRES scenarios
42 used for AR4 (note that the AR4 commitment experiment is not a scenario). In particular, at the low end,
43 the RCP2.6 radiative forcing is about 40% lower than SRES B1, the lowest SRES scenario used for AR4.
- 44 • The multi-model ensemble-mean model-diagnosed net climate forcing for 2091–2100 covers the range
45 2.2 (RCP2.6), 3.7 (RCP4.5), 4.1 (RCP6.0) and 7.2 (RCP8.5) W m^{-2} for concentrations-driven projections
46 in CMIP5. Note RCP6.0 is poorly sampled in these calculations. These diagnosed multi-model mean
47 forcings are in all cases substantially lower than the total forcings at 2100 as estimated in the RCP
48 database using more idealized calculations (2.7, 4.3, 5.5, 8.4 W m^{-2} respectively).
- 49 • While CMIP5 models and simulations have the potential for unprecedented insight and details for
50 projections, the lack of sufficient data at the time of writing of this draft limits the confidence with which
51 many of the statements can be made at this point. Very few publications have analysed CMIP5 data or
52 compared CMIP3 and CMIP5 so far.

54 **Temperature**

- 55 • It is *virtually certain* that global-mean surface temperature will continue to rise over the next few decades
56 irrespective of the GHG concentration pathways as represented by the RCPs. Around the mid-21st
57 century, the rate of global warming begins to be more strongly dependent on the radiative forcing. By

2100, the best estimate global-mean temperature change in the non-mitigation RCP8.5 is a factor of 3 higher than in the lowest RCP2.6, where warming stabilizes in the second half of this century.

- For RCP4.5, 6.0 and 8.5, global temperatures *likely* exceed 2°C warming with respect to present day by 2100. Based on model results and other studies, following the RCP2.6 (and similarly the E1 ENSEMBLES) concentrations pathway, it is only *about as likely as not* that the policy-relevant objective of no more than 2°C global warming relative to pre-industrial would be achieved. In some, but not all RCP2.6 model simulations, global temperatures exceed 2°C warming with respect to preindustrial. This scenario implies a rapid decrease of anthropogenic CO₂ emissions with negative emissions towards the end of the 21st century.
- Taking into account scaling arguments derived from earlier models and scenarios and the fact that the uncertainty assessments for equilibrium climate sensitivity, transient climate response and the carbon cycle-climate feedback have not changed significantly since AR4 (see below), the *likely* uncertainty in global temperature projections for the end of the 21st century remains about –40 to +60% around the CMIP5 mean.
- Future changes in global land surface air temperature exceed changes in global average ocean-area surface air temperature in a ratio of 1.5 ± 0.2 (one standard deviation), as was found in AR4. Studies since AR4 have identified a number of different mechanisms responsible for this involving boundary layer humidity, clouds and the ratio of surface sensible and latent heat fluxes.
- The Arctic region warms most under all scenarios, as was found in AR4 with a polar amplification factor raging from 1.8 to 3.3. The Arctic polar amplification peaks in early winter and has a minimum in the summer season. This polar amplification is not found in Antarctic regions due to the lesser land mass in the Southern Hemisphere and because of greater ocean heat uptake in the Southern Ocean.
- Regional surface air temperature warming has minima in the North Atlantic and Southern Oceans in all scenarios. Some models exhibit regional cooling in 2081–2100 over the North Atlantic Ocean under RCP4.5 forcing.
- Zonal temperature changes at the end of the 21st century show warming throughout the troposphere and cooling in the stratosphere. There is physical and pattern consistency in temperature changes between different generations of models. The consistency is especially clear in the tropical upper troposphere and the northern high latitudes, indicating that the greatest atmospheric warming is *very likely* to occur in these regions.
- It is *virtually certain* that in most places there will be more hot and fewer cold extremes as global temperature increases. Since AR4, the understanding of mechanisms and feedbacks leading to projected changes in extremes has been improved. Increases in the frequency, duration and magnitude of hot extremes along with heat stress are expected, however occasional cold winter extremes will continue to occur.
- Rare high and low temperature events are projected to experience greater increases than mean temperatures (i.e., the magnitude of both high and low temperature extremes increasing faster than the mean) with the largest changes in the rare low temperatures at high latitudes. It is *likely* that, in most regions, a 20 year maximum temperature event will become a one-in-two year event by the end of the 21st Century under RCP8.5, except for some regions of the high latitudes of the Northern Hemisphere where it is likely to become a one-in-five year event.

Pattern Scaling

- The well-established characteristic stability of geographical patterns of change during a transient experiment remains valid in the new generation of models participating in CMIP5. The robustness of these patterns across models and scenarios for temperature and, albeit in lesser measure, precipitation (especially for experiments where well-mixed and long-lived greenhouse gases represent the main forcing) underpins the representativeness of the maps shown in this chapter, which necessarily have to be limited by specific choices of scenario, multi-model summary, time horizon.

Clouds and Energy Budget of the Atmosphere

- Models simulate a decrease in cloud amount in the future over most of the tropics and mid-latitudes, due mostly to reductions in low cloud. Changes in marine boundary layer clouds in subtropical regions contribute to a large spread across models there. Increases in cloud fraction and cloud optical depth and therefore cloud reflection occur in high latitudes, poleward of 50°.
- The top of atmosphere (TOA) net flux into the climate system is very dependent on scenario, with increases over the 21st Century under RCP8.5 and increases then stabilization and even decreases for the

1 other scenarios. These projections reflect both future changes in radiative forcing and climate feedbacks,
2 and the flux imbalance at the TOA remains significantly smaller than the radiative forcing up to 2100.

4 **Atmospheric Circulation**

- 5 • As the climate warms, the Hadley and Walker circulations are projected to slow down. Weakening of
6 moisture transport from the boundary layer to the free atmosphere along ascending branches of these
7 tropical overturning circulations is associated with the imbalance between the increase in lower
8 tropospheric water vapour and global precipitation. A robust response to global warming is the widening
9 of the Hadley cell, which translates to broader tropical regions and a poleward encroachment of
10 subtropical dry zones.
- 11 • A robust feature of the pattern of mean sea level pressure change is a decrease in high latitudes and
12 increases in the mid-latitudes, associated with poleward shifts in the mid-latitude storm tracks and, in the
13 Southern Hemisphere, a positive trend in the annular mode. A poleward shift and intensification of the
14 Southern Hemisphere mid-latitude jet is seen at the higher GHG forcing of RCPs 4.5 and 8.5, which is a
15 response consistent with previous assessments. In austral summer, the additional influence of
16 stratospheric ozone recovery opposes changes due to greenhouse gases, though the net response varies
17 widely across models and scenarios.
- 18 • In Southern Hemisphere winter, there is a clear poleward shift in storm tracks of several degrees and a
19 small overall reduction in the frequency of storms under RCP4.5. The poleward shift at the end of the
20 century is consistent with a poleward shift in the Southern Hemisphere of the latitudes with strongest
21 atmospheric baroclinic zones and tropospheric jets. The consistency of behaviour between CMIP5 and
22 CMIP3 projections and the physical consistency of the storm response with other climatic changes
23 indicates that a poleward shift in Southern Hemisphere storm tracks is *very likely* by the end of the 21st
24 century under RCP4.5.
- 25 • In the Northern Hemisphere winter, there is an overall reduced frequency of storms and less indication of
26 a poleward shift in the tracks, except possibly over East Asia. The reduction in frequency is consistent
27 with weaker baroclinicity of the projected climate. A reduction in the occurrence of Northern Hemisphere
28 extratropical storms is *likely*, based on the consistency with previous projections, though, at least for
29 storms reaching Europe, simulation results and larger amount of thermal energy in the future climate
30 indicate a *likely* increase in the strength of the most intense extratropical storms.

32 **Water Cycle**

- 33 • On the planetary scale, relative humidity remains roughly constant in projected warmer climates.
34 However, a project differential warming of land and ocean promotes changes in atmospheric circulation
35 and resulting moisture transport that will lead to likely decreases in near-surface relative humidity over
36 most land areas with the notable exceptions of tropical Africa and polar regions.
- 37 • Global-scale precipitation is projected to gradually increase in the 21st century. It is *virtually certain*, that
38 precipitation increase will be much smaller, approximately $2\% \text{ K}^{-1}$, than the rate of lower tropospheric
39 water vapour increase ($\sim 7\% \text{ K}^{-1}$), due to global energetic constraints.
- 40 • It is *virtually certain* that average precipitation in a much warmer world will not be uniform, with regions
41 experiencing increases, or decreases or no much change at all. The high latitudes are *very likely* to
42 experience greater amounts of precipitation due to the additional water carrying capacity of the warmer
43 troposphere. Many mid-latitude arid and semi-arid regions will likely experience less precipitation and
44 many moist mid-latitude regions will *likely* experience more precipitation. The largest precipitation
45 changes over northern Eurasia and North America are projected to occur during the winter.
- 46 • Regional to global-scale projections of soil moisture and drought remain relatively uncertain compared to
47 other aspects of the hydrological cycle. Nonetheless, drying in the Mediterranean, southwestern U.S. and
48 south African regions are consistent with projected changes in Hadley circulation, so drying in these
49 regions as global temperatures increase is *likely*.
- 50 • Similarly, decreases in runoff are *likely* in southern Europe, the Middle East, and southwestern U.S. The
51 CMIP5 models project consistent increases in high latitude runoff, consistent with AR4, but confidence in
52 this projection is tempered by large biases in their simulation of present-day snow cover.
- 53 • Annual surface evaporation is projected to increase as global temperatures rise over most of the ocean and
54 is projected to either increase or decrease over land following roughly the same pattern as in precipitation.
55 Prominent areas of projected decreases in evaporation include the southwestern U.S./northwestern
56 Mexico, southern Africa and land bordering the Mediterranean. Evaporation increases over land in the
57 northern high latitudes, consistent with the increase in precipitation and an overall warming, increasing

1 potential evaporation. The consistency of this change across different generations of models and different
2 forcing scenarios along with an understanding of the underlying physical mechanisms indicates that these
3 changes in annual evaporation are *likely*.

- 4 • In addition to the changes in the seasonal pattern of mean precipitation described above, the frequency
5 distribution of precipitation events is projected to *very likely* undergo changes. For short-duration events,
6 a shift to more intense individual storms and fewer weak storms is projected. Over land areas where
7 increased evapotranspiration is projected, more frequent and more intense periods of agricultural drought
8 will follow despite an increase in the likelihood of more intense individual storms.

10 Cryosphere

- 11 • Climate models consistently project long-term reductions in sea ice areal coverage in both hemispheres.
12 In the Northern Hemisphere, the rate of decrease in sea ice extent over the late 20th century and the 21st
13 century is greatest in summertime. Overall, CMIP5 models better capture the rapid decline in summer
14 Arctic sea ice observed during the last decades than CMIP3 models. The spread across Arctic sea ice
15 projections remains wide and can partly be explained by the range of ice conditions in the late 20th
16 century in models. More than 90% of the CMIP5 models analyzed reach nearly ice-free September
17 conditions (sea ice extent less than 1×10^6 km²) in the Arctic by 2100 under RCP8.5. The most likely
18 range in global surface warming for a nearly ice-free Arctic Ocean is estimated to be 1.5 to 2.5°C above
19 1986–2005. In the Southern Hemisphere, given the large discrepancies in simulated historic sea ice
20 conditions compared to observations, future changes in sea ice remain highly uncertain.
- 21 • Summer Arctic sea ice loss has been rapid in observations and in many historical and future simulations.
22 Some models exhibit 5–10 year periods of very rapid summer decline - even greater than has occurred in
23 the last 5 years. Nonetheless, there is no evidence in models of a critical threshold in the transition from
24 perennial ice-covered to a seasonally ice-free Arctic Ocean beyond which further sea ice loss is
25 unstoppable and irreversible.
- 26 • Snow cover changes result from precipitation and ablation changes, which are sometimes opposite.
27 Projections of the Northern Hemisphere spring snow covered area in the CMIP5 models are fairly
28 coherent, with a decrease by the end of the 21st century between 9% (RCP2.6) and 24% (RCP8.5).
- 29 • The projected changes in permafrost are a response not only to warming, but also to changes in snow
30 cover, which exerts a control on the underlying soil. By the end of the 21st century, diagnosed near-
31 surface permafrost area is projected to decrease between 31% (RCP2.6) to 73% (RCP8.5).

33 Ocean

- 34 • While many model simulations have been conducted since the AR4 under a wide range of forcing
35 scenarios, projections of the AMOC behaviour has not changed. Based on the available CMIP5 models
36 and the literature, it remains *very likely* that the AMOC will weaken over the 21st century with a best
37 estimate decrease in 2100 of about 10–30% for the RCP 4.5 scenario and 20–40% for the RCP 8.5
38 scenario. It also remains *very unlikely* that the AMOC will undergo an abrupt transition or collapse in the
39 21st century for the scenarios considered.
- 40 • Climate model projects a concomitant southward movement of the Antarctic Circumpolar Current (ACC)
41 in response to a projected southward shift in the Southern Hemisphere mid-latitude westerlies.

43 Main Differences Between CMIP3 and CMIP5 Responses

- 44 • Using simple models to emulate the global mean temperature response from the CMIP5 models, it is
45 possible to estimate what those models would have shown if they had been used to run SRES A1B
46 scenario experiments. This has only been possible for a handful of CMIP5 models but will be eventually
47 used to attribute changes in AR4 and AR5 model projections to changes in models or changes in
48 scenarios. RCP4.5 is approximately analogue with SRES B1 and other scenarios may be approximately
49 paired according to the radiative forcing at the end of the 21st century, however important differences
50 remain in the transient behaviour because of the substantial difference in the 21st century concentration
51 pathways between SRES and RCPs.
- 52 • Multi-model average patterns of change in temperature and precipitation from CMIP3 and CMIP5
53 ensembles, once normalized per 1°C of global temperature change, present a high degree of pattern
54 correlation, with values larger than 0.9 for temperature change patterns and larger than 0.8 for
55 precipitation patterns. Differences in the latter are mainly located in Southeast Asia and differences in
56 black carbon and SO_x forcings between the two sets of scenarios are potentially responsible.

Long-Term Climate Change

- Continuing greenhouse gas emissions beyond 2100 as in the RCP8.5 extension induces a total radiative forcing above 12 W m^{-2} by 2300 that would lead to a warming of 8.7°C (range 5.0–11.6) by 2300 (relative to 1986–2005). Continuous negative emissions beyond 2100, inducing a total radiative forcing below 2 W m^{-2} by 2300 as in the RCP2.6 extension would reduce the warming to 0.6°C (range 0.3–1.0) by 2300.
- The climate system has multiple timescales associated with different thermal reservoirs and reservoirs of carbon. If radiative forcing were stabilized, the fraction of realized warming at that point is around $85 \pm 10\%$ of the total, and is almost independent of the forcing scenario. Equilibrium is reached only after centuries to millennia.
- The persistence of warming is substantially longer than the lifetime of anthropogenic greenhouse gases themselves, as a result of non-linear absorption effects as well as the slow heat transfer into and out of the ocean. In much the same way as the warming to a step increase of forcing is delayed, the cooling after setting radiative forcing to zero is also delayed. A positive temperature anomaly is maintained for decades to centuries to allow the ocean to lose its excess heat.
- For high climate sensitivities, and in particular if sulfate aerosol emissions are eliminated at the same time as greenhouse gas emissions, the commitment from past emission can be strongly positive, and is a superposition of a fast response to reduced aerosols emissions and a slow response to reduced CO_2 .
- Stabilization of global temperature does not imply stabilization for all aspects of the climate system, as some changes depend on the rate of increase or the type of forcing. Processes related to vegetation change, changes in the ice sheets, ocean acidification, deep ocean warming and associated sea level rise and potential feedbacks linking for example ocean and the ice sheets have their own intrinsic long timescales. Those may result in significant changes hundreds to thousands of years after global temperature is stabilized.
- Analysis of anthropogenic emission pathways shows that pathways that likely limit warming below 2°C (above pre-industrial) by 2100 show emission of about $31\text{--}46 \text{ GtCO}_2\text{eq yr}^{-1}$ and $17\text{--}23 \text{ GtCO}_2\text{eq yr}^{-1}$ by 2020 and 2050, respectively. Median 2010 emissions of all models are $48 \text{ GtCO}_2\text{eq yr}^{-1}$. In cumulative terms, the 2°C temperature target implies cumulative carbon emissions of about $1000\text{--}1300 \text{ GtC}$, of which about 520 GtC were emitted by 2011.

Equilibrium Climate Sensitivity, Transient Climate Response and Transient Response to Cumulative Carbon Emission

- Constraining climate sensitivity from the observed mean climate and variability remains difficult. Relationships between metrics of observable quantities and projections are often complex, and those found in perturbed physics ensembles may only hold in that ensemble. The range of equilibrium climate sensitivities (ECS) and transient responses (TCR) covered by CMIP3 and CMIP5 cannot be narrowed significantly by constraining the models with observations. Consistent with that, the range of TCR and ECS from the models available in CMIP5 is similar to CMIP3.
- This assessment still supports the conclusion from AR4 that equilibrium climate sensitivity (ECS) is *likely* in the range $2\text{--}4.5^\circ\text{C}$, and *very likely* above 1.5°C . The most *likely* value remains near 3°C . Values above 4.5°C are found in some models, and are not inconsistent with observed warming trends, but are less likely to agree with observations and reconstructions of past changes. The transient climate response (TCR) is *very likely* in the range $1\text{--}3^\circ\text{C}$, with a most *likely* value near 2°C based on the observed global changes in surface temperature and ocean heat uptake, the detection/attribution studies identifying the response patterns to increasing greenhouse gas concentrations, and the results of perturbed physics ensembles and CMIP3/5. While the uncertainties for both climate sensitivity and TCR are not significantly different from those estimated in AR4, the amount and quality of evidence has increased substantially. The results are supported by several different lines of evidence, each based on multiple studies, models and datasets.
- ECS and TCR remain useful concepts to characterize a temperature response, but there are limitations on the forcing and feedback concept. These include feedbacks that are much faster than the surface warming and slow feedbacks associated mainly with vegetation change and ice sheets on timescales of several centuries to millennia. The latter could cause ECS to be significantly different for millennia timescales.
- The ratio of global temperature change to total cumulative anthropogenic emissions (transient and equilibrium climate response to carbon emissions) is relatively constant and independent of the scenario, but is model dependent as it depends on the model airborne fraction and climate sensitivity. For any given temperature target, higher emissions in earlier decades therefore simply imply lower emissions by about

1 the same amount later on. The transient response to cumulative carbon emission (TRCE) is *very likely*
2 between 1–3°C/TtC (10^{12} metric tons of carbon), with a best estimate in the range of 1.5–2.0°C/TtC, for
3 cumulative emissions in the 0.5–2 TtC range until the time at which temperatures peak. Under these
4 conditions, and for low to medium estimates of climate sensitivity, the TRCE is near identical to the peak
5 response to cumulated carbon emissions (PRCE). For high climate sensitivity and/or strong carbon cycle
6 climate feedback and for larger cumulative emissions the peak warming can be delayed and PRCE may
7 be substantially larger than TRCE, but is poorly constrained by models and observations.
8

9 **Abrupt Change and Irreversibility**

- 10 • If anthropogenic carbon emissions were set to zero at some point in the future, slow surface to deep ocean
11 export of CO₂ and heat would lead to a near constant global temperature for several centuries, thus
12 making a large fraction of climate change largely irreversible on human time scales, except if net
13 anthropogenic emissions were strongly negative over a sustained period. For example, regions
14 experiencing increase or decrease in precipitation would essentially be locked in this new regime for
15 many centuries.
- 16 • Several components or phenomena in the climate system could potentially exhibit abrupt or nonlinear
17 changes, and some are known to have done so in the past. Examples include the Atlantic Meridional
18 Overturning Circulation, sea ice, the Greenland ice sheet, the Amazon forest and monsoonal circulations.
19 For some events, there is information on potential consequences, but in general there is low confidence
20 and little consensus on the likelihood of such events over the 21st century.
21
22
23

12.1 Introduction

Projections of future climate change are not like weather forecasts. It is not possible to make deterministic, definitive predictions of how climate will evolve over the next century and beyond as it is with short-term weather forecasts. It is not even possible to make predictions of the frequency of occurrence of all possible outcomes in the way that it might be possible with a calibrated probabilistic medium-range weather forecast. Predictions of climate change are both uncertain, first because these are primarily dependent on scenarios of future anthropogenic and natural forcings, second because of incomplete understanding and inadequate models of the climate system and finally because of the existence of natural climate variability. The term climate projection is used to indicate these uncertainties and dependencies. Nevertheless, as greenhouse gas concentrations continue to rise, we expect to see future changes to the climate system that are greater than those already observed and attributed to human activities.

This chapter assesses climate projections on time scales beyond those covered in Chapter 11, approximately from the mid-point of the 21st century. Information from a range of different modelling tools is used here; from simple energy balance models, through Earth System Models of Intermediate Complexity (EMICs) to complex dynamical climate and Earth System Models (ESMs). These tools are evaluated in Chapter 9 and, where possible, the evaluation is used in assessing the validity of the projections. This chapter also summarises some of the information on leading-order measures of the sensitivity of the climate system from other chapters and discusses the relevance of these for climate projections, commitments and irreversibility.

Since the AR4 (Meehl et al., 2007b) there have been a number of advances:

- New scenarios of future forcings have been developed to replace the SRES scenarios. The Representative Concentration Pathways (RCPs, see section 12.3) (Moss et al., 2010), have been designed to cover a wide range of possible magnitudes of climate change in models rather than being derived sequentially from storylines of socio-economic possibilities. The aim is to provide a range of climate responses from which individual socio-economic scenarios may be scaled and interpolated (some including explicit climate policy). Nevertheless, many studies that have been performed since AR4 have used SRES and, where appropriate, these are assessed. Simplified scenarios of future change, developed for understanding, are also synthesised.
- New models have been developed with higher spatial resolution, with better representation of processes and with the inclusion of more processes, in particular, processes that are important in simulating the carbon cycle of the Earth. In these models, emissions of greenhouse gases may be specified and these gases may be chemically active in the atmosphere or be exchanged with pools in terrestrial and oceanic systems before ending up as an airborne concentration (see Fig 10.1 of AR4).
- New types of model experiments have been performed, many coordinated by the Coupled Model Intercomparison Project version 5 (CMIP5), which exploit the addition of these new processes. Models may be driven by emissions of greenhouse gases, or driven by their concentrations with different Earth system feedback loops cut. This allows the separate assessment of different feedbacks in the system and of projections of physical climate variables and future emissions.
- Techniques to assess and quantify uncertainties in projections have been further developed and, where possible, projections are presented in the form of probability distribution functions (PDFs) that quantify the uncertainty. We make the distinction between the spread of a multi-model, an *ad hoc*, measure of the possible range of projections, and the quantification of uncertainty that combines information from models and observations using statistical algorithms. Just like climate models, different techniques for quantifying uncertainty exist and produce different outcomes. Where possible, different estimates of uncertainty are compared.

While not an advance, as time has moved on, the baseline period from which climate change is expressed has also moved on (a common baseline period of 1986–2005 is used throughout, consistent with the 2006 start-point for the RCP scenarios).

The focus of this chapter is on global and continental/ocean basin-scale climate projections. For many aspects of future climate change, it is possible to discuss generic features of projections and the processes that underpin them for such large scales. Where interesting or unique changes have been investigated at smaller scales, and there is a level of agreement between different studies of those smaller-scale changes, these may also be assessed in this chapter, although where changes are linked to phenomena such as El Niño,

1 the reader is referred to Chapter 14. An innovation for AR5 is Annex I, a collection of global and regional
2 maps of projected climate changes derived from model output. A detailed commentary on each of the maps
3 presented in Annex I is not provided here, but some discussion of generic features will be found.

4
5 Projections from regional models driven by boundary conditions from global models are not extensively
6 assessed but may be mentioned in the chapter. More detailed regional information may be found in Chapter
7 14 and is also now assessed in the Working Group II report where it can more easily be linked to impacts.

8 9 **12.2 Sources of Uncertainty from Emissions to Projections**

10 11 **12.2.1 General Concepts: Sources of Uncertainties**

12
13 The understanding of the sources of uncertainty affecting future climate change projections has not
14 substantially changed since AR4, but many experiments and studies since then have proceeded in
15 characterizing, and, at times, quantifying them. The latter involves much more than just a simple description
16 of the range of model outcomes, requiring an underlying statistical model that combines information from
17 both model experiments and observations.

18
19 Uncertainty affecting mid- to long-term projections of climatic changes stems from distinct but not
20 necessarily independent sources. Figure 12.1 shows a schematic of the chain from scenarios, through Earth
21 Systems Models to projections.

22 23 **[INSERT FIGURE 12.1 HERE]**

24 **Figure 12.1:** Links in the chain from scenarios, through models to climate projections. The Representative
25 Concentration Pathways (RCPs) are designed to sample a range of radiative forcing of the climate system at 2100. The
26 RCPs are translated into both emissions and concentrations of greenhouse gases using Integrated Assessment Models
27 (IAMs). These are then used as inputs to dynamical Earth System Models (ESMs) in simulations which are either
28 concentration-driven (the majority of projection experiments) or emissions-driven (only run for RCP8.5). Aerosols and
29 other forcing factors are implemented in subtly different ways in each ESM. The ESM projections each have a
30 potentially different radiative forcing, which may be viewed as an output of the model and which may not correspond to
31 precisely the level of radiative forcing indicated by the RCP. In addition, different models would produce different
32 responses even under the same radiative forcing. Uncertainty propagates through the chain and results in a spread of
33 ESM projections. This spread is only one way of assessing uncertainty in projections and alternative methods, which
34 combine information from simple and complex models and observations are also used to quantify that uncertainty.

35
36 **Emission scenarios:** Future anthropogenic emissions of greenhouse gases, aerosol particles and other
37 forcing agents such as land use change are dependent on socio-economic factors including global
38 geopolitical agreements to control those emissions. Systematic studies that attempt to quantify the likely
39 ranges of anthropogenic emission have been undertaken (Sokolov et al., 2010) but it is more common to use
40 a scenario approach of plausible pathways. AR4 made extensive use of the SRES scenarios developed using
41 a sequential approach, i.e., socio-economic factors feed into emissions scenarios which are then used either
42 to directly force the climate models or to determine concentrations of greenhouse gases and other agents
43 required to drive these models. This report also assesses outcomes of simulations that use the new RCP
44 scenarios, developed using a parallel process (Moss et al., 2010) whereby different targets in terms of
45 radiative forcing at 2100 were selected (2.6, 4.5, 6.0 and 8.5 W m⁻²) and greenhouse gas and aerosol
46 emissions consistent with those targets, and their corresponding socio-economic drivers were developed
47 simultaneously. Rather than being identified with one socio-economic storyline, RCP scenarios are
48 consistent with many possible economic futures. Their development was driven by the need to produce
49 scenarios more efficiently and to produce a wide range of possible model responses that may be scaled and
50 interpolated to estimate the response under other scenarios involving different measures of adaptation and
51 mitigation.

52
53 In terms of the uncertainties related to the RCP emissions scenarios, the following issues can be identified.

- 54 • It is not possible to attach probabilities or likelihoods to any of the RCP scenarios (as it is not for
55 SRES scenarios). Each of them should be considered plausible, though not necessarily equally likely.
- 56 • Despite the naming of the RCPs in terms of their 2100 radiative forcing, models translate
57 concentrations of forcing agents into forcing in different ways. Hence a model simulation of RCP6.0
58 may not attain exactly a radiative forcing of 6 W m⁻².

- Some model simulations are concentration-driven (greenhouse gas concentrations are specified) whereas some models, which have Earth Systems components, convert emission scenarios into concentrations. Different Earth System models driven by emissions may produce different concentrations of greenhouse gases and aerosols because of differences in the representation and/or parameterization of the processes responsible for the emission to concentration conversion.
- SRES and RCPs only account for future anthropogenic changes in radiative forcing. With regard to solar forcing, the 1985–2005 solar cycle is repeated. Neither projections of future deviations from this solar cycle, nor future volcanic radiative forcing and their uncertainties are considered.

Natural Variability: Any climate projection is subject to uncertainties that arise because of natural internal climate variability. In this chapter, the prediction of e.g., the amplitude or phase of some mode of variability that may be important on long time scales is not addressed (see Chapter 11). Any climate variable projection from an individual climate model's single simulation will be contaminated with a random sample of natural variability, whether it be a variable which involves a long time average (e.g., 20 years), a snapshot in time or some more complex diagnostic such as the variance computed from a time series over many years. No amount of time averaging can reduce natural variability to zero, although for some EMICs and simplified models, which may be used to reproduce the results of more complex model simulations, the representation of natural variability is excluded from the model specification. For different variables, and different spatial and time scale averages, the relative importance of natural variability in comparison with other sources of uncertainty will be different (see below). In general, natural variability becomes more important on shorter time scales and for more regional scale variables. The concept of signal-to-noise ratio may be used to quantify the relative magnitude of the forced response (signal) versus natural variability (noise). Natural variability may be sampled explicitly by running ensembles of simulations with slightly different initial conditions. In the case of both multi-model and perturbed physics ensembles, there is an implicit perturbation in the initial state, which means that these ensembles sample both modelling uncertainty and natural variability jointly.

Models: McWilliams (2007) argues that the ability of models to mimic nature is achieved by simplification choices that are non unique in terms of the fundamental numeric and algorithmic structures, forms and values of parameterizations, and number and kinds of coupled processes included. Simplifications and the interactions between parameterised and resolved processes induce 'errors' in models, which can have a leading-order impact on projections. It is possible to characterise the choices made when building and running models into structural -- indicating the numerical techniques used for solving the dynamical equations, the functional form of parameterisation schemes and the choices of inputs for fixed or varying boundary conditions -- and parametric -- indicating the choices made in setting the parameters which control the various components of the model. The community of climate modellers has regularly collaborated in producing coordinated experiments forming multiple model ensembles, MMEs from now on, (using both global and regional model families – e.g., CMIP3/5 - (Meehl et al., 2007a), ENSEMBLES - (Johns et al., 2011), through which structural uncertainty can be explored, and perturbed physics ensembles (PPEs - with e.g., HadCM3, MIROC, CCSM3 - (Yokohata et al., 2011)), through which uncertainties in parameterization choices can be assessed. As noted below, neither MMEs nor PPEs represent an adequate sample of all the possible choices one could make in building a climate model. Also, models may exclude some processes that could turn out to be important for projections (e.g., methane hydrate release).

The balance of uncertainties: The relative role of the different sources of uncertainty as one moves from short- to mid- to long term projections and considers different variables at different spatial scales has to be recognized and has been the object of several studies based on model simulations. Hawkins and Sutton (2009) and Hawkins and Sutton (2011), motivated by Cox and Stephenson (2007) have partitioned the total range in projections of average temperature or precipitation respectively, as expressed by the spread of different models' individual trajectories and their respective internal variability, under different scenarios. They show the three sources exchange relevance as the time horizon, the spatial scale and the variable change. In absolute terms, natural variability is estimated to remain approximately constant across the forecast horizon, with model variability and scenario variability increasing over time. For forecasts of global temperatures after mid-century, scenario and model uncertainty drown the amount of variation due to natural oscillations, with scenario uncertainty absorbing the largest fraction of the total variability in projections by the end of the century. For global average precipitation projections, scenario uncertainty has a much smaller role even by the end of the century and model uncertainty has the lion share across all forecast horizons. For

1 regional scales precipitation projections natural variability has the largest share for short term forecasting and
2 may maintain a significant portion of the whole up until middle of the century in some regions. [Cross
3 reference with chapter 11 here]

4 **12.2.2 From Ensembles to Uncertainty Quantification**

6 The opportunistic nature of the MME has been discussed in Tebaldi and Knutti (2007) and Knutti et al.
7 (2010a), highlighting how it does not represent a systematically sampled family of models, but relies on self
8 selection by the modelling groups. The models are therefore not designed to explore uncertainty in a
9 coordinated manner, and the range of their results cannot be straightforwardly interpreted as an exhaustive
10 range of plausible outcomes, with some studies arguing that the tail of distributions is by construction
11 undersampled (Raisanen, 2007). In general, the difficulty in producing quantitative estimates of uncertainty
12 based on multiple model output originates in their peculiarities as a statistical sample, neither random nor
13 systematic, with possible dependencies among the members and of spurious nature, often counting among
14 their members models with different degrees of complexities (different number of processes explicitly
15 represented or parameterized) even within the category of general circulation models. For some models,
16 relatively large ensembles sampling initial conditions have been performed, enabling better estimates of
17 natural variability uncertainty to be assessed (Deser et al., 2010).

19 Perturbed physics experiments (PPEs) differ radically for they can be, and have been, systematically
20 constructed and as such lend themselves to a more straightforward treatment through statistical modelling
21 (Rougier, 2007; Sanso and Forest, 2009). Uncertain parameters in a single modelling structure are chosen,
22 more often in the atmospheric component of the model (Collins et al., 2006a; Sanderson et al., 2008b) but
23 lately and more expensively also within the ocean component (Brierley et al., 2010; Collins et al., 2007),
24 attempting to focus on parameters to whose values model output is known to be sensitive. Parameters in the
25 land-surface schemes have also been subject to perturbation studies (Fischer et al., 2011). Ranges of possible
26 values are explored and often statistical emulators are introduced in order to sample a number of
27 combinations that would not be otherwise affordable as computing costs may be significant. The space of a
28 single model simulations (even when filtered through observational constraints) can show a large range of
29 outcomes for a given projection (Jackson et al., 2008). However, multi-model ensembles and perturbed
30 physics ensembles produce modes and distributions of climate responses that are different from one another,
31 demonstrating how one type of ensemble cannot be used as an analogue for the other (Collins et al., 2011;
32 Murphy et al., 2007; Sanderson et al., 2010).

34 Many studies have made use of results from these ensembles to characterize uncertainty in future
35 projections, and these will be referred to when describing specific aspects of future climate responses. PPEs
36 have been uniformly treated across the different studies through the statistical framework of analysis of
37 computer experiments (Harris et al., 2010; Rougier et al., 2009; Sanso et al., 2008) or, more plainly, as a
38 thorough exploration of alternative responses reweighted by observational constraints (Forest et al., 2008;
39 Piani et al., 2005). In all cases the construction of a probability distribution is facilitated by the systematic
40 nature of the experiments. MMEs have generated a much more diversified treatment, according to the choice
41 of applying weights to the different models on the basis of past performance or not, and according to the
42 fundamental notion of treating the different models as exchangeable among themselves or as a version of the
43 truth to which each model adds an error (Annan and Hargreaves, 2010). Many studies can be classified
44 according to these two criteria and their combination, but even within each of the four resulting categories
45 different studies produce different estimates of uncertainty, due to the preponderance of a-priori assumptions
46 (explicitly in those studies that approach the problem through a Bayesian perspective, or only implicit in the
47 choice of likelihood models, or weighting).

49 **12.2.3 Joint Projections of Multiple Variables**

51 While many of the key processes are understood, modeling studies are only starting to focus on projections
52 of joint variables. A few studies have addressed projected changes in joint variables, e.g., by combining
53 mean temperature and precipitation (Tebaldi and Lobell, 2008; Tebaldi and Sanso, 2009; Watterson and
54 Whetton, 2011; Watterson, 2011; Williams et al., 2007), linking soil moisture, precipitation and temperature
55 mean and variability (Fischer and Schär, 2009; Koster et al., 2009b; Koster et al., 2009c; Seneviratne et al.,
56 2006), or combining temperature and humidity (Diffenbaugh et al., 2007; Fischer and Schär, 2010; Willett

1 and Sherwood, 2011). Models may have difficulties simulating all relevant interactions between atmosphere
2 and land surface and the water cycle that determine the joint response, observations to evaluate models are
3 often limited (see Seneviratne 2010 ESR for a review), and model uncertainties are therefore large (Fischer
4 et al., 2011; Koster et al., 2006; Notaro, 2008). In some cases, correlations between e.g., temperature and
5 precipitation or accumulated precipitation and temperature have found to be too strong in climate models
6 (Hirschi et al., 2011; Trenberth and Shea, 2005). The situation is further complicated by the fact that model
7 biases in one variable affect other variables. The standard method for model projections is to subtract model
8 biases from control integrations (so called ‘constant bias’). Several studies note that this may be problematic
9 (Buser et al., 2009; Christensen et al., 2008), but there is no consensus at this stage for a method to treat
10 model biases in multiple variables more consistently. Statistical frameworks to deal with multivariate
11 projections are challenging even for just two variables, since they have to address a trade-off between
12 modeling the joint behavior at scales that are relevant for impacts – i.e., fine spatial and temporal scales,
13 often requiring complex spatio-temporal models – and maintaining computational feasibility. In one
14 instance (Tebaldi and Sanso, 2009) scales were investigated at the seasonal and subcontinental level, and
15 projections of the forced response of temperature and precipitation at those scales did not show significant
16 correlations, likely because of the heterogeneity of the relation between the variables within those large
17 averaged regions and seasons.

18
19 Recognizing the need for joint multivariate projections, the above limitations at this stage prevent a
20 quantitative assessment for most cases. A few robust qualitative relationships nonetheless emerge from the
21 literature and these are assessed, where appropriate, below.

22
23 For applications that are sensitive to relationships between variables, sampling from univariate ranges may
24 lead to unrealistic results when significant correlations exist. IPCC assessments often show model averages
25 as best estimates, but such averages can underestimate variability, are not plausible model states (Knutti et
26 al., 2010a) and do not necessarily represent the joint best estimate in a multivariate sense. For impact studies
27 that need dynamically coherent multivariate input from climate model simulations, using each climate model
28 output individually as a realization of joint variables to feed into the impact model is likely to be more
29 consistent, at least as far as the model captures the spatial covariance, the temporal co-evolution and the
30 relevant feedbacks that connect different variables.

31 32 **12.3 Projected Changes in Forcing Agents, including Emissions and Concentrations**

33
34 The experiments at the basis of global future projections discussed in this chapter are extensions of the
35 simulations of the observational record discussed in Chapters 9 and 10. The scenarios assessed in AR5,
36 introduced in Chapter 1, include four new scenarios designed to explore a wide range of future climate
37 characterised by representative long lived greenhouse gas (LLGHG) concentration trajectories. These are
38 described further in Section 12.3.1. The implementation of forcing agents in model projections, including
39 natural and anthropogenic aerosols, ozone, and land-use change are discussed in Section 12.3.2, with a
40 strong focus on CMIP5 experiments. Global mean emissions, concentrations and radiative forcings
41 applicable to the historical record simulations assessed in Chapters 9 and 10, and the future scenario
42 simulations assessed here, are illustrated in Annex II.

43 44 **12.3.1 Description of Scenarios**

45
46 Long-term climate change projections reflect how human activities or natural effects could alter the climate
47 over decades and centuries. In this context, defined scenarios are important, as assuming specific time series
48 of emissions, land-use, atmospheric concentrations or radiative forcing across multiple models allows for
49 coherent climate model intercomparisons and synthesis. Some scenarios are academic, they present an
50 idealized future, not accompanied by a socio-economic storyline and are used for process understanding.
51 More comprehensive scenarios are produced by Integrated Assessment Models (IAMs) as internally
52 consistent sets of emissions and socio-economic assumptions (e.g., regarding population and socio-economic
53 development) with the aim of presenting several plausible future worlds. Often, it is these scenarios that are
54 used for policy relevant climate change, impact, adaptation and mitigation analysis. Here, we focus on the
55 RCP scenarios used within the CMIP5 intercomparison exercise (Taylor et al., 2011) along with the SRES
56 scenarios developed for the IPCC TAR but still widely used by the community.

12.3.1.1 Idealized Concentration Scenarios

A 1%-per-annum compound increase of atmospheric CO₂ concentration until a doubling or a quadrupling of its initial value has been widely used since the second phase of CMIP (Meehl et al., 2000) and the SAR (Kattenberg et al., 1996). This idealized scenario is a useful benchmark for comparing coupled model climate sensitivity, climate feedback and transient climate response. The exponential increase of CO₂ concentrations induces approximately a linear increase in radiative forcing (Myhre et al., 1998) due to a ‘saturation effect’ of the strong absorbing bands. Thus, a linear ramp function results from these idealized pathways, adding to their suitability for comparative diagnostics of the models’ climate feedbacks and inertia. The CMIP5 intercomparison project again includes such a stylized pathway up to a quadrupling of CO₂ concentrations, in addition to an instantaneous quadrupling case, the latter allowing a better distinction between fast adjustments and longer-term feedbacks.

12.3.1.2 The Socio-Economic Driven SRES Scenarios

The climate change projections undertaken as part of CMIP3 and discussed in AR4 were based on the SRES A2, A1B and B2 scenarios (IPCC, 2000). These scenarios were developed using IAMs and resulted from specific socio-economic scenarios, i.e., from storylines about future demographic and economic development, regionalization, energy production and use, technology, agriculture, forestry, and land-use. All SRES scenarios assumed that no climate mitigation policy would be undertaken. Based on these SRES scenarios, global climate models were then forced with corresponding LLGHG and aerosol concentrations, although the degree to which models implemented these forcings differed (Meehl et al., 2007b, Table 10.1). The resulting climate projections, together with the socio-economic scenarios, were then the basis for further analysis by the impact, adaptation and vulnerability research community (Figure 12.1a).

12.3.1.3 The New Concentration Driven RCPs Scenarios, and their Extensions

As already detailed in Chapter 1, a new parallel process for scenario development was proposed in order to facilitate the interactions between the scientific communities working on climate change, adaptation and mitigation (Moss et al., 2010; Moss et al., 2008; van Vuuren et al., 2011b). These new scenarios, named "Representative Concentration Pathways" (RCPs), are referred to as pathways in order to emphasize that their primary purpose is to provide time-dependent projections of atmospheric greenhouse gas (GHG) concentrations. They are representative in that they are one of several different scenarios that have similar radiative forcing and emissions characteristics. The scenarios are identified by the stabilization value of the radiative forcing (in W m⁻²) (Figure 12.2): the lowest RCP, RCP2.6 (also referred as RCP3-PD), which peaks at 3 W m⁻² and then declines to approximately 2.6 W m⁻² by 2100; the medium-low RCP4.5 and the medium-high RCP6.0 aiming for stabilization at 4.5 and 6.0 W m⁻² respectively around 2100; and the highest one, RCP8.5, which implies a radiative forcing of 8.5 W m⁻² by 2100. Note that due to the substantial uncertainties in radiative forcing, these forcing values should be understood as comparative ‘labels’, not as exact definitions of the forcing that is effective in climate models. This is because not the radiative forcing, but rather the concentrations or emissions, are prescribed in the CMIP5 climate model runs. The forcing as it pertains to climate models is discussed in Section 12.3.3.

[INSERT FIGURE 12.2 HERE]

Figure 12.2: Time evolution of the anthropogenic radiative forcing between 2000 and 2300 due to the defined concentrations of long-lived greenhouse gases (CO₂, CH₄, N₂O, halogenated, chlorinated and fluorinated gases) for RCP scenarios and their extensions (continuous lines) and SRES scenarios (dashed lines). The four RCP scenarios used in CMIP5 are: RCP2.6 (blue), RCP4.5 (green), RCP6.0 (light blue) and RCP8.5 (red). The three SRES scenarios used in CMIP3 are: B1 (green), A1B (light blue) and A2 (red). The radiative forcing has been computed using the concentration of the different greenhouse gases for the different scenarios and the radiative efficiency published in the TAR (Table 6.7), using SRES scenario concentrations published in the TAR (Appendix II). It is illustrative of the LLGHG forcing that could result in climate models which are forced with the defined concentrations pathways.

Various steps were necessary to turn the selected ‘raw’ RCP emission scenarios from the IAMs to the datasets usable by the climate modelling community, including the extension with historical emissions (Granier et al., 2011; Smith et al., 2011), the harmonization and gridding of land-use datasets (Hurtt et al., 2011), the provision of atmospheric chemistry runs, particular for tropospheric ozone, and the harmonization of 2000–2005 GHG emission levels, extension of GHG concentrations with historical GHG

1 concentrations and harmonization of 2000–2005 GHG concentrations levels (Meinshausen et al., 2011c).
2 After these processing steps, the final RCP datasets comprise land-use data, harmonized GHG emissions and
3 concentrations, gridded reactive gas and aerosol emissions, as well as ozone and aerosol abundance fields.
4

5 The Four Representative Concentration Pathways (RCPs) are based through the end of the 21st century on
6 the IAMs. In order to investigate longer-term climate change implications, these RCPs were extended until
7 2300 (Meinshausen et al., 2011c). These extensions use simple assumptions on GHG emissions and
8 concentrations beyond 2100 and were designed as hypothetical ‘what-if’ scenarios, not as results of socio-
9 economic considerations beyond 2100. In order to continue to investigate a broad range of possible climate
10 futures, the two outer RCPs, RCP2.6 and RCP8.5 assume constant emissions after 2100, while the two
11 middle RCPs aim for a smooth stabilization of concentrations by 2150. RCP8.5 stabilizes concentrations
12 only by 2250, with CO₂ concentrations of approximately 2000 ppm, nearly 7 times the pre-industrial levels.
13 As the RCP2.6 implies net negative CO₂ emissions after around 2070 and throughout the extension, CO₂
14 concentrations are slowly reduced towards 360 ppm by 2300.
15

16 *12.3.1.4 Comparison of SRES and RCP Scenarios*

17 The four RCP scenarios used in CMIP5 lead to radiative forcing values that span a range larger than that of
18 the three SRES scenarios used in CMIP3 (Figure 12.2). RCP4.5 is close to SRES B1, RCP6.0 is in between
19 SRES B1 and SRES A1B and RCP8.5 is higher than SRES A2 and close to SRES A1FI. RCP2.6 is lower
20 than any SRES scenario and very close to the ENSEMBLES E1 scenario (Johns et al., 2011). Results
21 obtained with one GCM confirm that the only two SRES and RCP scenarios that are close are RCP4.5 and
22 SRES B1, and that the temperature increase with RCP8.5 is larger than that with SRES A2 (Duffresne et al.,
23 2011). The spread of projected global warming with the RCP scenarios is much larger than with SRES
24 scenarios. [PLACEHOLDER FOR SECOND ORDER DRAFT: to be updated when new literature and more
25 detailed analysis become available, specific points on aerosols and methane being considered.]
26
27

28 *12.3.1.5 Range of Other Scenarios used in the Literature*

29 Aside from the pathways and scenarios investigated as part of the CMIP5 experiments, there is a broad range
30 of scenarios and pathways in the literature. Some of these investigate emission implications of various
31 temperature or concentration-based climate targets, some are designed to investigate the climatic effect of
32 peaking or overshoot profile, yet others are meant to provide best-estimate predictions over the next decades.
33 Aside from this distinction regarding their purpose, the literature scenarios and pathways can be
34 distinguished regarding the coverage of gases, sectors and regions. For example, very specific emission
35 scenarios exist for single sectors, like the Eab and Edh (Électricité de France “a-base” and “d-high”) aviation
36 sector scenarios (Vedantham and Oppenheimer, 1998).
37
38

39 *12.3.2 Implementation of Forcings in CMIP5 Experiments*

40 The CMIP5 experimental protocol for long term transient climate experiments prescribes a common basis for
41 a comprehensive set of anthropogenic forcing agents acting as boundary conditions in three experimental
42 phases – historical, RCPs and ECPs (Taylor et al., 2011). To permit common implementations of this set of
43 forcing agents in CMIP5 models, self-consistent forcing data time series have been computed and provided
44 to participating models (see Sections 9.3.2.2 and 12.3.1.3) comprising emissions or concentrations of GHGs
45 and related compounds, atmospheric aerosols and their chemical precursors, and land use change.
46
47

48 Natural forcings (arising from solar variability and aerosol emissions via volcanic activity) are also specified
49 elements in the CMIP5 experimental protocol, but their future time evolutions are not prescribed very
50 precisely. A repeated 11-year cycle for total solar irradiance (Lean and Rind, 2009) is suggested for future
51 projections but the periodicity is not specified precisely as solar cycles vary in length. For volcanic eruptions,
52 no recommendation is given for future emissions or concentration data. The only recommendation is that
53 volcanic aerosols should either be omitted entirely both from the control experiment and future projections,
54 or the same background aerosols should be prescribed in both runs. Both options are *very unlikely* to be
55 realistic with respect to the mean future volcanic forcing, but simply provide a consistent framework for
56 model intercomparison given a lack of knowledge of when future large eruptions will occur.
57

1 For the other natural aerosols (dust, sea-salt, etc.), no emission or concentration data is recommended. The
2 emissions are potentially computed interactively by the models themselves and may change with climate, or
3 prescribed from separate model simulations carried out in the implementation of CMIP5 experiments.
4

5 The forcing agents applied in individual AOGCMs and ESMs used to make climate projections in CMIP5
6 are summarised in Table 12.1.
7

8 *12.3.2.1 “Emissions-Driven” versus “Concentrations-Driven” Experiments*

9

10 A novel feature within the CMIP5 experimental design is that experiments driven either by anthropogenic
11 emissions or prescribed concentration pathways for LLGHGs (Taylor et al., 2011) are included. The dual
12 forcing protocol allows “ESMs” (models possessing an interactive carbon cycle) and AOGCMs that do not
13 possess an interactive carbon cycle both to be forced with identical LLGHG concentration pathways to
14 derive a consistent range of climate responses from the two types of model. The range of climate responses
15 including climate-carbon cycle feedbacks can additionally be explored in ESMs driven with emissions rather
16 than concentrations, analogous to C⁴MIP experiments (Friedlingstein et al., 2006). Results from the two
17 types of experiment cannot be compared directly, but they provide complementary information. Firstly,
18 uncertainties in the forward climate response driven with specified emissions or concentrations can be
19 derived from all participating models, while concentrations-driven ESM experiments also permit a policy-
20 relevant diagnosis of the range of anthropogenic carbon emissions compatible with those concentration
21 pathways (Hibbard et al., 2007; Moss et al., 2010).
22

23 CMIP5 model implementations of concentrations-driven forcing by Long Lived Greenhouse Gases
24 (LLGHGs) conform closely in almost all cases to the standard protocol (Table 12.1; CO₂, CH₄, N₂O, CFCs),
25 imposing an effective control over the radiative forcing due to LLGHGs across the multi-model, apart from
26 the uncertainty arising from radiative transfer code (Collins et al., 2006b; Meehl et al., 2007b). The ability of
27 ESMs to determine their own LLGHG concentrations in “emissions-driven” experiments means that
28 radiative forcing due to LLGHGs is less tightly controlled in such experiments. Even in “concentrations-
29 driven” experiments, many models implement some emissions-driven forcing agents (most often aerosols,
30 but also ozone in some cases) leading to a potentially greater spread in both the concentrations and hence
31 radiative forcing of those emissions-driven agents.
32

33 **[INSERT TABLE 12.1 HERE]**

34 **Table 12.1:** [PLACEHOLDER FOR SECOND ORDER DRAFT: Radiative forcing agents in the CMIP5 multi-model
35 global climate projections. See Table 9.1 for descriptions of the models. ESMs are highlighted in bold. In most cases
36 forcing agents are implemented in conformance with standard prescriptions and datasets for CMIP5 (Taylor et al.,
37 2011). Entries mean: n.a.: Forcing agent excluded in both historical and scenario simulations; Y: Forcing agent included
38 (via prescribed concentrations, distributions or time series data); E: Forcing agent included (via specified emissions or
39 precursor emissions); Es: Forcing agent included (driven with specified emissions but with prescribed surface
40 concentrations); -: Simulations not performed; [?] – information not yet available. Numeric superscripts indicate model-
41 specific references and other superscripts denote particular variations in forcing implementations, as detailed in notes
42 following the table.]
43
44

45 *12.3.2.2 Variations between Model Forcing Specifications*

46

47 Apart from the distinction between concentrations-driven and emissions-driven protocols, a number of
48 variations are present in the implementation of similar forcing agents listed in Table 12.1, which generally
49 arise due to constraining characteristics of the model formulations, computational efficiency considerations,
50 or local implementation decisions (e.g., rescaling of prescribed data). In a number of models, off-line
51 modelling using an atmospheric chemistry-transport model or aerosol-transport model has been used to
52 convert emissions into concentrations compatible with the specific model formulation or characteristics. As a
53 result, although detailed prescriptions are given for the forcing agents in CMIP5 experiments, the variety of
54 modelling approaches leads to considerable variations in their actual implementations. This was also the case
55 in the ENSEMBLES multi-model projections, in which similar forcing agents to CMIP5 models were
56 applied but again with variations in the implementation of aerosol, ozone and land-use forcings, prescribing
57 the SRES A1B and E1 scenarios in a “concentrations-driven” protocol (Johns et al., 2011) akin to the CMIP5
58 protocol.

1
2 Methane, nitrous oxide and CFCs (typically with some aggregation of the multiple gases) are generally
3 prescribed with standard well-mixed concentrations in CMIP5 models, but in a number of models (CESM1
4 (WACCM), GFDL-CM3, GISS-E2 (TCAD,TCADI) and HadGEM2-ES) surface concentrations are
5 prescribed along with prescribed emissions., In the emissions-driven models, the 3-dimensional
6 concentrations in the atmosphere that are passed to the radiation scheme vary interactively.

7
8 Tropospheric and stratospheric ozone concentrations are in most models based on the CMIP5 standard ozone
9 dataset computed as part of the CCMVal-2/AC&C/SPARC activity (Cionni et al., 2011), but some models
10 base their input ozone concentrations on different datasets (e.g., MIROC-ESM, MIROC4h and MIROC5
11 used the Wang et al. (1995) historical dataset extended into the future). In some models (e.g., IPSL-CM5,
12 CCSM4) ozone is supplied as concentrations from off-line computations using a related atmospheric
13 chemistry-transport model. A few models (e.g., MIROC-ESM-CHEM, MRI-ESM1, and HadGEM2-ES for
14 tropospheric ozone only) determine ozone interactively from specified emissions via on-line atmospheric
15 chemistry. The CMIP5 standard ozone dataset does not include future solar cycle related ozone variations,
16 but some modelling groups modify the dataset to add stratospheric ozone variability related to solar forcing.
17 Computing ozone concentrations interactively, as is done in a minority of models, allows the fast coupling
18 between chemistry and climate to be captured, but modelling of chemistry processes has to be simplified in
19 comparison with full complexity chemistry-climate models (CCMs) due to computing constraints. However,
20 the CNRM-CM5 model reduces this computational burden by coupling interactively to a 2-dimensional
21 stratospheric chemistry model with linearized stratospheric ozone photochemistry (Cariolle and Teysse, 2007).
22
23

24 For atmospheric aerosols, either aerosol precursor emissions-driven or concentrations-driven forcings are
25 applied depending on individual model characteristics. A larger fraction of models in CMIP5 than CMIP3
26 prescribe aerosol precursor emissions rather than concentrations. Many still prescribe concentrations pre-
27 computed either using a directly related aerosol chemistry climate model or from output of another, complex,
28 emissions-driven aerosol chemistry model within the CMIP5 process, e.g., Lamarque et al. (2011; 2010).
29 Concentrations output from such simulations are used to drive the future RCP projections, helping to
30 reducing the computational burden of the projections themselves. In several of the concentrations-driven
31 models (CCSM4, IPSL-CM5A variants, MPI-ESM-LR, MPI_ESM_HR), additional emissions-driven
32 simulations have been undertaken so as to tailor the concentrations more closely to the model's individual
33 aerosol-climate characteristics. Compared with the CMIP3 models in AR4, a much large fraction of CMIP5
34 models now incorporate black and organic carbon aerosol forcings. A similar, larger, fraction of CMIP5
35 models include indirect aerosol effects, although in about half of those models that include the first indirect
36 effect it only includes the effect of sulphate aerosol, and the majority of models still exclude the second
37 indirect effect completely. No CMIP5 models represent urban aerosol pollution explicitly, and only one
38 model (GISS-E2) explicitly includes nitrate aerosol as a forcing in CMIP5 simulations. A study with a
39 version of the HadGEM2-ES models related to that used in CMIP5 suggests that, in contrast to the projected
40 decrease in sulphate aerosol, ammonium nitrate aerosol would increase over the 21st century, tending to
41 slow the decline in aerosol-related radiative forcing (Bellouin et al., 2011).
42

43 Land-use change is typically applied by blending anthropogenic land surface disturbance via crop and
44 pasture fraction changes with underlying land cover maps of natural vegetation, but model variations in the
45 underlying land cover maps and biome modelling mean that the land-use forcing agent is impossible to
46 impose in a completely common way at present (Pitman et al., 2009). Most CMIP5 models represent crop
47 and pasture disturbance separately, while some (CanESM2, MIROC4h, MIROC5) represent crop but not
48 pasture. Some models allow a dynamical representation of natural vegetation changes alongside
49 anthropogenic disturbance.

50
51 Treatment of the CO₂ emissions associated with land cover changes is also model-dependent. Some models
52 do not account for land cover changes at all, some simulate the biophysical effects but are still forced
53 externally by land cover change induced CO₂ emissions (in emission driven simulations), while the most
54 advanced ESMs simulate both the biophysical effects of land cover changes and their associated CO₂
55 emissions.
56

[PLACEHOLDER FOR SECOND ORDER DRAFT: Regarding information synthesized in Table 12.1, a more detailed assessment will be made of the different data sources and methods used to prescribe aerosol concentrations and/or total aerosol optical thickness in CMIP5 models, including the treatment of biomass burning black carbon aerosol as distinct from fossil fuel black carbon. Dust and sea-salt are modelled interactively in many but not all models but the entries in Table 12.1 do not discriminate between those models that prescribe them as concentrations and those which allow them to respond interactively to changes in climate (and vegetation in the case of dust); this will be done more consistently.]

12.3.3 Projected Radiative Forcing for the 21st Century

This section presents the projected radiative forcing estimated from the CMIP5 model projections and discusses the consistency with radiative forcing estimates determined using other methods in Chapters 7 and 8. Chapter 8 defines the radiative forcing concept in general and the methodology for computing radiative forcing directly from output of model projections which is used here. Quantification of future radiative forcing is of interest here as it is directly related to changes in the global energy balance of the climate system and resultant global warming.

Figure 12.3 illustrates the radiative forcing estimated in CMIP5 models through the 21st century for the four RCPs. The ensemble mean net climate forcing for 2091–2100 is 2.2, 3.7, 4.1 and 7.2 W m⁻² respectively for RCP2.6, RCP4.5, RCP6.0 and RCP8.5 in concentrations-driven projections. These ensemble mean estimated forcings are in all cases substantially lower than the total forcing at 2100 as estimated in the CMIP5 RCP database using idealized calculations (2.7, 4.3, 5.5, 8.4 W m⁻² respectively). For RCP2.6 and RCP4.5, the difference between the all-sky net forcing and LW clear-sky forcing decreases with time. For RCP2.6, the latter peaks around 2040 and then declines, consistent with the radiative forcing directly estimated from the GHG concentrations (Figure 12.2). The all-sky net forcing does not show this decrease but rather a stabilization. The reason is that the amount of aerosol decreases and, as the radiative forcing of aerosol is negative, the cooling effect of anthropogenic aerosols decreases, leading to an increase of the net forcing. This effect is also evident for RCP4.5, but not in RCP6.0 and RCP8.5 as the temperature increase is much larger for these two RCPs than for the two lower RCPs (Figure 12.4) which leads to a larger decrease of the average cloud fraction (section 12.4.3.5). This decrease in cloud fraction brings the net forcing closer to the LW clear-sky forcing, compensating for the effect of reducing the aerosol concentration. The net climate forcing in CMIP5 models at present day is generally lower than for CMIP3 models for the SRES-A1B scenario (Forster and Taylor, 2006) when compared using this same method.

[PLACEHOLDER FOR SECOND ORDER DRAFT: Currently the Figure 12.3 illustrates the climate forcing for individual CMIP5 models' computed using the Forster and Taylor (2006) method using top of atmosphere fluxes. When more data and analysis are available, the extent to which the climate forcing computed from model projections output this way is consistent with the sum of estimates of individual forcings and/or with forcings estimates using other methods presented elsewhere in the report, particularly Chapter 8, will be examined. The figure is expected to be updated or augmented with a box-whisker plot illustrating the multi-model range of forcing uncertainty for 20-year periods in the RCP projections up to 2100, in which individual model trajectories will not be identifiable.]

[INSERT FIGURE 12.3 HERE]

Figure 12.3: [PLACEHOLDER FOR SECOND ORDER DRAFT: Global mean climate forcings (W m⁻²) realised in the CMIP5 simulations diagnosed for four RCP scenarios. Thin green and orange lines correspond to net all-sky and longwave clear-sky climate forcings respectively. Climate forcing has been computed using the methodology of Forster and Taylor (2006), which includes rapid adjustment in the forcing term and further assumes each model has an invariant climate feedback parameter, which here has been calculated from the abrupt 4xCO₂ experiments using the method of Gregory et al. (2004). Climate forcings are referenced to the equivalent period (2005–2100 average) of the model's preindustrial control integration. Each of these lines represents a single CMIP5 model result averaged over all available ensemble members. Thick lines show the multi-model averaged climate forcing. Grey lines on the RCP6.0 panel show the net climate forcings diagnosed from 21 CMIP3 models for the SRES A1B scenario, taken from Forster and Taylor (2006).]

12.4 Projected Climate Change over the 21st Century

This section assesses projected changes in the climate system for the mid-21st century and beyond. Both physical and biogeochemical projections are described and draw heavily on climate model experiments performed for CMIP5, which have been evaluated in previous chapters. Projected climate changes are driven by changes in radiative forcing (see Section 12.3), which lead to imbalances in the energy budget and associated changes in temperature (Section 12.4.3), the water cycle (which is globally-linked to the energy cycle - Section 12.4.5), atmospheric circulation (Section 12.4.4), the cryosphere (Section 12.4.6) and the ocean (Section 12.4.7), as well as changes in concentrations of greenhouse gases and aerosols (Section 12.4.9). Multi-model mean changes under various RCPs are used to illustrate key changes (all models are given equal weight unless noted otherwise), with consideration for sources of uncertainty in these projections given throughout. In most multi model figures the number of models that are included is listed in the top right corner of each panel. Model robustness is indicated by stippling as described by Tebaldi et al. (2011). The use of pattern scaling to assess projections is discussed in Section 12.4.2 and a comparison with projections from the AR4 is given in Section 12.4.8.

12.4.1 Time-Evolving Global Quantities

12.4.1.1 Projected Changes in Global Mean Temperature and Precipitation

A consistent and robust feature across climate models is continuation of global warming in the 21st century (Figure 12.4 – showing changes in concentrations-driven models). Temperature increases are almost independent of the prescribed radiative forcing during the first two decades after 2005. At longer time scales, the warming rate begins to depend strongly on the specified GHG concentration pathway, being highest ($>0.3^{\circ}\text{C}$ per decade) in the highest RCP 8.5 and significantly lower in RCP 2.6, particularly after ~ 2050 when global surface temperature response stabilizes (and declines thereafter). The dependence of global temperature rise on GHG forcing at longer timescales has been confirmed by several studies (Meehl et al., 2007b). [PLACEHOLDER FOR SECOND ORDER DRAFT (TO BE CROSS-CHECKED WITH OBS CHAPTER): Global warming under RCP 2.6 approaches 2°C by 2100 relative to the pre-industrial period in the ensemble mean (assuming an observed warming of 0.7°C)], in agreement with previous studies of aggressive mitigation scenarios (Johns et al., 2011; Meehl et al., 2011) and in contrast to the non-mitigation pathways where all models project $>2^{\circ}\text{C}$ warming by 2100. In some model simulations of RCP2.6, warming does exceed 2°C change from pre-industrial. Emissions-driven model simulations are discussed in section 12.4.9.

[INSERT FIGURE 12.4 HERE]

Figure 12.4: Time series of global mean surface air temperature anomalies (relative to 1986–2005) from concentration-driven experiments from CMIP5. Projections are shown for each representative concentration pathway (RCP) for the multimodel mean (solid lines) and ± 1 standard deviation across the distribution of individual models (shading).

The multimodel global mean temperature changes under different radiative concentration pathways are summarized in Table 12.2. The relationship between cumulative anthropogenic carbon emissions and global temperature is assessed in Section 12.5. Also shown in Table 12.2 are regional average temperature changes under the RCPs. Land areas warm more rapidly than surface air temperatures over the ocean and northern polar regions warm more rapidly than the tropics (Section 12.4.3). The excess of land mass in the Northern Hemisphere in comparison with the Southern Hemisphere, coupled with the greater uptake of heat by the Southern Ocean in comparison with northern ocean basins means that the Northern Hemisphere generally warms more than the Southern. This partly contributes to the difference in warming between the Arctic and Antarctic, although the presence of the Antarctic ice sheet also contributes. The continental average temperatures reflect these generic features. Maps and timeseries of regional temperature changes are displayed in the Annex I Atlas.

Table 12.2: CMIP5 annual mean surface air temperature anomalies from the 1986–2005 reference period for selected time slices, regions and RCPs. Regions are defined as in AR4 (Hegerl et al., 2007). The multimodel mean ± 1 standard deviation range across the individual models is listed and the minimum and maximum values from the model distribution are given in brackets.

	RCP2.6	RCP4.5	RCP6.0	RCP8.5
Global: 2016–2035	0.8 ± 0.2 (0.5,1.2)	0.7 ± 0.2 (0.4,1.0)	0.7 ± 0.2 (0.4,1.0)	0.8 ± 0.2 (0.5,1.2)

2046–2065	1.2 ± 0.3 (0.8,1.7)	1.4 ± 0.4 (0.8,2.0)	1.4 ± 0.3 (1.1,1.9)	2.0 ± 0.4 (1.3,2.7)
2081–2100	1.2 ± 0.4 (0.8,1.7)	1.9 ± 0.5 (1.2,2.6)	2.4 ± 0.5 (1.7,3.1)	3.8 ± 0.8 (2.5,5.0)
2181–2200	0.8 ± 0.4 (0.5,1.2)	2.1 ± 0.4 (1.5,2.7)	-	7.2 ± 1.8 (4.4,9.1)
2281–2300	0.6 ± 0.4 (0.3,1.0)	2.3 ± 0.4 (1.7,2.8)	-	8.7 ± 2.4 (5.0,11.6)
Land: 2081–2100	1.6 ± 0.5 (1.0,2.3)	2.5 ± 0.6 (1.6,3.5)	3.2 ± 0.7 (2.3,4.2)	5.1 ± 1.1 (3.5,6.7)
Ocean: 2081–2100	1.0 ± 0.3 (0.6,1.5)	1.6 ± 0.4 (1.1,2.2)	2.0 ± 0.5 (1.4,2.7)	3.3 ± 0.7 (2.2,4.3)
Tropics: 2081–2100	1.0 ± 0.3 (0.6,1.6)	1.6 ± 0.4 (1.0,2.2)	2.1 ± 0.5 (1.5,2.7)	3.4 ± 0.7 (2.3,4.4)
Polar: Arctic: 2081–2100	3.0 ± 1.2 (1.6,4.7)	4.7 ± 1.5 (2.2,7.3)	5.5 ± 1.9 (3.0,8.6)	8.7 ± 2.1 (4.8, 12.1)
Polar: Antarctic: 2081–2100	1.2 ± 0.5 (0.2,2.0)	1.7 ± 0.6 (0.7,2.8)	2.0 ± 0.8 (1.1,3.3)	3.3 ± 0.9 (1.7,4.6)
Africa: 2081–2100	1.3 ± 0.4 (0.9,2.0)	2.3 ± 0.5 (1.4,3.2)	2.9 ± 0.6 (2.1,4.0)	4.8 ± 0.9 (3.5,5.9)
Asia: 2081–2100	1.7 ± 0.6 (1.0,2.8)	2.8 ± 0.8 (1.8,4.0)	3.5 ± 0.9 (2.3,4.9)	5.6 ± 1.3 (3.7,7.8)
Australia: 2081–2100	1.3 ± 0.3 (0.8,1.8)	2.1 ± 0.5 (1.4,2.7)	2.6 ± 0.6 (1.8,3.4)	4.2 ± 0.9 (2.6,5.5)
Europe: 2081–2100	1.6 ± 0.6 (1.0,2.6)	2.5 ± 0.7 (1.5,3.7)	3.1 ± 0.8 (2.2,4.4)	5.0 ± 1.2 (3.4,6.9)
North America: 2081–2100	2.0 ± 0.7 (1.3,3.2)	3.1 ± 1.0 (1.6,4.7)	3.9 ± 1.1 (2.5,5.5)	6.1 ± 1.5 (3.8,8.5)
South America: 2081–2100	1.3 ± 0.5 (0.8,2.1)	2.1 ± 0.6 (1.3,3.2)	2.6 ± 0.6 (2.0,3.4)	4.4 ± 1.1 (2.8,6.0)

1
2
3 Models project a gradual increase in global precipitation over the 21st century. An approximately linear
4 relationship with global temperature increase is found (Figure 12.5) which is physically consistent with the
5 temperature-water vapour positive feedback. The global precipitation sensitivity of less than 3% °C⁻¹ in most
6 models is less than the column integrated water vapour sensitivity of ~7% °C⁻¹ (Held and Soden, 2006;
7 Stephens and Ellis, 2008). The weaker precipitation sensitivity is attributed to an interaction of changes in
8 both the radiative budget (Andrews et al., 2010; Bala et al., 2010) and the increased water carrying capacity
9 of a warmer atmosphere (Allen and Ingram, 2002; Held and Soden, 2006; Vecchi and Soden, 2007) resulting
10 in a weaker moisture transport from the boundary layer to the free atmosphere. Not all models simulate the
11 same precipitation sensitivity and the slope of the global precipitation versus global temperature curves
12 differs for different scenarios, tending to be highest for RCP2.6 and RCP4.5. Different slopes across models
13 may be partly due to differences in the representation of the processes responsible for the basic model
14 precipitation sensitivity to increasing CO₂ (Chapter 9) and partly due to differences in the RCP radiative
15 forcing from different forcing agents. CMIP5 model behaviour is consistent with previous studies, including
16 CMIP3 model projections for SRES scenarios and commitment experiments, and ENSEMBLES multi-model
17 results for SRES A1B and E1 scenarios (Johns et al., 2011).
18

19 [INSERT FIGURE 12.5 HERE]

20 **Figure 12.5:** Global mean precipitation (mm/day) versus temperature (°C) changes relative to 1986 to 2005 for CMIP5
21 model projections for RCPs. Each coloured symbol represents the ensemble mean for a single model averaged over
22 successive decadal periods (2006 to 2015 up to 2086 to 2095). The black triangles are multi-model means.
23

24 12.4.1.2 Uncertainties in Global Quantities

25
26 Uncertainties in global mean quantities arise from variations in internal natural variability, model response
27 and forcing pathways. Table 12.2 gives two measures of uncertainty in the CMIP5 model projections, the
28 standard deviation and range across the model distribution, however, other techniques exist for assessing
29 uncertainty in future projections. Figure 12.6 summarises the uncertainty ranges in global mean temperature
30 changes at the end of the 21st century under the various scenarios for the CMIP5 models. Results for models
31 that have not simulated all scenarios were estimated based on a pulse response method (Good et al., 2011) to
32 give means and ranges that are comparable across scenarios. Estimates from the MAGICC model calibrated
33 to C4MIP and the climate sensitivity assessment of AR4 are given as yellow bars (Rogelj et al., 2011).
34 Taking into account scaling arguments derived from earlier models and scenarios (Knutti et al., 2008b) and
35 the fact that that the uncertainty assessments for equilibrium climate sensitivity, transient climate response
36 and the carbon cycle climate feedback have not changed significantly since AR4, the *likely* uncertainty in
37 global temperature projections for the end of the 21st century remains –40 to +60% around the CMIP5 mean,
38 as in AR4. Figure 12.7 shows maps of surface air temperature from each of the CMIP5 models highlighting
39 both similarities and differences between the responses of different models. The similarities may be
40 exploited to estimate temperature changes under different scenarios (next section).

1
2 **[INSERT FIGURE 12.6 HERE]**

3 **Figure 12.6:** Uncertainty estimates for global mean temperature change with respect to 1986–2005 using different
4 techniques. The yellow bars show the median, 33–66% range and 10–90% range based on (Rogelj et al., 2011a). The
5 solid black line indicates the CMIP5 ensemble mean and the grey bars show –40% and +60% of that mean.

6
7 **INSERT FIGURE 12.7 HERE]**

8 **Figure 12.7:** Surface air temperature change in 2081–2100 displayed as anomalies with respect to 1986–2005 for
9 RCP4.5 from each of the concentration-driven models available in the CMIP5 archive.

10
11 **12.4.2 Pattern Scaling**

12
13 **12.4.2.1 Definition and Use**

14
15 “Pattern scaling” is an approximation that has been explicitly suggested in the description of the new RCPs
16 (Moss et al., 2010) as a method for deriving impact-relevant regional projections for scenarios that have not
17 been simulated by global and regional climate models. It was first proposed by Santer et al. (1990) and relies
18 on the existence of a robust geographical pattern of temperature and – to a lesser degree especially when
19 aerosols are involved (Shiogama et al., 2010) – precipitation change. The pattern remains approximately
20 constant along the length of the simulation and across different scenarios and models, once it is scaled by the
21 corresponding global average temperature change. It is in the latter quantity that the dependence of the
22 evolution of the change in time on the model (e.g., its climate sensitivity) and the forcing (e.g., the emission
23 scenario) is encapsulated.

24
25 In analytical terms, it is assumed that the following relation approximately holds,

26
27
$$C(\mathbf{t}, \xi) = T_G(\mathbf{t}) \chi(\xi)$$

28
29 where the symbol ξ identifies the geographic location (model grid point or other spatial coordinates) and
30 possibly the time of year (for example a June-July-August average). The index \mathbf{t} runs along the length of the
31 forcing scenario of interest. $T_G(\mathbf{t})$ indicates global average temperature change at time \mathbf{t} under this scenario;
32 $\chi(\xi)$ is the time-invariant geographic pattern of change for the variable of interest (that by construction has a
33 spatial mean of unity) and $C(\mathbf{t}, \xi)$ is the actual field of change for that variable at the specific time \mathbf{t} under
34 this scenario. This way, regionally and temporally differentiated results under different scenarios or climate
35 sensitivities can be approximated by the product of a spatial pattern constant over time and a time evolving
36 global mean change in temperature. Characterizing the sensitivity to model and scenario is thus reduced to
37 obtaining the global mean temperature response, which can be done inexpensively, by simple climate
38 models. The spatial pattern can be estimated through the available coupled models simulations and, by
39 assumption, won’t depend on the actual scenario(s) under which those models were run.

40
41 The choice of the pattern in the studies available in the literature can be as simple as the ensemble average
42 field of change (across models and/or across scenarios, for the coupled experiments available), normalized
43 by the corresponding change in global average temperature, choosing a segment of the simulations when the
44 signal has emerged from the noise of natural variability from a baseline of reference (e.g., the last 20 years of
45 the 21st century compared to pre-industrial or current climate). Similar properties and results have been
46 obtained using more sophisticated multivariate procedures that optimize the variance explained by the
47 pattern (Holden and Edwards, 2010).

48
49 Pattern scaling and its applications have been documented in IPCC WG1 reports before (IPCC WG1 TAR,
50 section 13.5.2.1; AR4 section 10.3.2). It has been used extensively for regional temperature and precipitation
51 change projections, e.g., Murphy et al. (2007), Watterson (2008), Giorgi (2008), Harris et al. (2006) and
52 Harris et al. (2010), May et al. (2008a), Ruosteenoja and Ruokkoilainen (2007), Raisanen et al. (2006), Cabre
53 et al. (2010) and impacts studies, e.g., as described in Dessai et al. (2005) and Fowler et al. (2007b). Recent
54 studies have focused on patterns linked to warming at certain global average temperature change thresholds
55 (e.g., Sanderson et al., 2011).

1 There are basic limitations to this approach because the assumption holds only approximately and there exist
2 in fact differences between the patterns generated by different GCMs, but uncertainty can be characterized,
3 for example, by the inter-model spread in the pattern $\chi(\xi)$. The validity of this approximation is discussed by
4 Mitchell et al. (1999) and Mitchell (2003). Pattern scaling has been shown to be more accurate for
5 temperature than for precipitation projections. In fact, recent work with MIROC3.2 (Shiogama et al., 2010)
6 has revealed a dependence of the precipitation sensitivity (global average precipitation change per 1°C of
7 global warming – see Figure 12.5) on the scenario, and identified the reason for it in the fact that
8 precipitation is more sensitive to carbon aerosols than well-mixed greenhouse gases and there are significant
9 differences in black and organic carbon aerosol forcing between the emission scenarios investigated. This is
10 a behaviour that is linked to a more general limitation of pattern scaling, which breaks down if aerosol
11 forcing is significant, because the effects of aerosols have a regional nature and are thus dependent on the
12 future sources of pollution which are likely to vary geographically in the future and be difficult to predict.
13 For example, Asian and North American aerosol production are likely to have different time histories going
14 forward. (Schlesinger et al., 2000) extended the methodology of pattern scaling by isolating and recombining
15 patterns derived by dedicated experiments with a coupled climate model where sulfate aerosols were
16 increased for various regions in turn. More recently, in an extension of pattern scaling into a fully
17 probabilistic treatment of model, scenario and initial condition uncertainties, Frieler et al., (2011b) derived
18 joint probability distributions for regionally averaged temperature and precipitation changes as linear
19 functions of global average temperature and additional predictors including regionally specific SO_x and
20 black carbon emissions.

21
22 Pattern scaling is less accurate for stabilization scenarios. Manabe and Wetherald (1980) and Mitchell et al.
23 (1999) already pointed out that as the temperatures of the deep oceans reach equilibrium (over multiple
24 centuries) patterns of temperature change as well, one effect being that the warming of high latitudes in the
25 Southern hemisphere is much larger, relative to the global mean warming, than in the earlier periods. More
26 recently Held et al. (2010) showed how this slow warming pattern is in fact present during the initial
27 transient response of the system as well, albeit with much smaller amplitude.

28
29 Other areas where pattern scaling shows a lack of robustness are the edges of polar ice caps and sea ice
30 extent, where at an earlier time in the simulation ice melts and regions of sharp gradient surface, while later
31 in the simulation, in the absence of ice, the gradient will become less steep. Different models' ice
32 representations also make these regions' location much less robust across the model ensembles and the
33 scenarios.

34 35 12.4.2.2 CMIP5 Patterns

36
37 On the basis of CMIP5 simulations, we show geographical patterns (Figure 12.8) of warming and
38 precipitation change and indicate measures of their variability across models and across RCPs. The patterns
39 scaled to 1°C of warming above the reference period 1986–2005 for 2081–2100 (first row) and for the
40 commitment runs (thus excluding RCP8.5) at a time of stabilization, 2281–2300 (second row). Spatial
41 correlation of fields of temperature change is as high as [PLACEHOLDER FOR SECOND ORDER
42 DRAFT] in the model ensemble mean when considering different RCPs, and remain as high as 0.98 for
43 temperature and 0.90 for precipitation when comparing patterns at various times in the multi-century
44 simulations available under the RCPs (out to 2300). The zonal means shown to the side of each plot
45 represent each model by one line, colour coding the four different scenarios. They show good agreement of
46 models and scenarios over low and mid latitudes for temperature, but higher variability across models and
47 especially across scenarios for the areas subject to polar amplification, consistently with the previous
48 discussion of the role of the sea-ice edge. A comparison of the mean of the line to their spread indicates
49 overall the presence of a strong mean signal with respect to the spread of the ensemble. Precipitation shows
50 less structured variability of the ensemble across meridional zones, and suggests a lower signal-to-noise ratio
51 (measured as above). While we do not explicitly use pattern scaling in the sections that follow, it should be
52 borne in mind when trying to interpolate or extrapolate results to different scenarios or time periods, noting
53 the possibility that the scaling may break down at higher levels of global warming.

54
55 **[INSERT FIGURE 12.8 HERE]**

56 **Figure 12.8:** Temperature (left) and precipitation (right) change patterns derived from transient simulations from the
57 CMIP5 ensembles, scaled to 1°C of global average warming. The patterns have been calculated by computing 20-year

1 averages at the end of the 21st (top) and 22nd (bottom) Century and over the period 1986–2005 for the available
2 simulations under all RCPs, taking their difference (percentage difference in the case of precipitation) and normalizing
3 it, grid-point by grid-point, by the corresponding value of global average temperature change for each model and
4 scenario. The normalized patterns have then been averaged across models and scenarios. The colour scale represents °C
5 (in the case of temperature) and % (in the case of precipitation) per 1°C of global average warming and stippling
6 indicates the mean change averaged over all realisations is larger than the 95% percentile of the distribution. Zonal
7 means of the geographical patterns are shown for each individual model for RCP2.6 (blue), 4.5 (green), 6.0 (black) and
8 8.5 (red). RCP8.5 is excluded from the stabilisation figures.

11 **12.4.3 Changes in Temperature and Energy Budget**

12 **12.4.3.1 Patterns of Surface Warming**

13 Patterns of surface air temperature change for various RCPs show widespread warming during the 21st
14 century (Figure 12.9; see the Annex I Atlas for seasonal patterns). A key feature that has been present
15 throughout the history of coupled modelling is the larger warming over land compared to oceans, which
16 occurs in both transient and equilibrium climate change (e.g., Manabe et al., 1990). The degree to which
17 warming is larger over land than ocean is remarkably constant over time under transient warming (Lambert
18 and Chiang, 2007) and is predominantly a feature of the surface and lower atmosphere (Joshi et al., 2008).
19 Although heat capacity differences between land and ocean may seem intuitively relevant, studies have
20 found it occurs due to contrasts in surface Bowen ratio (Sutton et al., 2007) and boundary layer relative
21 humidity (Joshi et al., 2008) which are amplified by changes to cloudiness (Doutriaux-Boucher et al., 2009;
22 Fasullo, 2010), and due to soil moisture changes (Dong et al., 2009) under climate change. Globally
23 averaged warming over land and ocean is identified separately in Table 12.2 for the CMIP5 models, and the
24 ratio of land to ocean warming of $\sim 1.5 \pm 0.2$ is consistent with previous studies (Lambert et al., 2011). The
25 CMIP5 multimodel mean ratio is approximately constant from 2020 through to 2300 (based on an update of
26 Joshi et al., 2008 from available CMIP5 models).

27 **[INSERT FIGURE 12.9 HERE]**

28 **Figure 12.9:** 9-panel figure of multimodel ensemble average of surface air temperature change (compared to 1986–
29 2005 base period) for 2046–2065, 2081–2100, 2181–2200 for RCP 2.6, 4.5 and 8.5. Model agreement is assessed as in
30 (Tebaldi et al., 2011). Grid points are stippled where at least half of the models show significant change and >80% of
31 them agree on the sign, while white shading indicates at least half of the models show significant change but less than
32 80% of those agree on the sign.

33 Amplified surface warming in Arctic latitudes is also a consistent feature in climate model integrations (e.g.,
34 Manabe and Stouffer, 1980). This is often referred to as polar amplification, although as numerous studies
35 have shown in transient forcing integrations this is primarily an Arctic phenomenon (Manabe et al., 1991;
36 Meehl et al., 2007b). The lack of an amplified warming response in high Southern latitudes is attributed to
37 deep ocean mixing and heat uptake there. In equilibrium simulations, amplified warming occurs in both
38 polar regions.

39 On an annual average, the CMIP5 models currently available have a mean Arctic (70–90N) warming
40 approximately 2.7 times the global average warming for 2081–2100 compared to 1986–2005 (for the
41 RCP4.5 scenario). Similar polar amplification factors occur in the other RCPs and in earlier coupled model
42 simulations (e.g., Holland and Bitz, 2003; Winton, 2006b). This factor in models is a bit higher than the
43 observed central value, but is within the uncertainty of the best estimate from observations of the recent past
44 (Bekryaev et al., 2010). The uncertainty is large in the observed factor because station records are short and
45 sparse (ACIA, 2004). By contrast, model trends in surface air temperature are 2.5 to 5 times higher than
46 observed over Antarctica, but here also the observational estimates have a very large uncertainty, so, for
47 example, the CMIP3 ensemble mean is not inconsistent with observations (Monaghan et al., 2008).

48 The amplified Arctic warming in models has a distinct seasonal character (Holland and Bitz, 2003; Lu and
49 Cai, 2009; Manabe and Stouffer, 1980; Rind, 1987). The warming peaks in early winter (November–
50 December) with a CMIP5 multi-model mean warming of over 8K (over 4 times the global average
51 warming). The warming is a minimum in summer when excess heat goes to melting ice and warming the
52 surface ocean. Simulated Arctic warming also has a consistent vertical structure being surface based and
53

1 largest in the lower troposphere (e.g., Kay et al., 2011b; Manabe et al., 1991). This is in agreement with
2 recent observations (Screen and Simmonds, 2010; Serreze et al., 2009) but contrary to an earlier study which
3 suggested a larger warming aloft (Graversen et al., 2008). The discrepancy in observed vertical structure may
4 reflect inadequacies in datasets (Bitz and Fu, 2008; Grant et al., 2008; Thorne, 2008) and sensitivity to the
5 time period used for averaging.

6
7 There are many mechanisms that contribute to Arctic amplification, some of which were identified in early
8 modelling studies (Manabe and Stouffer, 1980). The surface albedo feedback associated primarily with
9 surface temperature driven albedo changes in sea ice and snow covered regions as well as the feedback
10 related to the insulation effect of sea ice amplify surface temperature change near the poles (Graversen and
11 Wang, 2009; Hall, 2004; Soden et al., 2008). The longwave radiation feedback associated with surface
12 temperature driven changes in the top of atmosphere longwave radiative loss to space opposes surface
13 warming at all latitudes, but less so in the Arctic (Soden et al., 2008; Winton, 2006b). Rising temperature
14 globally is expected to increase the latent heat transport by the atmosphere into the Arctic (Kug et al., 2010),
15 which warms primarily the lower troposphere. On average, CMIP3 models simulate enhanced latent heat
16 transport (Held and Soden, 2006), but north of about 65°N, the sensible heat transport declines enough to
17 more than offset the latent heat transport increase (Hwang et al., 2011). Ocean heat transport also plays a role
18 in the simulated Arctic amplification, with both large late 20th century transport (Mahlstein and Knutti,
19 2011a) and increases over the 21st century (Bitz et al., 2011) associated with higher amplification.
20 [PLACEHOLDER FOR SECOND ORDER DRAFT: Update these with CMIP5 analysis when possible] As
21 noted by Hwang et al. (2011) diagnosing the role of various factors in amplified warming is complicated by
22 coupling in the system in which local feedbacks interact with poleward heat transports.

23
24 While models consistently exhibit Arctic amplification in response to rising CO₂ concentrations, they differ
25 considerably on the magnitude. Previous work has implicated variations across climate models in numerous
26 factors including inversion strength (Boe et al., 2009a), ocean heat transport (Holland and Bitz, 2003;
27 Mahlstein and Knutti, 2011a), albedo feedback (Winton, 2006b), shortwave cloud feedback (Crook et al.,
28 2011; Kay et al., 2011b) as playing a role in the across-model scatter in polar amplification. In the CMIP5
29 models analyzed, amplification (defined as the 70–90N warming compared to the global average warming
30 for 2081–2100 versus 1986–2005) varies from 1.8 to 3.3 for the RCP4.5 scenario. Models with enhanced
31 warming amplification generally have less extensive late 20th century sea ice in June (Figure 12.10)
32 suggesting that the initial ice state influences the 21st century Arctic amplification. These models also tend
33 to simulate larger June ice loss (Figure 12.10).

34 [INSERT FIGURE 12.10 HERE]

35 **Figure 12.10:** Scatter diagram of initial June sea-ice extent versus polar amplification factor from the available CMIP5
36 models under RCP4.5.

37
38
39 Minimums in warming occur in the North Atlantic and Southern Oceans under transient forcing due to deep
40 ocean mixed layers and potential shifts in currents in those regions (Manabe et al., 1990; Xie et al., 2010).
41 Trenberth and Fasullo (2010) find that the large biases in the Southern Ocean energy budget in CMIP3
42 coupled models are negatively correlated with equilibrium climate sensitivity (see Section 12.5.3),
43 suggesting that an improved mean state in the Southern Ocean is needed before warming there can be
44 understood. In the equatorial Pacific, warming is enhanced in a narrow band which previous assessments
45 have described as ‘El Niño-like’, as may be expected from the projected decrease in atmospheric tropical
46 circulations (see Section 12.4.4). However, DiNezio et al. (2009) highlight that the tropical Pacific warming
47 in the CMIP3 models is not ‘El Niño-like’ as the pattern of warming and associated teleconnections is quite
48 distinct from that of an El Niño event. They attribute the enhanced equatorial warming to ocean dynamical
49 changes that can be decoupled from atmospheric changes. See also further discussion in Section 12.4.7.

50
51 These major features in warming are present in all pathways but with different magnitudes as discussed in
52 Section 12.4.2. Consistency over multiple generations of models indicates robust changes.

53 A further assessment of regional changes is presented in Table 12.2 and a number of figures are included in
54 the Atlas (Annex I). Warming continues and, except for RCP2.6, is enhanced beyond the 21st century with
55 similar patterns.

12.4.3.2 Zonal Temperature

Zonal temperature changes at the end of the 21st century in an ensemble of CMIP5 GCMs show warming throughout the troposphere and cooling in the stratosphere (Figure 12.11). The maximum in warming in the tropical upper troposphere is consistent with theoretical explanations and associated with a decline in the moist adiabatic lapse rate of temperature in the tropics as the climate warms (Bony et al., 2006). The northern polar regions also experience large warming due to the retreat of snow and ice. The patterns are similar to those in the TAR and AR4 with the RCP8.5 changes being similar in magnitude and distribution to the A1B changes in the AR4. Similar patterns appear for the RCP4.5 changes, but with reduced magnitudes, suggesting some degree of scaling with forcing change, similar to behaviour discussed in the AR4 and Section 12.4.2. This consistency over multiple generations of models indicates robust changes.

The RCP2.6 changes differ substantially from the RCP8.5 and 4.5 changes, not only in magnitude but also spatial distribution. The reduced magnitudes are understood as a consequence of reduced radiative forcing. The spatial distribution of change, however, departs substantially from those produced by RCP8.5 and 4.5. A warming maximum appears in the stratosphere over both poles, the lower stratosphere warms overall and only a weak maximum in warming occurs in the tropical upper troposphere. The multi-model polar stratospheric warming, especially in the southern hemisphere, appears to be similar to that found by Meehl et al. (2011) in CCSM4, who discuss the role of ozone recovery in determining the patterns (Baldwin et al., 2007; Son et al., 2010). Thus, the scaling of temperature changes seen in the AR4 for even the relatively weak “Commitment” scenario does not hold for the RCP2.6.

Away from the polar stratosphere, there is physical and pattern consistency in temperature changes between different generations of models. The consistency is especially clear in the tropical upper troposphere and the northern high latitudes and, coupled with physical understanding, indicates that the greatest warming is *very likely* to occur in these regions. However, there is remaining uncertainty about the magnitude of warming simulated in the tropical upper troposphere due to difficulties in assessing there the fidelity between models and observations (see Section 9.4.1.2 and 10.3.1.2.1).

[INSERT FIGURE 12.11 HERE]

Figure 12.11: CMIP5 multi-model changes in annual, zonal mean temperature relative to 1986–2005 for 2081–2100 under the RCP2.6 (left), RCP4.5 (centre) and RCP8.5 (right) forcing scenarios. Model agreement is assessed as in (Tebaldi et al., 2011). Grid points are stippled where at least half of the models show significant change and >80% of them agree on the sign, while white shading indicates at least half of the models show significant change but less than 80% of those agree on the sign.

12.4.3.3 Temperature Extremes

As the climate continues to warm, changes in several types of extremes in temperature are being observed (IPCC, 2012), and are *very likely* to continue in the future. Extremes occur on multiple time scales, from a single day or a few consecutive days (a heat spell or wave) to monthly and seasonal events and can be defined by indices e.g., percentage of days in a year when maximum temperature is above the 90th percentile of a present day distribution or by return periods or other measures. While changes in temperature extremes are a very robust signature of anthropogenic climate change, the magnitude of change and consensus among models varies with the characteristics of the event being considered (e.g., timescale, magnitude, duration and spatial extent) as well as the definition used to describe the extreme.

Since the AR4 many advances have been made in establishing global observed records of extremes (Alexander et al., 2006) against which models can be evaluated to give context to future projections (Alexander and Arblaster, 2009). Numerous regional assessments of future changes in extremes have also been performed and a comprehensive summary of these is given in IPCC Special Report on Extremes (IPCC, 2012). Here we summarise the key findings from IPCC (2012) and assess updates since then.

It is *virtually certain* that there will be more hot and less cold extremes as global temperature increases (Orlowsky and Seneviratne, 2011; Sillmann and Roeckner, 2008), increasing our confidence since the previous assessment (Meehl et al., 2007b). Figure 12.12 shows preliminary results from the CMIP5 multimodel experiments for seasonal changes in warm nights, cold days and warm days (based on an update of Tebaldi et al., 2006). A robust increase in warm temperature extremes and decrease in cold temperature

1 extremes is found at the end of the 21st Century, with the magnitude of the changes increasing with
2 increased anthropogenic forcing. Greatest percentile changes are found in the Tropics, with seasonal
3 differences between JJA and DJF due mostly to larger changes in the Northern Hemisphere extratropics.
4

5 It is *very likely* that, on average, there will be more record high than record cold temperatures in a warmer
6 average climate. For example, Meehl et al. (2009) found that the current ratio of 2 to 1 for record daily high
7 maxima to low minima over the United States was approximately 20 to 1 by the mid 21st century and 50 to 1
8 by late century in their model simulation. However, even at the end of the century there were still a few daily
9 record low minima, consistent with Kodra et al. (2011) who conclude that cold extremes will persist in a
10 warmer climate.

11
12 It is also *very likely* that heat waves will occur with a higher frequency and duration and these mainly follow
13 the increase in seasonal mean temperatures (Ballester et al., 2010a; Ballester et al., 2010b; Barnett et al.,
14 2006; Fischer and Schär, 2010). Changes in the magnitude of temperature extremes are also *very likely*
15 however these changes often differ from the mean temperature increase, as a result of changes in variability
16 and shape of the temperature distribution (Clark et al., 2006; Hegerl et al., 2004; Meehl and Tebaldi, 2004).
17 For example, summer temperature extremes over central and southern Europe are projected to warm
18 substantially more than the corresponding mean local temperatures as a result of enhanced temperature
19 variability at interannual to intraseasonal time scales (Clark et al., 2006; Fischer and Schär, 2009, 2010;
20 Fischer et al., 2007; Kjellstrom et al., 2007; Nikulin et al., 2011; Schar et al., 2004; Vidale et al., 2007).
21 Several recent studies have also argued that the probability of occurrence of the 2010 Russian heatwave
22 increases substantially (by a factor of 5 to 10 by the mid-century) along with increasing mean temperatures
23 and enhanced temperature variability (Barriopedro et al., 2011; Dole et al., 2011).
24

25 [INSERT FIGURE 12.12 HERE]

26 **Figure 12.12:** CMIP5 multimodel mean geographical changes in warm nights (the percentage of days when minimum
27 temperatures are above the 90th percentile) at the end of the 21st century (top row) and 20-year smoothed timeseries
28 (middle and bottom row) of globally averaged seasonal warm nights, cold days (the percentage of days when maximum
29 temperatures are below the 10th percentile) and warm days (the percentage of days when maximum temperatures are
30 above the 90th percentile) for RCP2.6, 4.5 and 8.5 based on available CMIP5 models. Shading in the timeseries
31 represents the ± 1 standard deviation across the individual models. Units are absolute values relative to the 1961–1990
32 base period.
33

34 Since the last assessment, an increased understanding of mechanisms and feedbacks leading to projected
35 changes in extremes has been gained. Climate models suggest that hot extremes are amplified by soil
36 moisture-temperature feedbacks (Diffenbaugh et al., 2007; Fischer and Schär, 2009; Lenderink et al., 2007;
37 Seneviratne et al., 2006; Vidale et al., 2007) in certain regions as the climate warms, consistent with previous
38 assessments. The largest increases in the magnitude of warm extremes are simulated over mid-latitude
39 continental areas, consistent with the drier conditions, and the associated reduction in evaporative cooling
40 from the land surface projected over these areas (Kharin et al., 2007). Winter cold extremes also warm more
41 than the local mean temperature over northern high latitudes (Orlowsky and Seneviratne, 2011) as a result of
42 reduced temperature variability related to declining snow cover (Fischer et al., 2011; Gregory and Mitchell,
43 1995; Kjellstrom et al., 2007). Changes in atmospheric circulation, induced by remote surface heating can
44 also modify the temperature distribution (Haarsma et al., 2009). Sillmann and Croci-Maspoli (2009) note
45 that cold winter extremes over Europe are driven by atmospheric blocking and changes to these blocking
46 patterns in the future results in a continued occurrence of cold winter extremes in that region even as global
47 temperatures increase.
48

49 Enhanced morbidity and mortality during heat waves relates not only to temperature but also humidity. Heat
50 stress, defined as the combined effect of temperature and humidity, is expected to increase along with
51 warming temperatures and far exceeds the local decrease in summer relative humidity due to soil drying
52 (Diffenbaugh et al., 2007; Fischer and Schär, 2010). Areas with abundant atmospheric moisture availability
53 and high present-day temperatures such as Mediterranean coastal regions are expected to experience the
54 greatest heat stress changes because the heat stress response scales with humidity and humidity becomes
55 increasingly important to heat stress at higher temperatures (Fischer and Schär, 2010; Sherwood and Huber,
56 2010; Willett and Sherwood, 2011).
57

Changes in rare temperature extremes can be assessed using extreme value theory based techniques (IPCC, 2012). Kharin et al. (2007), in an analysis of CMIP3 models, found large increases in the 20 year return values of the annual maximum and minimum daily averaged surface air temperatures (i.e., the size of an event that would be expected on average only once every 20 years, or with a 5% chance every year) with larger changes over land than ocean. Figure 12.13 displays the end of 21st century change in the magnitude of these rare events from the CMIP5 models in the RCP2.6, 4.5 and 8.5 scenarios. Comparison to the changes in mean temperature shown in figure 12.15 reveals that both high and low temperature rare events are projected to experience greater increases than the mean with the largest changes in the rare low temperatures at high latitudes. IPCC (2012) concluded from the CMIP3 models that it is *likely* that in most regions a 20 year maximum temperature event will become a one-in-two year event by the end of the 21st Century under A1B and A2 scenarios, except for some regions of the high latitudes of the Northern Hemisphere where it is *likely* to become a one-in-five year event. The SREX also notes that the limited number of detection and attribution studies suggest that the model changes may tend to be too large and these likelihood statements are somewhat less strongly stated than a direct interpretation of model output and its uncertainties. The CMIP5 models reinforce this assessment of large changes in frequency of rare events, particularly in the RCP8.5 scenario.

[INSERT FIGURE 12.13 HERE]

Figure 12.13: The CMIP5 multi-model median change in 20-yr return values of annual warm temperature extremes (left hand panels) and cold temperature extremes (right hand panels) as simulated by CMIP5 models in 2081–2100 relative to 1986–2005 in the RCP2.6 (top panels), RCP4.5 (middle panels), and RCP8.5 (bottom panels) experiments. Global averages of changes are indicated in the titles.

There is a high consensus amongst models in the sign of the future change in temperature extremes, with recent studies confirming this conclusion from the previous assessment (Meehl et al., 2007b; Orłowsky and Seneviratne, 2011; Tebaldi et al., 2006). However, the magnitude of the change remains uncertain due to scenario and model (both structural and parameter) uncertainty as well as internal variability. These uncertainties are much larger than corresponding uncertainties in the magnitude of mean temperature change (Barnett et al., 2006; Clark et al., 2006; Fischer and Schär, 2010; Fischer et al., 2011).

A summary of projected changes in temperature extremes is given in Table 12.3.

Table 12.3: [PLACEHOLDER FOR SECOND ORDER DRAFT: Long term changes in temperature extremes from (IPCC, 2012)]

Cold extremes	Warm extremes	Cold spells	Warm spells
<i>Virtually certain</i> decrease in number of unusually cold days and nights (as defined with 1961–1990 climate) on global scale	<i>Virtually certain</i> increase in number of unusually warm days and nights on global scale.	[No quantitative assessment in SREX but there are likely to be numerous studies on this topic in coming years.]	<i>Very likely</i> increase in length, frequency, and/or intensity of warm spells, including heatwaves over most land areas

12.4.3.4 Energy Budget

Anthropogenic or natural perturbations to the climate system produce radiative forcings that imbalance the global energy budget and affect the global mean temperature. The climate responds to a change in radiative forcing on multiple timescales and at longer timescales, the energy imbalance (i.e., the energy heating or cooling the Earth) is very close to the ocean heat uptake due to the much lower thermal inertia of the atmosphere and the continental surfaces (Knutti et al., 2008a; Murphy et al., 2009). The radiative response of the flux at TOA are generally analysed using the forcing-feedback framework and are presented in Chapter 9.

CMIP5 models simulate a small increase of the energy imbalance at the TOA over the 20th century (Figure 12.14a). The multimodel estimate of the current energy imbalance (1986–2005) is approximately -0.96 W m^{-2} ($-0.6, 1.3$) (preliminary estimate using available CMIP5 models), a value consistent with current estimates inferred from measurements of changes in ocean heat uptake: $0.9 \pm 0.3 \text{ W m}^{-2}$ (Lyman et al., 2010;

1 Stevens and Schwartz, 2011; see also Chapter 9 and Chapter 13). The future evolution of the imbalance is
2 very different depending on the scenario (Figure 12.14a): for RCP8.5 it continues to increase rapidly, much
3 less for RCP6.0, is almost constant for RCP4.5 and decreases for RCP2.6. This latter negative trend reveals
4 the quasi-stabilisation characteristic of RCP2.6.

5
6 The top of atmosphere (TOA) energy budget is the sum of the radiative forcings and of the climate response
7 and can be analysed separately in the shortwave (SW) and longwave (LW) domain. In the SW, the net flux at
8 TOA represents the SW flux that is absorbed by the Earth's atmosphere, ocean and land surface. The rapid
9 fluctuations that are simulated during the 20th century originate from volcanic eruptions that are prescribed
10 in the models (see Section 12.3.2). The volcanic aerosols reflect the solar radiation and thus decrease the
11 amount of SW radiation absorbed by the Earth (Figure 12.14c). The minimum of SW radiation absorbed by
12 the Earth during the period 1960–2000 is mainly due to two factors: a sequence of volcanic eruptions and an
13 increase of the reflecting aerosol burden due to human activities (see Chapter's 7 and 9). During the 21st
14 century, the absorbed SW radiation regularly increases for the RCP8.5 scenario, increases and progressively
15 stabilizes for the other scenarios, consistent with what has been previously obtained with CMIP3 models and
16 SRES scenarios (Trenberth and Fasullo, 2009). The two main contributions to the SW changes are the
17 change of clouds (see 12.4.3.5) and the change of the cryosphere (see Section 12.4.6) at high latitudes.
18 During this period, the amount of anthropogenic aerosols is constant or is reduced and aerosols have little
19 impact or contribution to increases in the amount of SW radiation that is absorbed. In the LW domain
20 (Figure 12.14b), the net flux at TOA represent the opposite of the flux that is emitted by the Earth's surface
21 and atmosphere toward space, i.e., a negative anomaly represents an increase of the emitted LW radiation.
22 The LW net flux depends mainly on two factors: the surface temperature and the magnitude of the
23 greenhouse effect of the atmosphere. The latter is driven mainly by the concentration of greenhouse gases,
24 the vertical temperature profile and the cloud properties. During the 20th century, the rapid fluctuations of
25 the LW radiation are the responses to the volcanic forcings: they decrease the absorbed SW radiation, which
26 decreases the surface temperature, which decreases the LW radiation emitted by the Earth toward space and
27 increases the net LW flux TOA. During the period 1960–2000, the fast increase of the greenhouse gas
28 concentrations also contributes to decrease the radiation emitted by the Earth. Then, in response to the net
29 heating of Earth, the temperature increases driving increases the emitted LW radiation. The change of the
30 temperature vertical profile, the water vapour and the cloud properties modulate this change in emitted LW
31 radiation (e.g., Bony et al., 2006; Randall et al., 2007).

32 [INSERT FIGURE 12.14 HERE]

33
34 **Figure 12.14:** Time evolution of the global mean (a) net total radiation anomaly at the TOA, (b) net longwave radiation
35 anomaly at the TOA and (c) net shortwave radiation anomaly at the TOA for the historical period and three RCP
36 scenarios from available models. All the fluxes are positive downward and units are $W m^{-2}$. The anomalies are
37 computed with respect to the 1900–1950 base period. [PLACEHOLDER FOR SECOND ORDER DRAFT: include
38 RCP6.0 and compute anomalies with respect to the control simulation].

39 [INSERT FIGURE 12.15 HERE]

40
41 **Figure 12.15:** CMIP multi-model changes in annual net radiation (R_T , left) net longwave radiation ($-OLR$, centre) and
42 absorbed solar radiation (ASR, bottom) at the TOA for the RCP4.5 scenario from available models. All fluxes are
43 positive downward, units are $W m^{-2}$ and $R_T = ASR - OLR$. The net radiation anomalies are computed with respect to the
44 1900–1950 base period. [PLACEHOLDER FOR SECOND ORDER DRAFT: the anomalies will be computed with
45 respect to the control simulation]

46
47 Since AR4, an increased attention has been given to the energetics of the climate system, and not only on the
48 flux at the top of the atmosphere (e.g., Andrews et al., 2009; Trenberth and Fasullo, 2010). An increased
49 number of models now consider a larger variety forcings, such as larger types of aerosols and varying
50 concentrations of ozone which impact the energy budget. The relationship between changes in the energy
51 budget and precipitation becomes more complicated and requires deeper analysis (see Section 12.4.5).

52 12.4.3.5 Clouds and Diurnal Temperature Range

53
54
55 Clouds are a major component of the climate system and play an important role in climate sensitivity (Cess
56 et al., 1990; Randall et al., 2007), the diurnal temperature range (DTR) over land (Zhou et al., 2009), and
57 land-sea contrast (see Section 12.4.3.1 and Chapter 7). The observed global mean cloud radiative forcing is
58 about $-20 W m^{-2}$ (Loeb et al., 2009), i.e., clouds have a net cooling effect. Current GCMs simulate clouds

1 through various complex parameterizations, and cloud feedback is a major source of the spread of the
2 climate sensitivity estimate (Dufresne and Bony, 2008; Randall et al., 2007; Soden and Held, 2006).

3
4 Under future projections the multimodel pattern of total cloud amount shows consistent decreases in the
5 subtropics, in conjunction with drying there, and increases at high latitudes. Another robust pattern is an
6 increase in cloud cover at all latitudes in the vicinity of the tropopause, and mostly decreases below (Meehl
7 et al., 2007b). Marine boundary layer clouds in subtropical regions were identified as a primary cause of
8 inter-model spread in cloud feedbacks in CMIP3 models (Bony and Dufresne, 2005; Webb et al., 2006;
9 Wyant et al., 2006). Since AR4, these results have been confirmed along with the positive feedbacks due to
10 high level clouds (Soden and Vecchi, 2011). The radiative effect of clouds mainly depends on their fraction,
11 optical depth and temperature. The contribution of these variables to the cloud feedback has been quantified
12 for the multi-model CMIP3 (Soden and Vecchi, 2011) and CFMIP1 database (Zelinka et al., 2011). These
13 findings may be summarized as follows and are consistent with the results with the CMIP5 models (Figure
14 12.16). The dominant contributor to the SW cloud feedback is the change in cloud fraction. The reduction of
15 cloud fraction between 50°S and 50°N, except along the equator (Figure 12.16), contributes to an increase in
16 the absorbed solar radiation (Figure 12.15c). Physical mechanisms and the role of different parametrizations
17 have been proposed to explain this reduction of low level clouds (Brient and Bony, 2011; Caldwell and
18 Bretherton, 2009; Zhang and Bretherton, 2008). Poleward of 50°, the cloud fraction and the cloud optical
19 depth increases, and therefore of the cloud reflectance. The signature is a decrease of the absorbed solar
20 radiation in a belt all around Antarctica, where there is no ice to reflect the solar radiation during summer
21 (Figure 12.15c). In the LW domain, the high cloud changes are the dominant effect. The rising of cloud
22 height is a robust results (Meehl et al., 2007b) that leads to a positive feedback with a dominant contribution
23 of tropical high clouds, that is clearly visible on the LW flux at the TOA (Figure 12.15b). Physical
24 explanations of this effect have been proposed (Hartmann and Larson, 2002; Lorenz and DeWeaver, 2007;
25 Zelinka and Hartmann, 2010). The decrease in cloudiness has the opposite effect on LW radiation and
26 reduces the effect of cloud rising, without cancelling it, as all CFMIP1 and CMIP3 models that have been
27 analysed show a positive global-mean LW cloud feedback and a global-mean SW cloud feedback that range
28 from slightly negative to strongly positive (Soden and Vecchi, 2011; Zelinka et al., 2011), the inter-model
29 spread being largely attributable to the low-level cloud feedbacks.

31 [INSERT FIGURE 12.16 HERE]

32 **Figure 12.16:** CMIP5 multi-model changes in annual total cloud amount relative to 1986–2005 for 2081–2100 under
33 the RCP2.6 (left), RCP4.5 (centre) and RCP8.5 (right) forcing scenarios. Model agreement is assessed as in (Tebaldi et
34 al., 2011). Grid points are stippled where at least half of the models show significant change and >80% of them agree
35 on the sign, while white shading indicates at least half of the models show significant change but less than 80% of those
36 agree on the sign.

37 12.4.4 Changes in Atmospheric Circulation

38
39 Projected changes in energy and water cycles couple with changes in atmospheric circulation and mass
40 distribution. Understanding this coupling is necessary to assess physical behaviour underlying projected
41 changes, revealing why changes occur and the realism of the changes.

42 12.4.4.1 Mean Sea Level Pressure and Upper-Air Winds

43
44 Sea level pressure gives an indication of surface changes in atmospheric circulation (Figure 12.17). As in
45 previous assessments, a robust feature of the pattern of change is a decrease in high latitudes and increases in
46 the mid latitudes, associated with poleward shifts in the mid latitude storm tracks (see Section 12.4.4.3) and
47 positive trends in the annular modes (e.g., Arblaster et al., 2011; Miller et al., 2006; Yin, 2005; see also
48 Chapter 14) as well as an expansion of the Hadley Cell (see Section 12.4.4.2). Large increases in seasonal
49 sea level pressure are also found in regions of sub-tropical drying such as the Mediterranean and northern
50 Africa in DJF and Australia in JJA. Tropical changes are less consistent across the models but in general
51 increases occur. This feature is not well understood although Gillett and Stott (2009) recently attributed
52 observed increases in tropical sea level pressure to anthropogenic forcing.

53 [INSERT FIGURE 12.17 HERE]

1 **Figure 12.17:** CMIP5 multimodel ensemble average of sea level pressure change (2081–2100 minus 1986–2005) for
2 RCP2.6, 4.5 and 8.5 for DJF and JJA seasons. Model agreement is assessed as in (Tebaldi et al., 2011). Grid points are
3 stippled where at least half of the models show significant change and >80% of those agree on the sign, while white
4 shading indicates at least half of the models show significant change but less than 80% of those agree on the sign.
5

6 Future changes in zonal mean zonal winds (Figure 12.18) are seen throughout the atmosphere with stronger
7 changes in higher RCPs. Large increases in winds are evident in the tropical upper stratosphere and a
8 poleward shift and intensification of the SH westerly jet stream is seen, associated with the increase in the
9 SH meridional temperature gradient. In the NH the response of the mid latitude jet stream is weaker and
10 complicated by the additional thermal forcing of polar amplification (Woollings, 2008).
11

12 The poleward shift and intensification of the SH mid latitude jet is seen to scale with the strength of GHG
13 forcing. While the poleward shift is extremely consistent across the models and *very likely* under increased
14 GHGs, the dynamical mechanisms by which the jet shifts poleward are still not completely understood and
15 have been explored in both simple and complex models (Butler et al., 2010; Chen et al., 2008; Lim and
16 Simmonds, 2009).
17

18 In austral summer the additional influence of stratospheric ozone recovery opposes changes due to
19 greenhouse gases, potentially leading to negligible or equatorward SH jet shifts in coming decades,
20 especially under lower GHGs. This has likely implications for southern high latitude climate (e.g.,
21 tropopause height, jet location, Hadley Cell extent, carbon uptake and sea-ice melt). Whether ozone or GHG
22 forcing dominates the summertime response varies widely across models and scenarios, with the multimodel
23 mean of the CCMVal-2 and CMIP3 (the subset that included ozone recovery) models suggesting a near-
24 cancellation of their impacts (Polvani et al., 2011; Son et al., 2010) but other studies indicating an
25 equatorward shift (McLandress et al., 2011; Perlwitz et al., 2008). Assessing these studies is complicated by
26 the different ozone forcing datasets used across them. In CMIP5 most models either include interactive
27 stratospheric chemistry or prescribed time varying ozone, for example from the AC&C/SPARC ozone
28 database (Cionni et al., 2011; see Table 12.1), in contrast to many models in CMIP3 which prescribed
29 constant ozone concentrations under future scenarios. Note that the evolution of ozone depleting substances
30 is similar to the SRES A1 scenario for all RCPs (Eyring et al., 2010b). [PLACEHOLDER FOR SECOND
31 ORDER DRAFT: update with CMIP5 once more models are available].
32

33 [INSERT FIGURE 12.18 HERE]

34 **Figure 12.18:** CMIP5 multimodel ensemble average of zonal wind change (2081–2100 minus 1986–2005) for RCP2.6,
35 4.5 and 8.5. Changes are shown for DJF and JJA. Black contours represent the multimodel mean average for the 1986–
36 2005 base period. Model agreement is assessed as in (Tebaldi et al., 2011). Grid points are stippled where at least half
37 of the models show significant change and >80% of them agree on the sign, while white shading indicates at least half
38 of the models show significant change but less than 80% of those agree on the sign. [PLACEHOLDER FOR SECOND
39 ORDER DRAFT: If chemistry-climate models show substantially different results from the standard CMIP5 models,
40 highlighting that in additional panels needs to be considered.]
41

42 12.4.4.2 Planetary-Scale Overturning Circulations

43
44 Large-scale atmospheric overturning circulations and their interaction with other atmospheric mechanisms
45 are significant in determining tropical climate and regional changes in response to enhanced radiative
46 forcing. There are indications of a weakening of tropical overturning of air as the climate warms (Chou and
47 Chen, 2010; Gastineau et al., 2008; Gastineau et al., 2009; Held and Soden, 2006; Vecchi and Soden, 2007).
48 Figure 12.19 shows an example of a weakening of the boreal winter (DJF) meridional overturning circulation
49 in a GCM experiment. In the SRESA1b scenario, AR4 models show a remarkable agreement in simulating a
50 weakening of the tropical atmospheric overturning circulation (Vecchi and Soden, 2007). Along the
51 ascending branches of tropical overturning cells, a reduction in convective mass flux from the boundary
52 layer to the free atmosphere is implied by the differential response to global warming of the boundary-layer
53 moisture content and surface evaporation. This weakening of vertical motion along the ascending regions of
54 both the tropical meridional and near-equatorial zonal cells is associated to the imbalance in the rate of
55 atmospheric moisture increase and that of global mean precipitation (Held and Soden, 2006). A reduction in
56 the compensating climatological subsidence along the downward branches of overturning circulations, where
57 the rate of increase of static stability exceeds radiative cooling, is implied.
58

1 The weakening of low-level convective mass flux along ascending regions of tropical overturning cells has
2 been ascribed to changes in the hydrologic cycle (Held and Soden, 2006; Vecchi and Soden, 2007).
3 Advection of dry air from subsidence regions towards the ascending branches of large-scale tropical
4 circulation has been suggested to be a feasible mechanism weakening ascent along the edges of convection
5 regions (Chou et al., 2009). Enhanced atmospheric stability associated with an increase in the vertical extent
6 of convection resulting from a deepening of the tropical troposphere in response to global warming has been
7 demonstrated to contribute to the slowdown of the overturning cells (Chou and Chen, 2010). An imbalance
8 between the increase in diabatic heating of the troposphere and static stability whereby the latter increase
9 more rapidly has also been thought to play a role in weakening tropical ascent (Lu et al., 2008).

10
11 **[INSERT FIGURE 12.19 HERE]**

12 **Figure 12.19:** [PLACEHOLDER FOR THE SECOND ORDER DRAFT: Boreal winter (DJF) and boreal summer
13 (JJA) zonal-mean stream function ($10^{10} \text{ kg s}^{-1}$) from CMIP3 model experiments. Contours show the model simulations
14 in an idealized 1%/year rise in CO_2 concentration. Shading displays the changes in the strength of the meridional
15 overturning circulation. The placeholder diagram is obtained from (Gastineau et al., 2008).]

16
17 The zonally asymmetric Walker Circulation is projected to weaken under global warming, more than the
18 Hadley circulation (Lu et al., 2007; Vecchi and Soden, 2007). Almost everywhere around the equatorial belt,
19 changes in the 500hPa pressure velocity oppose the climatological background motion, notably over the
20 maritime continent (Vecchi and Soden, 2007). Over the equatorial Pacific Ocean, where mid-tropospheric
21 ascent is projected to strengthen, changes in zonal SST hence sea-level pressure gradients induce low-level
22 westerly wind anomalies which act to weaken the low-level branch of the Pacific Walker circulation. These
23 projected changes in the tropical Pacific circulation, towards a more El-Niño-like state, are already occurring
24 (Zhang and Song, 2006).

25
26 Apart from changes in Hadley circulation strength, a robust feature in twenty-first century climate model
27 simulations is an increase in the cell's depth and width (Frierson et al., 2007; Lu et al., 2007; Lu et al., 2008;
28 Mitas and Clement, 2006), with the latter change translating to a broadening of tropical regions (Seidel and
29 Randel, 2007; Seidel et al., 2008) and a poleward displacement of subtropical dry zones (Lu et al., 2007).
30 The increase in the cell's depth is consistent with a tropical tropopause rise. The projected increase in the
31 height of the tropical tropopause and the associated increase in meridional temperature gradients close to the
32 tropopause slope have been proposed to be an important mechanism behind the Hadley cell expansion and
33 the poleward displacement of the subtropical westerly jet (Johanson and Fu, 2009; Lu et al., 2008). An
34 increase in subtropical and mid-latitude static stability has been found to be an important factor widening the
35 Hadley cell by shifting baroclinic eddy activity and the associated eddy-driven jet and subsidence poleward
36 (Lu et al., 2008; Mitas and Clement, 2006). As shown in Figure 12.20, the projected widening of the Hadley
37 cell, albeit weaker, is consistent with late twentieth century observations, where $\sim 2\text{--}5^\circ$ expansion was found
38 (Fu et al., 2006; Johanson and Fu, 2009; Seidel et al., 2008).

39
40 **[INSERT FIGURE 12.20 HERE]**

41 **Figure 12.20:** [PLACEHOLDER FOR THE SECOND ORDER DRAFT: Trends in Hadley cell width from
42 observations and GCM realizations under different GHG forcings. Trends show Hadley cell widening identified by a)
43 500hPa streamfunction (ψ_{500}) and b) outgoing long-wave radiation (OLR). In the models (observations), the boxes show
44 the 95% confidence interval (entire range) of the trends. The mean and median of each distribution are represented by
45 the circle and the horizontal bar, respectively. Figure from (Johanson and Fu, 2009)]

46
47 *12.4.4.3 Extratropical Storms: Tracks and Influences on Planetary-Scale Circulation and Transports*

48
49 Since the AR4, there has been further evaluation of changes in extratropical storm tracks under projected
50 global warming by CMIP3 models, as well as supporting studies using single models or idealized
51 simulations. These analyses generally confirm earlier studies, showing that extratropical storm tracks in both
52 hemispheres will tend to shift poleward (Bengtsson et al., 2009; Gastineau and Soden, 2009; Gastineau et al.,
53 2009; Perrie et al., 2010; Schuenemann and Cassano, 2010). Similar behaviour appears in CMIP3
54 simulations for the Southern Hemisphere (Figure 12.21). In Southern Hemisphere winter there is a clear
55 poleward shift in storm tracks of several degrees and a small overall reduction in the frequency of storms.
56 The poleward shift at the end of the century is consistent with a poleward shift in the Southern Hemisphere
57 of the latitudes with strongest atmospheric baroclinic zones (Figure 12.11) and tropospheric jets (Figure
58 12.18). The consistency of behaviour between CMIP5 and CMIP3 projections and the physical consistency

1 of the storm response with other climatic changes indicates that a poleward shift in Southern Hemisphere
2 storm tracks is *very likely*. In the Northern Hemisphere winter, the CMIP5 multi-model ensemble shows an
3 overall reduced frequency of storms and less indication of a poleward shift in the tracks, except possibly over
4 East Asia. Changes over the North Atlantic, in particular, may be tied to how the models simulate changes
5 there in the meridional overturning circulation (Catto et al., 2011; Woollings, 2008). The reduction in
6 frequency may be consistent with weaker baroclinicity of the projected climate (e.g., Figure 12.11). A
7 reduction in the occurrence of Northern Hemisphere extratropical storms is *likely*, based on the consistency
8 with previous projections.

9 10 **[INSERT FIGURE 12.21 HERE]**

11 **Figure 12.21:** Change in winter, extratropical storm track density for (2081–2100) – Historical Control (1986–2005)
12 for CMIP5 multi-model ensembles: (a) RCP 4.5 Northern Hemisphere DJF and (b) RCP 8.5 Northern Hemisphere DJF
13 (c) RCP 4.5 Southern Hemisphere JJA and (d) RCP 8.5 Northern Hemisphere JJA. Storm-track computation uses the
14 method of Bengtsson et al. (2006, their Figure 13a) applied to 850 hPa vorticity. Densities have units (number
15 density/month/unit area), where the unit area is equivalent to a 5° spherical cap ($\sim 10^6$ km²).

16
17 Additional analyses of CMIP3 GCMs have determined other changes in properties of extratropical storms.
18 Most analyses find that the frequency of storms decreases in projected climates (Favre and Gershunov, 2009;
19 Finnis et al., 2007), though the occurrence of strong storms tends to increase (Albrecht et al., 2009; Ulbrich
20 et al., 2009; Ulbrich et al., 2008). However, Della-Marta and Pinto (2009) find that strong North Atlantic
21 storms have unchanged return periods by the end of 21st century for both A1B and A2 scenarios, though
22 strong storms in the British Isles and North Sea do show shortened return periods. This behaviour is
23 consistent with analysis reported in the AR4. The strengthening of the strongest storms is consistent with the
24 presence of more thermal energy in the warmer climate system, though such consideration by itself does not
25 account for dynamical processes governing the size of storms (Kidston et al., 2010) and their genesis and
26 growth, all of which influence the structure and evolution of storms. Estimated future changes in wind
27 damage also indicate changes in extratropical storm frequency, location and intensity, especially for the
28 strongest storms. These analyses have tended to focus on Europe. A consistent outcome of several European
29 analyses (Debernard and Roed, 2008; Donat et al., 2010; Leckebusch et al., 2008; Pinto et al., 2007) is an
30 increase in damaging winds, an outcome of increased intensity for at least the strongest storms. Overall, the
31 simulation results and larger amount of thermal energy in the future climate indicate a *likely* increase in the
32 strength of the most intense extratropical storms.

33
34 Changes in extratropical storms in turn influence other large-scale climatic changes. Kug et al. (2010) show
35 that the poleward shift of storm tracks enhances polar warming and moistening. The Arctic Oscillation is
36 sensitive to synoptic eddy vorticity flux, so that projected changes in storm tracks can alter the Arctic
37 Oscillation (Choi et al., 2010). The net result is that changes in extratropical storms alter the climate in which
38 they are embedded, so that links between surface warming, extratropical storms and their influence on
39 climate are more complex than simple responses to changes in baroclinicity (e.g., O’Gorman, 2010).
40 Conclusive results on projected changes await further analysis.

41 42 **12.4.5 Changes in the Water Cycle**

43
44 The water cycle consists of water stored on the Earth in all its phases, along with the movement of water
45 through the Earth’s climate system. In the atmosphere, water occurs primarily as a gas, water vapor, but it
46 also occurs as solid ice and liquid water in clouds. The ocean is primarily liquid water, but is partly covered
47 by ice in polar regions. Terrestrial water in liquid form appears as surface water (lakes, rivers), soil moisture
48 and groundwater. Solid terrestrial water occurs in ice sheets, glaciers, frozen lakes, snow and ice on the
49 surface and permafrost. Projections of future changes in the water cycle are inextricably connected to
50 changes in the energy cycle (Section 12.4.3) and atmospheric circulation (Section 12.4.4).

51
52 Warmer air can contain more water vapor, but projected future changes in the water cycle are far more
53 complex than projected temperature changes. Some regions of the world will be subject to decreases in
54 hydrologic activity while others will be subject to increases. There are important local seasonal differences
55 among the responses of the water cycle to climate change as well.

56
57 At first sight, the CMIP3/5 models may appear to be inconsistent amongst each other, particularly at regional
58 scales. Anthropogenic changes to the water cycle are superimposed on complex naturally varying modes of

1 the climate (such as ENSO, AO, PDO, etc.) aggravating the differences between model projections.
2 However, by careful consideration of the interaction of the water cycle with changes in other aspects of the
3 climate system, the mechanisms of change are revealed, increasing confidence in projections.
4

5 12.4.5.1 Atmospheric Humidity

6

7 Atmospheric water vapour is the primary greenhouse gas in the atmosphere. Its changes affect all parts of the
8 water cycle. However, the amount of water vapour is controlled by naturally occurring processes rather than
9 directly through water vapour emissions from human activities. A common experience from past modelling
10 studies is that relative humidity (RH) remains approximately constant on climatological time scales and
11 planetary space scales, implying a strong constraint by the Clausius-Clapeyron relationship on how specific
12 humidity will change. However, underlying this fairly straight-forward behaviour are changes in RH that can
13 influence changes in cloud cover and atmospheric convection (Sherwood, 2010). Analysis of CMIP3 GCMs
14 under the A1B scenarios shows near-surface RH decreasing over most land areas with notable exceptions of
15 tropical Africa and polar regions (O’Gorman and Muller, 2010). A prominent contributor to changes in RH is
16 the land-ocean difference in temperature change during a warming scenario (Fasullo, 2010; Joshi et al.,
17 2008; O’Gorman and Muller, 2010), which controls RH over land by a last-saturation-temperature constraint.
18 Moisture originating over more slowly warming oceans will have its specific humidity level governed by
19 saturation temperatures of oceanic air (Sherwood et al., 2010). As this air moves over land and is warmed, its
20 relative humidity drops as any further moistening of the air over land is insufficient to maintain constant RH.
21 The differential warming of land and ocean can promote changes in atmospheric circulation and moisture
22 transports. An ensemble of five CMIP5 models (Figure 12.22) shows similar behaviour over land, although,
23 in contrast to the CMIP3 models, tropical Africa and the polar regions also show large areas of reduced RH.
24 Land-ocean differences in warming are projected to continue through the twenty-first century, and the
25 CMIP5 projections are consistent with a last-saturation constraint, indicating that reductions in near-surface
26 RH over most land areas is *likely*.
27

28 [INSERT FIGURE 12.22 HERE]

29 **Figure 12.22:** Changes in near-surface relative humidity under RCP 8.5 for the seasons DJF (left) and JJA (right)
30 relative to 1986–2005 for the periods 2046–2065 (top row), 2081–2100 (middle row) and 2181–2200 (bottom row).
31 Model agreement is assessed as in (Tebaldi et al., 2011). Grid points are stippled where at least half of the models show
32 significant change and >80% of them agree on the sign, while white shading indicates at least half of the models show
33 significant change but less than 80% of those agree on the sign.
34

35 12.4.5.2 Mean Precipitation

36

37 Global average precipitation is projected both by models and theoretical considerations to increase steadily
38 with temperature. The CMIP3 multi-model ensemble indicates about a 1–3% increase in global precipitation
39 and a 7.5% increase in atmospheric water vapor per °C global warming (Vecchi and Soden, 2007).
40

41 As seen in Section 12.4.5.1, water vapor increases are primarily a consequence of the Clausius-Clapeyron
42 relationship associated with increasing temperatures in the lower troposphere (where most atmospheric water
43 vapor resides) which has been observed to warm slightly less than the surface temperatures (CCSP_1.1,
44 2006; Pierrehumbert et al., 2007). In contrast, future precipitation increases are primarily the result of
45 changes in the energy balance of the atmosphere (Allen and Ingram, 2002; Boer, 1993; Held and Soden,
46 2006; Mitchell, 1983). The radiative budget of the atmosphere is balanced by latent heating (coming from
47 precipitation) and sensible heating. Relatively small changes in radiative fluxes are *likely* to cause substantial
48 changes to the global circulation (see Section 12.4.4.2) and water cycle. Since AR4, these changes have been
49 analyzed in detail for a large variety of forcings, simulations and models (Andrews et al., 2010; Bala et al.,
50 2010; Ming et al., 2010; Takahashi, 2009a). Precipitation changes may be decomposed as the sum of a fast
51 and a slow response. On short time scales, greenhouse gas forcing changes modify the radiative budget
52 causing a negative response in global precipitation for positive forcing (Andrews et al., 2010; Bala et al.,
53 2010). The inferred hydrological adjustment for zero warming under an instantaneous 4xCO₂ forcing
54 perturbation is in the range –0.18 to –0.11 mm day⁻¹ (or –7 to –4%) for CMIP5 models and is shown in
55 Figure 12.23. On longer time scales, resulting warmer temperatures and increased atmospheric water vapor
56 content causes changes in the radiative energy budget inducing a slow positive response in global
57 precipitation (Allen and Ingram, 2002; Held and Soden, 2006). For CO₂ forcing, the ratio between the
58 relative change of precipitation (dP/P) and the temperature change (dT) is in the range $dP/P/dT = 2\text{--}3\% \text{ K}^{-1}$

(Allen and Ingram, 2002; Held and Soden, 2006). The inter-model spread may be due to differences in modelled shortwave absorption by water vapor (Takahashi, 2009b). An increase of absorbing aerosols induces similar fast and slow responses in precipitation, but with a smaller impact on the global mean temperature than greenhouse gases and hence a smaller impact on the slow response of global precipitation (Andrews et al., 2010; Ming et al., 2010). Overall, the global-mean precipitation change may be estimated from a simple relationship between the global-mean temperature change, the tropospheric greenhouse gas forcing and the black carbon emissions (Frieler et al., 2011a) and its rate of increase per °C global warming is *very likely* to be less than that of atmospheric water vapor.

[INSERT FIGURE 12.23 HERE]

Figure 12.23: Global mean annual mean precipitation (mm/day) versus temperature changes for CMIP5 instantaneous 4 x CO₂ step experiments relative to the mean of their control simulations. Ordinary least squares regression linear fits of global mean precipitation against global mean temperature changes over the first 150 years of the 4 x CO₂ experiments, computed relative to the mean of the control experiment over the corresponding 150 years, are plotted. The fitted intercept at zero temperature change (F) and slope (Y) are also listed for each model.

Figure 12.24 shows the ratio between projected future relative changes in precipitation (%) and global mean temperature (°C) for 2079 to 2098 relative to 1986 to 2005 for CMIP5 model projections for the four RCPs. These projections exhibit a multi-model mean global-mean ratio varying from 2.4% °C⁻¹ for RCP2.6 to around 1.7% °C⁻¹ for RCP6.0 and RCP8.5, but a much larger range for individual models. The multi-model mean range across RCP projections is similar to that for AR4 SRES projections, and the RCP2.6 multi-model mean value is very close to that of the ENSEMBLES multi-model projections for the E1 scenario (Johns et al., 2011). The relatively high ratios exhibited by RCP2.6 and E1 projections (in which greenhouse gas radiative forcing peaks and then slowly declines) mirror the AR4 constant composition commitment experiment (2.3% °C⁻¹). As temperature approaches stabilisation in RCP2.6 projections the gradient of precipitation versus global temperature change steepens (Figure 12.24), in response to the perturbed radiative energy budget from the decline in greenhouse gas and aerosol forcings after the mid-century peak (Figure 12.3).

[INSERT FIGURE 12.24 HERE]

Figure 12.24: Percentage changes per °C of global warming in global, land and sea precipitation for CMIP5 model projections for the four RCPs in the period 2079 to 2098 relative to 1986 to 2005. Land and sea values use global mean temperature in the denominator. Each coloured symbol represents the ensemble mean for a single model. The black squares are multi-model means.

A general slowing down of the global circulation of the atmosphere (see Section 12.4.4.2) and an enhancement of the patterns of evaporation minus precipitation are robust features across the CMIP3 models in a warmer world (Held and Soden, 2006). It is *likely* that many arid and semi-arid regions will experience less precipitation and that many moist regions will experience more. However, verification of the muted response in global precipitation relative to water vapor as described by the physical mechanism detailed above and projected by all CMIP3 models the relatively short satellite observational record is mixed (Wentz et al., 2007). Due to the intermittent and highly variable nature of precipitation in most parts of the world, changes to average regional precipitation may not be easily discernible either in the recent past (see Chapter 10) or in the near future. Nonetheless, it is *virtually certain* that average precipitation in a much warmer world will be a mix of regions of increases, decreases or even regions of not much change at all.

The CMIP3 multi-model ensemble precipitation projections must be interpreted in this context of uncertainty. Multi-model projections are not probabilistic statements about the likelihood of changes. Maps of multi-model projected changes are smoothly varying but observed changes are and will continue to be much more granular. Projected precipitation changes vary greatly between models, much more so than for temperature projections. Part of this variance is due to genuine differences between the models. However, a large part of it is also the result of the small ensemble size from each model. This is especially true for regions of small projected change situated between two other regions, one experiencing significant increases while the other experiences significant decreases. Individual climate model realizations may differ in their projection of future precipitation changes in these regions due simply to their internal variability. Multi-model projections containing large numbers of realizations would tend to average to small changes in these regions. However, due to a limited number of available realizations this may not always be the case. As a

1 result, confidence in projections in regions of limited or no change in precipitation may be more difficult to
2 obtain than confidence in regions of large projected changes.

3
4 Storms in many regions of the Earth exhibit strong seasonal characteristics. Combining projections into an
5 annual quantity can hide regions where confidence may be high for particular seasons by mixing different
6 mechanisms of change. Figure 12.25 shows preliminary CMIP5 multi-model mean projections for percent
7 changes in seasonal average precipitation the RCP8.5 future scenario at the middle of the 21st century, the
8 end of the 21st century and the end of the 22nd century. Patterns of projected change are similar between the
9 SRES scenarios discussed in the AR4 and the RCP scenarios although the magnitudes and timing of changes
10 can substantially differ. For instance, the high latitudes are *very likely* to experience greater amounts of
11 precipitation due to the additional water carrying capacity of the warmer troposphere. The largest changes
12 over northern Eurasia and North America are projected to occur during the winter and are *likely* manifested
13 as increases in snowfall. Projected weakening and poleward expansion of the Hadley circulation (Gastineau
14 et al., 2009; Lu et al., 2007; Vecchi and Soden, 2007) evokes a strong tropical response. Compounded by an
15 associated projected weakening of the Walker circulation, these changes tend to decrease precipitation rates.
16 The net effect of a weakened atmospheric circulation and an increase in specific humidity is an increase in
17 the tropical precipitation together with a simultaneous suppression in the subtropics (Chou et al., 2009). The
18 predominant pattern of tropical and subtropical precipitation change detailed in the AR4 is reinforced in the
19 CMIP5 models; areas that are currently wet become wetter, areas that are currently dry become dryer. These
20 patterns become more evident as global climate change increases. As the overall climate warms, these
21 projected changes in precipitation exhibit the pattern scaling described in Section 12.4.2.

22 23 [INSERT FIGURE 12.25 HERE]

24 **Figure 12.25:** Multi-model CMIP5 average percent change in seasonal mean precipitation averaged over the periods
25 2045–2065, 2081–2100 and 2181–2200 under the RCP8.5 forcing scenarios. Model agreement is assessed as in
26 (Tebaldi et al., 2011). Grid points are stippled where at least half of the models show significant change and >80% of
27 them agree on the sign, while white shading indicates at least half of the models show significant change but less than
28 80% of those agree on the sign.

29 30 12.4.5.3 Soil Moisture

31
32 Near-surface soil moisture is the net result of a suite of complex processes (e.g., evapotranspiration,
33 drainage, overland flow, infiltration), uncertain inputs (e.g., precipitation), and heterogeneous and difficult-
34 to-characterize aboveground and belowground system properties (e.g., slope, soil texture). As a result,
35 regional to global-scale simulations of soil moisture and drought remain relatively uncertain (Burke and
36 Brown, 2008; Henderson-Sellers et al., 2008). The AR4 (Section 8.2.3.2) discussed the lack of assessments
37 of global-scale models in their ability to simulate soil moisture, and this problem appears to have persisted.
38 However, Koster et al. (2009a) argued that once climatological statistics affecting soil moisture were
39 accounted for, different models tend to agree on the temporal variability of soil moisture predictions. The
40 AR4 (Meehl et al., 2007b) summarized consistent (i.e., across models) projected 21st century annual mean
41 soil moisture changes as decreasing in the subtropics and Mediterranean region, and increasing in east Africa
42 and central Asia. An ensemble of six CMIP5 GCMs shows the same features in projected climates (Figure
43 12.26). The patterns are consistent across the RCPs, with the changes tending to become stronger as the
44 strength of the forcing change increases. Among individual ensemble members (not shown), the regions of
45 largest change show consistency across the ensemble for drying in the Mediterranean region, northeast South
46 America, southern Africa, and southwestern U.S. and moistening in tropical east Africa and the Indian
47 subcontinent. However, ensemble members do not show large regions of agreement on the sign of the
48 change in central Asia. The Mediterranean, southwestern U.S. and South African drying regions are
49 consistent with projected changes in Hadley circulation that inhibit precipitation in these regions and have
50 continued to appear across generations of projections, so drying in the Mediterranean and southwest U.S. is
51 *likely*.

52
53 More recent assessments include multi-model ensemble approaches, dynamical downscaling, and regional
54 climate models applied around the globe. Kolomyts and Surova (2010), using GISS and HadCM2 A2
55 projections, show that vegetation type has substantial influence on the development of pronounced drying
56 over the 21st century in Middle Volga Region forests. Analyses of the southwestern U.S. using CMIP3
57 models (Christensen and Lettenmaier, 2007; Seager et al., 2007) show consistent projections of drying,
58 primarily due to a decrease in winter precipitation. In contrast, Kellomaki et al. (2010) find A2 projections

1 for Finland yield decreased snow depth, but soil moisture generally increasing, consistent with the general
2 increase in precipitation occurring in high northern latitudes.

3
4 Changes often show substantial seasonal variation. For the Cline River watershed in western Canada,
5 Kienzle et al. (2011) find annual soil moisture increases 2.6% by the 2080s, but summer decreases. Sato et
6 al. (2007), using dynamical downscaling, find summer soil moisture decreases in Mongolia of up to 6% due
7 to increased potential evaporation in a warming climate and decreased precipitation and decreased
8 precipitation.

9
10 Soil moisture projections in high latitude permafrost regions are critically important for assessing future
11 climate feedbacks from trace-gas emissions (Riley et al., 2011; Zhuang et al., 2004) and vegetation changes
12 (Chapin et al., 2005). In addition to changes in precipitation, snow cover and evapotranspiration, future
13 changes in high latitude soil moisture also will depend on permafrost degradation, thermokarst evolution,
14 rapid changes in drainage (Smith et al., 2005), and changes in plant communities and their water demands.
15 Current understanding of these interacting processes at scales relevant to climate is poor, so that full
16 incorporation in current GCMs is lacking.

17 [INSERT FIGURE 12.26 HERE]

18
19 **Figure 12.26:** Percent change in annual soil moisture projected for 2081–2100 from a six-member CMIP5 ensemble for
20 (a) RCP 2.6, (b) RCP 4.5, and (c) RCP 8.5. Model agreement is assessed as in (Tebaldi et al., 2011). Grid points are
21 stippled where at least half of the models show significant change and >80% of them agree on the sign, while white
22 shading indicates at least half of the models show significant change but less than 80% of those agree on the sign.

23 12.4.5.4 Runoff and Evaporation

24
25
26 In the AR4 (Meehl et al., 2007b), 21st century runoff projections consistently (across models) decreased in
27 southern Europe, the Middle East, and southwestern U.S. and increased in Southeast Asia, tropical East
28 Africa, and at high northern latitudes. The largest changes by the end of the century reach 20% or more of
29 the simulated 1980 to 1999 values. The resulting discharges from high latitude rivers increased, while those
30 from major rivers in the Middle East, Europe, and southwestern U.S. tended to decrease. The same general
31 features appear in the ensemble change of CMIP5 GCMs (Figure 12.27) The features appear in late twenty-
32 first century changes for all three RCPs shown, with the areas of most intense change (>40%) typically
33 increasing with magnitude of forcing change. The large decreases in runoff in southern Europe and the
34 southwestern U.S. are consistent with increases in the intensity of the Hadley circulation and related
35 precipitation decreases and warming-induced evapotranspiration increases. The high northern latitude
36 increases are consistent with the greater precipitation possible in a warmer climate with more atmospheric
37 moisture. The consistency of changes across different generations of models and different forcing scenarios,
38 together with the physical consistency of change indicates that decreases are *likely* in runoff in southern
39 Europe, the Middle East, and southwestern U.S. The models project consistent increases in high latitude
40 runoff but confidence in this projection is tempered by large biases in their current snow cover.

41 [INSERT FIGURE 12.27 HERE]

42
43 **Figure 12.27:** Percent change in annual runoff projected for 2081–2100 from a six-member CMIP5 ensemble for (a)
44 RCP 2.6, (b) RCP 4.5, and (c) RCP 8.5. Model agreement is assessed as in (Tebaldi et al., 2011). Grid points are
45 stippled where at least half of the models show significant change and >80% of them agree on the sign, while white
46 shading indicates at least half of the models show significant change but less than 80% of those agree on the sign.

47
48 Annual surface evaporation in the AR4 increased over most of the ocean and increased or decreased over
49 land with largely the same pattern as increases and decreases in precipitation (Meehl et al., 2007b). Similar
50 behaviour occurs in an ensemble of CMIP5 models (Figure 12.28). Evaporation increases over most of the
51 ocean and land, with prominent areas of decrease over land occurring in the southwestern U.S./northwestern
52 Mexico, southern Africa and land bordering the Mediterranean. The areas of decrease correspond to areas
53 with reduced precipitation. The consistency of this change across different generations of models and
54 different forcing scenarios along with the physical basis for the precipitation decrease indicates that these
55 decreases in annual evaporation are *likely*. Annual evaporation increases over land in the northern high
56 latitudes are consistent with the increase in precipitation and the overall warming that would increase
57 potential evaporation. For the northern high latitudes, the physical consistency and the similar behaviour
58 across multiple generations and forcing scenarios indicates that annual evaporation increases there are *likely*.

1
2 A number of reports since the AR4 have updated findings from CMIP3 models and analyzed a large set of
3 mechanisms affecting runoff. Several studies have focused on the Colorado River basin in the United States
4 (Barnett and Pierce, 2008; Barnett et al., 2008; Christensen and Lettenmaier, 2007; McCabe and Wolock,
5 2007) showing that runoff reductions under global warming occur through a combination of
6 evapotranspiration increases and precipitation decreases, with the overall reduction in river flow exacerbated
7 by human water demands on the basin's supply.

8
9 CMIP3 analyses also showed seasonal shifts. Kienzle et al. (2011) studied climate change scenarios over the
10 Cline River watershed and projected (1) spring runoff and peak streamflow up to four weeks earlier than in
11 1961–1990; (2) significantly higher streamflow between October and June; and (3) lower streamflow
12 between July and September.

13
14 Evapotranspiration changes partly reflect changes in precipitation. However, some changes might come from
15 altered biological processes. For example, increased atmospheric CO₂ promotes stomatal closure and
16 reduced evapotranspiration (Betts et al., 2007; Cruz et al., 2010) which potentially can yield increased
17 runoff. There is potential for substantial feedback between vegetation changes and regional water cycles,
18 though the impact of such feedback remains uncertain at this point due to uncertainties plant response,
19 ecosystem shifts, and land management changes.

20 21 **[INSERT FIGURE 12.28 HERE]**

22 **Figure 12.28:** Percent change in annual evaporation projected for 2081–2100 from a multi-member CMIP5 ensemble
23 for (a) RCP 2.6, (b) RCP 4.5, and (c) RCP 8.5. Model agreement is assessed as in (Tebaldi et al., 2011). Grid points are
24 stippled where at least half of the models show significant change and >80% of them agree on the sign, while white
25 shading indicates at least half of the models show significant change but less than 80% of those agree on the sign.

26 27 *12.4.5.5 Extreme Events in the Water Cycle*

28
29 In addition to the changes in the seasonal pattern of mean precipitation described above, the distribution of
30 precipitation events is projected to *very likely* undergo profound changes (Boberg et al., 2010; Gutowski et
31 al., 2007; Sun et al., 2007). On short time scales, a shift to more intense individual storms and fewer weak
32 storms is projected (IPCC, 2012). On longer time scales, increased evapotranspiration over land can lead to
33 more frequent and more intense periods of agricultural drought.

34
35 A general relationship between changes in total precipitation and extreme precipitation does not exist (IPCC,
36 2012). Two possible mechanisms controlling short term extreme precipitation amounts are discussed at
37 length in the literature. The first consider that extreme precipitation events occur when most of the available
38 atmospheric water vapor rapidly precipitates out in a single storm. If the maximum amount of water vapor
39 air can control is controlled by the Clausius-Clapeyron relationship, as air temperature increases, this amount
40 of water also increases (Allan and Soden, 2008; Allen and Ingram, 2002; Kendon et al., 2010; Pall et al.,
41 2007). A second mechanism for extreme precipitation put forth by O’Gorman and Schneider (2009a, 2009b)
42 is that such events are controlled by anomalous horizontal moisture flux convergence and associated
43 convective updrafts which would change in a more complicated fashion in a warmer world (Sugiyama et al.,
44 2010). Li et al (2011b) found that both mechanisms contribute to extreme precipitation in a high-resolution
45 aquaplanet model with updrafts as the controlling element in the tropics and air temperature controlling the
46 mid latitudes. Additionally, Lenderink and Van Meijgaard (2008) found that very short extreme precipitation
47 events increase at a rate twice the amount predicted by Clausius-Clapeyron scaling in a very high-resolution
48 model over Europe suggesting that both mechanisms can interact jointly. However, Gastineau and Soden
49 (2009) found in the CMIP3 models that the updrafts associated with the most extreme tropical precipitation
50 events actually weaken despite an increase in the frequency of the heaviest rain rates further complicating
51 simple mechanistic explanations. Projections of future extreme precipitation often tend to be more robust at
52 the regional scales than for future mean precipitation. However, mechanisms of natural variability still are a
53 large factor in assessing the robustness of these projections (Kendon et al., 2008). In addition, the
54 mechanisms implicitly assume that circulation characteristics, such as storm tracks, will not change
55 substantially in a future climate. This assumption may be true for some regions and seasons (Gutowski et al.,
56 2008), but its generality remains to be analyzed.

1 What is considered extreme precipitation in one season at a particular place could be normal during a
2 different season or in a different location. The term “extreme” depends very much on context and is often
3 used in discussion of particular climate-related impacts. Commonly used indices to address precipitation
4 extremes summarize daily measurements into annual or seasonal quantities, like SDII, the simple daily
5 intensity index, R95p, the annual total precipitation falling in wet days with amounts larger than the 95th
6 quantile of the climatology, R5d, the annual maximum total precipitation in a pentad and CDD, the longest
7 spell of consecutive dry days in the year. The definition of these indices aims for statistical robustness,
8 applicability to a wide range of climates and a high signal-to-noise ratio together with a longer decorrelation
9 scale in the spatial domain when compared to daily extremes definitions (Alexander et al., 2006).

10 Consistently, climate models project future episodes of more intense precipitation in the wet seasons for
11 most of the land areas, especially in the Northern Hemisphere and its higher latitudes, and the monsoon
12 regions of the world, and at a global average scale. It is the case that the actual magnitude of the change is
13 dependent on the model used, but there is strong agreement across the models over the direction of change
14 (Chen and Knutson, 2008; Goubanova and Li, 2007; Haugen and Iversen, 2008; Kamiguchi et al., 2006;
15 Kysely and Beranova, 2009; May, 2008b; Tebaldi et al., 2006). Regional details are less robust in terms of
16 the relative magnitude of changes but remain in good accord across models in terms of the sign of the change
17 and the large scale geographical patterns (CCSP_3.3, 2008; Meehl et al., 2005a). In semi-arid regions of the
18 mid latitudes and subtropics like the Mediterranean, the southwest US, south-western Australia, southern
19 Africa and a large portion of South America, the tendency manifested in the majority of model simulations is
20 for longer dry periods and is consistent with the average decreases shown in Figure 12.25. Figure 12.29
21 shows changes in R95p over land regions obtained from the CMIP5 models. Globally, end of 21st century
22 changes range from 10% (RCP2.6) to 50% (RCP8.5) more precipitation on days with large storms. Locally,
23 the few regions where this index of extreme precipitation decreases in the late 21st century RCP8.5
24 projection coincide with areas of robust decreases in the mean precipitation of Figure 12.23d.

25 [INSERT FIGURE 12.29 HERE]

26 **Figure 12.29:** Projected changes (relative to the 1985–2005 baseline period) from the CMIP5 models in R95p, the
27 annual total precipitation occurring on days when the daily precipitation is greater than the 95th percentile of the 1961–
28 1990 period. a) Global average percent change over land regions for the RCP2.6, 4.5 and 8.5 scenarios. b) Percent
29 change over the 2081–2100 period in the RCP8.5. Equal model weighting.

30
31
32 Truly rare precipitation events can cause very significant impacts. These storms at the tails of the distribution
33 of precipitation are well described by Extreme Value Theory (EV) although there are significant biases in the
34 direct comparison of gridded model output and actual station data (Smith et al., 2009). There is also strong
35 evidence that model resolution plays a key role in replicating EV quantities estimated from gridded
36 observational data, suggesting that high-resolution models provide more confident projection of changes in
37 rare precipitation events (Fowler et al., 2007a; Wehner et al., 2011).

38 **12.4.6 Changes in Cryosphere**

39 **12.4.6.1 Changes in Sea Ice Cover**

40
41
42 Climate simulations conducted with both CMIP3 and CMIP5 models consistently project long-term
43 decreases in sea ice extent in both hemispheres in response to future increases in atmospheric greenhouse gas
44 concentrations and other anthropogenic forcings (Arzel et al., 2006; Bracegirdle et al., 2008; Körper et al.,
45 2011; Lefebvre and Goosse, 2008; Meehl et al., 2007b; NRC, 2011; Zhang and Walsh, 2006) (Figures 12.30
46 and 12.31). In the Northern Hemisphere, the rate of decrease in sea ice extent over the 21st century is
47 greatest in September. More than 90% of the CMIP5 models analyzed reach nearly ice-free conditions (ice
48 extent less than 1×10^6 km²) at the end of summer in the Arctic by 2100 under RCP8.5. However, for lower
49 forcing scenarios, the majority of models do not meet this criterion. In the Southern Hemisphere, most
50 CMIP5 models do not reach nearly ice-free conditions at any time during the year before the end of the 21st
51 century, even though the summertime sea ice extent at the start of the century is much lower than in the
52 Northern Hemisphere. In contrast to the Northern Hemisphere, the decreasing rate in Southern Hemisphere
53 sea ice areal coverage is largest in winter. Eisenman et al. (2011) argue that this hemispheric asymmetry in
54 the seasonality of sea ice loss is fundamentally related to the geometry of coastlines.

55 [INSERT FIGURE 12.30 HERE]

Figure 12.30: Anomalies in sea ice extent as simulated by CMIP5 models over the late 20th century and the whole 21st century using RCP2.6, RCP4.5, RCP6.0 and RCP8.5 for (a) Northern Hemisphere February, (b) Northern Hemisphere September, (c) Southern Hemisphere February and (d) Southern Hemisphere September. The solid curves show the multi-model means and the shading denotes the ± 1 standard deviation of the individual ensemble members. Sea ice extent is defined as the total area where sea ice concentration exceeds 15%. Anomalies are relative to the reference period 1986–2005. The number of models is given in the legend. Also plotted (solid pink curves) are the satellite data of Comiso (2008) over 1979–2005.

[INSERT FIGURE 12.31 HERE]

Figure 12.31: February and September CMIP5 multi-model mean sea ice concentrations (%) in the Northern and Southern Hemispheres for the periods (a) 1986–2005, (b) 2081–2100 under RCP4.5 and (c) 2081–2100 under RCP8.5. The pink lines show the observed 15% sea ice concentration limits averaged over 1986–2005 (Comiso, 2008).

A frequent criticism of the CMIP3 models is that these models as a whole significantly underestimate the rapid decline in summer Arctic sea ice observed during the satellite era (Stroeve et al., 2007; Winton, 2011). This concern has largely been eliminated for CMIP5 models. The CMIP5 multi-model mean trend in September Arctic sea ice extent over 1979–2005 amounts to $-0.47 \pm 0.70 \times 10^6 \text{ km}^2$ per decade (the uncertainty is two times the standard deviation of the model trends), compared to $-0.59 \pm 0.22 \times 10^6 \text{ km}^2$ per decade for satellite observations. About half of the models analyzed have an ensemble mean (or a single run if no ensemble is available) with a more negative trend than observed.

The change in September Arctic sea ice extent per degree annual mean global surface warming for 1979–2005 as derived from observations is $-3.4 \pm 1.6 \times 10^6 \text{ km}^2 \text{ }^\circ\text{C}^{-1}$ (the annual mean global surface temperature rise over this time period from the GISS Surface Temperature Analysis is $0.45 \pm 0.13^\circ\text{C}$; Hansen et al. (Hansen et al., 2010)). The corresponding number from CMIP5 models is $-2.0 \pm 2.5 \times 10^6 \text{ km}^2 \text{ }^\circ\text{C}^{-1}$. It can be seen from Figure 12.32 that the inter-model sensitivity is less scattered for CMIP5 models than for CMIP3 models. The average sensitivity of CMIP5 models is much lower than observed despite the closer agreement in September sea ice extent trends. This feature is due to the fact that the models on average warm too much during this period ($0.59 \pm 0.41^\circ\text{C}$). A similar result was found for the few CMIP3 models with losses in September Arctic sea ice comparable to observations (Mahlstein and Knutti, 2011a; Winton, 2011). Figure 12.32 indicates that, according to both CMIP3 and CMIP5 models, the September sea ice extent in the Northern Hemisphere could fall below $1 \times 10^6 \text{ km}^2$ with as little as about 1.5°C of global surface warming relative to 2000–2005. There are too few models in this figure with high sensitivity to give a reliable estimate of the upper bound of the global surface warming for which the September sea ice would remain above $1 \times 10^6 \text{ km}^2$ in extent. The models suggest a conservative estimate of 3°C , but it could be as high as 5°C . The most likely range is 1.5 to 2.5°C , which is consistent with estimates of Mahlstein and Knutti (2011b), who recalibrated an ensemble of CMIP3 models using observations (see below).

[INSERT FIGURE 12.32 HERE]

Figure 12.32: September Arctic sea ice extent versus annual mean global surface temperature change with respect to the period 2000–2005 for (a) CMIP3 models (SRES A1B scenario) and (b) CMIP5 models (all RCPs). Model outputs are averaged over five years. The black circle shows the mean observed September Arctic sea ice extent over 2000–2005 (Comiso, 2008).

A complete explanation for what controls the range of Arctic sea ice response in models over the 21st century remains elusive. A partial explanation has been found for the change in sea ice mass budget in relation to the mean late 20th century sea ice thickness distribution (Holland et al., 2010) and the fraction of thin ice cover (Boe et al., 2009b). Figure 12.33b shows that a related quantity, the late 20th century extent of sea ice below 1 m mean thickness in April, is a reasonable predictor of the 21st century September sea ice extent change. Thin ice is more susceptible to melt, and hence a larger area of thin ice results in a greater decrease in September sea ice extent. Nevertheless, the late 20th century average sea ice thickness has little influence on the 21st century September sea ice extent decline (not shown), despite the strong correlation between the annual mean ice thickness and the September ice extent in the late 20th century (Figure 12.33a). The late 20th century September sea ice extent is also a reasonable predictor of the 21st century September sea ice extent change (Figure 12.33d), but overall, less September sea ice extent leads to greater reduction in September sea ice extent. The strongest correlation is found between the late 20th century annual mean sea ice thickness and the 21st century change in annual mean sea ice thickness (Figure 12.33c). However, the negative relationship in Figure 12.33c is counter to the positive one in Figure 12.33d, which is perhaps one

1 reason why current conditions do not yield perfect relations for future change. Nonetheless, conditions in the
2 late 20th century have been shown to generally outweigh the influence of discrepancies in the strength of the
3 albedo feedback across different climate models (Bitz, 2008). It is therefore likely that the Northern
4 Hemisphere sea ice extent in the CMIP5 models is on average more sensitive to climate forcing and annual
5 mean global surface warming than CMIP3 models because sea ice in CMIP5 models is on average thinner
6 and overall less extensive for current climate conditions (Figure 12.33a).

7 8 **[INSERT FIGURE 12.33 HERE]**

9 **Figure 12.33:** Scatter plots of Northern Hemisphere sea ice quantities averaged over 1980–1999 or changes in mean
10 Northern Hemisphere sea ice quantities between 2040–2059 and 1980–1999. The ice thickness is averaged over the
11 ocean surface north of 70°N. The thin ice extent is the extent of ice which is less than 1 m thick. Correlations (R) are
12 shown in bold font if they are significant at the 95% confidence level. The blue and red circles correspond to CMIP3
13 (SRES A1B scenario) and CMIP5 (RCP4.5) models, respectively. Shading denotes the observed range spanning the ± 1
14 standard deviation about the mean value derived from Comiso (2008) satellite data for ice extent and about a bias
15 corrected estimate obtained with the Pan-Arctic Ice-Ocean Modeling and Assimilation System (PIOMAS), in which sea
16 ice concentration data were assimilated (Schweiger et al., 2011), for ice thickness. This bias correction is based on a
17 comparison of PIOMAS outputs with U.S. submarines and ICESat-derived ice thickness data.

18
19 These results lend support for weighting the models based on their present-day sea ice simulations. A
20 number of studies have done this by applying different metrics to the CMIP3 models. For example, Wang
21 and Overland (2009) sub-set the CMIP3 models based on their fidelity to the observed Arctic ice extent
22 seasonal cycle and mean September extent in the late 20th century. Boe et al. (2009b) used an observational
23 constraint of the recent (1979–2007) September ice extent trend and argued that this is physically-based
24 because it is related to the initial ice thickness distribution. Zhang (2010b) selected models based on the
25 regression between summer ice loss and Arctic surface temperature change. Estimates of future Arctic ice
26 loss rates have also utilized the observed record but with consideration of the model projected loss. For
27 example, Mahlstein and Knutti (2011b) used observationally calibrated regressions of ice extent change
28 relative to surface temperature increase to determine at what temperature rise September ice-free conditions
29 would result. These various methods lead to different timings for when a seasonally ice-free Arctic Ocean
30 might be realized (between the late 2030s and 2100 for the SRES A1B scenario). However, they all suggest a
31 faster rate of summer sea ice decline than the CMIP3 multi-model mean. Based on current research, the
32 optimal weighting for sea ice projections is not clear although we note that, to increase their reliability, these
33 metrics should have a credible underlying physical basis. Additionally caution is needed in using observed
34 sea ice trends as a metric given that the observed record is relatively short and Arctic sea ice trends on these
35 timescales bear a strong imprint of natural variability (Kay et al., 2011a; Mahlstein and Knutti, 2011b).

36
37 The potential irreversibility of the Arctic sea ice loss and the possibility of a rapid, non linear transition
38 towards an ice-free Arctic Ocean are discussed in Section 12.5.5.3.

39
40 In the Southern Hemisphere, all CMIP3 and CMIP5 models exhibit a reduction in sea ice extent by the end
41 of the 21st century, although the magnitude differs substantially across models (Arzel et al., 2006;
42 Bracegirdle et al., 2008; Körper et al., 2011; Lefebvre and Goosse, 2008; Meehl et al., 2007b; NRC, 2011)
43 (Figure 12.30). As their CMIP3 counterparts, the majority of CMIP5 models simulate a decreasing trend in
44 Antarctic sea ice extent for all seasons over 1979–2005, in contrast to the small observed increase. A large
45 variation in the modeled trends is present and a comparison of multiple ensemble members from the same
46 model suggests a strong imprint of natural variability over the late 20th century (e.g., Landrum et al., 2011).
47 The reasons for the discrepancies across models in late 20th century and projected trends are unclear. Studies
48 have suggested that missing (or inadequately parameterized) processes in climate models contribute to poor
49 model performance in the Southern Ocean. For example, changing ocean heat transport in response to
50 variations in Southern Ocean winds appears very dependent on the resolving or the method of
51 parameterizing ocean eddies (Farneti et al., 2010; Fyfe et al., 2007; Gent and Danabasoglu, 2011; Screen and
52 Simmonds, 2010; Spence et al., 2010) (Böning et al., 2008). This can have important consequences for the
53 ice-ocean heat exchange and sea ice response. Given discrepancies in simulated sea ice conditions compared
54 to observations, future changes in Southern Hemisphere sea ice are uncertain.

55 56 *12.4.6.2 Changes in Snow Cover and Frozen Ground*

1 The snow covered area (SCA) and snow water equivalent (SWE) respond sensitively to both temperature
2 and precipitation. SCA decreases are highly correlated with a shortening of the seasonal snow cover duration
3 (Brown and Mote, 2009). The snow cover season is shortened, with the snow accumulation season beginning
4 later in autumn ($+20 \pm 9$ days in CCSM3) and melt season beginning earlier in the spring (-14 ± 7 days in
5 CCSM3) (Lawrence and Slater, 2010). Projections for the change in annual maximum SWE are more mixed.
6 Warming decreases SWE both by reducing the fraction of precipitation that falls as snow and by increasing
7 snow melt, but projected increases in precipitation over much of the northern high latitudes during winter
8 months act to increase snow amounts. Whether snow covering the ground will become thicker or thinner
9 depends on the balance between these competing factors. According to the CMIP3 models, the average
10 borderline between increasing and decreasing mid-winter SWE coincides broadly with the -20°C isotherm
11 of the late 20th century November-to-March mean surface air temperature. On the colder side of this
12 isotherm, SWE generally increases and, on the warmer side, the reverse happens (Raisanen, 2008). The
13 Northern Hemisphere spring (March-April average) snow cover area changes are very coherent in the
14 CMIP5 MMD. Relative to the 1986–2005 reference period, weak changes of about $9 \pm 3\%$ are to expect for
15 RCP2.6 during the last two decades of the 21st century, while SCA decreases of about $12 \pm 3\%$ are
16 simulated for RCP4.5, $15 \pm 4\%$ for RCP6.0, and $24 \pm 5\%$ for RCP8.5 (Figure 12.34).

17 [INSERT FIGURE 12.34 HERE]

18 **Figure 12.34:** Northern Hemisphere spring (March to April average) relative snow covered area (RSCA) in the CMIP5
19 MMD, obtained through dividing the simulated 5-year box smoothed spring snow covered area (SCA) by the simulated
20 average spring SCA of 1986–2005 reference period. Blue: RCP2.6; Green: RCP4.5; Orange: RCP6.0; Red: RCP8.5.
21 Thick lines: MMD average. Shading and thin dotted lines indicate the inter-model spread (one standard deviation).
22

23
24 The strong projected warming across the northern high latitudes in climate model simulations has
25 implications for frozen ground. Recent projections of the extent of permafrost degradation continue to vary
26 widely, but virtually all of them indicate that a substantial amount of near-surface permafrost degradation
27 and thaw depth deepening over much of the permafrost area will occur (Koven et al., 2011; Lawrence et al.,
28 2011; Lawrence et al., 2008; Saito et al., 2007). Permafrost degradation at greater depths naturally occurs
29 much more slowly (Delisle, 2007), but very deep permafrost is less relevant as a component of the climate
30 system. Climate models are beginning to represent permafrost more accurately by accounting for the
31 insulating properties of organic soil and extending the depth over which soil temperature dynamics are
32 calculated to tens of meters (Alexeev et al., 2007; Koven et al., 2009; Lawrence et al., 2008; Nicolsky et al.,
33 2007; Rinke et al., 2008). The projected changes in permafrost are a response not only to warming, but also
34 to changes in snow conditions. Snow properties and their seasonal evolution exert significant control on soil
35 thermal state (Zhang, 2005). The projected changes in snow cover duration and mid-winter SWE can have
36 warming or cooling impacts on soil temperature (Lawrence and Slater, 2010). Applying the surface frost
37 index method (Nelson and Outcalt, 1987) to coupled climate model output of the CMIP5 MMD yields a
38 reduction of the diagnosed 2080–2099 near-surface permafrost area (continuous plus discontinuous
39 permafrost) by 31% (RCP2.6), 44% (RCP4.5), 51% (RCP6.0), and 73% (RCP8.5), compared to the 1986–
40 2005 diagnosed near-surface permafrost area (Figure 12.35). In summary, there is a high agreement across
41 CMIP5 and older model projections indicating substantial future near-surface permafrost degradation, with
42 amplitude depending on the emission scenario and on the processes taken into account.

43 [INSERT FIGURE 12.35 HERE]

44 **Figure 12.35:** Northern Hemisphere diagnosed near-surface permafrost area in the CMIP5 MMD following Nelson and
45 Outcalt (1987) and using 20-year average monthly surface air temperatures and snow depths. Blue: RCP2.6; Green:
46 RCP4.5; Orange: RCP6.0; Red: RCP8.5. Thick lines: MMD average. Shading and thin lines indicate the inter-model
47 spread (one standard deviation). Black symbols at the year 2000 represent the diagnosed near-surface permafrost
48 extents using reanalysis data (circle = ERA-I, up triangle=MERRA, down triangle=JRA, diamond=CFSRR).
49

50 12.4.7 Changes in the Ocean

51 12.4.7.1 Ocean Temperature, Salinity and Heat Transport

52
53 Projected warming of sea surface temperature (SST) over the next two decades is relatively insensitive to the
54 emissions trajectory. However, projected outcomes diverge as the 21st century progresses. Changes in
55 globally-averaged upper ocean heat content reflect changes in net global ocean surface heat fluxes. Recent
56 observations compiled by Levitus et al. (2009) indicate that ocean heat content (OHC) has increased at a rate
57
58

1 of $0.40 \times 10^{22} \text{ J yr}^{-1}$ since 1955. As in the case for SST, the differences in projected OHC for different RCP
2 forcing manifest themselves most profoundly as the century progresses. Subsurface warming is most
3 pronounced where North Atlantic deep water forms in the Northern Hemisphere and Antarctic Intermediate
4 Water forms in the Southern Hemisphere.

5
6 Durack and Wijffels (2010) examined trends in global ocean surface salinity (SSS) changes over the period
7 1950–2008. Their analysis revealed strong, spatially-coherent, trends in SSS over much of the global ocean,
8 with a pattern that bears “striking” resemblance to the climatological SSS field. The few CMIP5 climate
9 model projections available suggest that high SSS subtropical regions that are dominated by net evaporation
10 are typically getting more saline; lower SSS regions at high latitudes are typically getting fresher. They also
11 suggest a continuation of this trend in the Atlantic where subtropical surface waters become more saline as
12 the century progresses (Figure 12.36).

13
14 **[INSERT FIGURE 12.36 HERE]**

15 **Figure 12.36:** Projected sea surface salinity differences 2081–2100 for RCP8.5 relative to 1986–2005 from CMIP5
16 models. Model agreement is assessed as in (Tebaldi et al., 2011). Grid points are stippled where at least half of the
17 models show significant change and >80% of them agree on the sign, while white shading indicates at least half of the
18 models show significant change but less than 80% of those agree on the sign.

19
20 *12.4.7.2 Atlantic Meridional Overturning*

21
22 Almost all climate model projections reveal an increase of high latitude temperature and high latitude
23 precipitation (Meehl et al., 2007b). Both of these effects tend to make the high latitude surface waters lighter
24 and hence increase their stability. As seen in Figure 12.37, models show a weakening of the Atlantic
25 meridional overturning circulation (AMOC) over the course of the 21st century. Projected changes in the
26 strength of the AMOC at high latitudes appear stronger when density is used as a vertical coordinate instead
27 of depth (Zhang, 2010a). Once the radiative forcing is stabilized, the AMOC recovers to its preindustrial
28 level (Figure 12.37a). Gregory et al. (2005) found that for all eleven models analysed, the AMOC reduction
29 was caused more by changes in surface heat flux than changes in surface freshwater flux.

30
31 While many more model simulations have been conducted since the AR4 under a wide range of forcing
32 scenarios, projections of the AMOC behaviour has not changed. Based on the available CMIP5 models and
33 the literature, it remains very likely that the AMOC will weaken over the 21st century with a best estimate
34 decrease in 2100 of about 10–30% for the RCP 4.5 scenario and 20–40% for the RCP 8.5 scenario. It also
35 remains very unlikely that the AMOC will undergo an abrupt transition or collapse in the 21st century. As
36 assessed by Delworth et al. (2008), for an abrupt transition of the AMOC to occur, the sensitivity of the
37 AMOC to forcing would have to be far greater than that seen in current models. Alternatively, significant
38 ablation of the Greenland ice sheet greatly exceeding even the most aggressive of current projections would
39 be required. While neither possibility can be excluded entirely, it is unlikely that the AMOC will collapse
40 beyond the end of the 21st century because of global warming based on the models and range of scenarios
41 considered.

42
43 **[INSERT FIGURE 12.37 HERE]**

44 **Figure 12.37:** Multi model projections of Atlantic meridional overturning circulation (AMOC) strength at 30°N from
45 1850 through to the end of the RCP extensions. a) RCP2.6; b) RCP4.5; c) RCP6.0; d) RCP8.5. Results are based on a
46 small number of CMIP5 models available. Curves show results from only the first member (r1i1p1) of the submitted
47 ensemble of experiments.

48
49 *12.4.7.3 Southern Ocean*

50
51 A dominant and robust feature of the model outputs from the CMIP3 database analysed for IPCC AR4
52 (Meehl et al., 2007b) is the weaker surface warming at the end of the 21st century in the Southern Ocean
53 than at global scale. Furthermore, in response to the projected southward shift in the Southern Hemisphere
54 mid-latitude westerlies, the Antarctic Circumpolar Current (ACC) moves southwards in nearly all available
55 climate projections (Fyfe et al., 2007). This displacement induces a significant warming at 35°S–40°S in the
56 uppermost oceanic layers.

1 The additional analyses of the CMIP3 model outputs performed since the release of IPCC AR4 confirm and
2 refine the earlier findings (Lefebvre and Goosse, 2008; Sen Gupta et al., 2009; Wang and Meredith, 2008).
3 In addition to the abovementioned ACC shift, changes in the Southern Hemisphere oceanic circulation
4 projected for the end of the 21st century include, in many models, an intensification of subtropical and
5 subpolar gyres and a stronger upwelling of deep water (Sen Gupta et al., 2009; Wang and Meredith, 2008),
6 together with a reduced subduction of Subantarctic Mode Water and Antarctic Intermediate Water (Downes
7 et al., 2011). All those circulation changes must however be taken with caution as a number of studies
8 suggest that oceanic mesoscale eddies, which are not explicitly taken into account in models used for climate
9 projections, might noticeably affect the ACC response to changes in zonal wind stress (Downes et al., 2011;
10 Farneti and Gent, 2011; Farneti et al., 2010) (Böning et al., 2008).

11
12 Climate projections generally exhibit a decrease in mixed layer depth at southern mid- and high latitudes for
13 the end of the 21st century (Lefebvre and Goosse, 2008; Sen Gupta et al., 2009). This feature is a
14 consequence of the enhanced stratification resulting from surface warming and freshening, the latter
15 characteristics being mainly observed south of 45°S. Despite large intermodel differences, there is a robust
16 weakening of Antarctic Bottom Water (AABW) production and its northward outflow, which is consistent
17 with the decrease in surface density and which in turn is manifest as a warming signal close to the Antarctic
18 margin that reaches abyssal depths (Sen Gupta et al., 2009). In the vicinity of the Antarctic ice sheet, models
19 predict over the course of the 21st century an average warming of ~0.5°C at depths of 200–500 m for a mid-
20 range increase in atmospheric greenhouse gas concentrations, which could seriously impact on the mass
21 balance of ice shelves (Yin et al., 2011).

22
23 AOGCMs used in climate projections do not include any interactive ice sheet component. When climate–ice
24 sheet interactions are accounted for in an Earth system model of intermediate complexity under a $4 \times \text{CO}_2$
25 scenario, the melt water flux from the Antarctic ice sheet further reduces the surface density close to
26 Antarctica and the AABW formation rate (Swingedouw et al., 2008). Nevertheless, this effect becomes
27 significant only after more than one century.

28 29 *12.4.7.4 Other Projected Changes*

30
31 Using the model results from the IPCC AR4 simulations, Luo et al. (2009) found that the upper part of
32 Equatorial Undercurrent (EUC) strengthens in a warmer climate, whereas its lower part weakens. This EUC
33 anomaly is largely a result of the upward shift in the mean position of EUC maximum, and it has been shown
34 to closely follow the anomaly in buoyancy frequency along the equator (Saenko et al., 2011).

35
36 The weakening of the Pacific Walker circulation (Section 12.4.4.2) does not lead to the classical El Niño
37 response in the tropical Pacific Ocean (Collins et al., 2010; Vecchi and Soden, 2007). The weakening trade
38 winds leads to reduced equatorial upwelling which is accompanied by a flattening of the thermocline (i.e., a
39 reduction in the east-west tilt), a general thermocline shoaling (rising up) and a strengthening of the
40 temperature gradient across the thermocline (Yeh et al., 2009). The pattern of SST shows enhanced warming
41 on the equator and has a more zonal (north-south) symmetry than an east-west pattern associated with
42 interannual ENSO variability due to a reduced meridional heat-flux divergence throughout the equatorial
43 Pacific (DiNezio et al., 2009). In the west, cloud-cover feedbacks and evaporation balance the additional
44 dynamical heating as well as the greenhouse-gas-related radiative heating. In the east, increased cooling by
45 vertical heat transport within the ocean balances the additional warming over the cold tongue. The increased
46 cooling tendency arises from increased near-surface thermal stratification, despite a reduction in vertical
47 velocity associated with the weakened trades (An et al., 2008). Uncertainties in this picture arise because
48 many models show common biases including cold-tongues that extend too far into the west and ‘double
49 ITCZs’. Changes in ENSO interannual variability are assessed in Chapter 14.

50 51 *12.4.8 Consistency and Main Differences CMIP3/CMIP5 and SRES/RCPs*

52
53 In the experiments collected under CMIP5, both models and scenario have changed with respect to CMIP3
54 making a comparison with earlier results and the scientific literature they generated (on which some of this
55 chapter’s content is still based) complex. The set of models used in AR4 (the CMIP3 models) have been
56 superseded by the new CMIP5 models (Table 12.1, Chapter 9) and the SRES scenarios have been replaced

1 by four RCPs (section 12.3.1). In addition, the baseline period used to compute anomalies has advanced 6
2 years from 1980–1999 to 1986–2005.

3
4 Rerunning the full CMIP3 ensemble under the new RCPs and/or the full CMIP5 ensemble under the old
5 SRES scenarios in order to separate model and scenario effects has not been done. Thus we rely on
6 simplified modelling frameworks to emulate CMIP3/5 SRES/RCP model behavior. Figure 12.38 shows an
7 emulation of the global mean temperature response that we would expect from the CMIP5 models (those
8 available at the time of writing of the FOD) if they were run under SRES A1B. In this case anomalies are
9 computed with respect to 1980–1999 for direct comparison with AR4 figure 10.5, which is reproduced in the
10 lower panel. The method used to emulate the SRES A1B response of the CMIP5 is documented in (Good et
11 al., 2011) with the radiative forcing computed using the (Forster and Taylor, 2006) method and taking
12 ensemble mean forcing across all available CMIP3 and CMIP5 models (one initial condition ensemble
13 member per model). The simple model is only used to predict the temperature difference between A1B and
14 RCP8.5, and between A1B and RCP4.5 separately for each model. These differences are then added to
15 CMIP5 GCM simulations of RCP8.5 and RCP4.5 respectively, and averaged to give a single A1B estimate.

16
17 [PLACEHOLDER FOR SECOND ORDER DRAFT: discuss any major differences or highlight similarities
18 between upper and lower panels once more CMIP5 models are available.]

19 [INSERT 12.38 HERE]

20
21 **Figure 12.38:** Upper panel, an emulation of the global mean temperature response of the CMIP5 models run under
22 SRES A1B with anomalies computed with respect to 1980–1999. The emulation technique is described in (Good et al.,
23 2011). Lower panel, reproduction of part of Figure 10.5 of AR5 showing the CMIP3 model responses under SRES A1B
24 with the same anomaly period.

25
26 Meinshausen et al. (2011a; 2011b) tuned MAGICC6 to emulate 19 GCMs from CMIP3. The results are
27 temperature projections and their uncertainties (based on the empirical distribution of the ensemble) under
28 each of the RCPs, extended to year 2500 (under constant emissions for the lowest RCP and constant
29 concentrations for the remaining three). In the same paper, an ensemble produced by combining carbon cycle
30 parameter calibration to 9 C4MIP models with the 19 CMIP3 model parameter calibrations is also used to
31 estimate the emissions implied by the various concentration pathways had the CMIP3 models included a
32 carbon cycle component. Rogelj et al., (2011a) use the same tool but perform a fully probabilistic analysis of
33 the SRES and RCP scenarios using a parameter space that is consistent with CMIP3/C4MIP but a more
34 general uncertainty characterization for key quantities like equilibrium climate sensitivity, similarly to the
35 approach utilized in (Meinshausen et al., 2009). Observational or other historical constraints are also used in
36 this study and the analysis is consistent with the overall assessment of sources and ranges of uncertainties for
37 relevant quantities (equilibrium climate sensitivity above all) stemming from the AR4. Figure 12.39
38 summarizes results of this probabilistic comparison for global temperature. The RCPs span a large range of
39 stabilization, mitigation and non-mitigation pathways and the resulting range of temperature changes are
40 larger than those produced under SRES scenarios, which do not consider mitigation options. Emissions
41 under RCP8.5 are highest and the resulting temperature changes likely range from 4.0 to 6.1°C by 2100. The
42 lowest RCP2.6 assumes significant mitigation and the global temperature change likely remains below 2°C.

43 [INSERT FIGURE 12.39 HERE]

44
45 **Figure 12.39:** Temperature projections for SRES scenarios and the RCPs. (a) Time-evolving temperature distributions
46 (66 per cent range) for the four RCPs computed with this study's ECS distribution and a model setup representing
47 closely the carbon-cycle and climate system uncertainty estimates of the AR4 (grey areas). Median paths are drawn in
48 yellow. Red shaded areas indicate time periods referred to in panel b. (b) Ranges of estimated average temperature
49 increase between 2090 and 2099 for SRES scenarios and the RCPs respectively. Note that results are given both relative
50 to 1980–1999 (left scale) and relative to pre-industrial (right scale). Yellow ranges indicate results of this study; other
51 ranges show the AR4 estimates. Colour-coding of AR4 ranges is chosen to be consistent with the AR4.

52
53 Similar temperature change projections by the end of the 21st century are obtained under RCP8.5 and SRES
54 A1FI, RCP6 and SRES B2 and RCP4.5 and SRES B1. There remain large differences though in the transient
55 trajectories, with rates of change slower or faster for the different pairs. These differences can be traced back
56 to the interplay of the (negative) short-term effect of sulphate aerosols and the (positive) effect of long-lived
57 GHGs. Impact studies may be sensitive to the differences in these temporal profiles so care should be taken
58 in approximating SRES with RCPs and vice versa.

1
2 While simple models can separate the effect of the scenarios and the model response, no studies are currently
3 available that allow an attribution of the CMIP3-CMIP5 differences to changes in the transient climate
4 response, the carbon cycle, and the inclusion of new processes (chemistry, land surface, vegetation).
5 Figure 12.40 shows a comparison of the patterns of warming and precipitation change from CMIP3 and
6 CMIP5, utilizing the pattern scaling methodology (Section 12.4.2). The geographic patterns of mean change
7 are very similar across the two ensembles of models, with pattern correlations larger than 0.9 for temperature
8 and 0.8 for precipitation changes.

9
10 **[INSERT FIGURE 12.40 HERE]**

11 **Figure 12.40:** Patterns of temperature (left column) and percent precipitation change (right column) by the end of the
12 21st century (2081–2100 vs 1986–2005), for the CMIP3 models average (first row) and CMIP5 models average (second
13 row), scaled by the corresponding global average temperature changes.

14
15 **12.4.9 Changes Associated with Biogeochemical Feedbacks**

16
17 Future projections of major greenhouse gases and aerosols concentrations have been simulated by Earth
18 System Models (ESMs) or by Chemistry Climate Models (CCMs). With such models, projections account
19 for the imposed changes in anthropogenic emissions, but also for changes in natural sources and sinks as
20 they respond to changes in climate and atmospheric composition. If included in ESMs, the impact on
21 projected radiative forcing and hence on climate can be quantified.

22
23 **12.4.9.1 Carbon Dioxide**

24
25 **[PLACEHOLDER FOR SECOND ORDER DRAFT: Based on only one CMIP5 model available at the time**
26 **of the FIRST ORDER DRAFT submission]**

27
28 Within the CMIP5 sets of simulations, the historical and RCP8.5 emission-driven simulations allow to
29 evaluate the climate response of the Earth system when the atmospheric CO₂ and the climate system are
30 being calculated by the ESMs. In such ESMs, the atmospheric CO₂ is calculated as the difference between
31 the imposed anthropogenic emissions and the sum of land and ocean carbon uptakes. When compared to the
32 historical and RCP8.5 concentration driven simulations, the climate projections would differ if the simulated
33 atmospheric CO₂ is significantly different from the one used in the concentration driven simulations. This
34 could happen if the ESMs carbon cycle is different from the one simulated by MAGICC6, the model used to
35 calculate the greenhouse gases concentrations from emissions for the four RCPs (Meinshausen et al., 2011b;
36 Meinshausen et al., 2011c). Likewise, when driven by CO₂ concentration, the ESMs calculate the CO₂
37 emissions compatible to the prescribed atmospheric CO₂ trajectory allowing comparison with the emissions
38 estimated by the IAMs (Arora et al., 2011).

39
40 Figure 12.41 shows the simulated atmospheric CO₂ and global average surface air temperature for the
41 historical and RCP8.5 when *so far only one* model is driven by CO₂ emissions, compared with the CO₂
42 concentration driven simulation. *For that model*, simulated atmospheric CO₂ is reaching higher values than
43 the values used by ESM forced in CO₂ concentrations. As a result, *for that model*, emission driven scenarios
44 project larger warming by the end of the century (up to 0.5°C). The almost complete lack of data from
45 emission driven RCP simulations from ESMs at this stage prevents a comprehensive assessment and an
46 estimate of the uncertainty of the carbon cycle climate feedbacks beyond what is available from the C4MIP
47 generation of models assessed in AR4.

48
49 **[INSERT FIGURE 12.41 HERE]**

50 **Figure 12.41:** Comparison between ESM simulations with CO₂ emissions (red) or CO₂ concentration (black) as
51 external forcing. a) atmospheric CO₂ concentration (ppm), b) global average surface air temperature difference (°C).

52
53 **12.4.9.2 Methane**

54
55 Future projections of atmospheric methane (CH₄) concentration depend on the evolution of its sources and
56 sinks. Estimates of anthropogenic CH₄ sources are available for the SRES (IPCC, 2000) and RCP (van
57 Vuuren et al., 2011a) (Annex II). CH₄ has also significant natural sources. Some of these (in particular,
58 wetlands) are strongly linked to climate change (Gedney et al., 2004; Koven et al., 2011; Ringeval et al.,

2011; Shindell et al., 2004). There is a no general agreement on the climate change impact on CH₄ biogenic emissions. Earlier studies finding an increase in methane emissions, while the more recent study of Ringeval et al. (2011) shows that climate change induces a decrease of wetland extent and subsequently methane emissions. However, this study found that this climate effect is over-compensated by the increased flux density as a result of atmospheric CO₂ fertilisation leading to larger ecosystem productivity and hence to larger soil organic carbon available for anaerobic decomposition.

Climate change also affects CH₄ concentrations through change in the abundance of OH, which directly controls the methane lifetime (Isaksen et al., 2009; Shindell et al., 2007). There is a general agreement amongst CCMs that the enhanced water vapour level in a warmer climate leads to a larger production of the OH hydroxyl, leading to a reduction of the methane lifetime. However under the SRES scenarios, future changes in sources (mainly anthropogenic but also natural) dominate the simulated long-term trends in methane concentration.

12.4.9.3 Tropospheric Ozone

Under future climate change, tropospheric ozone may reduce due to increased destruction related to higher absolute humidities (Johnson et al., 2001) or may increase due to positive climate feedbacks such as an increased influx from the stratosphere (Eyring et al., 2010c; Hegglin and Shepherd, 2009), or higher biogenic VOC emissions (Hauglustaine et al., 2005; Sanderson et al., 2003). The net impact of climate change on tropospheric ozone is uncertain, but it is likely to vary significantly by region, altitude, and season (Isaksen et al., 2009; Jacob and Winner, 2009; Stevenson et al., 2006).

Since the AR4, new tropospheric ozone projections under the four RCP scenarios have been performed with the CAM3.5 chemistry-climate model with interactive tropospheric and stratospheric chemistry (Cionni et al., 2011; Lamarque et al., 2011). While emissions of ozone precursors are slightly different in the four RCPs, there are much larger differences for the GHGs concentrations and in particular for methane CH₄ concentration, with 2100 concentrations ranging between 1250 ppb (RCP2.6) and 3500 ppb (RCP 8.5) (Cionni et al., 2011). This large range in CH₄ concentration will directly affect projections of tropospheric ozone, with increase in tropospheric ozone for RCP8.5 and decrease in all other scenarios (Cionni et al., 2011, Lamarque et al., 2011) and the resulting radiative forcings (see Chapter 8). Surface ozone is projected to decrease in the future for all RCPs, this is due to the reduction of ozone precursors at the surface but also due to climate change and in particular increase in absolute humidity that enhances ozone destruction (Cionni et al., 2011). The RCP projections of surface ozone are significantly lower than the AR4 projections, mainly because of much lower emissions of NO_x in the RCPs than in the SRES scenarios (Prather et al., 2003).

12.4.9.4 Stratospheric Ozone

To project the future evolution of stratospheric ozone and attribute its behaviour to different forcings, CCMs with fully coupled stratospheric chemistry are now widely used. Simulations from 17 CCMs under the SRES A1B GHG scenario were recently examined to project the evolution of stratospheric ozone through the 21st century (Austin et al., 2010; Eyring et al., 2010a; Eyring et al., 2010c) as part of the second round of coordinated model inter-comparison organized by the Chemistry-Climate Model Validation Activity (CCMVal-2). As a result of the Montreal Protocol and its Amendments and Adjustments, the abundances of ozone-depleting substances (ODSs) are now slowly declining. As ODSs decrease, GHG induced changes in stratospheric climate and circulation (such as the cooling of the upper and middle stratosphere and the strengthening of the Brewer-Dobson circulation) are expected to have an increasing influence on the evolution of stratospheric ozone through the 21st century (Butchart et al., 2011; Eyring et al., 2010c; Haigh and Pyle, 1982).

The importance of these factors varies with region, time and GHG scenario. In the tropics, a return of tropical stratospheric column ozone to 1980 values is simulated around 2050 in the SRES A1B GHG scenario. This increase is followed by a continuous decrease in the second half of the 21st century mainly in the lower stratosphere, which is caused by an increase in the Brewer-Dobson circulation (Austin et al., 2010). The magnitude of ozone decrease depends on the GHG scenario, but in all RCP scenarios stratospheric column ozone in the tropics is projected to remain below its pre-1980 value at the end of the

21st century (Eyring et al., 2010b). In the mid-latitudes, the minimum of stratospheric column ozone is reached by ~2000 followed by a steady and significant increase well above pre-1980 values, in particular in the Northern Hemisphere. This increase is attributable to CO₂-cooling leading to increases in upper stratospheric ozone. In the Antarctic in spring, projected changes in ozone depleting substances (ODSs) are driving the changes in stratospheric column ozone, with ozone depletion being maximum around 2000 (~80 DU lower than its 1980 value), followed by a slow and steady increase until 2100 (Cionni et al., 2011). Evolution of spring-time stratospheric ozone in the Arctic is similar to the one projected in spring-time Antarctic, but with a less dramatic initial ozone hole (~23 DU lower than its 1980 value) and with larger recovery by the end of the 21st century (Austin et al., 2010; Eyring et al., 2010c, Cionni et al., 2011). Differences among GHG scenarios are found to be largest over northern mid-latitudes (~20 DU by 2100) and in the Arctic (~40 DU by 2100) with divergence mainly in the second half of the 21st century (Eyring et al., 2010b).

12.4.9.5 Land-Use

Future changes in land cover will have an impact on the climate system through biophysical and biogeochemical processes. Biophysical processes include change in surface albedo and changes in partitioning between latent and sensible heat, while biogeochemical feedbacks essentially include change in CO₂ sources and sinks (e.g., Pongratz et al., 2010) but could potentially also include changes in N₂O or CH₄ emissions. The biophysical response to future land cover changes has been investigated within the SRES scenarios. Using the SRES-A2 2100 land cover, Davin et al. (2007) simulated a global cooling of 0.14 K largely driven by change in albedo.

In the context of the LUCID activity (Pitman et al., 2009) ESMs performed additional simulations in order to separate the biophysical from the biogeochemical effects of land-use changes in the RCP scenarios. [PLACEHOLDER FOR SECOND ORDER DRAFT: Results from RCP-based LUCID simulations]

Regional analyses have been performed in order to quantify the biophysical impact of biofuels plantation (Georgescu et al., 2011; Loarie et al., 2011) generally finding a local to regional cooling when annual crops are replaced by bioenergy crops (such as sugar cane).

12.5 Long Term Climate Change, Commitment and Irreversibility

12.5.1 RCP Extensions

The CMIP5 intercomparison project includes simulations extending the four RCPs to the year 2300 (see section 12.3.1). This allows exploring the longer-term climate response to idealized GHG and aerosols forcings (Meinshausen et al., 2011c). By 2300, global warming reaches $8.7 \pm 2.4^\circ\text{C}$ (multi model average plus minus one standard deviation) under the RCP8.5; $2.3 \pm 0.4^\circ\text{C}$ under the RCP4.5 and 0.6 ± 0.4 under the RCP2.6 relative to 1986–2005. (Figure 12.4).

EMICs simulations have been performed following the same CMIP5 protocol for historical and RCPs extended to 2300. These scenarios have been prolonged beyond 2300 to investigate longer-term commitment and irreversibility (see below). Projected warming and the reduction of the AMOC up to 2300 as simulated by the EMICs is comparable to the one simulated by the CMIP5 ESMs (Figure 12.42)

[INSERT FIGURE 12.42 HERE]

Figure 12.42: Atmospheric CO₂ forcing, b) projected global mean surface temperature warming and c) projected change in meridional overturning circulation, as simulated by 6 EMICs (Bern3D, CLIMBER 2, CLIMBER 3-alpha, DCESS, MESMO and UVic) for the 4 RCPs up to 2300. A ten-year smoothing was applied.

12.5.2 Climate Change Commitment

Climate change commitment, the idea that the climate will change further after the forcing or emissions have been eliminated or held constant, has caught the attention of scientists and policy makers shortly before the completion of IPCC AR4 (Hansen et al., 2005a; Meehl et al., 2005b; Meehl et al., 2006; Wigley, 2005) (AR4 Section 10.7.1). However, the argument that the surface response would lag the radiative forcing due to the

1 large thermal reservoir of the ocean in fact goes back much longer (Hansen et al., 1985; Hansen et al., 1984;
2 Mitchell et al., 2000; Schlesinger, 1986; Siegenthaler and Oeschger, 1984; Wetherald et al., 2001). The
3 discussion in this section is framed largely in terms of temperature change, but other changes in the climate
4 system (e.g., precipitation) are closely related to changes in temperature (see Section 12.4.2). A summary of
5 how past emissions relate to future warming is also given in FAQ 12.3.

6
7 The Earth system has multiple response timescale related to different thermal reservoirs. For a step change in
8 forcing (instantaneous increase in the magnitude of the forcing and constant forcing after that), a large
9 fraction of the total of the surface temperature response will be realized in a few years (Brasseur and
10 Roeckner, 2005; Knutti et al., 2008a; Murphy et al., 2009). The remaining response over centuries is
11 controlled by the slow mixing of the energy perturbation into the ocean (Stouffer, 2004). The response
12 timescale depends on the amount of ocean mixing and the strength of climate feedbacks, and is longer for
13 higher climate sensitivity (Hansen et al., 1985; Knutti et al., 2005). The transient climate response is
14 therefore smaller than the equilibrium response, in particular for high climate sensitivities. Delayed
15 responses can also occur due to processes other than ocean warming, e.g., vegetation change (Jones et al.,
16 2009) or ice sheet melt that continues long after the forcing has been stabilized (see Section 12.5.2).

17
18 Another component that can delay a response to change in CO₂ emissions is the carbon cycle, which
19 involves similarly long timescales as the dominant long-term sink of anthropogenic CO₂ is controlled by the
20 surface to deep ocean mixing (e.g., Archer et al., 2009).

21
22 Several forms of commitment are often discussed in the literature. The most common is the “constant
23 composition commitment”, the warming that would occur after stabilizing all radiative constituents at a
24 given year (for example 2000) levels. AOGCMs estimated a most likely value of about 0.6°C for 2100
25 (relative to 1980–1999, AR4 Section 12.7.1) or 0.3°C (range 0.1–0.7°C across CMIP3) relative to the year
26 2000 (Knutti et al., 2008a). A year 2000 composition commitment simulations is not part of CMIP5, so
27 direct comparison with CMIP3 is not possible, however, the available CMIP5 results based on the RCP4.5
28 extensions (see section 12.5.1) are consistent with those numbers, with an additional warming of about 0.5°C
29 after stabilization of the forcing (Figure 12.4).

30
31 A measure of constant composition commitment is the fraction of realised warming which can be estimated
32 as the ratio of the warming at a given time to the long-term equilibrium warming (e.g., Solomon et al., 2009)
33 (Stouffer, 2004) (see also Meehl et al., 2007b, Section 10.7.2). EMICs simulations have been performed with
34 RCPs forcing up to 2300 prolonged until the end of the millennium with a constant forcing set at the value
35 reached by 2300. When the forcing stabilizes, the fraction of realized warming is around 85 ± 10%, and is
36 almost independent of the forcing scenario (Figure 12.43).

37 [INSERT FIGURE 12.43 HERE]

38 **Figure 12.43:** Atmospheric CO₂ forcing, b) projected global mean surface temperature warming and c) fraction of
39 realized warming calculate as the ratio of global temperature change at a given time to the change averaged over the
40 2980–2999 time period, as simulated by 4 EMICs (Bern3D, DCESS, MESMO and UVic) for the 4 RCPs up to 2300
41 followed by a constant (2300 level) radiative forcing up to the year 3000. A ten-year smoothing was applied.

42
43
44 “Constant emission commitment” is the warming that would result from keeping anthropogenic emissions
45 constant and is estimated for example at about 1–2.5°C by 2100 assuming constant (year 2010) emissions in
46 the future, based on the MAGICC model calibrated to CMIP3 and C4MIP (Meinshausen et al., 2011a;
47 Meinshausen et al., 2011b) (see FAQ 12.3).

48
49 Another form of commitment involves climate change when emissions are set to zero (“zero emission
50 commitment”). Results from a variety of models ranging from EMICs (Matthews and Caldeira, 2008; Meehl
51 et al., 2007b; Plattner et al., 2008; Solomon et al., 2009) to ESMs (Frolicher and Joos, 2010; Gillett et al.,
52 2011) show that abruptly switching carbon emissions to zero results in approximately constant global
53 temperature for several centuries onward. Those results indicate that past emissions commit us for hundreds
54 of years to approximately the amount of warming that has already been realized. On near equilibrium
55 timescales of a few centuries to about a millennia, the temperature response is controlled by climate
56 sensitivity (see Box 12.1) and the airborne fraction of CO₂ on these time-scales. After about a thousand years
57 (i.e., near thermal equilibrium), approximately 20–30% of the anthropogenic carbon emissions still remain in

1 the atmosphere (Archer et al., 2009; Frolicher and Joos, 2010; Montenegro et al., 2007; Plattner et al., 2008)
2 and produce a substantial temperature response long after emissions have ceased (Eby et al., 2009;
3 Friedlingstein and Solomon, 2005; Frolicher and Joos, 2010; Hare and Meinshausen, 2006; Lowe et al.,
4 2009; Matthews and Caldeira, 2008; Plattner et al., 2008; Solomon et al., 2009; Solomon et al., 2010). In the
5 transient phase, the approximately constant temperature results from a compensation of delayed commitment
6 warming (Meehl et al., 2005b; Wigley, 2005) with the reduction in atmospheric CO₂ resulting from deep
7 ocean carbon uptake as well as the nonlinear dependence of radiative forcing on atmospheric CO₂ (Meehl et
8 al., 2007b; Plattner et al., 2008; Solomon et al., 2009; Solomon et al., 2010). The commitment associated
9 with past emissions depends, as mentioned above, on the value of climate sensitivity and CO₂ airborne
10 fraction, but it also depends on the choices made for other radiative forcing constituents. In a CO₂ only case
11 and for sensitivities near the consensus value of 3°C, the warming commitment is near zero or slightly
12 negative. For high climate sensitivities, and in particular if aerosol emissions are eliminated at the same time,
13 the commitment from past emission can be strongly positive, and is a superposition of a fast response to
14 reduced aerosols emissions and a slow response associated with high climate sensitivities (Armour and Roe,
15 2011; Brasseur and Roeckner, 2005; Hare and Meinshausen, 2006; Knutti and Plattner, 2011) (see FAQ
16 12.3). All of the above studies support the conclusion that temperatures would decrease only slowly even for
17 strong reductions or complete elimination of CO₂ emissions, and might even increase temporarily for an
18 abrupt reduction of the short-lived gases (FAQ 12.3). The implications of this fact for climate stabilization
19 are discussed in Section 12.5.4.

20
21 New EMICs simulations with zero emissions beyond 2300 clearly confirm this behaviour (Figure 12.44)
22 seen in many earlier studies (see above). Switching off all anthropogenic emissions in 2300 leads to a
23 continuous slow decline of atmospheric CO₂, to a significantly slower decline of global temperature and to a
24 continuous increase in ocean thermal expansion over the course of the millennium. Larger forcings induce
25 longer delays before the Earth system would reach equilibrium. For RCP8.5, by year 3000 (700 years after
26 emissions have ceased) global temperature only drops by 1–2°C (relative to its peak value by 2300) and
27 thermal expansion has almost doubled (relative to 2300) and is still increasing.

28 29 **[INSERT FIGURE 12.44 HERE]**

30 **Figure 12.44:** a) compatible anthropogenic CO₂ emissions, b) projected atmospheric CO₂ concentration, c) global mean
31 surface temperature change and d) ocean thermal expansion, as simulated by 6 EMICs (Bern3D, CLIMBER
32 2, CLIMBER 3-alpha, DCESS, MESMO and UVic) for the 4 RCPs, assuming zero anthropogenic emissions after 2300.
33 A ten-year smoothing was applied.

34
35 The previous paragraph discussed climate change commitment from greenhouse gases that have already
36 been emitted. Another form of commitment refers to climate change associated with heat and carbon that has
37 gone into the land surface and oceans. This would be relevant to the consequences of a one-time removal of
38 all of the excess CO₂ in the atmosphere and is computed by taking a transient simulation and instantaneously
39 setting atmospheric CO₂ concentrations to initial (pre-industrial) values (Cao and Caldeira, 2010). In such an
40 extreme case, there would be a net flux of CO₂ from the ocean and land surface to the atmosphere, releasing
41 an amount of CO₂ representing about 30% of what was removed from the atmosphere. The net result is an
42 approximate halving of the warming on the time scale of centuries. A related form investigates the
43 consequences of an initial complete removal followed by sustained removal of any CO₂ returned to the
44 atmosphere from the land surface and oceans, and is computed by setting atmospheric CO₂ concentrations to
45 pre-industrial values and maintaining this concentration (Cao and Caldeira, 2010). In this case, only about
46 one-tenth of the pre-existing temperature perturbation persisted for more than half-century.

47
48 Several studies have demonstrated that the persistence of warming is substantially longer than anthropogenic
49 greenhouse gases themselves, as a result of non-linear absorption effects as well as the slow heat transfer into
50 and out of the ocean. In much the same way as the warming to a step increase of forcing is delayed, the
51 cooling after setting radiative forcing to zero is also delayed. A positive temperature anomaly is maintained
52 for decades to centuries to allow the ocean to lose its excess heat (Held et al., 2010; Solomon et al., 2010).

53
54 Beside the commitments described above, due inertia intrinsic to the climate system, there are a range of
55 different sources of inertia and hence commitments related the time-scales for energy system transitions
56 (Grubb, 1997). These sources of inertia in energy system transitions can be thought of as leading to
57 commitments in climate change. For example, Davis et al. (2010) estimated climate commitment of 1.3°C

(range 1.1–1.4°C, relative to preindustrial) from existing CO₂-emitting devices under the assumption that the lifetimes of these devices would not be extended beyond normal.

A more general form of commitment is therefore the question of how much can realistically be avoided and how much warming we are committed to (Washington et al., 2009). These forms of commitment however are strongly based on political, economic and social assumptions that are outside the domain of IPCC WGI and are not further considered here.

12.5.3 Global Measures of Climate Sensitivity and Transient Response

12.5.3.1 Ranges of CMIP5 and Observational Constraints Based on Climatology and Feedbacks

Equilibrium Climate Sensitivity (often termed ECS) in a model is usually defined as the equilibrium change in global surface temperature following a doubling of the atmospheric equivalent CO₂ concentration (see glossary). It measures the strength of all feedback processes that are important on long timescales in the model. The Transient Climate Response (TCR, the change in global surface temperature in a global coupled climate model in a 1% per year CO₂ increase experiment at the time of CO₂ doubling, see glossary) measures the transient temperature response to an external forcing, which depends both on the atmospheric, surface and land feedbacks but also on the transient ocean heat uptake. The two quantities are related in a nonlinear way, and the equilibrium response is larger than the transient. Both ECS and TCR are key benchmark numbers to characterize the temperature response to a given CO₂ forcing in a model. They provide important information for policy, to the extent that the concept of radiative forcing and climate feedbacks is applicable to the real world and to forcings other than greenhouse gases (see Section 12.5.3.2). The global temperature change on timescales of 50 to 100 years for scenarios with increasing forcing is approximately proportional to TCR because the ratio of temperature to forcing is nearly constant and invariant across scenarios (see AR4 Section 10.5.4.6, Appendix 10.A.1; (Gregory and Forster, 2008; Knutti et al., 2008b; Rogelj et al., 2011a). For climate stabilization (see Section 12.5.4), the equilibrium atmospheric CO₂ concentration and the equilibrium global temperature change are directly related through climate sensitivity. This section is an assessment focusing mainly on the recent literature and the reader is referred to IPCC AR4 (Sections 10.5.2.1, 10.5.4.4, 9.6, and Box 10.2) and recent reviews for a more comprehensive discussion of the large number of studies on climate sensitivity in particular (Edwards et al., 2007; Knutti and Hegerl, 2008).

From the models available so far, the range of climate sensitivities in CMIP5 is 2.1–4.6°C with a mean of 3.3°C. For the transient climate response the range is 1.3–2.5°C with a mean of 1.9°C. Note that in contrast to AR4, climate sensitivities are estimated as effective climate sensitivities from transient fully coupled rather than slab ocean simulations (see section 9.7.4). A scatter plot is shown in Figure 12.45, along with earlier estimates from AR4. Both means and standard deviations of climate sensitivities and transient responses in CMIP5 are similar to CMIP3.

[INSERT FIGURE 12.45 HERE]

Figure 12.45: Transient climate response (TCR) versus equilibrium climate sensitivity for the CMIP5 AOGCMs (red circles). Results from Meehl et al. (2007b) Figure 10.25 are given for comparison in black: circles mark CMIP3 models, triangles mark a perturbed physics ensemble of the HadCM3 AOGCM, crosses mark ranges covered by the IPCC TA AOGCMs for each quantity.

Several modelling groups have recently performed perturbed physics ensembles (PPE) to sample the parametric, and to some degree structural uncertainty (e.g., by switching between alternative parameterizations). The idea is to explore the range of possible model responses and to find relationships between model parameters and the simulated climate. Such relationships, if they exist, can be used to constrain model parameters, climate sensitivity, the transient response, or the regional response of any variable based on observations. The perturbation of atmospheric and surface albedo feedbacks in the Hadley Centre model leads to ranges of feedbacks and sensitivities much larger than the CMIP range (Collins et al., 2011; Knight et al., 2007; Piani et al., 2005; Sanderson et al., 2008a; Sanderson et al., 2008b; Stainforth et al., 2005). On the other hand, the range covered in the ECHAM and NCAR CCSM model are only about 2–5°C and 2.2–3.2°C, respectively (Klocke et al., 2011; Sanderson, 2011a, 2011b). A PPE based on perturbed land parameters yields an even narrower range of 0.5°C for climate sensitivity, dominated by the surface

1 albedo perturbations (Fischer et al., 2011). The spread in other variables and on small scales is of course
2 larger.

3
4 Relationships between climatological quantities and climate sensitivity are often found within a specific
5 PPE, but in many cases the relationship is not robust across PPEs from different models or in CMIP3
6 (Klocke et al., 2011; Knutti et al., 2006; Rougier et al., 2009; Sanderson, 2011b; Yokohata et al., 2010). This
7 implies that the model structure underlying a PPE is important (Masson and Knutti, 2011), and that a single
8 PPE is probably insufficient to constrain the climate sensitivity in the real world. Feedbacks related to clouds
9 and the water cycle are found to be particularly important for the spread of climate sensitivities (Rougier et
10 al., 2009; Sanderson et al., 2008b; Webb et al., 2006; Yokohata et al., 2010). Relationships between
11 observables and climate sensitivities in CMIP3 based on interannual variability (Wu and North, 2003), the
12 seasonal cycle (Knutti et al., 2006; Wu et al., 2008) and the regional radiation budget (Huber et al., 2011) are
13 generally weaker because models' structural uncertainty is also sampled. With one exception pointing to
14 higher sensitivities being more realistic (Shukla et al., 2006) most studies are unable to narrow the range of
15 climate sensitivities significantly if the observational uncertainty and the imperfect functional relationships
16 are properly accounted for. Several studies in fact point to a most likely value near 3°C that is similar to the
17 CMIP mean (Huber et al., 2011; Volodin, 2008; Wu et al., 2008) and most studies indicate a likely or very
18 likely range of about 2–5°C similar to the CMIP range (Huber et al., 2011; Wu et al., 2008). One
19 interpretation of this is that much of the climatological information available has been used to evaluate
20 AOGCMs already, and that the same data is therefore unable to constrain model behaviour further, at least
21 on a global scale. In contrast, local relationships between observable quantities and predicted changes across
22 models based on process understanding are more pronounced in a few cases, e.g., in the Southern Ocean
23 (Trenberth and Fasullo, 2010) or in the Arctic where models with more credible representations of the mean
24 climate, variability and observed trends predict stronger warming and sea ice melt and where the processes
25 are understood (Boe et al., 2009a; Boe et al., 2009b; Hall and Qu, 2006; Mahlstein and Knutti, 2011a;
26 Scherrer, 2011). However, results from CMIP5 are less clear for the Arctic, supporting the hypothesis that
27 biases to observations are often eliminated in newer models, without necessarily decreasing the spread of
28 projections (e.g., climate sensitivity).

29
30 This assessment of recently published constraints on climate sensitivity is consistent with several other
31 studies that attempt to link predictors of present day climate to the transient warming. Whetton et al. (2007)
32 and Knutti et al. (2010a) find that correlations between local to regional climatological values and projected
33 changes are small except for a few regions. Scherrer et al. (2011) find no robust relationship between the
34 ability of the CMIP3 models to represent interannual variability and their large scale transient projections.
35 Räisänen et al. (2010) report only small reductions (10–20%) in projected changes over the 21st century
36 when weighting the CMIP3 models by how well they reproduce present day climatology, and note that the
37 results are sensitive to the predictor variable and to some extent to the observational dataset.

38
39 The main difficulty in constraining AOGCMs with climatological data is measurement uncertainties, sparse
40 coverage in many observed variables, short time series for observed trends, lack of correlation between
41 observed quantities and projected past or future trends (Jun et al., 2008b; Knutti, 2010; Knutti et al., 2010a;
42 Tebaldi and Knutti, 2007), the ambiguity of possible metrics and the difficulty of associating them with
43 predictive skill (Eyring et al., 2005; Gleckler et al., 2008; Knutti et al., 2010b; Parker, 2006; Pierce et al.,
44 2009; Pincus et al., 2008; Reichler and Kim, 2008) and computational cost of running large samples of
45 coupled state of the art models at high resolution. In addition the sample of structurally different models is
46 small and many models share biases. The effective number of independent models is therefore likely to be
47 smaller than the actual number of models (Annan and Hargreaves, 2011b; Jun et al., 2008a; Knutti et al.,
48 2010b; Masson and Knutti, 2011; Tebaldi and Knutti, 2007). Another issue is selection bias, i.e., the fact that
49 statistical methods that test for correlations based on a large number of metrics, patterns and variables are
50 bound to find cases with significant correlations that appear by chance and are not robust when tested in a
51 different ensemble. This is particularly important for small ensembles like CMIP3 and if many predictors are
52 screened (DelSole and Shukla, 2009; Huber et al., 2011; Raisanen et al., 2010).

53
54 The assessed literature suggests that the range of climate sensitivities and transient responses covered by
55 CMIP3/5 cannot be narrowed significantly by constraining the models with observations of the mean climate
56 and variability. Studies based on PPE and CMIP3 support the conclusion that a credible representation of the
57 mean climate and variability is difficult to achieve with climate sensitivities below 2°C (Huber et al., 2011;

1 Klocke et al., 2011; Piani et al., 2005; Sanderson et al., 2008a; Sanderson et al., 2008b; Stainforth et al.,
2 2005). High climate sensitivity values above 5°C (in some cases above 10°C) are found in the PPE based on
3 HadAM/HadCM3. Several recent studies find that such high values cannot be excluded based on
4 climatological constraints, but are much less likely than values in the consensus range of 2–4.5°C (Knutti et
5 al., 2006; Piani et al., 2005; Rodwell and Palmer, 2007; Sanderson et al., 2008a; Sanderson, 2011a, 2011b;
6 Sanderson et al., 2010; Sanderson et al., 2008b). An overall assessment of climate sensitivity and transient
7 response is given in Box 12.1.

8
9 Observational constraints on the transient climate response mostly come from the observed warming over the
10 last century and are discussed in Section 10.9.1 and shown in Box 12.1, Figure 2.

11 12.5.3.2 Forcing and Response, Timescales of Feedbacks

12
13
14 Equilibrium climate sensitivity, transient climate response and climate feedbacks are useful concepts to
15 characterize the response of a model to an external forcing perturbation. However, there are limitations to the
16 concept of radiative forcing (Hansen et al., 2005b; Joshi et al., 2003; Shine et al., 2003; Stuber et al., 2005),
17 and the separation of forcings and fast feedbacks (e.g., clouds changing almost instantaneously as a result of
18 CO₂ induced heating rates rather than as a response to the slower surface warming) is sometimes difficult
19 (Andrews and Forster, 2008; Gregory and Webb, 2008). Equilibrium warming also depends on the type of
20 forcing (Davin et al., 2007; Hansen et al., 2005b; Stott et al., 2003). Climate sensitivity is time or state
21 dependent in some models (Boer et al., 2005; Gregory et al., 2004; Senior and Mitchell, 2000), and in some
22 but not all models climate sensitivity from a slab ocean version differs from that of coupled models or the
23 effective climate sensitivity (see glossary) diagnosed from a transient coupled integration (Danabasoglu and
24 Gent, 2009; Gregory et al., 2004; Li et al., 2011a). The cost of coupled AOGCMs is often prohibitively large
25 to run simulations to full equilibrium, and only a few models have performed those (Danabasoglu and Gent,
26 2009; Gregory et al., 2004; Li et al., 2011a; Manabe and Stouffer, 1994; Voss and Mikolajewicz, 2001).
27 Because of the time dependence of effective climate sensitivity, fitting simple models to AOGCMs over the
28 first few centuries may lead to errors in the response on multi-century timescales. In the HadCM3 case the
29 long term warming would be underestimated by 30% if extrapolated from the first century (Gregory et al.,
30 2004), in other models the warming of the slab and coupled model is almost identical (Danabasoglu and
31 Gent, 2009). The assumption that the response to different forcings is approximately additive appears to be
32 justified for large scale temperature (Jones et al., 2007; Meehl et al., 2004). A more complete discussion of
33 the concept of equilibrium climate sensitivity and the limitations is given in Knutti and Hegerl (2008).

34
35 A number of recent studies suggest that equilibrium sensitivities determined from AOGCMs and recent
36 warming trends may significantly underestimate the true Earth System sensitivity if equilibration on
37 millennial timescales is considered (Hansen et al., 2008; Lunt et al., 2010; Pagani et al., 2010; Rohling et al.,
38 2009). The argument is that slow feedbacks associated with vegetation changes and ice sheets have their own
39 intrinsic long timescales and are not considered in most models (Jones et al., 2009). Additional feedbacks are
40 mostly thought to be positive but negative feedbacks of smaller magnitude are also simulated (Goelzer et al.,
41 2011; Swingedouw et al., 2008). The climate sensitivity of a model may therefore not reflect the sensitivity
42 of the full Earth system because those feedback processes are not considered. Feedbacks determined in very
43 different base state (e.g., the Last Glacial Maximum) differ from those in the current warm period, and
44 relationships between observables and climate sensitivity are model dependent (Crucifix, 2006; Edwards et
45 al., 2007; Hargreaves et al., 2007; Schneider von Deimling et al., 2006). Estimates of climate sensitivity
46 based on paleoclimate archives (Hansen et al., 2008; Lunt et al., 2010; Pagani et al., 2010; Rohling et al.,
47 2009) are therefore not necessarily representative for an estimate of climate sensitivity in a world warmer
48 than the current. Also it is uncertain on which timescale some of those Earth system feedbacks would
49 become significant.

50
51 Equilibrium climate sensitivity undoubtedly remains a key quantity that is useful to relate a change in
52 greenhouse gases or other forcings to a global temperature change. But the above caveats imply that
53 estimates based on past climate states very different from today, based on timescales different than those
54 relevant for climate stabilization (e.g., the eruption of Pinatubo), or based on forcings other than greenhouses
55 gases (e.g., spatially non-uniform land cover changes, volcanic eruptions or solar forcing) may differ from
56 the climate sensitivity measuring the climate feedbacks of the Earth system today, and that again may be
57 different from the sensitivity of the Earth in a much warmer state on timescales of millennia.

12.5.4 Climate Stabilization and Long-term Climate Targets

This section discusses the relation between emission and climate targets, based on uncertainties in both the transient and the equilibrium climate responses to emissions. This includes both the stabilization at a given temperature and avoiding a warming beyond a predefined threshold. The latter idea of limiting peak warming is a more general concept that stabilization of temperature and atmospheric CO₂, and one that is more likely to happen than an exact climate stabilization which would require perpetual non-zero positive emissions to counteract the otherwise ineluctable long-term slow decrease in global temperature (Figure 12.44).

12.5.4.1 Background

Limiting climate impacts requires stabilizing climate change at an appropriate level or returning to it before these impacts become too large. The concept of stabilization is strongly linked to the ultimate objective of the UNFCCC which is “to achieve [...] stabilization of greenhouse gas concentrations in the atmosphere at a level that would prevent dangerous anthropogenic interference with the climate system.” Recent policy discussions focused on a global temperature increase, rather than on greenhouse gas concentrations. The most prominent target currently supported is the 2°C temperature target, i.e., to limit global temperature increase relative to preindustrial times to below 2°C. The 2°C target has been used first by the European Union as a policy target in 1996 but can be traced further back (Jaeger and Jaeger, 2011; Randalls, 2010). Climate impacts however are geographically diverse and different for each sector, and no objective threshold separates dangerous from acceptable interference. Some changes may be delayed or irreversible, and some impacts are likely to be beneficial. It is thus not possible to define a single critical threshold without making value judgments and assumptions about cost and benefit and about aggregating and comparing values today and in the future. Targets other than 2°C have been proposed (e.g., 1.5°C relative to preindustrial), or 350 ppm (Hansen et al., 2008), and the rate of change may also be important (e.g., for adaptation). This section does not advocate or defend any threshold, nor does it judge the economic or political feasibility of such goals, but simply assesses the implications of different illustrative climate targets on allowed carbon emissions, based on our current understanding of climate and carbon cycle feedbacks.

12.5.4.2 Constraints on Cumulative Carbon Emissions

The total amount of anthropogenic CO₂ released in the atmosphere (often termed cumulative carbon emission) is a good measure of peak atmospheric CO₂ and hence of the global transient or peak warming response. The ratio of global temperature to total cumulative anthropogenic emissions (transient and equilibrium climate response to carbon emissions) is relatively constant and independent of the scenario, but is model dependent as it depends on the model airborne fraction and climate sensitivity (Allen et al., 2009; Knutti and Plattner, 2011; Matthews and Caldeira, 2008; Matthews et al., 2009; Meinshausen et al., 2009; Zickfeld et al., 2009). This is consistent with an earlier study indicating that the global warming potential is approximately independent of the scenario (Caldeira and Kasting, 1993).

Assuming constant climate sensitivity and given carbon cycle feedbacks, stabilization of global temperatures requires to stabilize atmospheric concentrations, which would lead to eventual temperature stabilization at equilibrium after several centuries. This requires decreasing emissions to the level of natural carbon sinks, and eventually to near-zero (Allen et al., 2009; Jones et al., 2006; Knutti and Plattner, 2011; Matthews and Caldeira, 2008; Meehl et al., 2007b; Meinshausen et al., 2009; Plattner et al., 2008; Weaver et al., 2007; Zickfeld et al., 2009).

The relationships between cumulative emissions and temperature for various studies is shown in Figure 12.46. Note that some lines mark the evolution of temperature as a function of emissions over time while other panels show peak temperatures for different simulations. Also some models prescribe only CO₂ emissions while others use multi gas scenarios, and the time horizons differ. Matthews et al. (2009) estimated the transient climate response to emission (TCRE) as 1–2.1°C/TtC (5–95%) based on the C4MIP model range (Figure 12.46). Allen et al. (2009) used a simple model and found 1.3–3.9°C/TtC (5–95%) for peak warming. The EMIC simulations so far suggest a range of about 2–3°C/TtC (12.46f). Rogelj et al. (2011a) estimate a 5–95% range of about 1–2°C/TtC (Figure 12.46d) based on the MAGICC model calibrated

1 to the C4MIP model range and the likely range of 2–4.5°C for climate sensitivity given in AR4. The
2 ENSEMBLES E1 show a range of 1–4°C/TtC (scaled from 0.5–2°C for 0.5TtC, Figure 12.46c) (Johns et al.,
3 2011). The results by Meinshausen et al. (2009) confirm the approximate linearity between temperature and
4 emissions. Their results are difficult to compare due to the short time period considered, but the model was
5 found to be consistent with that of Allen et al. (2009). Zickfeld et al. (2009) find a best estimate of about
6 1.5°C/TtC. Another estimate of TCRE can be obtained from the very likely range of transient climate
7 response of 1–3°C. The current airborne fraction is about 45% and slightly increasing (Le Quere et al.,
8 2009). For an assumed airborne fraction range of 50±5% for 1 TtC and simply combining the extreme
9 assumptions for both ranges, this would imply a very likely range of 1.8±1°C/TtC.

10
11 Expert judgement based on the available evidence therefore suggest that the transient response to cumulative
12 carbon emission (TRCE) is *very likely* between 1–3°C/TtC (10^{12} metric tons of carbon), with a best estimate
13 in the range of 1.5–2.0°C/TtC, for cumulative emissions in the 0.5–2 TtC range until the time at which
14 temperatures peak. Under these conditions, and for low to medium estimates of climate sensitivity, the
15 TRCE is near identical to the peak response to cumulated carbon emissions (PRCE). For high climate
16 sensitivity and/or strong carbon cycle climate feedback and for larger cumulative emissions the peak
17 warming can be delayed and PRCE may be substantially larger than TRCE, but is poorly constrained by
18 models and observations. The best estimate is similar to other recent attempts to synthesize the available
19 evidence (Matthews et al., 2011; NRC, 2011). The upper bound is more uncertain and there is less agreement
20 across studies, but in general the results from various methods and models are consistent. The results by
21 Schwartz et al. (2011) are inconsistent with the above evidence and are questioned in the literature (Knutti
22 and Plattner, 2011). They are not based on a climate model and neglect the relevant response timescales.

23
24 An equilibrium climate response to emissions (ECRE) on a timescale of about 1000 years after emission
25 cease can in principal be estimated based on the likely range of equilibrium climate sensitivity (2–4.5°C) and
26 an airborne fraction after about 1000 yrs of $25 \pm 5\%$ (Archer et al., 2009). Again combining the extreme
27 values would suggest a range of 0.8–2.7°C/TtC with a best estimate of 1.5°C. The most likely warming
28 estimated for 1000 years is slightly lower than the peak warming, consistent with small decrease of
29 temperature seen in many simple models and EMICs after zeroing emissions (Armour and Roe, 2011; Meehl
30 et al., 2007b; Plattner et al., 2008; Solomon et al., 2009) (see also FAQ 12.3, Figure1). However, this
31 equilibrium estimate is based on feedbacks estimated for the present day climate. Both climate and carbon
32 cycle feedbacks increase substantially on long timescales and for high cumulative emissions (see 12.5.3.2),
33 introducing large uncertainties in particular on the upper bound.

34 [INSERT FIGURE 12.46 HERE]

35
36 **Figure 12.46:** Global temperature change vs. cumulative emissions for different scenarios and models. a) Transient
37 global temperature increase vs. cumulative carbon emissions for C4MIP (Matthews et al., 2009), b) maximum
38 temperature increase until 2100 vs. cumulative Kyoto-gas emissions (CO₂ equivalent) (Meinshausen et al., 2009), c) as
39 in panel a but for the ENSEMBLES E1 scenario (Johns et al., 2011), d) transient temperature increase for the RCP
40 scenarios based on the MAGICC model constrained to C4MIP, observed warming, and the IPCC AR4 climate
41 sensitivity range (Rogelj et al., 2011a), e) peak CO₂ induced warming vs. cumulative CO₂ emissions to 2200 (Allen et
42 al., 2009; Bowerman et al., 2011), f) transient temperature increase from the new EMIC simulations (see Figure 12.44).

43 44 [START BOX 12.1 HERE]

45 **Box 12.1: Equilibrium Climate Sensitivity and Transient Climate Response**

46
47 Equilibrium climate sensitivity and the transient climate response can be estimated based on feedback
48 analysis in climate models (see Section 9.7.4), the patterns of mean climate and variability in models
49 compared to observations (Section 12.5.3.1), and based on paleoclimate archives, short term perturbations of
50 the energy balance like the Pinatubo eruption, and the observed surface and ocean temperature trends since
51 preindustrial (see Section 10.9.3).

52
53 Newer studies of the observed 20th century warming, based on simple and intermediate complexity models,
54 improved statistical methods, and several different and newer datasets largely confirm earlier studies
55 showing that climate sensitivity is likely in the 2–4.5°C range, and TCR is very likely in the 1–3°C range.
56 Despite substantial uncertainty ranges, the results from those methods, along with the feedbacks simulated
57
58

1 by AOGCMs are the ones that translate in the most direct way to quantifying future warming on century
2 timescales. Results based on shorter climate variations and paleoclimate evidence are consistent with those
3 ranges, and sometimes more narrow, but make stronger structural assumptions (see section 12.5.3.2). A few
4 studies argued for low values of climate sensitivity, but almost all of them have received criticism in the
5 literature (see Knutti and Hegerl (2008) and references therein). A summary of published ranges and PDFs
6 of climate sensitivity is given in Box 12.1, Figure 1. Distributions and ranges for the transient climate
7 response are shown in Box 12.1, Figure 2.

8
9 **[INSERT BOX 12.1, FIGURE 1 HERE]**

10 **Box 12.1, Figure 1:** Probability density functions, distributions and ranges for equilibrium climate sensitivity, based on
11 Figure 10.20b plus climatological constraints shown in IPCC AR4 Box 12.2 Figure 1.

12
13 **[INSERT BOX 12.1, FIGURE 2 HERE]**

14 **Box 12.1, Figure 2:** Probability density functions, distributions and ranges (5–95%) for the transient climate response
15 from different studies. See Figure 10.20a for details.

16
17 Combining information from different constraints from the observed warming trends, volcanic eruptions,
18 model climatology, and paleoclimate, e.g., by using a distribution obtained from the Last Glacial Maximum
19 as a prior for the 20th century analysis, yields a more narrow range for climate sensitivity (Annan and
20 Hargreaves, 2006; Annan and Hargreaves, 2011a; Hegerl et al., 2006). However, those methods are sensitive
21 to the assumptions on the independence of the various lines of evidence, the possibility of shared biases in
22 models or feedback estimates (Lemoine, 2010), and the assumption that each individual line of evidence is
23 unbiased. The assessed literature provides no consensus on a formal statistical method to combine different
24 lines of evidence. All methods in general are sensitive to the assumed prior distributions (Annan and
25 Hargreaves, 2011a; Frame et al., 2005; Hegerl et al., 2006; Tomassini et al., 2007). Annan and Hargreaves
26 (2011a) criticize the use of uniform priors and argue that sensitivities above 4.5°C are extremely unlikely
27 (<5%). On the other hand fourteen experts in a recent expert elicitation on average allocate a probability of
28 22% to sensitivities above 4.5°C (Zickfeld et al., 2010), indicating still little consensus on the probability for
29 high climate sensitivity.

30
31 Despite considerable advances in climate models and in understanding and quantifying climate feedbacks,
32 the assessed literature and recent reviews (Edwards et al., 2007; Knutti and Hegerl, 2008) still supports the
33 conclusion from AR4 that climate sensitivity is likely in the range 2–4.5°C, and very likely above 1.5°C. The
34 most likely value remains near 3°C. Values above 4.5°C are found in some models, and are not inconsistent
35 with observed warming trends, but are less likely to agree with observations and reconstructions of past
36 changes (see sections 10.9.4 and 12.5.1).

37
38 Paleoclimate and modelling evidence suggest that on timescales of centuries to millennia, additional positive
39 or negative feedbacks not currently represented in most models, associated for example with ice sheet
40 melting (Goelzer et al., 2011) or vegetation change (Jones et al., 2009) may change the sensitivity of the
41 system. In contrast to the classical ‘Charney sensitivity’ which only considers the feedbacks associated with
42 water vapour, lapse rate, clouds and albedo, this ‘Earth system sensitivity’ may be significantly higher
43 (Hansen et al., 2008; Jones et al., 2009; Lunt et al., 2010; Pagani et al., 2010; Rohling et al., 2009), implying
44 that lower atmospheric CO₂ concentrations are needed to meet a given temperature target. A number of
45 caveats however apply to those studies (see section 12.5.3.2). For climate stabilization, the allowed
46 cumulative carbon emissions are another useful metric relating emissions directly to temperature. It
47 considers carbon cycle feedbacks and uncertainties, but not additional feedbacks associated for example with
48 the release of methane hydrates or large amounts of carbon from permafrost (see Section 12.5.4, FAQ 12.3).

49
50 The assessment suggests that the transient climate response (TCR) is very likely in the range 1–3°C, with a
51 most likely value near 2°C based on the observed global changes in surface temperature and ocean heat
52 uptake, the detection/attribution studies identifying the response patterns to increasing greenhouse gas
53 concentrations (Section 10.9.1), and the results of CMIP3/5 (Figure 12.45). Estimating TCR is partly limited
54 by the difficulty in accurately estimating the current disequilibrium of the Earth, but suffers from fewer
55 difficulties in terms of time-dependent feedbacks (see Section 12.5.3.2), and is more relevant for projections
56 on timescales of a few decades. While the uncertainties for both climate sensitivity and TCR are not
57 significantly different from those estimated in AR4, the amount and quality of evidence has increased

1 substantially. The results are supported by several different lines of evidence, each based on multiple studies,
2 models and datasets.

3
4 Another quantity relevant for temperature stabilization is the transient response to cumulative carbon
5 emission (TRCE) is *very likely* between 1–3°C/TtC (10^{12} metric tons of carbon), with a best estimate in the
6 range of 1.5–2.0°C/TtC, for cumulative emissions in the 0.5–2 TtC range until the time at which
7 temperatures peak. Under these conditions, and for low to medium estimates of climate sensitivity, the
8 TRCE is near identical to the peak response to cumulated carbon emissions (PRCE). For high climate
9 sensitivity and/or strong carbon cycle climate feedback and for larger cumulative emissions the peak
10 warming can be delayed and PRCE may be substantially larger than TRCE, but is poorly constrained by
11 models and observations (see section 12.5.4). Those values have the advantage of directly relating
12 temperature change to emissions, but as a result of combining the uncertainty in both the climate sensitivity
13 or TCR and the carbon cycle response, they are also similarly uncertain.

14
15 **[END BOX 12.1 HERE]**

16 17 18 *12.5.4.3 Limitations and Conclusions*

19
20 One general limitation is that stabilization of global temperature does not imply stabilization for all aspects
21 of the climate system. For example, some models find significant hysteresis behaviour in the global water
22 cycle, because global precipitation depends on both atmospheric CO₂ and temperature (Wu et al., 2010).
23 Processes related to vegetation change (Jones et al., 2009) or changes in the ice sheets (Ridley et al., 2010) as
24 well as ocean acidification, deep ocean warming and associated sea level rise (Meehl et al., 2005b; Wigley,
25 2005) and potential feedbacks linking for example ocean and the ice sheets (Gillett et al., 2011; Goelzer et
26 al., 2011) have their own intrinsic long timescales. Those may result in significant changes hundreds to
27 thousands of years after global temperature is stabilized.

28
29 The simplicity of the concept of a cumulative carbon budget makes it attractive for policy (WBGU, 2009).
30 Higher emissions in earlier decades simply imply lower emissions by the same amount later on. This is
31 illustrated based on the RCP2.6 scenario in Figure 12.47a/b. Two idealized emission pathways with initially
32 higher emissions (even sustained at high level for a decade in one case) lead to the same warming if
33 emissions are then reduce much more rapidly. Even a step-wise emission pathway with levels constant at
34 2010 and zero near mid century leads to a similar temperature evolution as they all have identical cumulative
35 emissions. However, there are also limitations to the concept of a cumulative carbon budget. First, the ratio
36 of global temperature and cumulative carbon is only approximately constant. It is the result of an interplay of
37 several compensating carbon cycle and climate feedback processes, which operate at different timescales.
38 This assessment tries to account for that by providing a best estimate and range for the transient, peak, and
39 equilibrium warming. Second, the ratio strongly depends on the model's climate sensitivity and climate-
40 carbon cycle feedbacks, thus the allowed emissions for a given temperature target are uncertain (see Figure
41 12.43) (Knutti and Plattner, 2011; Matthews et al., 2009). Third, non-CO₂ forcing constituents are important,
42 which requires assumptions on how CO₂ emission reductions are linked to changes in other forcings
43 (Meinshausen et al., 2006; Meinshausen et al., 2009). So far, most studies ignored non-CO₂ altogether.
44 Those which consider them find non-negligible effects in particular for abrupt reductions in emissions of
45 short-lived species (Armour and Roe, 2011; Brasseur and Roeckner, 2005; Hare and Meinshausen, 2006)
46 (see also FAQ 12.3). Fourth, most models do not consider the possibility that long term feedbacks (Hansen et
47 al., 2007; Jones et al., 2009; Knutti and Hegerl, 2008) may be different (see Section 12.5.2). Despite the fact
48 that stabilization refers to equilibrium, the results assessed here are primarily relevant for the next few
49 centuries and may differ for millennial scales. Finally, the concept of cumulative carbon implies that higher
50 initial emissions can be compensated by a faster decline in emissions later or by negative emissions.
51 However, in the real world short-term and long term goals are not independent and mitigation rates are
52 limited by economic constraints and existing infrastructure (Davis et al., 2010; Meinshausen et al., 2009;
53 Mignone et al., 2008; Rive et al., 2007). Likewise, assuming a cumulative carbon budget that requires
54 negative emissions at a later stage will imply a temporal overshoot of a given target. An updated analysis of
55 193 published emission pathways with an energy balance model (Rogelj et al., 2011b; UNEP, 2010) is
56 shown in Figure 12.47c/d. Those emission pathways that likely limit warming below 2°C (above pre-
57 industrial) by 2100 show emission of about 31–46 GtCO₂eq and 17–23 GtCO₂eq by 2020 and 2050,

1 respectively. Median 2010 emissions of all models are 48 GtCO₂eq. In cumulative terms, the best estimate for
2 the transient climate response to cumulative carbon emissions (TCRE) is in the range of 1.5–2.0°C/TtC,
3 implying a most likely value for the cumulative budget compatible with stabilization at 2°C of about 1000–
4 1300 GtC, of which about 520 GtC have been emitted by 2011. Note that, as opposed to 12.47a/b, these
5 scenarios still have positive emissions by 2100, implying that the warming would probably exceed the target
6 in the longer-term.

7 8 **[INSERT FIGURE 12.47 HERE]**

9 **Figure 12.47:** a) CO₂ emissions for the RCP3PD scenario (black) and three illustrative modified emission pathways
10 leading to the same warming, b) global temperature change relative to preindustrial for the pathways shown in panel a.
11 c) Coloured bands show IAM emission pathways over the twenty-first century. The pathways were grouped based on
12 ranges of “likely” avoided temperature increase in the twenty-first century. Pathways in the yellow, orange and red
13 bands likely stay below 2°C, 3°C, 4°C by 2100, respectively, while those in the purple band are higher than that.
14 Emission corridors were defined by, at each year, identifying the 20th to 80th percentile range of emissions and drawing
15 the corresponding coloured bands across the range. Individual scenarios that follow the upper edge of the bands early
16 on tend to follow the lower edge of the band later on, d) global temperature relative to preindustrial for the pathways in
17 panel a. Data in panels c,d based on Rogelj et al. (2011b).

18 19 **12.5.5 Abrupt Change and Irreversibility**

20 21 *12.5.5.1 Introduction*

22
23 For the purposes of this section we adopt the definition of abrupt climate change used in Synthesis and
24 Assessment Product 3.4 of the U.S. Climate Change Science Program CCSP (CCSP_3.4, 2008). We define
25 *abrupt climate change* as a large-scale change in the climate system that takes place over a few decades or
26 less, persists (or is anticipated to persist) for at least a few decades, and causes substantial disruptions in
27 human and natural systems.

28
29 A number of elements within the Earth system are thought to possess critical thresholds, or *tipping points*,
30 beyond which transitions to new states of the element ensue. These so-called *tipping elements* (Lenton et al.,
31 2008) include the Atlantic meridional overturning, sea ice, the Greenland ice sheet, the Amazon forest, and
32 monsoonal circulation. These and other tipping elements are addressed in the remainder of this section.

33
34 Abrupt climate change may arise as a consequence of an element passing a tipping point. Such a change is
35 said to be irreversible on a given time scale if the removal of the perturbation that caused the system to pass
36 a tipping point does not lead to a recovery of the tipping element due to natural processes within this time
37 scale. In the context of interest here, the pertinent time scale is centennial to millennial.

38 39 *12.5.5.2 The Atlantic Meridional Overturning*

40
41 Models for which the stability has been systematically assessed by suitably designed hysteresis experiments
42 robustly show a threshold beyond which the Atlantic thermohaline circulation cannot be sustained
43 (Rahmstorf et al., 2005). It is very likely that global warming will move the climate system towards this
44 threshold. However, how close we are to this threshold is highly model-dependent and influenced by factors
45 that are currently poorly understood. Moreover there is some indication that most climate models may
46 overestimate the stability of the Atlantic ocean circulation (Drijfhout et al., 2010; Hofmann and Rahmstorf,
47 2009). In addition to the main threshold for a complete breakdown of the circulation, others may exist that
48 involve more limited changes, such as a cessation of Labrador Sea deep water formation (Wood et al., 1999)
49 (see also section 12.4.7.2). Rapid melting of the Greenland ice sheet causes increases in freshwater runoff,
50 potentially weakening the Atlantic meridional overturning circulation (AMOC). However, Jungclaus et al.
51 (2006), Mikolajewicz et al. (2007a), Driesschaert et al. (2007) and Hu et al. (2009) found only a small
52 temporary effect of increased melt water fluxes on the AMOC, that was either small compared to the effect
53 of enhanced poleward atmospheric moisture transport or only noticeable in the most extreme scenarios.

54 55 *12.5.5.3 Sea Ice*

56
57 Several studies (e.g., Lenton et al., 2008; Lindsay and Zhang, 2005) and the popular media have questioned
58 whether the loss of the summer Arctic sea ice might reach a tipping point with a critical threshold beyond

1 which sea ice loss is irreversible. In some climate projections, the future decrease in summer Arctic sea ice
2 coverage is not gradual but is instead punctuated by 5–10 year periods of rapid ice loss (Holland et al.,
3 2006). However, rapid sea ice loss events do not necessarily require a critical threshold or irreversible
4 behaviour (Amstrup et al., 2010). For example, the events discussed by Holland et al. (2006) appear to result
5 from the combination of the large interannual climate variability and forced change in the Arctic (Holland et
6 al., 2008), and the sea ice variability is made up of periods of rapid sea ice advance as often as retreat.

7
8 Further work using a single-column energy balance model (Eisenman and Wettlaufer, 2009) and
9 atmosphere-ocean general circulation models (Amstrup et al., 2010; Armour et al., 2011; Sedlacek et al.,
10 2011; Tietsche et al., 2011) found no evidence of a critical threshold in the transition from perennial ice-
11 covered to a seasonally ice-free Arctic Ocean beyond which further sea ice loss is unstoppable and
12 irreversible (on centennial timescales for present forcing). Research shows that sea ice can recover because
13 thin ice and snow cover promotes strong longwave radiation loss to space and high ice growth rates (Bitz and
14 Roe, 2004; Notz, 2009; Tietsche et al., 2011). These stabilizing negative feedbacks in the system are enough
15 to overcome the positive surface albedo feedback, which acts to amplify the sea ice response. In most models
16 the relationship between temperature and sea ice cover is approximately linear, and the results from the
17 newer CMIP5 models support those conclusions (see Section 12.4.6).

18
19 In contrast, some studies have questioned whether the transition from seasonal to year-round ice-free
20 conditions, after raising CO₂ to very high levels, exhibits a critical threshold in a few CMIP3 models (Ridley
21 et al., 2007; Winton, 2006a). Winton (2006a; 2008) hypothesize that the small ice cap instability (North,
22 1984) could cause such an abrupt transition. Eisenman and Wettlaufer (2009) also found that a critical
23 threshold in the transition from seasonal ice to year-round ice-free conditions is plausible, but they concluded
24 that the cause is a loss of the stabilizing effect of sea ice growth when the ice season shrinks in time.
25 However, recent work (Armour et al., 2011) suggests that, when reversibility is directly assessed in one
26 CMIP3 model, the loss of year-round Arctic sea ice is reversible under reductions in greenhouse gas
27 concentrations and there is no evidence for multiple stable ice cover states.

28
29 Regardless of the cause, rapid sea ice loss has consequences throughout the climate system as noted by
30 Vavrus et al. (2011) for cloud cover and Lawrence et al. (2008) for the high-latitude ground thermal state.
31 Furthermore, the interannual-decadal variability in the summer Arctic sea ice extent is predicted to increase
32 in response to global warming (Goosse et al., 2009; Holland et al., 2008). These studies suggest that large
33 anomalies in sea ice coverage, like the one that occurred in 2007, might become increasingly frequent. Thus,
34 while instances of rapid summer Arctic sea ice loss are likely to occur in the future, it appears unlikely that
35 these result from a critical threshold in the system.

36 37 *12.5.5.4 Ice Sheets*

38
39 All available modelling studies agree that the Greenland ice sheet will significantly decrease in area and
40 volume in a warmer climate. If the warming is maintained for a sufficiently long period, a total decay of the
41 ice sheet results. Modelling studies of the threshold temperature increase (with respect to preindustrial
42 levels) that is necessary for near-complete GIS decay strongly depends on the processes taken into account
43 and on the boundary conditions applied (Bougamont et al., 2007; Gregory and Huybrechts, 2006; Stone et
44 al., 2010). This threshold might therefore lie outside, and in particular below, the range of $3.1 \pm 0.8^\circ\text{C}$ global
45 mean annual temperature change suggested by Gregory and Huybrechts (2006) based on the notion that a
46 negative spatially integrated surface mass balance is a sufficient but not necessary condition for ice-sheet
47 decay. Results from the few available long-term Antarctic ice sheet (AIS) simulations with coupled climate-
48 ice sheet models are contradictory due to differences in the treatment of surface mass balance, grounding-
49 line migration and ice sheet–ice shelf interactions in their respective AIS components. In some experiments
50 (Mikolajewicz et al., 2007a; Mikolajewicz et al., 2007b; Vizcaino et al., 2008), the AIS grows under all
51 warming scenarios considered because of increased snowfall, while a different treatment of the surface mass
52 balance in Vizcaino et al. (2010) led to mass loss under a 4 x CO₂ scenario after about 150 years.

53
54 Irreversibility of ice-sheet volume and extent changes can arise because of the surface-elevation feedback
55 that operates when a decrease of the elevation of the ice sheet induces a decreased surface mass balance
56 (generally through increased melting), and therefore essentially applies to Greenland. Using a high-
57 resolution ice sheet model coupled to HadCM3, Ridley et al. (2010) found that the present-day GIS could be

1 reformed only if the volume had not fallen below a threshold of irreversibility, situated between 80 and 90%
2 of the original value. Depending on the degree of warming, this point-of-no-return could be reached within a
3 few hundred years, sooner than global climate could revert to its pre-industrial state. Charbit et al. (2008)
4 linked irreversible decay of the Greenland ice sheet to a cumulative CO₂ emission above 3000 GtC. For
5 weaker emissions, the Greenland ice sheet could recover over several thousand years.

6
7 Ice-sheet volume and extent changes can be abrupt because of the so-called grounding line instability. This
8 can occur in coastal regions where bedrock is retrograde (Schoof, 2007; Weertmann, 1974). In this case, the
9 grounding line could in theory rapidly retreat until a position with opposite bedrock slope is attained.
10 Bedrock is below sea level in large portions of West Antarctica, but also in parts of East Antarctica, notably
11 in Wilkes Land (Le Brocq et al., 2010; Roberts et al., 2011). If the grounding line attains the limits of these
12 sub-glacial basins during initially gradual ice sheet retreat, grounding line instability might occur in these
13 regions. However, an assessment of the potential for the future occurrence of abrupt ice sheet retreat due to
14 grounding line instabilities, and to what degree these possible abrupt changes would be irreversible on
15 centennial time scales, is currently impossible due to incomplete process understanding and model
16 limitations.

17 18 *12.5.5.5 Hydrologic Variability: Megadroughts and Monsoonal Circulation*

19 20 *12.5.5.5.1 Megadroughts*

21 As noted in Sections 5.5.2.4 and 5.6.2, megadroughts are a recurring feature of Holocene paleoclimate
22 records in North America, east and south Asia, Europe, Africa and India. The transitions into and out of the
23 megadroughts take many years and do not appear abrupt in the sense of indicating nonlinearity in the
24 physical system. Since the megadroughts all ended they are also not irreversible. Nonetheless transitions
25 over years to a decade into a state of elevated aridity would have seriously stressed human populations and
26 would do so again should a megadrought reoccur.

27
28 While previous megadroughts in southwest North America arose from natural causes, climate models project
29 that this region will undergo progressive aridification as part of a general drying and poleward expansion of
30 the subtropical dry zones driven by rising greenhouse gases (Held and Soden, 2006; Seager and Vecchi,
31 2010; Seager et al., 2007). The models project the aridification to intensify steadily as radiative forcing and
32 global warming progress without abrupt changes. Solomon et al. (2009) has considered the question of how
33 precipitation will be changed in the future for the hypothetical case of increasing CO₂ emissions followed by
34 immediate cessation of emissions. According to Solomon et al. (2009), carbon cycle modelling indicates that
35 after ending emissions 40% of the peak CO₂ concentration enhancement over the pre-industrial value
36 remains in the atmosphere on millennium timescale. Solomon et al. (2009) show that if, for example, CO₂
37 rises to 600 ppm followed by zero emissions, the quasi-equilibrium CO₂ is about 400 ppm which, it is
38 claimed on the basis of the climate models used in AR4, would reduce precipitation in key areas such as
39 southwest North America, southern Europe and western Australia by as much as 15%. Multiyear droughts in
40 the past that led to significant social crises (such as the U.S. Dust Bowl of the 1930s) had comparable
41 precipitation reductions. Action to ensure a lower peak CO₂ or allowing CO₂ to peak even higher would lead
42 to less or more aridification. If CO₂ concentrations are allowed to peak at around twice pre-industrial levels,
43 hydrological changes of serious amplitude would be irreversible on the millennium timescale in the absence
44 of carbon capture from the atmosphere.

45 46 *12.5.5.5.2 Monsoonal circulation*

47 Climate model simulations and paleo-reconstructions provide evidence of past abrupt changes in Saharan
48 vegetation, with the “green Sahara” conditions (Hoelzmann et al., 1998) of the African Humid Period (AHP)
49 during the mid-Holocene serving as the most recent example (see section 5.6.2). However, Claussen et al.
50 (2003) note the mid-Holocene is not a direct analogue for future greenhouse gas-induced climate change
51 since the forcings are different, with a maximum shortwave forcing in the Northern Hemisphere summer
52 versus a globally and seasonally uniform longwave forcing, respectively. Paleoclimate examples suggest that
53 a strong radiative or SST forcing is needed to achieve a rapid climate change, and that the rapid changes are
54 reversible when the forcing is withdrawn. Both the abrupt onset and termination of the AHP were triggered
55 when northern African summer insolation was 4.2% higher than present day, representing an increase of
56 about 19 W m⁻² (deMenocal et al., 2000). The 1.66 W m⁻² greenhouse gas forcing from 1750 to 2005
57 estimated in the IPCC AR4 is much smaller. Indeed, a climate model of intermediate complexity simulates a

1 rapid Saharan greening under very high levels (1000 ppm) but not under lower levels (560 ppm) of
2 atmospheric CO₂ (Claussen et al., 2003). Abrupt Saharan vegetation changes of the Younger Dryas are
3 linked with a rapid AMOC weakening which is considered very unlikely during the 21st century and
4 unlikely beyond that as a consequence of global warming.

5
6 Climate model derived projections of changes in runoff by Milly et al. (2008) suggest widespread drying and
7 drought across most of southwestern North America and many other subtropical regions by the middle of the
8 21st century. Some studies suggest that this subtropical drying may have already begun in southwestern
9 North America (Barnett et al., 2008; Pierce et al., 2008; Seager et al., 2007; Seidel and Randel, 2007). More
10 recent studies (Dai, 2011; Hoerling et al., 2010; Seager and Vecchi, 2010; Seager and Naik, 2011) suggest
11 that regional reductions in precipitation are primarily due to natural variability and the anthropogenic forced
12 trends remain currently weak compared to those caused by internal variability within the climate system.

13
14 Studies with conceptual models (Levermann et al., 2009; Zickfeld et al., 2005) have shown that the Indian
15 summer monsoon can operate in two stable regimes: besides the “wet” summer monsoon, a stable state
16 exists which is characterized by low precipitation over India. These studies suggest that any perturbation of
17 the radiative budget which tends to weaken the driving pressure gradient has the potential to induce abrupt
18 transitions between these two regimes.

19
20 Numerous studies with coupled ocean-atmosphere models have explored the potential impact of
21 anthropogenic forcing on the Indian monsoon. When forced with anticipated increases in greenhouse gas
22 concentrations, the majority of these studies show an intensification of the rainfall associated with the Indian
23 summer monsoon (Cherchi et al., 2010; Douville et al., 2000; Hu et al., 2000; Kitoh et al., 1997; Kripalani et
24 al., 2007; May, 2002; Meehl and Washington, 1993; Stowasser et al., 2009; Ueda et al., 2006). Despite the
25 intensification of precipitation, several of these modeling studies show a weakening of the summer monsoon
26 circulation (Cherchi et al., 2010; Kitoh et al., 1997; Kripalani et al., 2007; May, 2002; Stowasser et al., 2009;
27 Ueda et al., 2006). The net effect is nevertheless an increase of precipitation due to enhanced moisture
28 transport into the Asian monsoon region (Ueda et al., 2006). In recent years, studies with general circulation
29 models have also explored the direct effect of aerosol forcing on the Indian monsoon (Collier and Zhang,
30 2009; Lau et al., 2006; Meehl et al., 2008; Randles and Ramaswamy, 2008). Considering absorbing aerosols
31 (black carbon) only, Meehl et al. (2008) found an increase in pre-monsoonal precipitation, but a decrease in
32 summer monsoon precipitation over parts of South Asia. In contrast, Lau et al. (2006) found an increase in
33 May-June-July precipitation in that region. If an increase in scattering aerosols only is considered, the
34 monsoon circulation weakens and precipitation is inhibited (Randles and Ramaswamy, 2008). Given that the
35 effect of increased atmospheric loading of aerosols will be opposed by the concomitant increases in
36 greenhouse gas concentrations, it is unlikely that an abrupt transition to the dry summer monsoon regime
37 will be triggered in the 21st century. However, a scenario is conceivable whereby aerosol control policies
38 (meant to mitigate intolerable impacts on human health, food production and ecosystems reductions in air
39 pollution in Asia) could, by reducing the damping effects of aerosols on the monsoon, result in sudden
40 monsoon strengthening (Zickfeld et al., 2005).

41 42 *12.5.5.6 Amazon Rainforest and Boreal Forest*

43 44 *12.5.5.6.1 Amazon rainforest*

45 In today’s climate, the strongest growth in the Amazon rainforest occurs during the dry season when strong
46 insolation is combined with water drawn from underground aquifers that store the previous wet season’s
47 rainfall. AOGCMs do not agree about how the dry season length in the Amazon may change in the future
48 due to greenhouse gas increases (Bombardi and Carvalho, 2009), but simulations with coupled regional
49 climate/potential vegetation models are consistent in simulating an increase in dry season length, a 70%
50 reduction in the areal extent of the rainforest, and an eastward expansion of the caatinga vegetation (Cook
51 and Vizy, 2008; Sorensson et al., 2010). The transition could be abrupt when the dry season becomes too
52 long for the vegetation to survive, although the resilience of the vegetation to a longer dry period may be
53 increased by the CO₂ fertilization effect (Zelazowski et al., 2011). Deforestation may also increase dry
54 season length (Costa and Pires, 2010) and drier conditions increase the likelihood of wildfires that, combined
55 with fire ignition associated with human activity, can undermine the forest’s resiliency to climate change. If
56 climate change brings drier conditions closer to those supportive of seasonal forests rather than rainforest,
57 fire can act as a trigger to abruptly and irreversibly change the ecosystem (Malhi et al., 2009). However the

1 existence of refugia is an important determinant of the potential for the reemergence of the vegetation
2 (Walker et al., 2009).

3
4 Analysis of projected change in the climate-biome space of current vegetation distributions suggest that the
5 risk of Amazonian forest die-back is small (Malhi et al., 2009), a finding supported by modeling when strong
6 carbon dioxide fertilization effects on Amazonian vegetation are assumed (Rammig et al., 2010). However,
7 the strength of carbon dioxide fertilization on tropical vegetation is poorly known. Uncertainty concerning
8 the existence of tipping point in the Amazonian rainforest purely driven by climate change therefore remains
9 high. The likelihood of a tipping point being crossed in precipitation volume is low, but cannot be ruled out.
10 The transitions of the Amazonian rainforest into a lower biomass state could however be the result of the
11 combined effects of limits to carbon fertilization, climate warming, potential precipitation decline in
12 interaction with the effects of human land-use.

13 14 *12.5.5.6.2 Boreal forest*

15 Evidence from field observations and biogeochemical modelling make it scientifically conceivable that
16 regions of the boreal forest could tip into a different vegetation state under climate warming, but
17 uncertainties on the likelihood of this occurring are very high (Allen et al., 2010; Lenton et al., 2008). This is
18 mainly due to large gaps in knowledge concerning relevant ecosystemic and plant physiological responses to
19 warming (Niinemets, 2010). The main effect is a potential transition from a forest to a woodland or grassland
20 state on the dry southern edges of the boreal forest in the continental interiors leading to an overall increase
21 in herbaceous vegetation cover in the affected parts of the boreal zone (Lucht et al., 2006). The proposed
22 potential mechanisms for decreased forest growth and/or increased forest mortality are: increased drought
23 stress under warmer summer conditions in regions with low soil moisture (Barber et al., 2000; Dulamsuren et
24 al., 2010; Dulamsuren et al., 2009); desiccation of saplings with shallow roots due to summer drought
25 periods in the top soil layers, causing suppression of forest reproduction (Hogg and Schwarz, 1997); leaf
26 tissue damage due to high leaf temperatures during peak summer temperatures under strong climate
27 warming; increased insect, herbivory and subsequent fire damage in damaged or struggling stands
28 (Dulamsuren et al., 2008). The balance of effects controlling standing biomass, fire type and frequency,
29 permafrost thaw depth, snow volume and soil moisture remains uncertain. While the existence of and the
30 thresholds controlling this potential tipping element are highly uncertain, its existence cannot at present be
31 ruled out.

32 33 *12.5.5.7 Permafrost Carbon Storage*

34
35 Since the IPCC AR4, estimates of the amount of carbon stored in permafrost have been significantly revised
36 upwards (Tarnocai et al., 2009), putting the permafrost carbon stock to an equivalent of twice the
37 atmospheric carbon pool (Dolman et al., 2010). Because of low carbon input at high latitudes, permafrost
38 carbon is to a large part of Pleistocene (Zimov et al., 2006) or Holocene (Smith et al., 2004) origin, and its
39 potential vulnerability is dominated by decomposition (Eglin et al., 2010). The conjunction of a long carbon
40 accumulation time scale on one hand and potential decomposition under climatic conditions leading to
41 permafrost thaw (Kuhry et al., 2010; Schuur et al., 2009; Zimov et al., 2006) on the other hand suggests
42 potential irreversibility of permafrost carbon decomposition (leading to an increase of atmospheric CO₂
43 and/or CH₄ concentrations) on timescales of hundreds to thousands of years in a warming climate. The few
44 existing modelling studies of permafrost carbon balance under future warming that take into account
45 essential permafrost-related processes (Khvorostyanov et al., 2008; Koven et al., 2011; Schaefer et al., 2011;
46 Schneider von Deimling et al., 2011; Wania et al., 2009) do not yield coherent results. This also reflects an
47 insufficient understanding of the relevant soil processes during and after permafrost thaw, including
48 processes leading to stabilization of unfrozen soil carbon (Schmidt et al., 2011). As such, a firm assessment
49 of the amplitude of these irreversible changes in permafrost carbon loss is premature.

50 51 *12.5.5.8 Atmospheric Methane*

52
53 Model simulations (Fyke and Weaver, 2006; Lamarque, 2008; Reagan and Moridis, 2007, 2009) suggest that
54 clathrate deposits in shallow regions (in particular at high latitude regions and in the Gulf of Mexico) are
55 susceptible to destabilization via ocean warming. However, concomitant sea level rise enhances clathrate
56 stability in the ocean. A recent assessment of the potential for a future catastrophic release of methane was
57 undertaken by the U.S. Climate Change Science Program (Synthesis and Assessment Product 3.4 see Brook

1 et al. (2008)). They concluded that it was very unlikely that such a catastrophic release would occur this
2 century. However, they argued that anthropogenic warming will very likely lead to enhanced methane
3 emissions from both terrestrial and oceanic clathrates (Brooke et al., 2008). While difficult to formally
4 assess, initial estimates of the 21st century feedback from methane clathrate destabilization are small but not
5 insignificant (Archer, 2007; Fyke and Weaver, 2006; Lamarque, 2008). On multi-millennial timescales, such
6 methane emissions will provide a significant positive feedback to anthropogenic warming (Archer, 2007;
7 Archer and Buffett, 2005; Brooke et al., 2008). Once more, due to the difference between release and
8 accumulation timescales, such emissions are irreversible.

9
10 The largest natural source of methane emissions arises from the anaerobic decay of organic matter in
11 tropical, boreal and Arctic wetlands. Brooke et al. (2008) conclude that methane emissions from wetlands
12 will very likely increase as a consequence of anthropogenic warming. However, the modelling study of Avis
13 et al. (2010) suggests that as permafrost degrades, the overall areal extent of boreal and arctic wetlands
14 decreases. Their results suggest that the future global production of methane from high latitude wetlands will
15 have a complicated signal over the next century with decreasing overall wetland extent counteracting a
16 greater number of wet days in remaining wetlands. However, a modelling study with interactive wetland
17 extents by Ringeval et al. (2011) yielded increased future methane emissions from wetlands essentially due
18 to increased flux density as a result of CO₂ fertilisation leading to a larger soil carbon reservoir available for
19 anaerobic decomposition.

20
21
22 **[START FAQ 12.1 HERE]**

23 **FAQ 12.1: Why are so Many Models and Scenarios Used to Project Climate Change?**

24
25
26 Future climate is determined by assumptions on future emissions of greenhouse gases, aerosol precursors
27 and other forcings on one hand, and the response of the Earth to those forcings on the other hand. In
28 addition, natural variability inherent in the climate system will be superimposed on the forced response.

29 **Scenarios**

30
31
32 Predicting future patterns of socio-economic development is arguably even more difficult than predicting
33 future patterns in the evolution of a physical system, the former involving prediction of human behavior,
34 policy choices, international competition and cooperation. The common approach is to use scenarios of
35 plausible future human activities from which future emissions of greenhouse gases and other forcing agents
36 such as aerosol particles are derived. It has not, in general, been possible to assign likelihoods to individual
37 forcing scenarios.

38
39 In AR4, much use was made of the SRES scenarios that characterised human behaviour into different
40 families of storylines. The SRES scenarios were developed in a sequential fashion; socio-economics to
41 emissions to concentrations. For this report a new set of scenarios have been developed – the Representative
42 Concentration Pathways (RCPs). The RCPs were developed in a parallel fashion by first choosing different
43 levels of radiative forcing at 2100 (2.6, 4.5, 6.0 and 8.5 W m⁻²) and the developing the greenhouse gas and
44 aerosol emissions and their corresponding socio-economic drivers simultaneously. Rather than being
45 identified with one socio-economic storyline, RCP scenarios are consistent with many possible economic
46 futures.

47
48 Their development was driven by the need to produce scenarios more efficiently and to produce a wide range
49 of possible model responses. The reasoning behind this is that often climate models produce patterns of
50 climate change that may be simply scaled by the level of global mean temperature change (pattern scaling),
51 hence other scenarios involving, for example, pathways to adaptation and mitigation may be scaled and
52 interpolated from the RCPs.

53
54 Despite the naming of the RCPs in terms of their 2100 radiative forcing, uncertainties in the way models
55 translate emissions to concentrations and uncertainties in the way models convert those concentrations into a
56 radiative forcing, means that e.g., RCP4.5 does not necessarily equate to 4.5 W m⁻² forcing in 2100.

1 FAQ 12.1, Figure 1 shows the global mean temperature response of the CMIP5 models for the historical
2 simulations and the four RCP scenarios up the year 2100.

3 4 **Models**

5
6 Climate models are the principal tools used to make projections of future climate change. Models are derived
7 from physical and empirical understanding and represent the complex and interacting climate processes that
8 are needed to simulate past climate and climate change, and projections. The use of analogues from past
9 observations, or the extrapolation of recent trends is, for the majority of projection problems, not an adequate
10 strategy for producing projections.

11
12 Although it is possible to write down the equations of fluid motion that determine the behaviour of the
13 atmosphere and ocean, it is not possible to directly solve these without recourse to computer simulation and
14 without making approximations. There simply is not a computer big enough to solve the equations on a fine
15 enough grid. In addition, there are other small-scale processes, for example cloud-particle interactions that
16 are not described by those equations. In addition, many models now include biological and chemical
17 processes that have some mathematical basis, for example in terms of conservation laws, but for which
18 empirical understanding is common.

19
20 It is seen as a healthy aspect of the community of climate models that different groups have adopted different
21 numerical techniques for solving the dynamical equations and approximating physical, chemical and
22 biological processes. This model diversity permits decisions about model formulation to be made differently
23 by different groups, resulting in a diversity of different projections of climate change at global and regional
24 scales. The uncertainty in the projections that comes from the different approximations and choices that
25 could be made, is sampled in some way. Of course, the sampling is not systematic or comprehensive and
26 there are inadequacies that are common to all models.

27
28 The use of models of varying complexity for different projection problems is also common – a faster model
29 with lower resolution or a simplified description of the processes may be used in case where long multi-
30 century simulations are required or where multiple realisations are needed.

31
32 The coordination of model experiments and model output by groups such as CMIP has resulted in increased
33 capacity in the community to evaluate and inter-compare the ability of models to simulate past climate and
34 climate change and to evaluate and inter-compare the future projections. The “multi-model” approach is now
35 a kind of industry-standard technique that is used when looking at projections of a specific climate variable.
36 Other approaches include the “perturbed-physics” approach that involves the perturbation to parameters from
37 the components of models that approximate physical processes that cannot be resolved (the parameterisation
38 schemes). While this allows large numbers of realisations to be produced (larger ensembles) the perturbed
39 physics approach cannot sample all the possible choices that could be made during model formulation.

40
41 FAQ 12.2, Figure 1 shows the temperature response by the end of the 21st century for three illustrative
42 models and the highest and lowest scenario.

43
44 Models agree on large scale patterns of warming at the surface, e.g., land warming faster than ocean and the
45 Arctic warming faster than the tropics. But models differ in the magnitude of their global response for the
46 same scenario, and in small scale, regional aspects of their response. For example, the magnitude of Arctic
47 amplification varies among different models, and a subset of models show a weaker warming or slight
48 cooling in the North Atlantic as a result of the reduction in deepwater formation and shifts in currents.

49
50 Because neither multi-model or perturbed-physics ensembles provide an adequate sample of all the possible
51 outcomes of future climate change, and because the raw ensemble output does not take into account the
52 validity of each member of the ensemble, statistical techniques have been developed to formulate projections
53 in terms of probability distribution functions. These statistical techniques themselves have approximations
54 and choices so cannot be regarded as providing final assessments of uncertainty, nevertheless, they provide
55 useful tools for integrating information from ensembles, theory and observations via their use in model
56 evaluation.

1 **[INSERT FAQ 12.1, FIGURE 1 HERE]**

2 **FAQ 12.1, Figure 1:** Global mean temperature change (mean and one standard deviation, relative to 1986–2005) for
3 the CMIP5 models and the four RCP scenarios. For the highest (RCP8.5) and lowest (RCP2.6) scenario, illustrative
4 maps of surface temperature change at the end of the 21st century (relative to 1986–2005) are shown for three CMIP5
5 models. These models are chosen to show a rather broad range of response but this particular set of models is not
6 representative of any measure of model response uncertainty.

7
8 **[END FAQ 12.1 HERE]**

9
10
11 **[START FAQ 12.2 HERE]**

12 **FAQ 12.2: How will the Earth’s Water Cycle Change?**

13
14
15 The flow and storage of water in the Earth’s climate system is highly variable, but changes beyond natural
16 variability are expected to occur by the end of the current century. In a warmer world, the water cycle will
17 intensify, leading to an overall increase of rainfall, surface evaporation and plant transpiration. In some
18 locations, the more intense water cycle will yield an accumulation of water on land. In others, the amount of
19 water will decrease due to regional drying and loss of snow and ice cover.

20
21 The water cycle consists of water stored on the Earth in all its phases, along with the movement of water
22 through the Earth’s climate system (FAQ 12.2, Figure 1). In the atmosphere, water occurs primarily as a gas,
23 water vapour, but it also occurs as ice and liquid water in clouds. The ocean of course is primarily liquid
24 water, but the ocean is partly covered by ice in polar regions. Terrestrial water in liquid form appears as
25 surface water (lakes, rivers), soil moisture and groundwater. Solid terrestrial water occurs in ice sheets,
26 glaciers, snow and ice on the surface and permafrost.

27
28 Statements about future climate sometimes say that the water cycle will accelerate, but this can be
29 misleading, for strictly speaking, it implies that the cycling of water will occur more and more quickly with
30 time and at all locations. Parts of the world will indeed experience intensification of the water cycle, with
31 larger transports of water and more rapid movement of water into and out of storage reservoirs. However,
32 other parts of the climate system will experience substantial depletion of water and thus less movement of
33 water, and some water reservoirs may even vanish.

34
35 As the Earth warms, some general features of change should occur simply in response to a warmer climate.
36 Ice in all forms should melt more rapidly and be less pervasive. The atmosphere should have more water
37 present, and observations and model results indicate that it already has. Water should evaporate more quickly
38 from the surface. Sea level should rise due to the slight expansion of warming ocean waters and the flow into
39 the ocean of water from melting of land ice. These general changes are modified by the complexity of the
40 climate system, so that they should not be expected to occur equally in all locations or at the same pace. For
41 example, circulation of water in the atmosphere, on land and in the ocean can change as climate changes,
42 concentrating water in some locations and depleting it in others. Humans also intervene directly in the water
43 cycle through water management and through changes in land-use, and changing population distributions
44 and water practices would produce additional changes in the water cycle.

45
46 Water cycle processes can vary substantially over short periods of time (minutes, days, hours) and distance
47 (meters, kilometers). Despite this complexity, projections of future climate show changes that are common
48 among many models and climate forcing scenarios, suggesting some robust types of change, even if
49 magnitudes vary with model and forcing. We focus here on changes over land, where changes in the water
50 cycle have their largest impact on human and natural systems.

51
52 Projected climate changes generally show an increase in precipitation in the tropics, a decrease in the
53 subtropics and increases at higher latitudes. In the tropics, these changes appear to be governed by increases
54 in atmospheric water vapour and changes in atmospheric circulation that promote more tropical rainfall. In
55 the subtropics, these circulation changes simultaneously promote less rainfall. Because the subtropics are
56 home to most of the world’s deserts, these changes imply increasing aridity in already dry areas and possible
57 expansion of deserts. Increases at higher latitudes are governed by warmer temperatures that allow more

1 water in the atmosphere and thus more water that can precipitate. These high latitude changes are more
2 pronounced during the colder seasons.

3
4 Whether land becomes drier or wetter depends partly on precipitation changes but also on changes in surface
5 evaporation and transpiration from plants (together denoted evapotranspiration). Because a warmer
6 atmosphere can contain more water vapour, it can induce greater evapotranspiration where there is sufficient
7 terrestrial water. In the tropics, increased evapotranspiration tends to mute the effects of increased
8 precipitation, whereas in the subtropics, the relatively low amounts of soil moisture to start with means that
9 little change in evapotranspiration can occur. At higher latitudes, the increased precipitation generally
10 outweighs increased evapotranspiration in projected climates, yielding increased annual runoff (Figure
11 12.27), but mixed changes in soil moisture (Figure 12.26).

12
13 A further complicating factor is the character of rainfall when it occurs. Model projections show rainfall
14 becoming more intense, not only because more moisture may be present in the atmosphere, but also because
15 precipitation events tend to occur less frequently. The reduced frequency of days with rain produces two
16 seemingly contradictory changes: more intense downpours leading to more flooding and longer periods
17 between rain events, promoting more drought.

18
19 At high latitudes and at high elevation, additional changes occur due to the loss of frozen water. Some of
20 these are resolved by the present generation of global climate models (GCMs), and some changes can only
21 be inferred because they involve features such as glaciers that typically are not resolved or included in
22 models. The warmer climate means that snow tends to start accumulating later in the fall and melt earlier in
23 the spring. The earlier spring melt alters the timing of peak springtime flow in rivers receiving snow melt.
24 As a result, later flowrates will decrease, potentially affecting water resource management. These features
25 appear in GCM simulations. Loss of permafrost, a feature not included in most of the current GCMs, will
26 allow moisture to seep more deeply into the ground, but it will also allow the ground to warm, which could
27 enhance evapotranspiration. In addition, even though current GCMs do not explicitly include their evolution,
28 we can expect that glaciers will continue to recede and the volume of water they provide to rivers in the
29 summer may disappear in some locations as glaciers disappear. They will also contribute to a reduction in
30 springtime river flow. These results do not necessarily mean that annual river flow will decrease, if overall
31 annual precipitation as either snow or rain increases.

32
33 **[INSERT FAQ 12.2, FIGURE 1 HERE]**

34 **FAQ 12.2, Figure 1:** Schematic diagram of the water cycle and projected changes. The blue arrows indicate major
35 types of water movement through the Earth's climate system: precipitation from the atmosphere, evaporation from the
36 surface and runoff from the land to the oceans. The shaded regions denoted as 'drier' and 'wetter' indicate areas with
37 decrease and increased rainfall, respectively. Yellow arrows indicate an important atmospheric circulation, the Hadley
38 circulation, whose upward motion promotes tropical rainfall while suppressing subtropical rainfall. Model projections
39 indicate that this circulation will shift its downward branch poleward in both the Northern and Southern Hemispheres,
40 with associated drying. Wetter conditions are projected at high latitudes because a warmer atmosphere will allow
41 greater precipitation.

42
43 **[END FAQ 12.2 HERE]**

44
45
46 **[START FAQ 12.3 HERE]**

47
48 **FAQ 12.3: What would Happen to Future Climate if We Stopped Emissions Today?**

49
50 Stopping emissions today is a scenario that is not plausible. But it is one of several idealized cases that
51 provide insight into the response of the climate system and carbon cycle. As a result of the multiple
52 timescales in the climate system, the relation between change in emissions and climate response is quite
53 complex, with some changes still occurring long after emissions ceased.

54
55 When emitted in the atmosphere, greenhouse gases get removed through chemical reactions with other
56 reactive components or, in the case of CO₂, get exchanged with the ocean and the land. These processes
57 characterize the lifetime of the gas in the atmosphere which is defined by the time it takes for a concentration
58 pulse to naturally decrease by a factor of e (2.71). How long greenhouse gases persist in the atmosphere

1 varies over a wide range, from days to thousands of years. For example, methane has a lifetime of about 10
2 years, N₂O of about 100 years and C₂F₆ of about 10,000 years. CO₂ is more complicated as it is removed
3 from the atmosphere through multiple physical and biogeochemical processes in the land and the ocean; all
4 operating at different time scales. About half of the anthropogenic CO₂ is removed within a few decades but
5 the remaining fraction stays in the atmosphere for much longer. About 20% of emitted CO₂ is still in the
6 atmosphere after 1000 years.

7
8 As a result of the significant lifetimes of major anthropogenic greenhouse gases, the change in atmospheric
9 concentration due to past emissions will persist long after emissions are ceased. Concentration of greenhouse
10 gases would not return immediately to their pre-industrial levels if emissions were halted. Methane
11 concentration would return to values close to pre-industrial level in about 50 years, N₂O concentrations
12 would need several centuries, while CO₂ would essentially never (on human time scales) come back to its
13 preindustrial level. Changes in short lived species like aerosols or tropospheric ozone on the other hand
14 cause a forcing that is nearly instantaneous. This is the commitment from past emissions (or zero emission
15 commitment).

16
17 The implication is that even if anthropogenic greenhouse gases emissions were halted now, the radiative
18 forcing due to these long-lived greenhouse gases concentrations would only slowly decrease in the future.
19 Moreover, the climate response of the Earth system would be even slower. Global temperature would not
20 respond quickly to the greenhouse gas concentration changes. Eliminating short lived negative forcings from
21 sulphate aerosols at the same time would cause a temporary warming of a few tenths of a degree, as shown
22 in blue in FAQ 12.3, Figure 1.

23
24 The climate system is characterized by a long inertia, mainly driven by the ocean. The ocean has a very large
25 capacity of absorbing heat, which means that it will take several centuries for the whole ocean to warm up so
26 to reach equilibrium with the altered radiative forcing. The surface ocean (and hence the continents) will
27 continue to warm until it reaches a surface temperature in equilibrium with this new radiative forcing. The
28 AR4 showed that if concentration of greenhouse gases were held constant at present day level, the Earth
29 surface would still continue to warm of about 0.3°C over the 21st century relative to the year 2000. This is
30 the climate commitment to past concentrations (or constant composition commitment), shown in grey in
31 FAQ 12.3, Figure 1. Constant emissions at current levels would further increase the atmospheric
32 concentration and result in much more warming than observed so far (FAQ 12.3, Figure 1, red lines).

33
34 Setting emissions to zero will therefore lead to a near stabilization of the climate for multiple centuries. The
35 concentration of GHG would decrease and hence the radiative forcing as well, but the inertia of the climate
36 system would delay the temperature response. The implications are that long-term global temperature is
37 largely controlled by total CO₂ emissions that have accumulated over time, irrespective of the time when
38 they were emitted. Limiting global warming below a given level (e.g., 2°C above pre-industrial) requires
39 stabilizing the atmospheric CO₂ concentration and requires near zero CO₂ emissions eventually. A higher
40 climate target allows for a higher CO₂ concentration, and hence delays the necessary emission reduction.
41 Global temperature is a useful aggregate number to describe the magnitude of climate change, but not all
42 changes will scale linearly global temperature. Changes in the water cycle for example also depend on the
43 type of forcing (e.g., greenhouse gases, aerosols, land use change), slower components of the Earth System
44 such as sea level rise and ice sheet would take even longer to respond, and there may be tipping points or
45 irreversible changes in the climate system.

46
47 **[INSERT FAQ 12.3, FIGURE 1 HERE]**

48 **FAQ 12.3, Figure 1:** Projections based on the energy balance carbon cycle model MAGICC for constant atmospheric
49 composition (constant forcing, grey), constant emissions (red) and zero emissions (blue) starting in 2010, with
50 probabilistic estimates of uncertainty. Figure adapted from Hare and Meinshausen (2006) based on the MAGICC
51 calibration to all CMIP3 and C4MIP models (Meinshausen et al., 2011a; Meinshausen et al., 2011b).

52
53 **[END FAQ 12.3 HERE]**

References

- ACIA, 2004: Arctic Climate Impact Assessment (ACIA): Impacts of a Warming Arctic, 140 pp pp.
- Albrecht, A., D. Schindler, K. Grebhan, U. Kohnle, and H. Mayer, 2009: Storminess over the North-Atlantic European region under climate change - a review. *Allgemeine Forst und Jagdzeitung*, **180**, 109-118.
- Alexander, L. V., and J. M. Arblaster, 2009: Assessing trends in observed and modelled climate extremes over Australia in relation to future projections. *International Journal of Climatology*, **29**, 417-435.
- Alexander, L. V., et al., 2006: Global observed changes in daily climate extremes of temperature and precipitation. *Journal of Geophysical Research-Atmospheres*, **111**, D05109.
- Alexeev, V., D. Nicolsky, V. Romanovsky, and D. Lawrence, 2007: An evaluation of deep soil configurations in the CLM3 for improved representation of permafrost. *Geophysical Research Letters*, **34**, L09502.
- Allan, R., and B. Soden, 2008: Atmospheric warming and the amplification of precipitation extremes. *Science*, **321**, 1481-1484.
- Allen, C., et al., 2010: A global overview of drought and heat-induced tree mortality reveals emerging climate change risks for forests. *Forest Ecology and Management*, **259**, 660-684.
- Allen, M., and W. Ingram, 2002: Constraints on future changes in climate and the hydrologic cycle. *Nature*, **419**, 224-232.
- Allen, M. R., D. J. Frame, C. Huntingford, C. D. Jones, J. A. Lowe, M. Meinshausen, and N. Meinshausen, 2009: Warming caused by cumulative carbon emissions towards the trillionth tonne. *Nature*, **458**, 1163-1166.
- Amstrup, S., E. DeWeaver, D. Douglas, B. Marcot, G. Durner, C. Bitz, and D. Bailey, 2010: Greenhouse gas mitigation can reduce sea-ice loss and increase polar bear persistence. *Nature*, **468**, 955-958.
- An, S. I., J. S. Kug, Y. G. Ham, and I. S. Kang, 2008: Successive modulation of ENSO to the future greenhouse warming. *Journal of Climate*, **21**, 3-21.
- Andrews, T., and P. Forster, 2008: CO₂ forcing induces semi-direct effects with consequences for climate feedback interpretations. *Geophysical Research Letters*, **35**, L04802.
- Andrews, T., P. M. Forster, and J. M. Gregory, 2009: A Surface Energy Perspective on Climate Change. *Journal of Climate*, **22**, 2557-2570.
- Andrews, T., P. Forster, O. Boucher, N. Bellouin, and A. Jones, 2010: Precipitation, radiative forcing and global temperature change. *Geophysical Research Letters*, **37**, L14701.
- Annan, J., and J. Hargreaves, 2006: Using multiple observationally-based constraints to estimate climate sensitivity. *Geophysical Research Letters*, **33**, L06704.
- Annan, J. D., and J. C. Hargreaves, 2010: Reliability of the CMIP3 ensemble. *Geophysical Research Letters*, **37**, L02703.
- , 2011a: On the generation and interpretation of probabilistic estimates of climate sensitivity. *Climatic Change*, **104**, 423-436.
- Annan, J. D., and J. C. Hargreaves, 2011b: Understanding the CMIP3 multi-model ensemble. *Journal of Climate*, **24**, 4529-4538.
- Arblaster, J. M., G. A. Meehl, and D. J. Karoly, 2011: Future climate change in the Southern Hemisphere: Competing effects of ozone and greenhouse gases. *Geophys. Res. Lett.*, **38**, L02701.
- Archer, D., 2007: Methane hydrate stability and anthropogenic climate change. *Biogeosciences*, **4**, 521-544.
- Archer, D., and B. Buffett, 2005: Time-dependent response of the global ocean clathrate reservoir to climatic and anthropogenic forcing. *Geochemistry Geophysics Geosystems*, **6**, Q03002.
- Archer, D., et al., 2009: Atmospheric Lifetime of Fossil Fuel Carbon Dioxide. *Annual Review of Earth and Planetary Sciences*, **37**, 117-134.
- Armour, K., and G. Roe, 2011: Climate commitment in an uncertain world. *Geophysical Research Letters*, **38**, L01707.
- Armour, K., I. Eisenman, E. Blanchard-Wrigglesworth, K. McCusker, and C. Bitz, 2011: The reversibility of sea ice loss in a state-of-the-art climate model. *Geophysical Research Letters*, **38**, L16705.
- Arora, V. K., et al., 2011: Carbon emission limits required to satisfy future representative concentration pathways of greenhouse gases. *Geophysical Research Letters*, **38**, L05805.
- Arzel, O., T. Fichefet, and H. Goosse, 2006: Sea ice evolution over the 20th and 21st centuries as simulated by current AOGCMs. *Ocean Modelling*, **12**, 401-415.
- Austin, J., et al., 2010: Decline and recovery of total column ozone using a multimodel time series analysis. *Journal of Geophysical Research-Atmospheres*, **115**, D00M10, doi:10.1029/2010JD013857.
- Avis, C. A., A. J. Weaver, and K. J. Meissner, 2010: Evolution of high-latitude wetlands in response to permafrost thaw. *Nature Geoscience*, **4**, 444-448.
- Bala, G., K. Caldeira, and R. Nemani, 2010: Fast versus slow response in climate change: implications for the global hydrological cycle. *Climate Dynamics*, **35**, 423-434.
- Baldwin, M. P., M. Dameris, and T. G. Shepherd, 2007: Atmosphere - How will the stratosphere affect climate change? *Science*, **316**, 1576-1577.
- Ballester, J., F. Giorgi, and X. Rodo, 2010a: Changes in European temperature extremes can be predicted from changes in PDF central statistics. *Climatic Change*, **98**, 277-284.
- Ballester, J., X. Rodo, and F. Giorgi, 2010b: Future changes in Central Europe heat waves expected to mostly follow summer mean warming. *Climate Dynamics*, **35**, 1191-1205.

- 1 Barber, V., G. Juday, and B. Finney, 2000: Reduced growth of Alaskan white spruce in the twentieth century from
2 temperature-induced drought stress. *Nature*, **405**, 668-673.
- 3 Barnett, D. N., S. J. Brown, J. M. Murphy, D. M. H. Sexton, and M. J. Webb, 2006: Quantifying uncertainty in changes
4 in extreme event frequency in response to doubled CO₂ using a large ensemble of GCM simulations. *Climate*
5 *Dynamics*, **26**, 489-511.
- 6 Barnett, T., and D. Pierce, 2008: When will Lake Mead go dry? *Water Resources Research*, **44**, W03201.
- 7 Barnett, T., et al., 2008: Human-induced changes in the hydrology of the western United States. *Science*, **319**, 1080-
8 1083.
- 9 Barriopedro, D., E. M. Fischer, J. Luterbacher, R. Trigo, and R. Garcia-Herrera, 2011: The Hot Summer of 2010:
10 Redrawing the Temperature Record Map of Europe. *Science*, **332**, 220-224.
- 11 Bekryaev, R. V., I. V. Polyakov, and V. A. Alexeev, 2010: Role of Polar Amplification in Long-Term Surface Air
12 Temperature Variations and Modern Arctic Warming. *Journal of Climate*, **23**, 3888-3906.
- 13 Bellouin, N., J. Rae, A. Jones, C. Johnson, J. Haywood, and O. Boucher, 2011: Aerosol forcing in the Hadley Centre
14 CMIP5 simulations and the role of ammonium nitrate. *Journal of Geophysical Research*, **116**, D20206.
- 15 Bengtsson, L., K. I. Hodges, and E. Roeckner, 2006: Storm tracks and climate change. *Journal of Climate*, **19**, 3518-
16 3543.
- 17 Bengtsson, L., K. I. Hodges, and N. Keenlyside, 2009: Will Extratropical Storms Intensify in a Warmer Climate?
18 *Journal of Climate*, **22**, 2276-2301.
- 19 Betts, R., et al., 2007: Projected increase in continental runoff due to plant responses to increasing carbon dioxide.
20 *Nature*, **448**, 1037-1041.
- 21 Bitz, C., and G. Roe, 2004: A mechanism for the high rate of sea ice thinning in the Arctic Ocean. *Journal of Climate*,
22 **17**, 3623-3632.
- 23 Bitz, C., and Q. Fu, 2008: Arctic warming aloft is data set dependent. *Nature*, **455**, E3-E4.
- 24 Bitz, C. M., 2008: Some aspects of uncertainty in predicting sea ice thinning. *Arctic Sea Ice Decline: Observations,*
25 *Projections, Mechanisms, and Implications*, E. T. DeWeaver, C. M. Bitz, and L. B. Tremblay, Eds., Amer.
26 Geophys. Union, 63-76.
- 27 Bitz, C. M., J. K. Ridley, M. M. Holland, and H. Cattle, 2011: 20th and 21st century Arctic climate in global climate
28 models. *Arctic Climate Change – The ACSYS Decade and Beyond*, P. Lemke, Ed.
- 29 Boberg, F., P. Berg, P. Thejll, W. Gutowski, and J. Christensen, 2010: Improved confidence in climate change
30 projections of precipitation evaluated using daily statistics from the PRUDENCE ensemble. *Climate Dynamics*,
31 **35**, 1097-1106.
- 32 Boe, J., A. Hall, and X. Qu, 2009a: Current GCMs' Unrealistic Negative Feedback in the Arctic. *Journal of Climate*, **22**,
33 4682-4695.
- 34 Boe, J., A. Hall, and X. Qu, 2009b: September sea-ice cover in the Arctic Ocean projected to vanish by 2100. *Nature*
35 *Geoscience*, **2**, 341-343.
- 36 Boer, G., K. Hamilton, and W. Zhu, 2005: Climate sensitivity and climate change under strong forcing. *Climate*
37 *Dynamics*, **24**, 685-700.
- 38 Boer, G. J., 1993: Climate change and the regulation of the surface moisture and energy budgets. *Climate Dynamics*, **8**,
39 225-239.
- 40 Bombardi, R., and L. Carvalho, 2009: IPCC global coupled model simulations of the South America monsoon system.
41 *Climate Dynamics*, **33**, 893-916.
- 42 Böning, C., A. Dispert, M. Visbeck, S. Rintoul, and F. Schwarzkopf, 2008: The response of the Antarctic Circumpolar
43 Current to recent climate change. *Nature Geoscience*, **1**, 864-869.
- 44 Bony, S., and J. L. Dufresne, 2005: Marine boundary layer clouds at the heart of tropical cloud feedback uncertainties
45 in climate models. *Geophysical Research Letters*, **32**.
- 46 Bony, S., et al., 2006: How well do we understand and evaluate climate change feedback processes? *Journal of Climate*,
47 **19**, 3445-3482.
- 48 Bougamont, M., et al., 2007: Impact of model physics on estimating the surface mass balance of the Greenland ice
49 sheet. *Geophysical Research Letters*, **34**, L17501.
- 50 Bowerman, N., D. Frame, C. Huntingford, J. Lowe, and M. Allen, 2011: Cumulative carbon emissions, emissions floors
51 and short-term rates of warming: implications for policy. *Philosophical Transactions of the Royal Society a-*
52 *Mathematical Physical and Engineering Sciences*, **369**, 45-66.
- 53 Bracegirdle, T., W. Connolley, and J. Turner, 2008: Antarctic climate change over the twenty first century. *Journal of*
54 *Geophysical Research-Atmospheres*, **113**, D03103.
- 55 Brasseur, G., and E. Roeckner, 2005: Impact of improved air quality on the future evolution of climate. *Geophysical*
56 *Research Letters*, **32**, L23704.
- 57 Brient, F., and S. Bony, 2011: Interpretation of the positive low-cloud feedback predicted by a climate model under
58 global warming. *Climate Dynamics*. submitted.
- 59 Brierley, C. M., M. Collins, and A. J. Thorpe, 2010: The impact of perturbations to ocean-model parameters on climate
60 and climate change in a coupled model. *Climate Dynamics*, **34**, 325-343, doi:10.1007/s00382-00008-00486-
61 00383.
- 62 Brooke, E., D. Archer, E. Dlugokencky, S. Frolking, and D. Lawrence, 2008: Potential for abrupt changes in
63 atmospheric methane.

- 1 Brown, R., and P. Mote, 2009: The Response of Northern Hemisphere Snow Cover to a Changing Climate. *Journal of*
2 *Climate*, **22**, 2124-2145.
- 3 Burke, E., and S. Brown, 2008: Evaluating uncertainties in the projection of future drought. *Journal of*
4 *Hydrometeorology*, **9**, 292-299.
- 5 Buser, C. M., H. R. Kunsch, D. Luthi, M. Wild, and C. Schär, 2009: Bayesian multi-model projection of climate: bias
6 assumptions and interannual variability. *Climate Dynamics*, **33**, 849-868, doi:810.1007/s00382-00009-00588-
7 00386.
- 8 Butchart, N., et al., 2011: Multi-model climatologies of the stratosphere. *Journal of Geophysical Research*, **116**,
9 D05102.
- 10 Butler, A. H., D. W. J. Thompson, and R. Heikes, 2010: The Steady-State Atmospheric Circulation Response to
11 Climate Change-like Thermal Forcings in a Simple General Circulation Model. *Journal of Climate*, **23**, 3474-
12 3496.
- 13 Cabre, M. F., S. A. Solman, and M. N. Nunez, 2010: Creating regional climate change scenarios over southern South
14 America for the 2020's and 2050's using the pattern scaling technique: validity and limitations. *Climatic Change*,
15 **98**, 449-469.
- 16 Caldeira, K., and J. F. Kasting, 1993: Insensitivity of global warming potentials to carbon-dioxide emission scenarios.
17 *Nature*, **366**, 251-253.
- 18 Caldwell, P., and C. S. Bretherton, 2009: Response of a Subtropical Stratocumulus-Capped Mixed Layer to Climate and
19 Aerosol Changes. *Journal of Climate*, **22**, 20-38.
- 20 Cao, L., and K. Caldeira, 2010: Atmospheric carbon dioxide removal: long-term consequences and commitment.
21 *Environmental Research Letters*, **5**, 024011.
- 22 Cariolle, D., and H. Teysseire, 2007: A revised linear ozone photochemistry parameterization for use in transport and
23 general circulation models: multi-annual simulations. *Atmospheric Chemistry and Physics*, **7**, 2183-2196.
- 24 Catto, J. L., L. C. Shaffrey, and K. I. Hodges, 2011: Northern Hemisphere Extratropical Cyclones in a Warming
25 Climate in the HiGEM High-Resolution Climate Model. *Journal of Climate*, **24**, 5336-5352.
- 26 CCSP_1.1, 2006: Temperature Trends in the Lower Atmosphere: Steps for Understanding and Reconciling Differences.
27 CCSP_3.3, 2008: Weather and Climate Extremes in a Changing Climate, 164 pp pp.
- 28 CCSP_3.4, 2008: Abrupt Climate Change.
- 29 Cess, R., et al., 1990: Intercomparison and interpretation of climate feedback processes in 19 atmospheric general-
30 circulation models. *Journal of Geophysical Research-Atmospheres*, **95**, 16601-16615.
- 31 Chapin, F., et al., 2005: Role of land-surface changes in Arctic summer warming. *Science*, **310**, 657-660.
- 32 Charbit, S., D. Paillard, and G. Ramstein, 2008: Amount of CO2 emissions irreversibly leading to the total melting of
33 Greenland. *Geophysical Research Letters*, **35**, L12503.
- 34 Chen, C. T., and T. Knutson, 2008: On the verification and comparison of extreme rainfall indices from climate models.
35 *Journal of Climate*, **21**, 1605-1621.
- 36 Chen, G., J. Lu, and D. M. W. Frierson, 2008: Phase Speed Spectra and the Latitude of Surface Westerlies: Interannual
37 Variability and Global Warming Trend. *Journal of Climate*, **21**, 5942-5959.
- 38 Cherchi, A., A. Alessandri, S. Masina, and A. Navarra, 2010: Effect of increasing CO2 levels on monsoons. *Climate*
39 *Dynamics*, 10.1007/s00382-010-0801-7. online first.
- 40 Choi, D. H., J. S. Kug, W. T. Kwon, F. F. Jin, H. J. Baek, and S. K. Min, 2010: Arctic Oscillation responses to
41 greenhouse warming and role of synoptic eddy feedback. *Journal of Geophysical Research-Atmospheres*, **115**,
42 D17103.
- 43 Chou, C., and C. Chen, 2010: Depth of Convection and the Weakening of Tropical Circulation in Global Warming.
44 *Journal of Climate*, **23**, 3019-3030.
- 45 Chou, C., J. Neelin, C. Chen, and J. Tu, 2009: Evaluating the "Rich-Get-Richer" Mechanism in Tropical Precipitation
46 Change under Global Warming. *Journal of Climate*, **22**, 1982-2005.
- 47 Christensen, J. H., F. Boberg, O. B. Christensen, and P. Lucas-Picher, 2008: On the need for bias correction of regional
48 climate change projections of temperature and precipitation. *Geophysical Research Letters*, **35**, L20709.
- 49 Christensen, N., and D. Lettenmaier, 2007: A multimodel ensemble approach to assessment of climate change impacts
50 on the hydrology and water resources of the Colorado River Basin. *Hydrology and Earth System Sciences*, **11**,
51 1417-1434.
- 52 Cionni, I., et al., 2011: Ozone database in support of CMIP5 simulations: results and corresponding radiative forcing.
53 *Atmospheric Chemistry and Physics Discussion*. submitted.
- 54 Clark, R. T., S. J. Brown, and J. M. Murphy, 2006: Modeling northern hemisphere summer heat extreme changes and
55 their uncertainties using a physics ensemble of climate sensitivity experiments. *Journal of Climate*, **19**, 4418-
56 4435.
- 57 Claussen, M., V. Brovkin, A. Ganopolski, C. Kubatzki, and V. Petoukhov, 2003: Climate change in northern Africa:
58 The past is not the future. *Climatic Change*, **57**, 99-118.
- 59 Collier, J., and G. Zhang, 2009: Aerosol direct forcing of the summer Indian monsoon as simulated by the NCAR
60 CAM3. *Climate Dynamics*, **32**, 313-332.
- 61 Collins, M., C. M. Brierley, M. MacVean, B. B. Booth, and G. R. Harris, 2007: The sensitivity of the rate of
62 transient climate change to ocean physics perturbations. *Journal of Climate*, **20**, 2315-2320,
63 doi:2310.1175/jcli4116.2311.

- 1 Collins, M., B. B. Booth, G. R. Harris, J. M. Murphy, D. M. H. Sexton, and M. J. Webb, 2006a: Towards
2 quantifying uncertainty in transient climate change. *Climate Dynamics*, **27**, 127-147, doi:10.1007/s00382-
3 00006-00121-00380.
- 4 Collins, M., B. Booth, B. Bhaskaran, G. Harris, J. Murphy, D. Sexton, and M. Webb, 2011: Climate model errors,
5 feedbacks and forcings: a comparison of perturbed physics and multi-model ensembles. *Climate Dynamics*, DOI
6 10.1007/s00382-010-0808-0. 1737-1766.
- 7 Collins, M., et al., 2010: The impact of global warming on the tropical Pacific ocean and El Nino. *Nature Geoscience*,
8 **3**, 391-397.
- 9 Collins, W., et al., 2006b: Radiative forcing by well-mixed greenhouse gases: Estimates from climate models in the
10 Intergovernmental Panel on Climate Change (IPCC) Fourth Assessment Report (AR4). *Journal of Geophysical*
11 *Research-Atmospheres*, **111**, D14317.
- 12 Comiso, J. C., 2008: Bootstrap Sea Ice Concentrations from Nimbus-7 SMMR and DMSP SSM/I, 1979-2005. National
13 Snow and Ice Data Center, Boulder, Colorado, U.S.A., Digital Media.
- 14 Cook, K., and E. Vizzy, 2008: Effects of twenty-first-century climate change on the Amazon rain forest. *Journal of*
15 *Climate*, **21**, 542-560.
- 16 Costa, M., and G. Pires, 2010: Effects of Amazon and Central Brazil deforestation scenarios on the duration of the dry
17 season in the arc of deforestation. *International Journal of Climatology*, **30**, 1970-1979.
- 18 Cox, P., and D. Stephenson, 2007: Climate change - A changing climate for prediction. *Science*, **317**, 207-
19 208, doi:210.1126/science.1145956.
- 20 Crook, J. A., P. M. Forster, and N. Stuber, 2011: Spatial Patterns of Modeled Climate Feedback and Contributions to
21 Temperature Response and Polar Amplification. *Journal of Climate*, **24**, 3575-3592.
- 22 Crucifix, M., 2006: Does the Last Glacial Maximum constrain climate sensitivity? *Geophysical Research Letters*, **33**,
23 L18701.
- 24 Cruz, F. T., A. J. Pitman, J. L. McGregor, and J. P. Evans, 2010: Contrasting Regional Responses to Increasing Leaf-
25 Level Atmospheric Carbon Dioxide over Australia. *Journal of Hydrometeorology*, **11**, 296-314.
- 26 Dai, A., 2011: Drought under global warming: a review. *Wiley Interdisciplinary Reviews: Climate Change*, **2**, 45-65.
- 27 Danabasoglu, G., and P. Gent, 2009: Equilibrium Climate Sensitivity: Is It Accurate to Use a Slab Ocean Model?
28 *Journal of Climate*, **22**, 2494-2499.
- 29 Davin, E., N. de Noblet-Ducoudre, and P. Friedlingstein, 2007: Impact of land cover change on surface climate:
30 Relevance of the radiative forcing concept. *Geophysical Research Letters*, **34**, L13702,
31 doi:10.1029/2007GL029678.
- 32 Davis, S., K. Caldeira, and H. Matthews, 2010: Future CO2 Emissions and Climate Change from Existing Energy
33 Infrastructure. *Science*, **329**, 1330-1333.
- 34 Debernard, J. B., and L. P. Roed, 2008: Future wind, wave and storm surge climate in the Northern Seas: a revisit.
35 *Tellus Series a-Dynamic Meteorology and Oceanography*, **60**, 427-438.
- 36 Delisle, G., 2007: Near-surface permafrost degradation: How severe during the 21st century? *Geophysical Research*
37 *Letters*, **34**, L09503.
- 38 Della-Marta, P. M., and J. G. Pinto, 2009: Statistical uncertainty of changes in winter storms over the North Atlantic
39 and Europe in an ensemble of transient climate simulations. *Geophysical Research Letters*, **36**, L14703.
- 40 DelSole, T., and J. Shukla, 2009: Artificial Skill due to Predictor Screening. *Journal of Climate*, **22**, 331-345.
- 41 Delworth, T. L., et al., 2008: The potential for abrupt change in the Atlantic Meridional Overturning Circulation. *Abrupt*
42 *Climate Change. A report by the U.S. Climate Change Science Program and the Subcommittee on Global*
43 *Change Research*, 258-359.
- 44 deMenocal, P., J. Ortiz, T. Guilderson, J. Adkins, M. Sarnthein, L. Baker, and M. Yarusinsky, 2000: Abrupt onset and
45 termination of the African Humid Period: rapid climate responses to gradual insolation forcing. *Quaternary*
46 *Science Reviews*, **19**, 347-361.
- 47 Deser, C., A. Phillips, V. Bourdette, and H. Teng, 2010: Uncertainty in climate change projections: the role of internal
48 variability. *Climate Dynamics*, 10.1007/s00382-010-0977-x. online first, doi:10.1007/s00382-00010-00977-x.
- 49 Dessai, S., X. F. Lu, and M. Hulme, 2005: Limited sensitivity analysis of regional climate change probabilities for the
50 21st century. *Journal of Geophysical Research-Atmospheres*, **110**, D19108.
- 51 Diffenbaugh, N. S., J. S. Pal, F. Giorgi, and X. J. Gao, 2007: Heat stress intensification in the Mediterranean climate
52 change hotspot. *Geophysical Research Letters*, **34**, L11706.
- 53 DiNezio, P. N., A. C. Clement, G. A. Vecchi, B. J. Soden, and B. P. Kirtman, 2009: Climate Response of the Equatorial
54 Pacific to Global Warming. *Journal of Climate*, **22**, 4873-4892.
- 55 Dole, R., et al., 2011: Was there a basis for anticipating the 2010 Russian heat wave? *Geophysical Research Letters*, **38**.
- 56 Dolman, A., G. van der Werf, M. van der Molen, G. Ganssen, J. Erisman, and B. Strengers, 2010: A Carbon Cycle
57 Science Update Since IPCC AR-4. *Ambio*, **39**, 402-412.
- 58 Donat, M. G., G. C. Leckebusch, J. G. Pinto, and U. Ulbrich, 2010: European storminess and associated circulation
59 weather types: future changes deduced from a multi-model ensemble of GCM simulations. *Climate Research*,
60 **42**, 27-43.
- 61 Dong, B. W., J. M. Gregory, and R. T. Sutton, 2009: Understanding Land-Sea Warming Contrast in Response to
62 Increasing Greenhouse Gases. Part I: Transient Adjustment. *Journal of Climate*, **22**, 3079-3097.

- 1 Doutriaux-Boucher, M., M. J. Webb, J. M. Gregory, and O. Boucher, 2009: Carbon dioxide induced stomatal closure
2 increases radiative forcing via a rapid reduction in low cloud. *Geophysical Research Letters*, **36**.
- 3 Douville, H., J. Royer, J. Polcher, P. Cox, N. Gedney, D. Stephenson, and P. Valdes, 2000: Impact of CO2 doubling on
4 the Asian summer monsoon: Robust versus model-dependent responses. *Journal of the Meteorological Society
5 of Japan*, **78**, 421-439.
- 6 Downes, S., A. Budnick, J. Sarmiento, and R. Farneti, 2011: Impacts of wind stress on the Antarctic Circumpolar
7 Current fronts and associated subduction. *Geophysical Research Letters*, **38**, L11605.
- 8 Driesschaert, E., et al., 2007: Modeling the influence of Greenland ice sheet melting on the Atlantic meridional
9 overturning circulation during the next millennia. *Geophysical Research Letters*, **34**, L10707.
- 10 Drijfhout, S. S., S. Weber, and E. van der Waluw, 2010: The stability of the MOC as diagnosed from the model
11 projections for the pre-industrial, present and future climate. *Climate Dynamics*. online first.
- 12 Dufresne, J.-L., et al., 2011: Climate change projections using the IPSL-CM5 Earth System Model: from CMIP3 to
13 CMIP5. *Climate Dynamics*. submitted.
- 14 Dufresne, J. L., and S. Bony, 2008: An assessment of the primary sources of spread of global warming estimates from
15 coupled atmosphere-ocean models. *Journal of Climate*, **21**, 5135-5144.
- 16 Dulamsuren, C., M. Hauck, and M. Muhlenberg, 2008: Insect and small mammal herbivores limit tree establishment in
17 northern Mongolian steppe. *Plant Ecology*, **195**, 143-156.
- 18 Dulamsuren, C., M. Hauck, and C. Leuschner, 2010: Recent drought stress leads to growth reductions in *Larix sibirica*
19 in the western Khentey, Mongolia. *Global Change Biology*, **16**, 3024-3035.
- 20 Dulamsuren, C., et al., 2009: Water relations and photosynthetic performance in *Larix sibirica* growing in the forest-
21 steppe ecotone of northern Mongolia. *Tree Physiology*, **29**, 99-110.
- 22 Durack, P., and S. Wijffels, 2010: Fifty-Year Trends in Global Ocean Salinities and Their Relationship to Broad-Scale
23 Warming. *Journal of Climate*, **23**, 4342-4362.
- 24 Eby, M., K. Zickfeld, A. Montenegro, D. Archer, K. Meissner, and A. Weaver, 2009: Lifetime of Anthropogenic
25 Climate Change: Millennial Time Scales of Potential CO2 and Surface Temperature Perturbations. *Journal of
26 Climate*, **22**, 2501-2511.
- 27 Edwards, T., M. Crucifix, and S. Harrison, 2007: Using the past to constrain the future: how the palaeorecord can
28 improve estimates of global warming. *Progress in Physical Geography*, **31**, 481-500.
- 29 Eglin, T., et al., 2010: Historical and future perspectives of global soil carbon response to climate and land-use changes.
30 *Tellus Series B-Chemical and Physical Meteorology*, **62**, 700-718.
- 31 Eisenman, I., and J. Wettlaufer, 2009: Nonlinear threshold behavior during the loss of Arctic sea ice. *Proceedings of the
32 National Academy of Sciences of the United States of America*, **106**, 28-32.
- 33 Eisenman, I., T. Schneider, D. S. Battisti, and C. M. Bitz, 2011: Consistent changes in the sea ice seasonal cycle in
34 response to global warming. *Journal of Climate*. in press.
- 35 Eyring, V., T. G. Shepherd, and D. W. Waugh, 2010a: SPARC CCMVal, SPARC Report on the Evaluation of
36 Chemistry-Climate Models.
- 37 Eyring, V., et al., 2010b: Sensitivity of 21st century stratospheric ozone to greenhouse gas scenarios. *Geophys. Res.
38 Lett.*, **37**, L16807.
- 39 Eyring, V., et al., 2005: A strategy for process-oriented validation of coupled chemistry-climate models. *Bulletin of the
40 American Meteorological Society*, **86**, 1117-1133.
- 41 Eyring, V., et al., 2010c: Multi-model assessment of stratospheric ozone return dates and ozone recovery in CCMVal-2
42 models. *Atmospheric Chemistry and Physics*, **10**, 9451-9472.
- 43 Farneti, R., and P. Gent, 2011: The effects of the eddy-induced advection coefficient in a coarse-resolution coupled
44 climate model. *Ocean Modelling*, **39**, 135-145.
- 45 Farneti, R., T. Delworth, A. Rosati, S. Griffies, and F. Zeng, 2010: The Role of Mesoscale Eddies in the Rectification of
46 the Southern Ocean Response to Climate Change. *Journal of Physical Oceanography*, **40**, 1539-1557.
- 47 Fasullo, J. T., 2010: Robust Land-Ocean Contrasts in Energy and Water Cycle Feedbacks. *Journal of Climate*, **23**,
48 4677-4693.
- 49 Favre, A., and A. Gershunov, 2009: North Pacific cyclonic and anticyclonic transients in a global warming context:
50 possible consequences for Western North American daily precipitation and temperature extremes. *Climate
51 Dynamics*, **32**, 969-987.
- 52 Finnis, J., M. M. Holland, M. C. Serreze, and J. J. Cassano, 2007: Response of Northern Hemisphere extratropical
53 cyclone activity and associated precipitation to climate change, as represented by the Community Climate
54 System Model. *Journal of Geophysical Research-Biogeosciences*, **112**, G04S42.
- 55 Fischer, E. M., and C. Schär, 2009: Future changes in daily summer temperature variability: driving processes and role
56 for temperature extremes. *Climate Dynamics*, **33**, 917-935.
- 57 ———, 2010: Consistent geographical patterns of changes in high-impact European heatwaves. *Nature Geoscience*, **3**,
58 398-403.
- 59 Fischer, E. M., D. M. Lawrence, and B. M. Sanderson, 2011: Quantifying uncertainties in projections of extremes-a
60 perturbed land surface parameter experiment. *Climate Dynamics*, **37**, 1381-1398.
- 61 Fischer, E. M., S. I. Seneviratne, D. Lüthi, and C. Schär, 2007: Contribution of land-atmosphere coupling to recent
62 European summer heat waves. *Geophysical Research Letters*, **34**, L06707.

- 1 Forest, C. E., P. H. Stone, and A. P. Sokolov, 2008: Constraining climate model parameters from observed 20th century
2 changes. *Tellus Series a-Dynamic Meteorology and Oceanography*, **60**, 911-920, doi:910.1111/j.1600-
3 0870.2008.00346.x.
- 4 Forster, P., and K. Taylor, 2006: Climate forcings and climate sensitivities diagnosed from coupled climate model
5 integrations. *Journal of Climate*, 6181-6194.
- 6 Fowler, H., M. Ekstrom, S. Blenkinsop, and A. Smith, 2007a: Estimating change in extreme European precipitation
7 using a multimodel ensemble. *Journal of Geophysical Research-Atmospheres*, **112**, D18104.
- 8 Fowler, H. J., S. Blenkinsop, and C. Tebaldi, 2007b: Linking climate change modelling to impacts studies: recent
9 advances in downscaling techniques for hydrological modelling. *International Journal of Climatology*, **27**, 1547-
10 1578.
- 11 Frame, D., B. Booth, J. Kettleborough, D. Stainforth, J. Gregory, M. Collins, and M. Allen, 2005: Constraining climate
12 forecasts: The role of prior assumptions. *Geophysical Research Letters*, **32**, L09702.
- 13 Friedlingstein, P., and S. Solomon, 2005: Contributions of past and present human generations to committed warming
14 caused by carbon dioxide. *Proceedings of the National Academy of Sciences of the United States of America*,
15 **102**, 10832-10836.
- 16 Friedlingstein, P., et al., 2006: Climate-carbon cycle feedback analysis: Results from the (CMIP)-M-4 model
17 intercomparison. *Journal of Climate*, 3337-3353.
- 18 Frieler, K., M. Meinhausen, T. Schneider von Deimling, T. Andrews, and P. Forster, 2011a: Changes in global-mean
19 precipitation in response to warming, greenhouse gas forcing and black carbon. *Geophysical Research Letters*,
20 **38**, L04702.
- 21 Frieler, K., M. Meinshausen, M. Mengel, N. Braun, and W. Hare, 2011b: A scaling approach to probabilistic
22 assessment of regional climate. *Journal of Climate*, 10.1175/JCLI-D-11-00199.1. In press.
- 23 Frierson, D., J. Lu, and G. Chen, 2007: Width of the Hadley cell in simple and comprehensive general circulation
24 models. *Geophysical Research Letters*, **34**, L18804.
- 25 Frolicher, T., and F. Joos, 2010: Reversible and irreversible impacts of greenhouse gas emissions in multi-century
26 projections with the NCAR global coupled carbon cycle-climate model. *Climate Dynamics*, **35**, 1439-1459.
- 27 Fu, Q., C. M. Johanson, J. M. Wallace, and T. Reichler, 2006: Enhanced mid-latitude tropospheric warming in satellite
28 measurements. *Science*, **312**, 1179-1179.
- 29 Fyfe, J., O. Saenko, K. Zickfeld, M. Eby, and A. Weaver, 2007: The role of poleward-intensifying winds on Southern
30 Ocean warming. *Journal of Climate*, **20**, 5391-5400.
- 31 Fyke, J., and A. Weaver, 2006: The effect of potential future climate change on the marine methane hydrate stability
32 zone. *Journal of Climate*, **19**, 5903-5917.
- 33 Gastineau, G., and B. J. Soden, 2009: Model projected changes of extreme wind events in response to global warming.
34 *Geophysical Research Letters*, **36**, L10810.
- 35 Gastineau, G., H. Le Treut, and L. Li, 2008: Hadley circulation changes under global warming conditions indicated by
36 coupled climate models. *Tellus Series a-Dynamic Meteorology and Oceanography*, **60**, 863-884.
- 37 Gastineau, G., L. Li, and H. Le Treut, 2009: The Hadley and Walker Circulation Changes in Global Warming
38 Conditions Described by Idealized Atmospheric Simulations. *Journal of Climate*, **22**, 3993-4013.
- 39 Gedney, N., P. Cox, and C. Huntingford, 2004: Climate feedback from wetland methane emissions. *Geophys. Res. Lett.*,
40 **31**, L20503, doi:20510.21029/22004GL020919.
- 41 Gent, P. R., and G. Danabasoglu, 2011: Climate model response to increasing Southern Hemisphere winds in CCSM4.
42 *Journal of Climate*, **24**, 4992-4998.
- 43 Georgescu, M., D. Lobell, and C. Field, 2011: Direct climate effects of perennial bioenergy crops in the United States.
44 *Proc Natl Acad Sci USA*, **109**, 4307-4312.
- 45 Gillett, N. P., and P. A. Stott, 2009: Attribution of anthropogenic influence on seasonal sea level pressure. *Geophys.*
46 *Res. Lett.*, **36**, L23709.
- 47 Gillett, N. P., V. K. Arora, K. Zickfeld, S. Marshall, and W. Merryfield, 2011: Ongoing climate change following a
48 complete cessation of carbon dioxide emissions. *Nature Geoscience*, **4**, 83-87.
- 49 Giorgi, F., 2008: A simple equation for regional climate change and associated uncertainty. *Journal of Climate*, **21**,
50 1589-1604, doi:1510.1175/2007jcli1763.1581.
- 51 Gleckler, P., K. Taylor, and C. Doutriaux, 2008: Performance metrics for climate models. *Journal of Geophysical*
52 *Research-Atmospheres*, **113**, D06104.
- 53 Goelzer, H., P. Huybrechts, M. Loutre, H. Goosse, T. Fichefet, and A. Mouchet, 2011: Impact of Greenland and
54 Antarctic ice sheet interactions on climate sensitivity. *Climate Dynamics*, **37**, 1005-1018.
- 55 Good, P., J. M. Gregory, and J. A. Lowe, 2011: A step-response simple climate model to reconstruct and interpret
56 AOGCM projections. *Geophysical Research Letters*, **38**, L01703.
- 57 Goosse, H., O. Arzel, C. Bitz, A. de Montety, and M. Vancoppenolle, 2009: Increased variability of the Arctic summer
58 ice extent in a warmer climate. *Geophysical Research Letters*, **36**, L23702.
- 59 Goubanova, K., and L. Li, 2007: Extremes in temperature and precipitation around the Mediterranean basin in an
60 ensemble of future climate scenario simulations. *Global and Planetary Change*, **57**, 27-42.
- 61 Granier, C., et al., 2011: Evolution of anthropogenic and biomass burning emissions at global and regional scales
62 during the 1980-2010 period. *Climatic Change*, **109**, 163-190.

- 1 Grant, A., S. Brönnimann, and L. Haimberger, 2008: Recent Arctic warming vertical structure contested. *Nature*, **455**,
2 E2-E3.
- 3 Graversen, R., and M. Wang, 2009: Polar amplification in a coupled climate model with locked albedo. *Climate*
4 *Dynamics*, **33**, 629-643.
- 5 Graversen, R., T. Mauritsen, M. Tjernstrom, E. Kallen, and G. Svensson, 2008: Vertical structure of recent Arctic
6 warming. *Nature*, **541**, 53-56.
- 7 Gregory, J., and P. Huybrechts, 2006: Ice-sheet contributions to future sea-level change. *Philosophical Transactions of*
8 *the Royal Society a-Mathematical Physical and Engineering Sciences*, **364**, 1709-1731.
- 9 Gregory, J., and M. Webb, 2008: Tropospheric adjustment induces a cloud component in CO₂ forcing. *Journal of*
10 *Climate*, **21**, 58-71.
- 11 Gregory, J., and P. Forster, 2008: Transient climate response estimated from radiative forcing and observed temperature
12 change. *Journal of Geophysical Research-Atmospheres*, **113**, D23105.
- 13 Gregory, J., et al., 2004: A new method for diagnosing radiative forcing and climate sensitivity. *Geophysical Research*
14 *Letters*, **31**, L03205.
- 15 Gregory, J., et al., 2005: A model intercomparison of changes in the Atlantic thermohaline circulation in response to
16 increasing atmospheric CO₂ concentration. *Geophysical Research Letters*, **32**, L12703.
- 17 Gregory, J. M., and J. F. B. Mitchell, 1995: Simulation of daily variability of surface-temperature and precipitation over
18 Europe in the current and 2xCO₂ climates using the UKMO climate model. *Quarterly Journal of the Royal*
19 *Meteorological Society*, **121**, 1451-1476.
- 20 Grubb, M., 1997: Technologies, energy systems and the timing of CO₂ emissions abatement - An overview of
21 economic issues. *Energy Policy*, **25**, 159-172.
- 22 Gutowski, W., K. Kozak, R. Arritt, J. Christensen, J. Patton, and E. Takle, 2007: A possible constraint on regional
23 precipitation intensity changes under global warming. *Journal of Hydrometeorology*, **8**, 1382-1396.
- 24 Gutowski, W., S. Willis, J. Patton, B. Schwedler, R. Arritt, and E. Takle, 2008: Changes in extreme, cold-season
25 synoptic precipitation events under global warming. *Geophysical Research Letters*, **35**, L20710.
- 26 Haarsma, R. J., F. Selten, B. V. Hurk, W. Hazeleger, and X. L. Wang, 2009: Drier Mediterranean soils due to
27 greenhouse warming bring easterly winds over summertime central Europe. *Geophysical Research Letters*, **36**,
28 L04705.
- 29 Haigh, J., and J. Pyle, 1982: Ozone perturbation experiments in a two-dimensional circulation model. *Quarterly Journal*
30 *of the Royal Meteorological Society*, **108**, 551-574.
- 31 Hall, A., 2004: The role of surface albedo feedback in climate. *Journal of Climate*, **17**, 1550-1568.
- 32 Hall, A., and X. Qu, 2006: Using the current seasonal cycle to constrain snow albedo feedback in future climate change.
33 *Geophysical Research Letters*, **33**, L03502.
- 34 Hansen, J., R. Ruedy, M. Sato, and K. Lo, 2010: Global surface temperature change. *Reviews of Geophysics*, **48**,
35 RG4004.
- 36 Hansen, J., G. Ruessell, A. Lacis, I. Fung, D. Rind, and P. Stone, 1985: Climate response-times - dependence on climate
37 sensitivity and ocean mixing. *Science*, **229**, 857-859.
- 38 Hansen, J., M. Sato, P. Kharecha, G. Russell, D. Lea, and M. Siddall, 2007: Climate change and trace gases.
39 *Philosophical Transactions of the Royal Society a-Mathematical Physical and Engineering Sciences*, **365**, 1925-
40 1954.
- 41 Hansen, J., et al., 1984: Climate sensitivity: Analysis of feedback mechanisms. *Climate Processes and Climate*
42 *Sensitivity*, J. Hansen, and T. Takahashi, Eds., American Geophysical Union.
- 43 Hansen, J., et al., 2008: Target Atmospheric CO₂: Where Should Humanity Aim? *The Open Atmospheric Science*
44 *Journal*, **2**, 217-231.
- 45 Hansen, J., et al., 2005a: Earth's energy imbalance: Confirmation and implications. *Science*, **308**, 1431-1435.
- 46 Hansen, J., et al., 2005b: Efficacy of climate forcings. *Journal of Geophysical Research-Atmospheres*, **110**, D18104.
- 47 Hare, B., and M. Meinshausen, 2006: How much warming are we committed to and how much can be avoided?
48 *Climatic Change*, **75**, 111-149.
- 49 Hargreaves, J., A. Abe-Ouchi, and J. Annan, 2007: Linking glacial and future climates through an ensemble of GCM
50 simulations. *Climate of the Past*, **3**, 77-87.
- 51 Harris, G. R., M. Collins, D. M. H. Sexton, J. M. Murphy, and B. B. B. Booth, 2010: Probabilistic projections for 21st
52 century European climate. *Natural Hazards and Earth System Sciences*, **10**, 2009-2020, doi:2010.5194/nhess-
53 2010-2009-2010.
- 54 Harris, G. R., D. M. H. Sexton, B. B. B. Booth, M. Collins, J. M. Murphy, and M. J. Webb, 2006: Frequency
55 distributions of transient regional climate change from perturbed physics ensembles of general circulation model
56 simulations. *Climate Dynamics*, **27**, 357-375.
- 57 Hartmann, D. L., and K. Larson, 2002: An important constraint on tropical cloud - climate feedback. *Geophysical*
58 *Research Letters*, **29**, 1951.
- 59 Haugen, J., and T. Iversen, 2008: Response in extremes of daily precipitation and wind from a downscaled multi-model
60 ensemble of anthropogenic global climate change scenarios. *Tellus Series a-Dynamic Meteorology and*
61 *Oceanography*, **60**, 411-426.
- 62 Hauglustaine, D., J. Lathiere, S. Szopa, and G. Folberth, 2005: Future tropospheric ozone simulated with a climate-
63 chemistry-biosphere model. *Geophys. Res. Lett.*, **32**, L24807, doi:24810.21029/22005GL024031.

- 1 Hawkins, E., and R. Sutton, 2009: The potential to narrow uncertainty in regional climate predictions. *Bulletin of the*
2 *American Meteorological Society*, **90**, 1095-1107, doi:10.1175/2009BAMS2607.1091.
- 3 ———, 2011: The potential to narrow uncertainty in projections of regional precipitation change. *Climate Dynamics*, **37**,
4 407-418.
- 5 Hegerl, G., T. Crowley, W. Hyde, and D. Frame, 2006: Climate sensitivity constrained by temperature reconstructions
6 over the past seven centuries. *Nature*, **440**, 1029-1032.
- 7 Hegerl, G. C., F. W. Zwiers, P. A. Stott, and V. V. Kharin, 2004: Detectability of anthropogenic changes in annual
8 temperature and precipitation extremes. *Journal of Climate*, **17**, 3683-3700.
- 9 Hegerl, G. C., et al., 2007: Understanding and Attributing Climate Change. *Climate Change 2007: The Physical*
10 *Science Basis. Contribution of Working Group I to the Fourth Assessment Report of the Intergovernmental*
11 *Panel on Climate Change*, Cambridge University Press.
- 12 Hegglin, M., and T. Shepherd, 2009: Large climate-induced changes in ultraviolet index and stratosphere-to-
13 troposphere ozone flux. *Nature Geoscience*, **2**, 687-691.
- 14 Held, I., and B. Soden, 2006: Robust responses of the hydrological cycle to global warming. *Journal of Climate*, **19**,
15 5686-5699.
- 16 Held, I. M., M. Winton, K. Takahashi, T. Delworth, F. R. Zeng, and G. K. Vallis, 2010: Probing the Fast and Slow
17 Components of Global Warming by Returning Abruptly to Preindustrial Forcing. *Journal of Climate*, **23**, 2418-
18 2427.
- 19 Henderson-Sellers, A., P. Irannejad, and K. McGuffie, 2008: Future desertification and climate change: The need for
20 land-surface system evaluation improvement. *Global and Planetary Change*, **64**, 129-138.
- 21 Hibbard, K. A., G. A. Meehl, P. A. Cox, and P. Friedlingstein, 2007: A strategy for climate change stabilization
22 experiments. *EOS Transactions AGU*, **88**, 217-221.
- 23 Hirschi, M., et al., 2011: Observational evidence for soil-moisture impact on hot extremes in southeastern Europe.
24 *Nature Geoscience*, **4**, 17-21.
- 25 Hoelzmann, P., D. Jolly, S. Harrison, F. Laarif, R. Bonnefille, and H. Pachur, 1998: Mid-Holocene land-surface
26 conditions in northern Africa and the Arabian Peninsula: A data set for the analysis of biogeophysical feedbacks
27 in the climate system. *Global Biogeochemical Cycles*, **12**, 35-51.
- 28 Hoerling, M., J. Eischeid, and J. Perlwitz, 2010: Regional Precipitation Trends: Distinguishing Natural Variability from
29 Anthropogenic Forcing. *Journal of Climate*, **23**, 2131-2145.
- 30 Hofmann, M., and S. Rahmstorf, 2009: On the stability of the Atlantic meridional overturning circulation. *Proceedings*
31 *of the National Academy of Sciences of the United States of America*, **106**, 20584-20589.
- 32 Hogg, E., and A. Schwarz, 1997: Regeneration of planted conifers across climatic moisture gradients on the Canadian
33 prairies: implications for distribution and climate change. *Journal of Biogeography*, **24**, 527-534.
- 34 Holden, P. B., and N. R. Edwards, 2010: Dimensionally reduced emulation of an AOGCM for application to integrated
35 assessment modelling. *Geophysical Research Letters*, **37**, L21707.
- 36 Holland, M., C. Bitz, and B. Tremblay, 2006: Future abrupt reductions in the summer Arctic sea ice. *Geophysical*
37 *Research Letters*, **33**, L23503.
- 38 Holland, M., M. Serreze, and J. Stroeve, 2010: The sea ice mass budget of the Arctic and its future change as simulated
39 by coupled climate models. *Climate Dynamics*, **34**, 185-200.
- 40 Holland, M. M., and C. M. Bitz, 2003: Polar amplification of climate change in coupled models. *Climate Dynamics*, **21**,
41 221-232.
- 42 Holland, M. M., C. M. Bitz, B. Tremblay, and D. A. Bailey, 2008: The role of natural versus forced change in future
43 rapid summer Arctic ice loss. *Arctic Sea Ice Decline: Observations, Projections, Mechanisms, and Implications*,
44 E. T. DeWeaver, C. M. Bitz, and L. B. Tremblay, Eds., Amer. Geophys. Union, 133-150.
- 45 Hu, A., G. Meehl, W. Han, and J. Yin, 2009: Transient response of the MOC and climate to potential melting of the
46 Greenland Ice Sheet in the 21st century. *Geophysical Research Letters*, **36**, L10707.
- 47 Hu, Z., M. Latif, E. Roeckner, and L. Bengtsson, 2000: Intensified Asian summer monsoon and its variability in a
48 coupled model forced by increasing greenhouse gas concentrations. *Geophysical Research Letters*, **27**, 2681-
49 2684.
- 50 Huber, M., I. Mahlstein, M. Wild, J. Fasullo, and R. Knutti, 2011: Constraints on Climate Sensitivity from Radiation
51 Patterns in Climate Models. *Journal of Climate*, **24**, 1034-1052.
- 52 Hurtt, G., et al., 2011: Harmonization of land-use scenarios for the period 1500-2100: 600 years of global gridded
53 annual land-use transtions, wood harvest, and resulting secondary lands. *Climatic Change*, doi:10.1007/s10584-
54 011-0153-2.
- 55 Hwang, Y.-T., D. M. W. Frierson, B. J. Soden, and I. M. Held, 2011: The corrigendum for Held and Soden
56 (2006). *Journal of Climate*. in press.
- 57 IPCC, 2000: IPCC Special Report on Emissions Scenarios. Prepared by Working Group III of the Intergovernmental
58 Panel on Climate Change.
- 59 ———, 2012: Changes in Climate Extremes and their Impacts on the Natural Physical Environment, in press pp.
- 60 Isaksen, I., et al., 2009: Atmospheric composition change: Climate-Chemistry interactions. *Atmospheric Environment*,
61 **43**, 5138-5192.
- 62 Jackson, C. S., M. K. Sen, G. Huerta, Y. Deng, and K. P. BoW man, 2008: Error Reduction and Convergence in
63 Climate Prediction. *Journal of Climate*, **21**, 6698-6709, doi:6610.1175/2008jcli2112.6691.

- 1 Jacob, D., and D. Winner, 2009: Effect of climate change on air quality. *Atmospheric Environment*, **43**, 51-63.
- 2 Jaeger, C., and J. Jaeger, 2011: Three views of two degrees. *Regional Environmental Change*, **11**, S15-S26.
- 3 Johanson, C. M., and Q. Fu, 2009: Hadley Cell Widening: Model Simulations versus Observations. *Journal of Climate*,
4 **22**, 2713-2725.
- 5 Johns, T. C., et al., 2011: Climate change under aggressive mitigation: the ENSEMBLES multi-model experiment.
6 *Climate Dynamics*, **37**, 1975-2003.
- 7 Johnson, C., D. Stevenson, W. Collins, and R. Derwent, 2001: Role of climate feedback on methane and ozone studied
8 with a coupled ocean-atmosphere-chemistry model. *Geophys. Res. Lett.*, **28**, 1723-1726.
- 9 Jones, A., J. Haywood, and O. Boucher, 2007: Aerosol forcing, climate response and climate sensitivity in the Hadley
10 Centre climate model. *Journal of Geophysical Research-Atmospheres*, **112**, D20211.
- 11 Jones, C., P. Cox, and C. Huntingford, 2006: Climate-carbon cycle feedbacks under stabilization: uncertainty and
12 observational constraints. *Tellus Series B-Chemical and Physical Meteorology*, DOI 10.1111/j.1600-
13 0889.2006.00215.x. 603-613.
- 14 Jones, C., J. Lowe, S. Liddicoat, and R. Betts, 2009: Committed terrestrial ecosystem changes due to climate change.
15 *Nature Geoscience*, **2**, 484-487.
- 16 Jones, C. D., et al., 2011: The HadGEM2-ES implementation of CMIP5 centennial simulations. *Geoscientific Model
17 Development*, **4**, 543-570.
- 18 Joshi, M., K. Shine, M. Ponater, N. Stuber, R. Sausen, and L. Li, 2003: A comparison of climate response to different
19 radiative forcings in three general circulation models: towards an improved metric of climate change. *Climate
20 Dynamics*, DOI 10.1007/s00382-003-0305-9. 843-854.
- 21 Joshi, M. M., J. M. Gregory, M. J. Webb, D. M. H. Sexton, and T. C. Johns, 2008: Mechanisms for the land/sea
22 warming contrast exhibited by simulations of climate change. *Climate Dynamics*, **30**, 455-465.
- 23 Jun, M., R. Knutti, and D. Nychka, 2008a: Local eigenvalue analysis of CMIP3 climate model errors. *Tellus Series a-
24 Dynamic Meteorology and Oceanography*, DOI 10.1111/j.1600-0870.2008.00356.x. 992-1000.
- 25 Jun, M., R. Knutti, and D. W. Nychka, 2008b: Spatial Analysis to Quantify Numerical Model Bias and Dependence:
26 How Many Climate Models Are There? *Journal of the American Statistical Association*, **103**, 934-947.
- 27 Jungclaus, J., H. Haak, M. Esch, E. Roeckner, and J. Marotzke, 2006: Will Greenland melting halt the thermohaline
28 circulation? *Geophysical Research Letters*, **33**, L17708.
- 29 Kamiguchi, K., A. Kitoh, T. Uchiyama, R. Mizuta, and A. Noda, 2006: Changes in Precipitation-based Extremes
30 Indices Due to Global Warming Projected by a Global 20-km-mesh Atmospheric Model. *SOLA*, **2**, 64-67.
- 31 Kattenberg, A., et al., 1996: Climate Models - Projections of Future Climate. *Climate Change 1995 - The Science of
32 Climate Change. Contribution of WGI to the Second Assessment Report of the Intergovernmental Panel on
33 Climate Change*. Cambridge University Press.
- 34 Kay, J., M. Holland, and A. Jahn, 2011a: Inter-annual to multi-decadal Arctic sea ice extent trends in a warming world.
35 *Geophysical Research Letters*, **38**, L15708.
- 36 Kay, J. E., M. M. Holland, C. Bitz, E. Blanchard-Wrigglesworth, A. Gettelman, A. Conley, and D. Bailey, 2011b: The
37 influence of local feedbacks and northward heat transport on the equilibrium Arctic climate response to
38 increased greenhouse gas forcing in coupled climate models. submitted.
- 39 Kellomaki, S., M. Maajarvi, H. Strandman, A. Kilpelainen, and H. Peltola, 2010: Model Computations on the Climate
40 Change Effects on Snow Cover, Soil Moisture and Soil Frost in the Boreal Conditions over Finland. *Silva
41 Fennica*, **44**, 213-233.
- 42 Kendon, E., D. Rowell, and R. Jones, 2010: Mechanisms and reliability of future projected changes in daily
43 precipitation. *Climate Dynamics*, **35**, 489-509.
- 44 Kendon, E., D. Rowell, R. Jones, and E. Buonomo, 2008: Robustness of future changes in local precipitation extremes.
45 *Journal of Climate*, **17**, 4280-4297.
- 46 Kharin, V. V., F. W. Zwiers, X. B. Zhang, and G. C. Hegerl, 2007: Changes in temperature and precipitation extremes
47 in the IPCC ensemble of global coupled model simulations. *Journal of Climate*, **20**, 1419-1444.
- 48 Khvorostyanov, D., P. Ciaia, G. Krinner, and S. Zimov, 2008: Vulnerability of east Siberia's frozen carbon stores to
49 future warming. *Geophysical Research Letters*, **35**, L10703.
- 50 Kidston, J., S. M. Dean, J. A. Renwick, and G. K. Vallis, 2010: A robust increase in the eddy length scale in the
51 simulation of future climates. *Geophysical Research Letters*, **37**, L03806.
- 52 Kienzle, S. W., M. W. Nemeth, J. M. Byrne, and R. J. MacDonald, 2011: Simulating the hydrological impacts of
53 climate change in the upper North Saskatchewan River basin, Alberta, Canada. *Journal of Hydrology*. in press.
- 54 Kitoh, A., S. Yukimoto, A. Noda, and T. Motoi, 1997: Simulated changes in the Asian summer monsoon at times of
55 increased atmospheric CO2. *Journal of the Meteorological Society of Japan*, **75**, 1019-1031.
- 56 Kjellstrom, E., L. Barring, D. Jacob, R. Jones, G. Lenderink, and C. Schar, 2007: Modelling daily temperature
57 extremes: recent climate and future changes over Europe. *Climatic Change*, **81**, 249-265.
- 58 Klocke, D., R. Pincus, and J. Quaas, 2011: On constraining estimates of climate sensitivity with present-day
59 observations through model weighting. *Journal of Climate*. in press.
- 60 Knight, C., et al., 2007: Association of parameter, software, and hardware variation with large-scale behavior across
61 57,000 climate models. *Proceedings of the National Academy of Sciences of the United States of America*, **104**,
62 12259-12264.
- 63 Knutti, R., 2010: The end of model democracy? *Climatic Change*, **102**, 395-404.

- 1 Knutti, R., and G. Hegerl, 2008: The equilibrium sensitivity of the Earth's temperature to radiation changes. *Nature*
2 *Geoscience*, **1**, 735-743.
- 3 Knutti, R., and G.-K. Plattner, 2011: Comment on 'Why Hasn't Earth Warmed as Much as Expected?' by Schwartz et
4 al. 2010. *Journal of Climate*. in press.
- 5 Knutti, R., G. A. Meehl, M. R. Allen, and D. A. Stainforth, 2006: Constraining climate sensitivity from the seasonal
6 cycle in surface temperature. *Journal of Climate*, **19**, 4224-4233.
- 7 Knutti, R., S. Krahenmann, D. Frame, and M. Allen, 2008a: Comment on "Heat capacity, time constant, and sensitivity
8 of Earth's climate system" by S. E. Schwartz. *Journal of Geophysical Research-Atmospheres*, **113**, D15103.
- 9 Knutti, R., F. Joos, S. Muller, G. Plattner, and T. Stocker, 2005: Probabilistic climate change projections for CO₂
10 stabilization profiles. *Geophysical Research Letters*, **32**, L20707.
- 11 Knutti, R., R. Furrer, C. Tebaldi, J. Cermak, and G. Meehl, 2010a: Challenges in Combining Projections from Multiple
12 Climate Models. *Journal of Climate*, **23**, 2739-2758.
- 13 Knutti, R., G. Abramowitz, M. Collins, V. Eyring, P. J. Gleckler, B. Hewitson, and L. Mearns, 2010b: Good Practice
14 Guidance Paper on Assessing and Combining Multi Model Climate Projections.
- 15 Knutti, R., et al., 2008b: A review of uncertainties in global temperature projections over the twenty-first century.
16 *Journal of Climate*, **21**, 2651-2663.
- 17 Kodra, E., K. Steinhaeuser, and A. R. Ganguly, 2011: Persisting cold extremes under 21st-century warming scenarios.
18 *Geophysical Research Letters*, **38**, L08705.
- 19 Kolomyts, E., and N. Surova, 2010: Predicting the Impact of Global Warming on Soil Water Resources in Marginal
20 Forests of the Middle Volga Region. *Water Resources*, **37**, 89-101.
- 21 Körper, J., et al., 2011: The Effect of Aggressive Mitigation on Sea Level Rise and Sea Ice Changes. *Climate*
22 *Dynamics*. submitted.
- 23 Koster, R., Z. Guo, R. Yang, P. Dirmeyer, K. Mitchell, and M. Puma, 2009a: On the Nature of Soil Moisture in Land
24 Surface Models. *Journal of Climate*, **22**, 4322-4335.
- 25 Koster, R., et al., 2006: GLACE: The Global Land-Atmosphere Coupling Experiment. Part I: Overview. *Journal of*
26 *Hydrometeorology*, **7**, 590-610.
- 27 Koster, R. D., S. D. Schubert, and M. J. Suarez, 2009b: Analyzing the Concurrence of Meteorological Droughts and
28 Warm Periods, with Implications for the Determination of Evaporative Regime. *Journal of Climate*, **22**, 3331-
29 3341.
- 30 Koster, R. D., H. L. Wang, S. D. Schubert, M. J. Suarez, and S. Mahanama, 2009c: Drought-Induced Warming in the
31 Continental United States under Different SST Regimes. *Journal of Climate*, **22**, 5385-5400.
- 32 Koven, C., P. Friedlingstein, P. Ciais, D. Khvorostyanov, G. Krinner, and C. Tarnocai, 2009: On the formation of high-
33 latitude soil carbon stocks: Effects of cryoturbation and insulation by organic matter in a land surface model.
34 *Geophysical Research Letters*, **36**, L21501.
- 35 Koven, C. D., et al., 2011: Permafrost carbon-climate feedbacks accelerate global warming. *Proceedings of the*
36 *National Academy of Sciences of the United States of America*, **108**, 14769-14774.
- 37 Kripalani, R., J. Oh, A. Kulkarni, S. Sabade, and H. Chaudhari, 2007: South Asian summer monsoon precipitation
38 variability: Coupled climate model simulations and projections under IPCC AR4. *Theoretical and Applied*
39 *Climatology*, **90**, 133-159.
- 40 Kug, J., D. Choi, F. Jin, W. Kwon, and H. Ren, 2010: Role of synoptic eddy feedback on polar climate responses to the
41 anthropogenic forcing. *Geophysical Research Letters*, **37**, L14704.
- 42 Kuhry, P., E. Dorrepaal, G. Hugelius, E. Schuur, and C. Tarnocai, 2010: Potential Remobilization of Belowground
43 Permafrost Carbon under Future Global Warming. *Permafrost and Periglacial Processes*, **21**, 208-214.
- 44 Kysely, J., and R. Beranova, 2009: Climate-change effects on extreme precipitation in central Europe: uncertainties of
45 scenarios based on regional climate models. *Theoretical and Applied Climatology*, **95**, 361-374.
- 46 Lamarque, J.-F., et al., 2011: Global and regional evolution of short-lived radiatively-active gases and aerosols in the
47 Representative Concentration Pathways. *Climatic Change*, **109**, 191-212.
- 48 Lamarque, J., 2008: Estimating the potential for methane clathrate instability in the 1%-CO₂ IPCC AR-4 simulations.
49 *Geophysical Research Letters*, **35**, L19806.
- 50 Lamarque, J., et al., 2010: Historical (1850-2000) gridded anthropogenic and biomass burning emissions of reactive
51 gases and aerosols: methodology and application. *Atmospheric Chemistry and Physics*, **10**, 7017-7039.
- 52 Lambert, F. H., and J. C. H. Chiang, 2007: Control of land-ocean temperature contrast by ocean heat uptake.
53 *Geophysical Research Letters*, **34**, L13704.
- 54 Lambert, F. H., M. J. Webb, and M. J. Joshi, 2011: The relationship between land-ocean surface temperature contrast
55 and radiative forcing. *Journal of Climate*, **24**, 3239-3256.
- 56 Landrum, L., M. M. Holland, D. P. Schneider, and E. Hunke, 2011: Antarctic sea ice climatology, variability and late
57 20th century change in CCSM4. *Journal of Climate*. submitted.
- 58 Lau, K., M. Kim, and K. Kim, 2006: Asian summer monsoon anomalies induced by aerosol direct forcing: the role of
59 the Tibetan Plateau. *Climate Dynamics*, **26**, 855-864.
- 60 Lawrence, D., and A. Slater, 2010: The contribution of snow condition trends to future ground climate. *Climate*
61 *Dynamics*, **34**, 969-981.
- 62 Lawrence, D., A. Slater, and S. Swenson, 2011: Simulation of Present-day and Future Permafrost and Seasonally
63 Frozen Ground Conditions in CCSM4. *Journal of Climate*. in press.

- 1 Lawrence, D., A. Slater, V. Romanovsky, and D. Nicolsky, 2008: Sensitivity of a model projection of near-surface
2 permafrost degradation to soil column depth and representation of soil organic matter. *Journal of Geophysical*
3 *Research-Earth Surface*, **113**, F02011.
- 4 Le Brocq, A. M., A. J. Payne, and A. Vieli, 2010: An improved Antarctic dataset for high resolution numerical ice sheet
5 models (ALBMAP v1). *Earth Syst. Sci. Data*, **2**, 247-260.
- 6 Le Quere, C., et al., 2009: Trends in the sources and sinks of carbon dioxide. *Nature Geoscience*, **2**, 831-836.
- 7 Lean, J., and D. Rind, 2009: How will Earth's surface temperature change in future decades? *Geophysical Research*
8 *Letters*, **36**, L15708.
- 9 Leckebusch, G. C., A. Weimer, J. G. Pinto, M. Meyers, and P. Speth, 2008: Extreme wind storms over Europe in
10 present and future climate: a cluster analysis approach. *Meteorologische Zeitschrift*, **17**, 67-82.
- 11 Lefebvre, W., and H. Goosse, 2008: Analysis of the projected regional sea-ice changes in the Southern Ocean during
12 the twenty-first century. *Climate Dynamics*, **30**, 59-76.
- 13 Lemoine, D. M., 2010: Climate Sensitivity Distributions Dependence on the Possibility that Models Share Biases.
14 *Journal of Climate*, **23**, 4395-4415.
- 15 Lenderink, G., and E. Van Meijgaard, 2008: Increase in hourly precipitation extremes beyond expectations from
16 temperature changes. *Nature Geoscience*, **1**, 511-514.
- 17 Lenderink, G., A. van Ulden, B. van den Hurk, and E. van Meijgaard, 2007: Summertime inter-annual temperature
18 variability in an ensemble of regional model simulations: analysis of the surface energy budget. *Climatic*
19 *Change*, **81**, 233-247.
- 20 Lenton, T., H. Held, E. Kriegler, J. Hall, W. Lucht, S. Rahmstorf, and H. Schellnhuber, 2008: Tipping elements in the
21 Earth's climate system. *Proceedings of the National Academy of Sciences of the United States of America*, **105**,
22 1786-1793.
- 23 Levermann, A., J. Schewe, V. Petoukhov, and H. Held, 2009: Basic mechanism for abrupt monsoon transitions.
24 *Proceedings of the National Academy of Sciences of the United States of America*, **106**, 20572-20577.
- 25 Levitus, S., J. Antonov, T. Boyer, R. Locarnini, H. Garcia, and A. Mishonov, 2009: Global ocean heat content 1955-
26 2008 in light of recently revealed instrumentation problems. *Geophysical Research Letters*, **36**, L07608.
- 27 Li, C., J.-S. von Storch, and J. Marotzke, 2011a: Deep-ocean Heat Uptake and Equilibrium Climate Response. *Climate*
28 *Dynamics*. submitted.
- 29 Li, F., W. Collins, M. Wehner, D. Williamson, J. Olson, and C. Algieri, 2011b: Impact of horizontal resolution on
30 simulation of precipitation extremes in an aqua-planet version of Community Atmospheric Model (CAM3).
31 *Tellus*, **63**, 884-892.
- 32 Lim, E. P., and I. Simmonds, 2009: Effect of tropospheric temperature change on the zonal mean circulation and SH
33 winter extratropical cyclones. *Climate Dynamics*, **33**, 19-32.
- 34 Lindsay, R., and J. Zhang, 2005: The thinning of Arctic sea ice, 1988-2003: Have we passed a tipping point? *Journal of*
35 *Climate*, **18**, 4879-4894.
- 36 Loarie, S. R., D. B. Lobell, G. P. Asner, Q. Z. Mu, and C. B. Field, 2011: Direct impacts on local climate of sugar-cane
37 expansion in Brazil. *Nature Climate Change*, **1**, 105-109.
- 38 Loeb, N. G., et al., 2009: Toward Optimal Closure of the Earth's Top-of-Atmosphere Radiation Budget. *Journal of*
39 *Climate*, **22**, 748-766.
- 40 Lorenz, D. J., and E. T. DeWeaver, 2007: Tropopause height and zonal wind response to global warming in the IPCC
41 scenario integrations. *Journal of Geophysical Research-Atmospheres*, **112**.
- 42 Lowe, J., C. Huntingford, S. Raper, C. Jones, S. Liddicoat, and L. Gohar, 2009: How difficult is it to recover from
43 dangerous levels of global warming? *Environmental Research Letters*, **4**, 014012.
- 44 Lu, J., and M. Cai, 2009: Seasonality of polar surface warming amplification in climate simulations. *Geophysical*
45 *Research Letters*, **36**, L16704.
- 46 Lu, J., G. Vecchi, and T. Reichler, 2007: Expansion of the Hadley cell under global warming. *Geophysical Research*
47 *Letters*, **34**, L06805.
- 48 Lu, J., G. Chen, and D. Frierson, 2008: Response of the Zonal Mean Atmospheric Circulation to El Nino versus Global
49 Warming. *Journal of Climate*, **21**, 5835-5851.
- 50 Lucht, W., S. Schaphoff, T. Ebrecht, U. Heyder, and W. Cramer, 2006: Terrestrial vegetation redistribution and carbon
51 balance under climate change. *Carbon Balance and Management*, **1**.
- 52 Lunt, D., A. Haywood, G. Schmidt, U. Salzmann, P. Valdes, and H. Dowsett, 2010: Earth system sensitivity inferred
53 from Pliocene modelling and data. *Nature Geoscience*, **3**, 60-64.
- 54 Luo, Y., L. Rothstein, and R. Zhang, 2009: Response of Pacific subtropical-tropical thermocline water pathways and
55 transports to global warming. *Geophysical Research Letters*, **36**, L04601.
- 56 Lyman, J. M., et al., 2010: Robust warming of the global upper ocean. *Nature*, **465**, 334-337.
- 57 Mahlstein, I., and R. Knutti, 2011a: Ocean Heat Transport as a Cause for Model Uncertainty in Projected Arctic
58 Warming. *Journal of Climate*, **24**, 1451-1460.
- 59 Mahlstein, I., and R. Knutti, 2011b: September Arctic sea ice predicted to disappear near 2°C global warming above
60 present. *Journal of Geophysical Research*. submitted.
- 61 Malhi, Y., et al., 2009: Exploring the likelihood and mechanism of a climate-change-induced dieback of the Amazon
62 rainforest. *Proceedings of the National Academy of Sciences of the United States of America*, **106**, 20610-20615.

- 1 Manabe, S., and R. T. Wetherald, 1980: Distribution of climate change resulting from an increase in CO₂ content of the
2 atmosphere. *Journal of the Atmospheric Sciences*, **37**, 99-118.
- 3 Manabe, S., and R. Stouffer, 1980: Sensitivity of a global climate model to an increase of CO₂ concentration in the
4 atmosphere. *Journal of Geophysical Research-Oceans and Atmospheres*, **85**, 5529-5554.
- 5 ———, 1994: Multiple-century response of a coupled ocean-atmosphere model to an increase of atmospheric carbon-
6 dioxide. *Journal of Climate*, **7**, 5-23.
- 7 Manabe, S., K. Bryan, and M. J. Spelman, 1990: Transient-response of a global ocean atmosphere model to a doubling
8 of atmospheric carbon-dioxide. *Journal of Physical Oceanography*, **20**, 722-749.
- 9 Manabe, S., R. J. Stouffer, M. J. Spelman, and K. Bryan, 1991: TRANSIENT RESPONSES OF A COUPLED OCEAN
10 ATMOSPHERE MODEL TO GRADUAL CHANGES OF ATMOSPHERIC CO₂. I. ANNUAL MEAN
11 RESPONSE. *Journal of Climate*, **4**, 785-818.
- 12 Masson, D., and R. Knutti, 2011: Climate model genealogy. *Geophysical Research Letters*, **38**, L08703,
13 doi:08710.01029/02011GL046864.
- 14 Matthews, H., and K. Caldeira, 2008: Stabilizing climate requires near-zero emissions. *Geophysical Research Letters*,
15 **35**, L04705.
- 16 Matthews, H., N. Gillett, P. Stott, and K. Zickfeld, 2009: The proportionality of global warming to cumulative carbon
17 emissions. *Nature*, **459**, 829-832.
- 18 Matthews, H. D., S. Solomon, and R. Pierrehumbert, 2011: Cumulative carbon as a policy framework for achieving
19 climate stabilization. *Philosophical Transactions of the Royal Society*. in press.
- 20 May, W., 2002: Simulated changes of the Indian summer monsoon under enhanced greenhouse gas conditions in a
21 global time-slice experiment. *Geophysical Research Letters*, **29**, 1118.
- 22 May, W., 2008a: Climatic changes associated with a global "2 degrees C-stabilization" scenario simulated by the
23 ECHAM5/MPI-OM coupled climate model. *Climate Dynamics*, **31**, 283-313.
- 24 May, W., 2008b: Potential future changes in the characteristics of daily precipitation in Europe simulated by the
25 HIRHAM regional climate model. *Climate Dynamics*, **30**, 581-603.
- 26 McCabe, G., and D. Wolock, 2007: Warming may create substantial water supply shortages in the Colorado River
27 basin. *Geophysical Research Letters*, **34**, L22708.
- 28 McLandress, C., T. G. Shepherd, J. F. Scinocca, D. A. Plummer, M. Sigmond, A. I. Jonsson, and M. C. Reader, 2011:
29 Separating the Dynamical Effects of Climate Change and Ozone Depletion. Part II Southern Hemisphere
30 Troposphere. *Journal of Climate*, **24**, 1850-1868.
- 31 McWilliams, J. C., 2007: Irreducible imprecision in atmospheric and oceanic simulations. *Proceedings of the National
32 Academy of Sciences of the United States of America*, **104**, 8709-8713.
- 33 Meehl, G., and W. Washington, 1993: South Asian summer monsoon variability in a model with doubled atmospheric
34 carbon-dioxide concentration. *Science*, **260**, 1101-1104.
- 35 Meehl, G., J. Arblaster, and C. Tebaldi, 2005a: Understanding future patterns of increased precipitation intensity in
36 climate model simulations. *Geophysical Research Letters*, **32**, L18719.
- 37 Meehl, G., J. Arblaster, and W. Collins, 2008: Effects of black carbon aerosols on the Indian monsoon. *Journal of
38 Climate*, **21**, 2869-2882.
- 39 Meehl, G., G. Boer, C. Covey, M. Latif, and R. Stouffer, 2000: The Coupled Model Intercomparison Project (CMIP).
40 *Bull. Amer. Meteorol. Soc.*, **81**, 313-318.
- 41 Meehl, G., W. Washington, C. Ammann, J. Arblaster, T. Wigley, and C. Tebaldi, 2004: Combinations of natural and
42 anthropogenic forcings in twentieth-century climate. *Journal of Climate*, **17**, 3721-3727.
- 43 Meehl, G., et al., 2005b: How much more global warming and sea level rise? *Science*, **307**, 1769-1772.
- 44 Meehl, G., et al., 2006: Climate change projections for the twenty-first century and climate change commitment in the
45 CCSM3. *Journal of Climate*, **19**, 2597-2616.
- 46 Meehl, G. A., and C. Tebaldi, 2004: More intense, more frequent, and longer lasting heat waves in the 21st century.
47 *Science*, **305**, 994-997.
- 48 Meehl, G. A., C. Tebaldi, G. Walton, D. Easterling, and L. McDaniel, 2009: Relative increase of record high maximum
49 temperatures compared to record low minimum temperatures in the U. S. *Geophysical Research Letters*, **36**,
50 L23701.
- 51 Meehl, G. A., et al., 2007a: The WCRP CMIP3 multimodel dataset - A new era in climate change research. *Bulletin of
52 the American Meteorological Society*, **88**, 1383-1394.
- 53 Meehl, G. A., et al., 2011: Climate system response to external forcings and climate change projections in CCSM4.
54 *Journal of Climate*. in press.
- 55 Meehl, G. A., et al., 2007b: Global Climate Projections. *Climate Change 2007: The Physical Science Basis.
56 Contribution of Working Group I to the Fourth Assessment Report of the Intergovernmental Panel on Climate
57 Change*, Cambridge University Press.
- 58 Meinshausen, M., S. Raper, and T. Wigley, 2011a: Emulating coupled atmosphere-ocean and carbon cycle models with
59 a simpler model, MAGICC6-Part 1: Model description and calibration. *Atmospheric Chemistry and Physics*, **11**,
60 1417-1456.
- 61 Meinshausen, M., T. Wigley, and S. Raper, 2011b: Emulating atmosphere-ocean and carbon cycle models with a
62 simpler model, MAGICC6-Part 2: Applications. *Atmospheric Chemistry and Physics*, **11**, 1457-1471.

- 1 Meinshausen, M., B. Hare, T. Wigley, D. Van Vuuren, M. Den Elzen, and R. Swart, 2006: Multi-gas emissions
2 pathways to meet climate targets. *Climatic Change*, **75**, 151-194.
- 3 Meinshausen, M., et al., 2009: Greenhouse-gas emission targets for limiting global warming to 2 degrees C. *Nature*,
4 **458**, 1158-1162.
- 5 Meinshausen, M., et al., 2011c: The RCP Greenhouse Gas Concentrations and their Extensions from 1765 to 2300.
6 *Climatic Change*, **109**, 213-241.
- 7 Mignone, B., R. Socolow, J. Sarmiento, and M. Oppenheimer, 2008: Atmospheric stabilization and the timing of carbon
8 mitigation. *Climatic Change*, **88**, 251-265.
- 9 Mikolajewicz, U., M. Vizcaino, J. Jungclaus, and G. Schurgers, 2007a: Effect of ice sheet interactions in anthropogenic
10 climate change simulations. *Geophysical Research Letters*, **34**, L18706.
- 11 Mikolajewicz, U., M. Groger, E. Maier-Reimer, G. Schurgers, M. Vizcaino, and A. Winguth, 2007b: Long-term effects
12 of anthropogenic CO₂ emissions simulated with a complex earth system model. *Climate Dynamics*, **28**, 599-633.
- 13 Miller, R. L., G. A. Schmidt, and D. T. Shindell, 2006: Forced annular variations in the 20th century intergovernmental
14 panel on climate change fourth assessment report models. *Journal of Geophysical Research-Atmospheres*, **111**,
15 D18101.
- 16 Milly, P., J. Betancourt, M. Falkenmark, R. Hirsch, Z. Kundzewicz, D. Lettenmaier, and R. Stouffer, 2008: Climate
17 change - Stationarity is dead: Whither water management? *Science*, **319**, 573-574.
- 18 Ming, Y., V. Ramaswamy, and G. Persad, 2010: Two opposing effects of absorbing aerosols on global-mean
19 precipitation. *Geophysical Research Letters*, **37**, L13701.
- 20 Mitas, C., and A. Clement, 2006: Recent behavior of the Hadley cell and tropical thermodynamics in climate models
21 and reanalyses. *Geophysical Research Letters*, **33**, -.
- 22 Mitchell, J., T. Johns, W. Ingram, and J. Lowe, 2000: The effect of stabilising atmospheric carbon dioxide
23 concentrations on global and regional climate change. *Geophysical Research Letters*, **27**, 2977-2980.
- 24 Mitchell, J. F. B., 1983: The seasonal response of a general-circulation model to changes in CO₂ and sea temperatures.
25 *Quarterly Journal of the Royal Meteorological Society*, **109**, 113-152.
- 26 Mitchell, J. F. B., T. C. Johns, M. Eagles, W. J. Ingram, and R. A. Davis, 1999: Towards the construction of climate
27 change scenarios. *Climatic Change*, **41**, 547-581.
- 28 Mitchell, T. D., 2003: Pattern scaling - An examination of the accuracy of the technique for describing future climates.
29 *Climatic Change*, **60**, 217-242.
- 30 Monaghan, A., D. Bromwich, and D. Schneider, 2008: Twentieth century Antarctic air temperature and snowfall
31 simulations by IPCC climate models. *Geophysical Research Letters*, **35**, L07502.
- 32 Montenegro, A., V. Brovkin, M. Eby, D. Archer, and A. Weaver, 2007: Long term fate of anthropogenic carbon.
33 *Geophysical Research Letters*, **34**, L19707.
- 34 Moss, R. H., et al., 2010: The next generation of scenarios for climate change research and assessment. *Nature*, **463**,
35 747-756.
- 36 Moss, R. H., et al., 2008: Towards New Scenarios for Analysis of Emissions, Climate Change, Impacts, and Response
37 Strategies., 132 pp.
- 38 Murphy, D. M., S. Solomon, R. W. Portmann, K. H. Rosenlof, P. M. Forster, and T. Wong, 2009: An observationally
39 based energy balance for the Earth since 1950. *Journal of Geophysical Research-Atmospheres*, **114**, D17107.
- 40 Murphy, J. M., B. B. Booth, M. Collins, G. R. Harris, D. M. H. Sexton, and M. J. Webb, 2007: A methodology for
41 probabilistic predictions of regional climate change from perturbed physics ensembles. *Philosophical
42 Transactions of the Royal Society a-Mathematical Physical and Engineering Sciences*, **365**, 1993-2028.
- 43 Myhre, G., E. Highwood, K. Shine, and F. Stordal, 1998: New estimates of radiative forcing due to well mixed
44 greenhouse gases. *Geophysical Research Letters*, **25**, 2715-2718.
- 45 Nelson, F., and S. Outcalt, 1987: A computational method for prediction and regionalization of permafrost. *Arctic and
46 Alpine Research*, **19**, 279-288.
- 47 Nicolsky, D., V. Romanovsky, V. Alexeev, and D. Lawrence, 2007: Improved modeling of permafrost dynamics in a
48 GCM land-surface scheme. *Geophysical Research Letters*, **34**, L08501.
- 49 Niinemets, U., 2010: Responses of forest trees to single and multiple environmental stresses from seedlings to mature
50 plants: Past stress history, stress interactions, tolerance and acclimation. *Forest Ecology and Management*, **260**,
51 1623-1639.
- 52 Nikulin, G., E. Kjellstrom, U. Hansson, G. Strandberg, and A. Ullerstig, 2011: Evaluation and future projections of
53 temperature, precipitation and wind extremes over Europe in an ensemble of regional climate simulations. *Tellus
54 Series a-Dynamic Meteorology and Oceanography*, **63**, 41-55.
- 55 North, G., 1984: The small ice cap instability in diffuse climate models. *Journal of the Atmospheric Sciences*, **41**, 3390-
56 3395.
- 57 Notaro, M., 2008: Statistical identification of global hot spots in soil moisture feedbacks among IPCC AR4 models.
58 *Journal of Geophysical Research-Atmospheres*, **113**, D09101.
- 59 Notz, D., 2009: The future of ice sheets and sea ice: Between reversible retreat and unstoppable loss. *Proceedings of the
60 National Academy of Sciences of the United States of America*, **106**, 20590-20595.
- 61 NRC, 2011: *Climate Stabilization Targets: Emissions, Concentrations, and Impacts over Decades to Millennia*.
62 National Academies Press, 298 pp.

- 1 O'Gorman, P., and T. Schneider, 2009a: Scaling of Precipitation Extremes over a Wide Range of Climates Simulated
2 with an Idealized GCM. *Journal of Climate*, **22**, 5676-5685.
- 3 ———, 2009b: The physical basis for increases in precipitation extremes in simulations of 21st-century climate change.
4 *Proceedings of the National Academy of Sciences of the United States of America*, **106**, 14773-14777.
- 5 O'Gorman, P. A., 2010: Understanding the varied response of the extratropical storm tracks to climate change.
6 *Proceedings of the National Academy of Sciences of the United States of America*, **107**, 19176-19180.
- 7 O'Gorman, P. A., and C. J. Muller, 2010: How closely do changes in surface and column water vapor follow Clausius-
8 Clapeyron scaling in climate change simulations? *Environmental Research Letters*, **5**, 025207.
- 9 Orłowski, B., and S. I. Seneviratne, 2011: Global changes in extremes events: Regional and seasonal dimension.
10 *Climatic Change*. online first.
- 11 Pagani, M., Z. Liu, J. LaRiviere, and A. Ravelo, 2010: High Earth-system climate sensitivity determined from Pliocene
12 carbon dioxide concentrations. *Nature Geoscience*, **3**, 27-30.
- 13 Pall, P., M. Allen, and D. Stone, 2007: Testing the Clausius-Clapeyron constraint on changes in extreme precipitation
14 under CO2 warming. *Climate Dynamics*, **28**, 351-363.
- 15 Parker, W. S., 2006: Understanding pluralism in climate modeling. *Foundations of Science*, **11**, 349-368.
- 16 Perlwitz, J., S. Pawson, R. Fogt, J. Nielsen, and W. Neff, 2008: Impact of stratospheric ozone hole recovery on
17 Antarctic climate. *Geophys. Res. Lett.*, **35**, L08714.
- 18 Perrie, W., Y. H. Yao, and W. Q. Zhang, 2010: On the impacts of climate change and the upper ocean on midlatitude
19 northwest Atlantic landfalling cyclones. *Journal of Geophysical Research-Atmospheres*, **115**, D23110.
- 20 Piani, C., D. J. Frame, D. A. Stainforth, and M. R. Allen, 2005: Constraints on climate change from a multi-thousand
21 member ensemble of simulations. *Geophysical Research Letters*, **32**, L23825.
- 22 Pierce, D., et al., 2008: Attribution of Declining Western US Snowpack to Human Effects. *Journal of Climate*, **21**,
23 6425-6444.
- 24 Pierce, D. W., T. P. Barnett, B. D. Santer, and P. J. Gleckler, 2009: Selecting global climate models for regional climate
25 change studies. *Proceedings of the National Academy of Sciences of the United States of America*, **106**, 8441-
26 8446.
- 27 Pierrehumbert, R. T., H. Brogniez, and R. Roca, 2007: On the relative humidity of the atmosphere. *The Global*
28 *Circulation of the Atmosphere*, T. Schneider, and A. Sobel, Eds., Princeton University Press.
- 29 Pincus, R., C. Batstone, R. Hofmann, K. Taylor, and P. Glecker, 2008: Evaluating the present-day simulation of clouds,
30 precipitation, and radiation in climate models. *Journal of Geophysical Research-Atmospheres*, **113**, D14209.
- 31 Pinto, J. G., E. L. Frohlich, G. C. Leckebusch, and U. Ulbrich, 2007: Changing European storm loss potentials under
32 modified climate conditions according to ensemble simulations of the ECHAM5/MPI-OM1 GCM. *Natural*
33 *Hazards and Earth System Sciences*, **7**, 165-175.
- 34 Pitman, A., et al., 2009: Uncertainties in climate responses to past land cover change: First results from the LUCID
35 intercomparison study. *Geophys. Res. Lett.*, **36**, L14814.
- 36 Plattner, G., et al., 2008: Long-term climate commitments projected with climate-carbon cycle models. *Journal of*
37 *Climate*, **21**, 2721-2751.
- 38 Polyani, L. M., M. Previdi, and C. Deser, 2011: Large cancellation, due to ozone recovery, of future Southern
39 Hemisphere atmospheric circulation trends. *Geophysical Research Letters*, **38**, L04707.
- 40 Pongratz, J., C. Reick, T. Raddatz, and M. Claussen, 2010: Biogeophysical versus biogeochemical climate response to
41 historical anthropogenic land cover change. *Geophys. Res. Lett.*, **37**, L08702.
- 42 Prather, M., et al., 2003: Fresh air in the 21st century? *Geophys. Res. Lett.*, **30**, 1100.
- 43 Rahmstorf, S., et al., 2005: Thermohaline circulation hysteresis: A model intercomparison. *Geophysical Research*
44 *Letters*, **32**, L23605.
- 45 Raisanen, J., 2007: How reliable are climate models? *Tellus Series a-Dynamic Meteorology and Oceanography*, **59**, 2-
46 29.
- 47 Raisanen, J., 2008: Warmer climate: less or more snow? *Climate Dynamics*, **30**, 307-319.
- 48 Raisanen, J., and L. Ruokolainen, 2006: Probabilistic forecasts of near-term climate change based on a resampling
49 ensemble technique. *Tellus Series a-Dynamic Meteorology and Oceanography*, **58**, 461-472.
- 50 Raisanen, J., L. Ruokolainen, and J. Ylhäisi, 2010: Weighting of model results for improving best estimates of climate
51 change. *Climate Dynamics*, **35**, 407-422.
- 52 Rammig, A., et al., 2010: Estimating the risk of Amazonian forest dieback. *New Phytologist*, **187**, 694-706.
- 53 Randall, D. A., et al., 2007: Climate Models and Their Evaluation. *Climate Change 2007: The Physical Science Basis.*
54 *Contribution of Working Group I to the Fourth Assessment Report of the Intergovernmental Panel on Climate*
55 *Change*, Cambridge University Press.
- 56 Randalls, S., 2010: History of the 2°C climate target. *Wiley Interdisciplinary Reviews: Climate Change*, **1**, 598-605.
- 57 Randles, C., and V. Ramaswamy, 2008: Absorbing aerosols over Asia: A Geophysical Fluid Dynamics Laboratory
58 general circulation model sensitivity study of model response to aerosol optical depth and aerosol absorption.
59 *Journal of Geophysical Research-Atmospheres*, **113**, D21203.
- 60 Reagan, M., and G. Moridis, 2007: Oceanic gas hydrate instability and dissociation under climate change scenarios.
61 *Geophysical Research Letters*, **34**, L22709.
- 62 ———, 2009: Large-scale simulation of methane hydrate dissociation along the West Spitsbergen Margin. *Geophysical*
63 *Research Letters*, **36**, L23612.

- 1 Reichler, T., and J. Kim, 2008: How well do coupled models simulate today's climate? *Bulletin of the American*
2 *Meteorological Society*, **89**, 303-311.
- 3 Ridley, J., J. Lowe, C. Brierley, and G. Harris, 2007: Uncertainty in the sensitivity of Arctic sea ice to global warming
4 in a perturbed parameter climate model ensemble. *Geophysical Research Letters*, **34**, L19704.
- 5 Ridley, J., J. Gregory, P. Huybrechts, and J. Lowe, 2010: Thresholds for irreversible decline of the Greenland ice sheet.
6 *Climate Dynamics*, **35**, 1049-1057.
- 7 Riley, W. J., Z. M. Subin, M. S. Torn, L. Meng, M. Mahowald, P. G. Hess, and D. M. Lawrence, 2011: Barriers to
8 predicting changes in global terrestrial methane fluxes: Analyses using CLM4ME, a methane biogeochemistry
9 model integrated in CESM. *Biogeosciences*. submitted.
- 10 Rind, D., 1987: The doubled CO2 climate - impact of the sea-surface temperature-gradient. *Journal of the Atmospheric*
11 *Sciences*, **44**, 3235-3268.
- 12 Ringeval, B., P. Friedlingstein, C. Koven, P. Ciais, N. de Noblet-Ducoudré, B. Decharme, and P. Cadule, 2011:
13 Climate-CH4 feedback from wetlands and its interaction with climate-CO2 feedbacks. *Biogeosciences*, **8**, 2137-
14 2157.
- 15 Rinke, A., P. Kuhry, and K. Dethloff, 2008: Importance of a soil organic layer for Arctic climate: A sensitivity study
16 with an Arctic RCM. *Geophysical Research Letters*, **35**, L13709.
- 17 Rive, N., A. Torvanger, T. Berntsen, and S. Kallbekken, 2007: To what extent can a long-term temperature target guide
18 near-term climate change commitments? *Climatic Change*, **82**, 373-391.
- 19 Roberts, J. L., et al., 2011: Refined broad-scale sub-glacial morphology of Aurora Subglacial Basin, East Antarctica
20 derived by an ice-dynamics-based interpolation scheme. *The Cryosphere*, **5**, 511-560.
- 21 Rodwell, M., and T. Palmer, 2007: Using numerical weather prediction to assess climate models. *Quarterly Journal of*
22 *the Royal Meteorological Society*, **133**, 129-146.
- 23 Rogelj, J., M. Meinshausen, and R. Knutti, 2011a: Global warming under old and new scenarios using IPCC climate
24 sensitivity range estimates. *Nature Climate Change*. submitted.
- 25 Rogelj, J., et al., 2011b: Emission pathways consistent with a 2°C global temperature limit. *Nature Climate Change*, **1**,
26 413-418.
- 27 Rohling, E., K. Grant, M. Bolshaw, A. Roberts, M. Siddall, C. Hemleben, and M. Kucera, 2009: Antarctic temperature
28 and global sea level closely coupled over the past five glacial cycles. *Nature Geoscience*, **2**, 500-504.
- 29 Rougier, J., 2007: Probabilistic inference for future climate using an ensemble of climate model evaluations. *Climatic*
30 *Change*, **81**, 247-264.
- 31 Rougier, J., D. M. H. Sexton, J. M. Murphy, and D. Stainforth, 2009: Analyzing the Climate Sensitivity of the HadSM3
32 Climate Model Using Ensembles from Different but Related Experiments. *Journal of Climate*, **22**, 3540-3557.
- 33 Ruosteenoja, K., H. Tuomenvirta, and K. Jylha, 2007: GCM-based regional temperature and precipitation change
34 estimates for Europe under four SRES scenarios applying a super-ensemble pattern-scaling method. *Climatic*
35 *Change*, **81**, 193-208.
- 36 Saenko, O. A., X.-Y. Yang, M. H. England, and W. G. Lee, 2011: Subduction and transport in the Indian and Pacific
37 Oceans in a 2xCO2 climate. *Journal of Climate*, **24**, 1821-1838.
- 38 Saito, K., M. Kimoto, T. Zhang, K. Takata, and S. Emori, 2007: Evaluating a high-resolution climate model: Simulated
39 hydrothermal regimes in frozen ground regions and their change under the global warming scenario. *Journal of*
40 *Geophysical Research-Earth Surface*, **112**, F02S11.
- 41 Sanderson, B., C. Piani, W. Ingram, D. Stone, and M. Allen, 2008a: Towards constraining climate sensitivity by linear
42 analysis of feedback patterns in thousands of perturbed-physics GCM simulations. *Climate Dynamics*, **30**, 175-
43 190.
- 44 Sanderson, B. M., 2011a: A Multimodel Study of Parametric Uncertainty in Predictions of Climate Response to Rising
45 Greenhouse Gas Concentrations. *Journal of Climate*, **25**, 1362-1377.
- 46 ———, 2011b: On the estimation of systematic error in regression-based predictions of climate sensitivity. *Climatic*
47 *Change*. submitted.
- 48 Sanderson, B. M., K. M. Shell, and W. Ingram, 2010: Climate feedbacks determined using radiative kernels in a multi-
49 thousand member ensemble of AOGCMs. *Climate Dynamics*, **35**, 1219-1236, doi:1210.1007/s00382-00009-
50 00661-00381.
- 51 Sanderson, B. M., et al., 2008b: Constraints on model response to greenhouse gas forcing and the role of subgrid-scale
52 processes. *Journal of Climate*, **21**, 2384-2400, doi:2310.1175/2008jcli1869.2381.
- 53 Sanderson, M., C. Jones, W. Collins, C. Johnson, and R. Derwent, 2003: Effect of climate change on isoprene
54 emissions and surface ozone levels. *Geophys. Res. Lett.*, **30**, 1936, doi:1910.1029/2003GL017642.
- 55 Sanderson, M. G., D. L. Hemming, and R. A. Betts, 2011: Regional temperature and precipitation changes under high-
56 end (≥ 4 degrees C) global warming. *Philosophical Transactions of the Royal Society a-Mathematical Physical*
57 *and Engineering Sciences*, **369**, 85-98.
- 58 Sanso, B., and C. Forest, 2009: Statistical calibration of climate system properties. *Journal of the Royal Statistical*
59 *Society Series C-Applied Statistics*, **58**, 485-503, doi:410.1111/j.1467-9876.2009.00669.x.
- 60 Sanso, B., C. E. Forest, and D. Zantedeschi, 2008: Inferring Climate System Properties Using a Computer Model.
61 *Bayesian Analysis*, **3**, 1-37.
- 62 Santer, B. D., T. M. L. Wigley, M. E. Schlesinger, and J. F. B. Mitchell, 1990: Developing climate scenarios from
63 equilibrium GCM results, 29 pp. pp.

- 1 Sato, T., F. Kimura, and A. Kitoh, 2007: Projection of global warming onto regional precipitation over Mongolia using
2 a regional climate model. *Journal of Hydrology*, **333**, 144-154.
- 3 Schaefer, K., T. Zhang, L. Bruhwiler, and A. Barrett, 2011: Amount and timing of permafrost carbon release in
4 response to climate warming. *Tellus Series B-Chemical and Physical Meteorology*, **63**, 165-180.
- 5 Schar, C., P. L. Vidale, D. Luthi, C. Frei, C. Haberli, M. A. Liniger, and C. Appenzeller, 2004: The role of increasing
6 temperature variability in European summer heatwaves. *Nature*, **427**, 332-336.
- 7 Scherrer, S., 2011: Present-day interannual variability of surface climate in CMIP3 models and its relation to future
8 warming. *International Journal of Climatology*, **31**, 1518-1529.
- 9 Schlesinger, M., 1986: Equilibrium and transient climatic warming induced by increased atmospheric CO₂. *Climate
10 Dynamics*, **1**, 35-51.
- 11 Schlesinger, M., et al., 2000: Geographical distributions of temperature change for scenarios of greenhouse gas and
12 sulfur dioxide emissions. *Technological Forecasting and Social Change*, **65**, 167-193.
- 13 Schmidt, M. W. I., et al., 2011: Persistence of soil organic matter as an ecosystem property. *Nature*, **478**, 49-56.
- 14 Schneider von Deimling, T., H. Held, A. Ganopolski, and S. Rahmstorf, 2006: Climate sensitivity estimated from
15 ensemble simulations of glacial climate. *Climate Dynamics*, **27**, 149-163.
- 16 Schneider von Deimling, T., M. Meinshausen, A. Levermann, V. Huber, K. Frieler, D. Lawrence, and V. Brovkin,
17 2011: Estimating the permafrost-carbon feedback on global warming. *Biogeosciences Discussions*, **8**, 4727-
18 4761.
- 19 Schoof, C., 2007: Ice sheet grounding line dynamics: Steady states, stability, and hysteresis. *Journal of Geophysical
20 Research-Earth Surface*, **112**, F03S28.
- 21 Schuenemann, K. C., and J. J. Cassano, 2010: Changes in synoptic weather patterns and Greenland precipitation in the
22 20th and 21st centuries: 2. Analysis of 21st century atmospheric changes using self-organizing maps. *Journal of
23 Geophysical Research-Atmospheres*, **115**, D05108.
- 24 Schuur, E., J. Vogel, K. Crummer, H. Lee, J. Sickman, and T. Osterkamp, 2009: The effect of permafrost thaw on old
25 carbon release and net carbon exchange from tundra. *Nature*, **459**, 556-559.
- 26 Schweiger, A., R. Lindsay, J. Zhang, M. Steele, H. Stern, and R. Kwok, 2011: Uncertainty in modeled Arctic sea ice
27 volume. *Journal of Geophysical Research-Oceans*, **116**, C00D07.
- 28 Screen, J., and I. Simmonds, 2010: The central role of diminishing sea ice in recent Arctic temperature amplification.
29 *Nature*, **464**, 1334-1337.
- 30 Seager, R., and G. A. Vecchi, 2010: Greenhouse warming and the 21st century hydroclimate of the southwestern North
31 America. *Proc. Nat. Acad. Sci.*, **107**, 21277-21282.
- 32 Seager, R., and N. Naik, 2011: A mechanism-based approach to detecting recent anthropogenic hydroclimate change. *J.
33 Clim.* submitted.
- 34 Seager, R., et al., 2007: Model projections of an imminent transition to a more arid climate in southwestern North
35 America. *Science*, **316**, 1181-1184.
- 36 Sedlacek, J., R. Knutt, O. Martius, and U. Beyerle, 2011: Impact of a reduced Arctic sea-ice cover on ocean and
37 atmospheric properties. *Journal of Climate*. in press.
- 38 Seidel, D., and W. Randel, 2007: Recent widening of the tropical belt: Evidence from tropopause observations. *Journal
39 of Geophysical Research-Atmospheres*, **112**, D20113.
- 40 Seidel, D. J., Q. Fu, W. J. Randel, and T. J. Reichler, 2008: Widening of the tropical belt in a changing climate. *Nature
41 Geoscience*, **1**, 21-24.
- 42 Sen Gupta, A., A. Santoso, A. Taschetto, C. Ummenhofer, J. Trevena, and M. England, 2009: Projected Changes to the
43 Southern Hemisphere Ocean and Sea Ice in the IPCC AR4 Climate Models. *Journal of Climate*, **22**, 3047-3078.
- 44 Seneviratne, S. I., D. Luthi, M. Litschi, and C. Schar, 2006: Land-atmosphere coupling and climate change in Europe.
45 *Nature*, **443**, 205-209.
- 46 Senior, C., and J. Mitchell, 2000: The time-dependence of climate sensitivity. *Geophysical Research Letters*, **27**, 2685-
47 2688.
- 48 Serreze, M., A. Barrett, J. Stroeve, D. Kindig, and M. Holland, 2009: The emergence of surface-based Arctic
49 amplification. *Cryosphere*, **3**, 11-19.
- 50 Sherwood, S. C., 2010: Direct versus indirect effects of tropospheric humidity changes on the hydrologic cycle.
51 *Environmental Research Letters*, **5**, 025206.
- 52 Sherwood, S. C., and M. Huber, 2010: An adaptability limit to climate change due to heat stress. *Proceedings of the
53 National Academy of Sciences of the United States of America*, **107**, 9552-9555.
- 54 Sherwood, S. C., W. Ingram, Y. Tsushima, M. Satoh, M. Roberts, P. L. Vidale, and P. A. O'Gorman, 2010: Relative
55 humidity changes in a warmer climate. *Journal of Geophysical Research-Atmospheres*, **115**, D09104.
- 56 Shindell, D., B. Walter, and G. Faluvegi, 2004: Impacts of climate change on methane emissions from wetlands.
57 *Geophys. Res. Lett.*, **31**, L21202, doi:21210.21029/22004GL021009.
- 58 Shindell, D., et al., 2007: Climate response to projected changes in short-lived species under an A1B scenario from
59 2000-2050 in the GISS climate model. *J. Geophys. Res.*, **112**, D20103, doi:20110.21029/22007JD008753.
- 60 Shine, K., J. Cook, E. Highwood, and M. Joshi, 2003: An alternative to radiative forcing for estimating the relative
61 importance of climate change mechanisms. *Geophysical Research Letters*, **30**, 2047.
- 62 Shiogama, H., et al., 2010: Emission scenario dependencies in climate change assessments of the hydrological cycle.
63 *Climatic Change*, **99**, 321-329.

- 1 Shukla, J., T. DelSole, M. Fennessy, J. Kinter, and D. Paolino, 2006: Climate model fidelity and projections of climate
2 change. *Geophysical Research Letters*, **33**, L07702.
- 3 Siegenthaler, U., and H. Oeschger, 1984: Transient temperature changes due to increasing CO₂ using simple models.
4 *Annals of Glaciology*, 153-159.
- 5 Sillmann, J., and E. Roeckner, 2008: Indices for extreme events in projections of anthropogenic climate change.
6 *Climatic Change*, **86**, 83-104.
- 7 Sillmann, J., and M. Croci-Maspoli, 2009: Present and future atmospheric blocking and its impact on European mean
8 and extreme climate. *Geophysical Research Letters*, **36**, L10702.
- 9 Smith, L., Y. Sheng, G. MacDonald, and L. Hinzman, 2005: Disappearing Arctic lakes. *Science*, **308**, 1429-1429.
- 10 Smith, L., et al., 2004: Siberian peatlands a net carbon sink and global methane source since the early Holocene.
11 *Science*, **303**, 353-356.
- 12 Smith, R. L., C. Tebaldi, D. Nychka, and L. O. Mearns, 2009: Bayesian Modeling of Uncertainty in Ensembles of
13 Climate Models. *Journal of the American Statistical Association*, **104**, 97-116, doi:110.1198/jasa.2009.0007.
- 14 Smith, S. J., J. van Aardenne, Z. Klimont, R. J. Andres, A. Volke, and S. Delgado Arias, 2011: Anthropogenic sulfur
15 dioxide emissions: 1850-2005. *Atmos. Chem. Phys.*, **11**, 1101-1116.
- 16 Soden, B., I. Held, R. Colman, K. Shell, J. Kiehl, and C. Shields, 2008: Quantifying climate feedbacks using radiative
17 kernels. *Journal of Climate*, **21**, 3504-3520.
- 18 Soden, B. J., and I. M. Held, 2006: An assessment of climate feedbacks in coupled ocean-atmosphere models. *Journal*
19 *of Climate*, **19**, 3354-3360.
- 20 Soden, B. J., and G. A. Vecchi, 2011: The vertical distribution of cloud feedback in coupled ocean-atmosphere models.
21 *Geophysical Research Letters*, **38**, L12704.
- 22 Sokolov, A. P., et al., 2010: Probabilistic forecast for twenty-first-century climate based on uncertainties in emissions
23 (without policy) and climate parameters. *Journal of Climate*, **23**, 2230-2231, doi:2210.1175/2009jcli3566.2231.
- 24 Solomon, S., G. Plattner, R. Knutti, and P. Friedlingstein, 2009: Irreversible climate change due to carbon dioxide
25 emissions. *Proceedings of the National Academy of Sciences of the United States of America*, **106**, 1704-1709.
- 26 Solomon, S., J. Daniel, T. Sanford, D. Murphy, G. Plattner, R. Knutti, and P. Friedlingstein, 2010: Persistence of
27 climate changes due to a range of greenhouse gases. *Proceedings of the National Academy of Sciences of the*
28 *United States of America*, **107**, 18354-18359.
- 29 Son, S. W., et al., 2010: Impact of stratospheric ozone on Southern Hemisphere circulation change: A multimodel
30 assessment. *Journal of Geophysical Research-Atmospheres*, **115**, D00M07.
- 31 Sorensson, A., C. Menendez, R. Ruscica, P. Alexander, P. Samuelsson, and U. Willen, 2010: Projected precipitation
32 changes in South America: a dynamical downscaling within CLARIS. *Meteorologische Zeitschrift*, **19**, 347-355.
- 33 Spence, P., J. Fyfe, A. Montenegro, and A. Weaver, 2010: Southern Ocean Response to Strengthening Winds in an
34 Eddy-Permitting Global Climate Model. *Journal of Climate*, **23**, 5332-5343.
- 35 Stainforth, D., et al., 2005: Uncertainty in predictions of the climate response to rising levels of greenhouse gases.
36 *Nature*, **433**, 403-406.
- 37 Stephens, G. L., and T. D. Ellis, 2008: Controls of Global-Mean Precipitation Increases in Global Warming GCM
38 Experiments. *Journal of Climate*, **21**, 6141-6155.
- 39 Stevens, B., and S. E. Schwartz, 2011: Observing and Modeling Earth's Energy Flow. *Surveys in Geophysics*.
40 submitted.
- 41 Stevenson, D., et al., 2006: Multimodel ensemble simulations of present-day and near-future tropospheric ozone. *J.*
42 *Geophys. Res.*, **111**, D08301, doi:08310.01029/02005JD006338.
- 43 Stone, E., D. Lunt, I. Rutt, and E. Hanna, 2010: Investigating the sensitivity of numerical model simulations of the
44 modern state of the Greenland ice-sheet and its future response to climate change. *Cryosphere*, **4**, 397-417.
- 45 Stott, P., G. Jones, and J. Mitchell, 2003: Do models underestimate the solar contribution to recent climate change?
46 *Journal of Climate*, **16**, 4079-4093.
- 47 Stouffer, R., 2004: Time scales of climate response. *Journal of Climate*, **17**, 209-217.
- 48 Stowasser, M., H. Annamalai, and J. Hafner, 2009: Response of the South Asian Summer Monsoon to Global
49 Warming: Mean and Synoptic Systems. *Journal of Climate*, **22**, 1014-1036.
- 50 Stroeve, J., M. Holland, W. Meier, T. Scambos, and M. Serreze, 2007: Arctic sea ice decline: Faster than forecast.
51 *Geophysical Research Letters*, **34**, L09501.
- 52 Stuber, N., M. Ponater, and R. Sausen, 2005: Why radiative forcing might fail as a predictor of climate change. *Climate*
53 *Dynamics*, **24**, 497-510.
- 54 Sugiyama, M., H. Shiogama, and S. Emori, 2010: Precipitation extreme changes exceeding moisture content increases
55 in MIROC and IPCC climate models. *Proceedings of the National Academy of Sciences of the United States of*
56 *America*, **107**, 571-575.
- 57 Sun, Y., S. Solomon, A. Dai, and R. W. Portmann, 2007: How often will it rain? *Journal of Climate*, **20**, 4801-4818.
- 58 Sutton, R. T., B. W. Dong, and J. M. Gregory, 2007: Land/sea warming ratio in response to climate change: IPCC AR4
59 model results and comparison with observations. *Geophysical Research Letters*, **34**, L02701.
- 60 Swingedouw, D., T. Fichefet, P. Huybrechts, H. Goosse, E. Driesschaert, and M. Loutre, 2008: Antarctic ice-sheet
61 melting provides negative feedbacks on future climate warming. *Geophysical Research Letters*, **35**, L17705.
- 62 Szopa, S., et al., 2011: Aerosol and Ozone changes as forcing for Climate Evolution between 1850 and 2100. *Climate*
63 *Dynamics*. submitted.

- 1 Takahashi, K., 2009a: Radiative Constraints on the Hydrological Cycle in an Idealized Radiative-Convective
2 Equilibrium Model. *Journal of the Atmospheric Sciences*, **66**, 77-91.
- 3 ———, 2009b: The Global Hydrological Cycle and Atmospheric Shortwave Absorption in Climate Models under CO₂
4 Forcing. *Journal of Climate*, **22**, 5667-5675.
- 5 Tarnocai, C., J. Canadell, E. Schuur, P. Kuhry, G. Mazhitova, and S. Zimov, 2009: Soil organic carbon pools in the
6 northern circumpolar permafrost region. *Global Biogeochemical Cycles*, **23**, GB2023.
- 7 Taylor, K. E., R. J. Stouffer, and G. A. Meehl, 2011: A Summary of the CMIP5 Experiment Design.
- 8 Tebaldi, C., and R. Knutti, 2007: The use of the multi-model ensemble in probabilistic climate projections.
9 *Philosophical Transactions of the Royal Society a-Mathematical Physical and Engineering Sciences*, **365**, 2053-
10 2075.
- 11 Tebaldi, C., and D. B. Lobell, 2008: Towards probabilistic projections of climate change impacts on global crop yields.
12 *Geophysical Research Letters*, **35**, L08705.
- 13 Tebaldi, C., and B. Sanso, 2009: Joint projections of temperature and precipitation change from multiple climate
14 models: a hierarchical Bayesian approach. *Journal of the Royal Statistical Society Series a-Statistics in Society*,
15 **172**, 83-106.
- 16 Tebaldi, C., J. M. Arblaster, and R. Knutti, 2011: Mapping model agreement on future climate projections. *Geophysical*
17 *Research Letters*, doi:10.1029/2011GL049863. in press.
- 18 Tebaldi, C., K. Hayhoe, J. M. Arblaster, and G. A. Meehl, 2006: Going to the extremes. *Climatic Change*, **79**, 185-211.
- 19 Thorne, P., 2008: Arctic tropospheric warming amplification? *Nature*, **455**, E1-E2.
- 20 Tietsche, S., D. Notz, J. H. Jungclaus, and J. Marotzke, 2011: Recovery mechanisms of Arctic summer sea ice.
21 *Geophys. Res. Lett.*, **38**, L02707.
- 22 Tomassini, L., P. Reichert, R. Knutti, T. F. Stocker, and M. E. Borsuk, 2007: Robust Bayesian uncertainty analysis of
23 climate system properties using Markov chain Monte Carlo methods. *Journal of Climate*, **20**, 1239-1254.
- 24 Trenberth, K. E., and D. J. Shea, 2005: Relationships between precipitation and surface temperature. *Geophysical*
25 *Research Letters*, **32**, L14703.
- 26 Trenberth, K. E., and J. T. Fasullo, 2009: Global warming due to increasing absorbed solar radiation. *Geophysical*
27 *Research Letters*, **36**, L07706.
- 28 ———, 2010: Simulation of Present-Day and Twenty-First-Century Energy Budgets of the Southern Oceans. *Journal of*
29 *Climate*, **23**, 440-454.
- 30 Ueda, H., A. Iwai, K. Kuwako, and M. Hori, 2006: Impact of anthropogenic forcing on the Asian summer monsoon as
31 simulated by eight GCMs. *Geophysical Research Letters*, **33**, L06703.
- 32 Ulbrich, U., G. C. Leckebusch, and J. G. Pinto, 2009: Extra-tropical cyclones in the present and future climate: a
33 review. *Theoretical and Applied Climatology*, **96**, 117-131.
- 34 Ulbrich, U., J. G. Pinto, H. Kupfer, G. C. Leckebusch, T. Spanghel, and M. Reyers, 2008: Changing northern
35 hemisphere storm tracks in an ensemble of IPCC climate change simulations. *Journal of Climate*, **21**, 1669-
36 1679.
- 37 UNEP, 2010: The emissions gap report: Are the Copenhagen Accord pledges sufficient to limit global warming to 2°C
38 or 1.5°C?, 55 pp., <http://www.unep.org/publications/ebooks/emissionsgapreport/> pp.
- 39 van Vuuren, D., et al., 2011a: The representative concentration pathways: an overview. *Climatic Change*, **109**, 5-31.
- 40 van Vuuren, D. P., et al., 2011b: RCP3-PD: Exploring the possibilities to limit global mean temperature change to less
41 than 2°C. *Climatic Change*, **109**, 95-116.
- 42 Vavrus, S., M. M. Holland, and D. A. Bailey, 2011: Changes in clouds during intervals of rapid ice loss. *Clim. Dyn.*,
43 10.1007/s00382-010-0816-0. in press.
- 44 Vecchi, G. A., and B. J. Soden, 2007: Global warming and the weakening of the tropical circulation. *Bulletin of the*
45 *American Meteorological Society*, **88**, 1529-1530.
- 46 Vedantham, A., and M. Oppenheimer, 1998: Long-term scenarios for aviation: Demand and emissions of CO₂ and
47 NO_x. *Energy Policy*, **26**, 625-641.
- 48 Vidale, P. L., D. Luthi, R. Wegmann, and C. Schar, 2007: European summer climate variability in a heterogeneous
49 multi-model ensemble. *Climatic Change*, **81**, 209-232.
- 50 Vizcaino, M., U. Mikolajewicz, J. Jungclaus, and G. Schurgers, 2010: Climate modification by future ice sheet changes
51 and consequences for ice sheet mass balance. *Climate Dynamics*, **34**, 301-324.
- 52 Vizcaino, M., U. Mikolajewicz, M. Groger, E. Maier-Reimer, G. Schurgers, and A. Winguth, 2008: Long-term ice
53 sheet-climate interactions under anthropogenic greenhouse forcing simulated with a complex Earth System
54 Model. *Climate Dynamics*, **31**, 665-690.
- 55 Voltaire, A., et al., 2011: The CNRM-CM5.1 global climate model: Description and basic evaluation. *Climate*
56 *Dynamics*. submitted.
- 57 Volodin, E., 2008: Relation between temperature sensitivity to doubled carbon dioxide and the distribution of clouds in
58 current climate models. *Izvestiya Atmospheric and Oceanic Physics*, **44**, 288-299.
- 59 Voss, R., and U. Mikolajewicz, 2001: Long-term climate changes due to increased CO₂ concentration in the coupled
60 atmosphere-ocean general circulation model ECHAM3/LSG. *Climate Dynamics*, **17**, 45-60.
- 61 Walker, R., et al., 2009: Protecting the Amazon with protected areas. *Proceedings of the National Academy of Sciences*
62 *of the United States of America*, **106**, 10582-10586.

- 1 Wang, M., and J. Overland, 2009: A sea ice free summer Arctic within 30 years? *Geophysical Research Letters*, **36**,
2 L07502.
- 3 Wang, W., X. Liang, M. Dudek, D. Pollard, and S. Thompson, 1995: Atmospheric Ozone as a Climate Gas.
4 *Atmospheric Research*, **37**, 247-256.
- 5 Wang, Z., and M. Meredith, 2008: Density-driven Southern Hemisphere subpolar gyres in coupled climate models.
6 *Geophysical Research Letters*, **35**, L14605.
- 7 Wania, R., I. Ross, and I. Prentice, 2009: Integrating peatlands and permafrost into a dynamic global vegetation model:
8 2. Evaluation and sensitivity of vegetation and carbon cycle processes. *Global Biogeochemical Cycles*, **23**,
9 GB3015.
- 10 Washington, W., et al., 2009: How much climate change can be avoided by mitigation? *Geophysical Research Letters*,
11 **36**, L08703.
- 12 Watanabe, S., et al., 2011: MIROC-ESM 2010: model description and basic results of CMIP5-20c3m experiments.
13 *Geoscientific Model Development*, **4**, 845-872.
- 14 Watterson, I. G., 2008: Calculation of probability density functions for temperature and precipitation change under
15 global warming. *Journal of Geophysical Research-Atmospheres*, **113**, D12106,
16 doi:12110.11029/12007JD009254.
- 17 Watterson, I. G., and P. H. Whetton, 2011: An application of joint PDFs of climate in future decades to wheat crop
18 yield. *Australian Meteorological and Oceanographic Journal*. submitted.
- 19 Watterson, I. M., 2011: Calculation of joint PDFs for climate change with properties matching Australian projections.
20 *Australian Meteorological and Oceanographic Journal*. submitted.
- 21 WBGU, 2009: Solving the climate dilemma: The budget approach, 59 pp., ISBN 53-936191-936127-936191 pp.
- 22 Weaver, A., K. Zickfeld, A. Montenegro, and M. Eby, 2007: Long term climate implications of 2050 emission
23 reduction targets. *Geophysical Research Letters*, **34**, L19703.
- 24 Webb, M., et al., 2006: On the contribution of local feedback mechanisms to the range of climate sensitivity in two
25 GCM ensembles. *Climate Dynamics*, **27**, 17-38.
- 26 Weertmann, J., 1974: Stability of the junction of an ice sheet and an ice shelf. 3-11.
- 27 Wehner, M., D. R. Easterling, J. H. Lawrimore, R. R. Heim Jr., R. S. Vose, and B. Santer, 2011: Projections of Future
28 Drought in the Continental United States and Mexico. *Journal of Hydrometeorology*. submitted.
- 29 Wentz, F., L. Ricciardulli, K. Hilburn, and C. Mears, 2007: How much more rain will global warming bring? *Science*,
30 **317**, 233-235.
- 31 Wetherald, R., R. Stouffer, and K. Dixon, 2001: Committed warming and its implications for climate change.
32 *Geophysical Research Letters*, **28**, 1535-1538.
- 33 Whetton, P., I. Macadam, J. Bathols, and J. O'Grady, 2007: Assessment of the use of current climate patterns to
34 evaluate regional enhanced greenhouse response patterns of climate models. *Geophysical Research Letters*, **34**,
35 L14701.
- 36 Wigley, T., 2005: The climate change commitment. *Science*, **307**, 1766-1769.
- 37 Willett, K. M., and S. C. Sherwood, 2011: Exceedance of WBGT thresholds for 15 regions under a warming climate.
38 *International Journal of Climatology*, DOI: 10.1002/joc.2257. in press.
- 39 Williams, J. W., S. T. Jackson, and J. E. Kutzbach, 2007: Projected distributions of novel and disappearing climates by
40 2100 AD. *Proceedings of the National Academy of Sciences of the United States of America*, **104**, 5738-5742.
- 41 Winton, M., 2006a: Does the Arctic sea ice have a tipping point? *Geophysical Research Letters*, **33**, L23504.
- 42 —, 2006b: Amplified Arctic climate change: What does surface albedo feedback have to do with it? *Geophysical
43 Research Letters*, **33**, L03701.
- 44 Winton, M., 2008: Sea ice-albedo feedback and nonlinear Arctic climate change. *Arctic Sea Ice Decline: Observations,
45 Projections, Mechanisms, and Implications*, E. T. DeWeaver, C. M. Bitz, and L. B. Tremblay, Eds., Amer.
46 Geophys. Union, 111-131.
- 47 Winton, M., 2011: Do Climate Models Underestimate the Sensitivity of Northern Hemisphere Sea Ice Cover? *Journal
48 of Climate*, **24**, 3924-3934.
- 49 Wood, R., A. Keen, J. Mitchell, and J. Gregory, 1999: Changing spatial structure of the thermohaline circulation in
50 response to atmospheric CO₂ forcing in a climate model. *Nature*, **399**, 572-575.
- 51 Woollings, T., 2008: Vertical structure of anthropogenic zonal-mean atmospheric circulation change. *Geophys. Res.
52 Lett.*, **35**, L19702.
- 53 Wu, P., R. Wood, J. Ridley, and J. Lowe, 2010: Temporary acceleration of the hydrological cycle in response to a CO₂
54 rampdown. *Geophysical Research Letters*, **37**, L12705.
- 55 Wu, Q., and G. North, 2003: Statistics of calendar month averages of surface temperature: A possible relationship to
56 climate sensitivity. *Journal of Geophysical Research-Atmospheres*, **108**, 4071.
- 57 Wu, Q., D. Karoly, and G. North, 2008: Role of water vapor feedback on the amplitude of season cycle in the global
58 mean surface air temperature. *Geophysical Research Letters*, **35**, L08711.
- 59 Wu, T., et al., 2011: The 20th century global carbon cycle from the Beijing Climate Center Climate System Model
60 (BCC_CSM). *Climate Dynamics*. submitted.
- 61 Wyant, M. C., et al., 2006: A comparison of low-latitude cloud properties and their response to climate change in three
62 AGCMs sorted into regimes using mid-tropospheric vertical velocity. *Climate Dynamics*, **27**, 261-279.

- 1 Xie, S. P., C. Deser, G. A. Vecchi, J. Ma, H. Y. Teng, and A. T. Wittenberg, 2010: Global Warming Pattern Formation:
2 Sea Surface Temperature and Rainfall. *Journal of Climate*, **23**, 966-986.
- 3 Yeh, S., J. Kug, B. Dewitte, M. Kwon, B. Kirtman, and F. Jin, 2009: El Nino in a changing climate. *Nature*, **461**, 511-
4 514.
- 5 Yin, J., J. Overpeck, S. Griffies, A. Hu, J. Russell, and R. Stouffer, 2011: Different magnitudes of projected subsurface
6 ocean warming around Greenland and Antarctica. *Nature Geoscience*, **4**, 524-528.
- 7 Yin, J. H., 2005: A consistent poleward shift of the storm tracks in simulations of 21st century climate. *Geophys. Res.*
8 *Lett.*, **32**, L18701.
- 9 Yokohata, T., M. Webb, M. Collins, K. Williams, M. Yoshimori, J. Hargreaves, and J. Annan, 2010: Structural
10 Similarities and Differences in Climate Responses to CO2 Increase between Two Perturbed Physics Ensembles.
11 *Journal of Climate*, **23**, 1392-1410.
- 12 Yokohata, T., J. D. Annan, J. C. Hargreaves, C. S. Jackson, M. Tobis, M. Webb, and M. Collins, 2011: Reliability of
13 multi-model and structurally different single-model ensembles. *Climate Dynamics*. submitted.
- 14 Zelazowski, P., Y. Malhi, C. Huntingford, S. Sitch, and J. Fisher, 2011: Changes in the potential distribution of humid
15 tropical forests on a warmer planet. *Philosophical Transactions of the Royal Society a-Mathematical Physical*
16 *and Engineering Sciences*, **369**, 137-160.
- 17 Zelinka, M., and D. Hartmann, 2010: Why is longwave cloud feedback positive? *Journal of Geophysical Research-*
18 *Atmospheres*, **115**, D16117.
- 19 Zelinka, M. D., S. A. Klein, and D. L. Hartmann, 2011: Computing and partitioning cloud feedbacks using cloud
20 property histograms. Part II: Attribution to Changes in Cloud Amount, Altitude, and Optical Depth. *Journal of*
21 *Climate*. submitted.
- 22 Zhang, M., and H. Song, 2006: Evidence of deceleration of atmospheric vertical overturning circulation over the
23 tropical Pacific. *Geophysical Research Letters*, **33**, -.
- 24 Zhang, M. H., and C. Bretherton, 2008: Mechanisms of low cloud-climate feedback in idealized single-column
25 simulations with the Community Atmospheric Model, version 3 (CAM3). *Journal of Climate*, **21**, 4859-4878.
- 26 Zhang, R., 2010a: Northward intensification of anthropogenically forced changes in the Atlantic meridional overturning
27 circulation (AMOC). *Geophysical Research Letters*, **37**, L24603.
- 28 Zhang, T., 2005: Influence of the seasonal snow cover on the ground thermal regime: An overview. *Reviews of*
29 *Geophysics*, **43**, RG4002.
- 30 Zhang, X., 2010b: Sensitivity of arctic summer sea ice coverage to global warming forcing: towards reducing
31 uncertainty in arctic climate change projections. *Tellus Series a-Dynamic Meteorology and Oceanography*, **62**,
32 220-227.
- 33 Zhang, X., and J. Walsh, 2006: Toward a seasonally ice-covered Arctic Ocean: Scenarios from the IPCC AR4 model
34 simulations. *Journal of Climate*, **19**, 1730-1747.
- 35 Zhou, L. M., R. E. Dickinson, P. Dirmeyer, A. Dai, and S. K. Min, 2009: Spatiotemporal patterns of changes in
36 maximum and minimum temperatures in multi-model simulations. *Geophysical Research Letters*, **36**, L02702.
- 37 Zhuang, Q., et al., 2004: Methane fluxes between terrestrial ecosystems and the atmosphere at northern high latitudes
38 during the past century: A retrospective analysis with a process-based biogeochemistry model. *Global*
39 *Biogeochemical Cycles*, **18**, GB3010.
- 40 Zickfeld, K., B. Knopf, V. Petoukhov, and H. Schellnhuber, 2005: Is the Indian summer monsoon stable against global
41 change? *Geophysical Research Letters*, **32**, L15707.
- 42 Zickfeld, K., M. Eby, H. Matthews, and A. Weaver, 2009: Setting cumulative emissions targets to reduce the risk of
43 dangerous climate change. *Proceedings of the National Academy of Sciences of the United States of America*,
44 **106**, 16129-16134.
- 45 Zickfeld, K., M. Morgan, D. Frame, and D. Keith, 2010: Expert judgments about transient climate response to
46 alternative future trajectories of radiative forcing. *Proceedings of the National Academy of Sciences of the*
47 *United States of America*, **107**, 12451-12456.
- 48 Zimov, S., S. Davydov, G. Zimova, A. Davydova, E. Schuur, K. Dutta, and F. Chapin, 2006: Permafrost carbon: Stock
49 and decomposability of a globally significant carbon pool. *Geophysical Research Letters*, **33**, L20502.
- 50
51

1 **Tables**

2

3 **Table 12.1:** [PLACEHOLDER FOR SECOND ORDER DRAFT: Radiative forcing agents in the CMIP5 multi-model global climate projections. See Table 9.1 for descriptions of
 4 the models. ESMs are highlighted in bold. In most cases forcing agents are implemented in conformance with standard prescriptions and datasets for CMIP5 (Taylor et al., 2011).
 5 Entries mean: n.a.: Forcing agent excluded in both historical and scenario simulations; Y: Forcing agent included (via prescribed concentrations, distributions or time series data); E:
 6 Forcing agent included (via specified emissions or precursor emissions); Es: Forcing agent included (driven with specified emissions but with prescribed surface concentrations); -:
 7 Simulations not performed; [?] – information not yet available. Numeric superscripts indicate model-specific references and other superscripts denote particular variations in forcing
 8 implementations, as detailed in notes following the table.]

9

Model	Forcing Agents																		
	Greenhouse Gases						Aerosols										Other		
	CO ₂	CH ₄	N ₂ O	Trop O ₃	Strat O ₃	CFCs	SO ₄	Urban	Black carbon	Organic carbon	Nitrate	First indirect effect	Second indirect effect	Dust	Volcanic	Sea salt	Land use	Solar	
ACCESS-1.0	Y	Y	Y	Y	Y	Y	E	n.a.	E	E	n.a.	Y	Y	Y	Y	Y	[?]	Y	
BCC-CSM1.1 ¹	Y/E ^{cc}	Y	Y	Y	Y	Y	Y	n.a.	Y	Y	n.a.	n.a.	n.a.	Y	Y	Y	n.a.	Y	
BNU-ESM	Y/E ^{cc}	Y	Y	Y	Y	Y	Y	n.a.	Y	Y	n.a.	Y	Y	Y	n.a.	Y	n.a.	Y	
CanAM4	Y	Y	Y	Y	Y	Y	E	n.a.	E	E	n.a.	Y ^{so}	n.a.	Y	Y/E st	Y	n.a.	Y	
CanCM4	Y	Y	Y	Y	Y	Y	E	n.a.	E	E	n.a.	Y ^{so}	n.a.	Y	Y/E st	Y	n.a.	Y	
CanESM2	Y/E ^{cc}	Y	Y	Y	Y	Y	E	n.a.	E	E	n.a.	Y ^{so}	n.a.	Y	Y/E st	Y	Y ^{cr}	Y	
CCSM4 ²	Y	Y	Y	Y ^a	Y ^a	Y	Y ^a	n.a.	Y ^a	Y ^a	n.a.	n.a.	n.a.	Y	Y	Y	Y	Y	
CESM1(BGC)	Y/E ^{cc}	Y	Y	Y ^a	Y ^a	Y	Y ^a	n.a.	Y ^a	Y ^a	n.a.	n.a.	n.a.	Y	Y	Y	Y	Y	
CESM1(CAM5)	Y	Y	Y	Y ^a	Y ^a	Y	E	n.a.	E	E	n.a.	Y	Y	E	Y/E	E	Y	Y	
CESM1(WACCM)	Es	Es	Es	E/Es ^{op}	E/Es ^{op}	Es	Y	n.a.	Y	Y	n.a.	n.a.	n.a.	Y	Y	Y	Y	Y	
CMCC-CESM	Y	Y	Y	Y	Y	Y	Y	n.a.	n.a.	n.a.	n.a.	Y ^{so}	n.a.	Y	n.a.	n.a.	n.a.	Y	
CMCC-CM	Y	Y	Y	Y	Y	Y	Y	n.a.	n.a.	n.a.	n.a.	Y ^{so}	n.a.	Y	n.a.	n.a.	n.a.	Y	
CMCC-CMS	Y	Y	Y	Y	Y	Y	Y	n.a.	n.a.	n.a.	n.a.	Y ^{so}	n.a.	Y	n.a.	n.a.	n.a.	Y	
CNRM-CM5 ³	Y	Y	Y	Y	Y ^{oc}	Y	Y ^b	n.a.	Y ^b	Y ^b	n.a.	Y ^{so}	n.a.	Y ^b	Y	Y ^b	n.a.	Y	
CSIRO-Mk3.6	Y	Y	Y	Y	Y	Y	E	n.a.	E	E	n.a.	Y	Y	Y	Y	Y	n.a.	Y	
EC-EARTH	Y	Y	Y	Y	Y	Y	Y	n.a.	Y	Y	n.a.	n.a.	n.a.	Y	Y	Y	Y	Y	
FIO-ESM	Y/E ^{cc}	Y	Y	Y	Y	Y	Y	n.a.	n.a.	Y	n.a.	n.a.	n.a.	Y	Y	Y	n.a.	Y	
GFDL-CM3	Y	Y/Es ^{rc}	Y/Es ^{rc}	E	E	Y	E	n.a.	E	E	n.a.	Y	Y	E	Y	Y	Y	Y	
GFDL-ESM2G	Y/E ^{cc}	Y	Y	Y	Y	Y	Y	n.a.	Y	Y	n.a.	n.a.	n.a.	Y	Y	Y	Y	Y	
GFDL-ESM2M	Y/E ^{cc}	Y	Y	Y	Y	Y	Y	n.a.	Y	Y	n.a.	n.a.	n.a.	Y	Y	Y	Y	Y	

GISS-E2(NINT) ⁴	Y	Y	Y	Y	Y	Y	Y	n.a.	Y	Y	Y	Y	n.a.	n.a.	Y	n.a.	Y	Y
GISS-E2(TCAD) ⁴	Y	Es/E ^{hf}	Es	E	E	Es/E ^{hf}	E	n.a.	E	E	E	Y	n.a.	E	Y	E	Y	Y
GISS-E2(TCADI) ⁴	Y	Es/E ^{hf}	Es	E	E	Es/E ^{hf}	E	n.a.	E	E	E	Y	n.a.	E	Y	E	Y	Y
HadGEM2-ES ⁵	Y/E ^{cc}	Es	Y	E	Y	Y	E	n.a.	E	E	n.a.	Y	Y	Y	Y	Y	Y	Y
INM-CM4	Y/E ^{cc}	Y	Y	Y	Y	n.a.	Y	n.a.	n.a.	n.a.	n.a.	Y ^{so}	n.a.	n.a.	Y	n.a.	Y	Y
IPSL-CM5A-LR ⁶	Y/E ^{cc}	Y	Y	Y ^b	Y ^b	Y	Y ^b	n.a.	Y ^b	Y ^b	n.a.	Y	n.a.	Y ^b	Y	Y	Y	Y
IPSL-CM5A-MR ⁶	Y/E ^{cc}	Y	Y	Y	Y	Y	Y	n.a.	Y	Y	n.a.	Y	n.a.	Y	Y	Y	Y	Y
IPSL-CM5B-LR ⁶	Y	Y	Y	Y	Y	Y	Y	n.a.	Y	Y	n.a.	Y	n.a.	Y	Y	Y	Y	Y
MIROC-ESM ⁷	Y/E ^{cc}	Y	Y	Y	Y	Y	E	n.a.	E	E	n.a.	Y	Y	Y	Y	Y	Y	Y
MIROC-ESM-CHEM ⁷	Y	Y	Y	E	E	Y	E	n.a.	E	E	n.a.	Y	Y	Y	Y	Y	Y	Y
MIROC4h	Y	Y	Y	Y	Y	Y	E	n.a.	E	E	n.a.	Y	Y	Y	Y	Y	Y ^{cr}	Y
MIROC5	Y	Y	Y	Y	Y	Y	E	n.a.	E	E	n.a.	Y	Y	Y	Y	Y	Y ^{cr}	Y
MPI-ESM-LR	Y/E ^{cc}	Y	Y	Y	Y	Y	Y	n.a.	[?]	[?]	n.a.	[?]	[?]	[?]	Y	[?]	Y	Y
MPI-ESM-MR	Y/E ^{cc}	Y	Y	Y	Y	Y	Y	n.a.	[?]	[?]	n.a.	[?]	[?]	[?]	Y	[?]	Y	Y
MRI-CGCM3	Y	Y	Y	Y	Y	Y	E	n.a.	E	E	n.a.	Y	Y	E	E	E	Y	Y
MRI-ESM1	-/E ^{cc}	Y	Y	E	E	Y	E	n.a.	E	E	n.a.	Y	Y	E	E	E	Y	Y
NorESM1-M	Y	Y	Y	Y	Y	Y	E	n.a.	E	E	n.a.	Y	Y	E	E	E	Y	Y
NorESM1-ME	Y/E ^{cc}	Y	Y	Y	Y	Y	E	n.a.	E	E	n.a.	Y	Y	E	E	E	Y	Y

1 Notes

2 **Model-specific references:**3 ¹ Wu et al. (2011)4 ² Meehl et al. (2011)5 ³ Voldoire et al. (2011)6 ⁴ GISS-E2-R and GISS-E2-H models are forced similarly and both represented here as GISS-E2. Both -R and -H model versions have three variants: in the NINT and TCAD variants the aerosol indirect effect is parametrised following Hansen et al. (2005), whereas in the TCADI variant it is calculated interactively.7 ⁵ Jones et al. (2011)8 ⁶ Dufresne et al. (2011)9 ⁷ Watanabe et al. (2011)10 **Additional notes:**11 ^{cc} Separate entries for ESMs denote “concentrations-driven” and “emissions-driven” experiments respectively.12 ^{rc} Separate entries for different treatments used for radiation and chemistry respectively.13 ^{hf} Separate entries denote historical and future (RCPs) respectively.14 ^a Three-dimensional tropospheric ozone, stratospheric ozone and aerosol distributions specified as monthly mean concentrations, computed off-line using CAM-Chem – a modified version of CAM3.5 with interactive chemistry – driven with specified emissions for the historical period (Lamarque et al., 2010) and RCPs (Lamarque et al., 2011) with sea surface temperature and sea ice boundary conditions based on CCSM3's projections for the closest corresponding AR4 scenarios. These historical and projected RCP concentrations are also used in some other models.

- 1 ^b Aerosol concentrations or optical depths and/or ozone prescribed from output of a closely-related aerosol-transport chemistry model simulations forced with CMIP5 prescribed
2 emissions - Szopa et al. (2011) for CNRM-CM5 and IPSL-CM5A-LR.
3 ^{op} Separate entries denote different ozone chemistry precursors.
4 ^{oc} Linearized 2D ozone chemistry scheme (Cariolle and Teyssedre, 2007) including transport and photochemistry, reactive to stratospheric chlorine perturbations but not tropospheric
5 chemical emissions.
6 ^{so} First indirect effect from sulphate aerosol only. st Separate entries denote stratosphere and troposphere respectively.
7 ^{cf} Land use change represented via crop change only.

Chapter 12: Long-term Climate Change: Projections, Commitments and Irreversibility

Coordinating Lead Authors: Matthew Collins (UK), Reto Knutti (Switzerland)

Lead Authors: Julie Arblaster (Australia), Ken Caldeira (USA), Jean-Louis Dufresne (France), Thierry Fichet (Belgium), Pierre Friedlingstein (UK), Xuejie Gao (China), William Gutowski (USA), Tim Johns (UK), Gerhard Krinner (France), Mxolisi Shongwe (Swaziland), Claudia Tebaldi (USA), Andrew Weaver (Canada), Michael Wehner (USA)

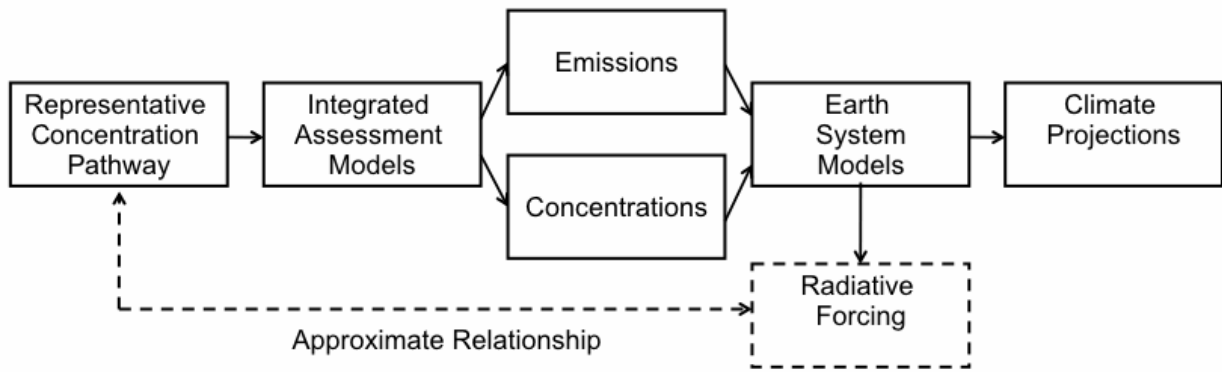
Contributing Authors: Myles R. Allen, Tim Andrews, Cecilia Bitz, Claire Brutel, Mark Cane, Robin Chadwick, Ed Cook, Kerry H. Cook, Michael Eby, Veronika Eyring, Erich M. Fischer, Piers Forster, Peter Good, Hugues Goosse, Kevin I. Hodges, Marika Holland, Philippe Huybrechts, Manoj Joshi, Viatcheslav Kharin, Yochanan Kushnir, David Lawrence, Robert W. Lee, Spencer Liddicoat, Wolfgang Lucht, Damon Matthews, François Massonnet, Malte Meinshausen, Christina M. Patricola, Gwenaëlle Philippon, Prabhat, Stefan Rahmstorf, William J. Riley, Joeri Rogelj, Oleg Saenko, Richard Seager, Jan Sedlacek, Len Shaffrey, Jana Sillmann, Andrew Slater, Robert Webb, Giuseppe Zappa, Kirsten Zickfeld

Review Editors: Sylvie Joussaume (France), Abdalah Mokssit (Morocco), Karl Taylor (USA), Simon Tett (UK)

Date of Draft: 16 December 2011

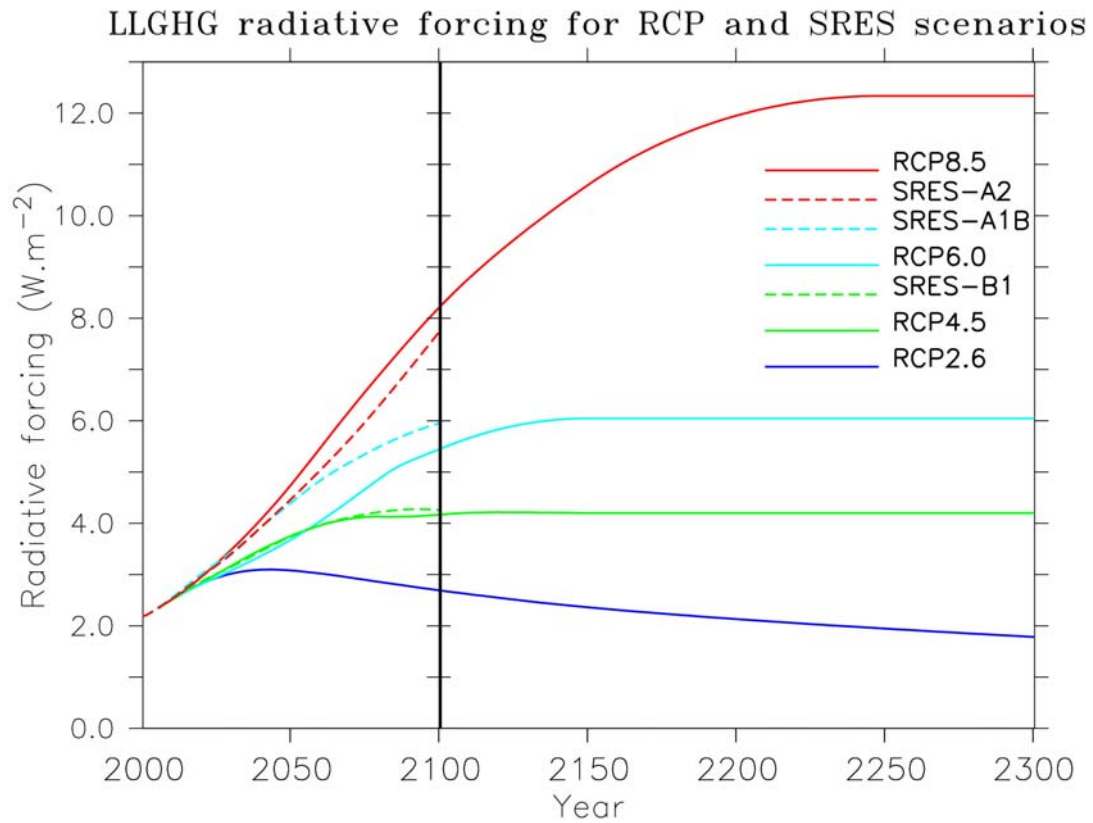
Notes: TSU Compiled Version

1 **Figures**



3
4
5 **Figure 12.1:** Links in the chain from scenarios, through models to climate projections. The Representative
6 Representative Concentration Pathways (RCPs) are designed to sample a range of radiative forcing of the climate system at 2100. The
7 RCPs are translated into both emissions and concentrations of greenhouse gases using Integrated Assessment Models
8 (IAMs). These are then used as inputs to dynamical Earth System Models (ESMs) in simulations which are either
9 concentration-driven (the majority of projection experiments) or emissions-driven (only run for RCP8.5). Aerosols and
10 other forcing factors are implemented in subtly different ways in each ESM. The ESM projections each have a
11 potentially different radiative forcing, which may be viewed as an output of the model and which may not correspond to
12 precisely the level of radiative forcing indicated by the RCP. In addition, different models would produce different
13 responses even under the same radiative forcing. Uncertainty propagates through the chain and results in a spread of
14 ESM projections. This spread is only one way of assessing uncertainty in projections and alternative methods, which
15 combine information from simple and complex models and observations are also used to quantify that uncertainty.
16

1



2

3

4

5

6

7

8

9

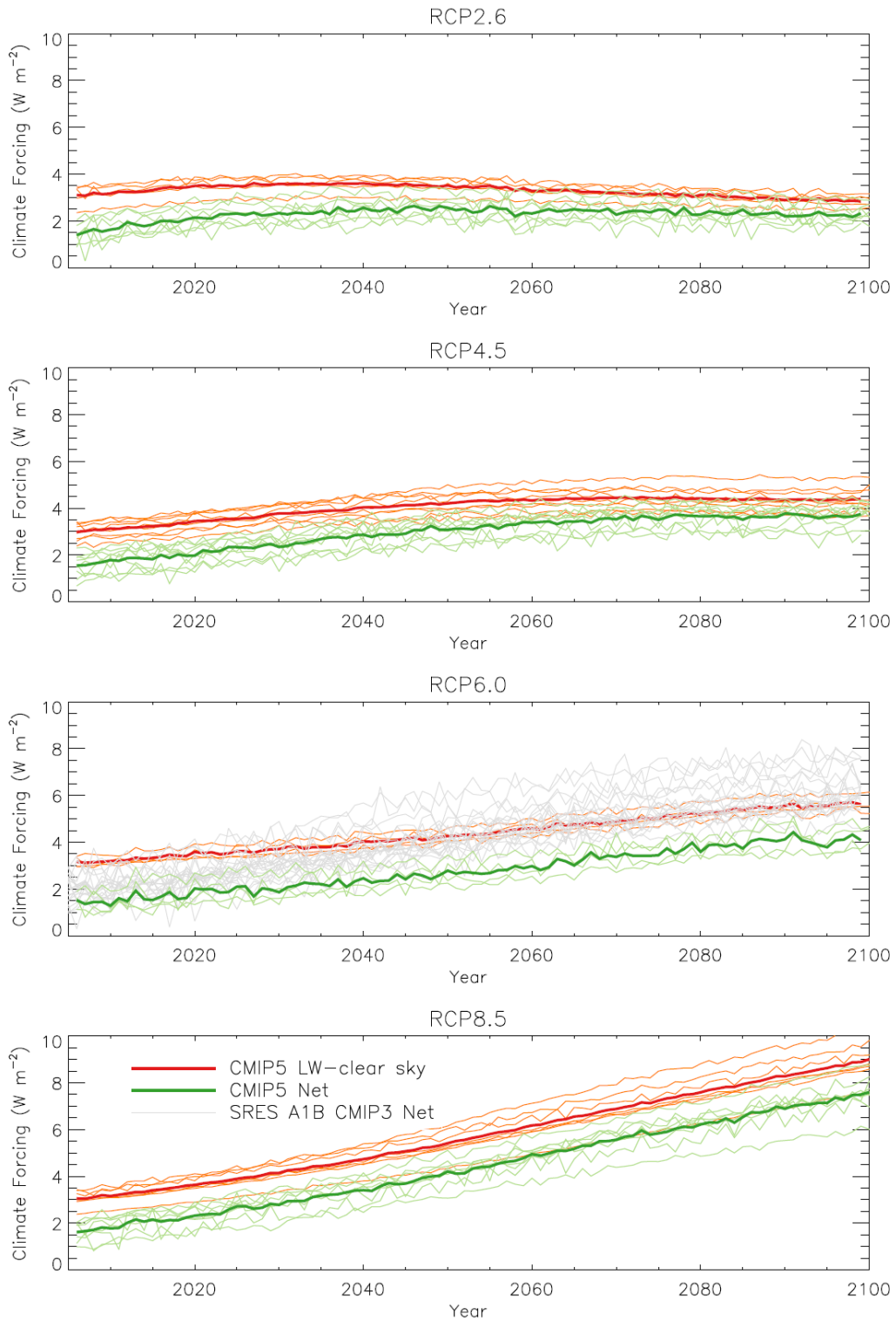
10

11

12

Figure 12.2: Time evolution of the anthropogenic radiative forcing between 2000 and 2300 due to the defined concentrations of long-lived greenhouse gases (CO₂, CH₄, N₂O, halogenated, chlorinated and fluorinated gases) for RCP scenarios and their extensions (continuous lines) and SRES scenarios (dashed lines). The four RCP scenarios used in CMIP5 are: RCP2.6 (blue), RCP4.5 (green), RCP6.0 (light blue) and RCP8.5 (red). The three SRES scenarios used in CMIP3 are: B1 (green), A1B (light blue) and A2 (red). The radiative forcing has been computed using the concentration of the different greenhouse gases for the different scenarios and the radiative efficiency published in the TAR (Table 6.7), using SRES scenario concentrations published in the TAR (Appendix II). It is illustrative of the LLGHG forcing that could result in climate models which are forced with the defined concentrations pathways.

1



2

3

4

5

6

7

8

9

10

11

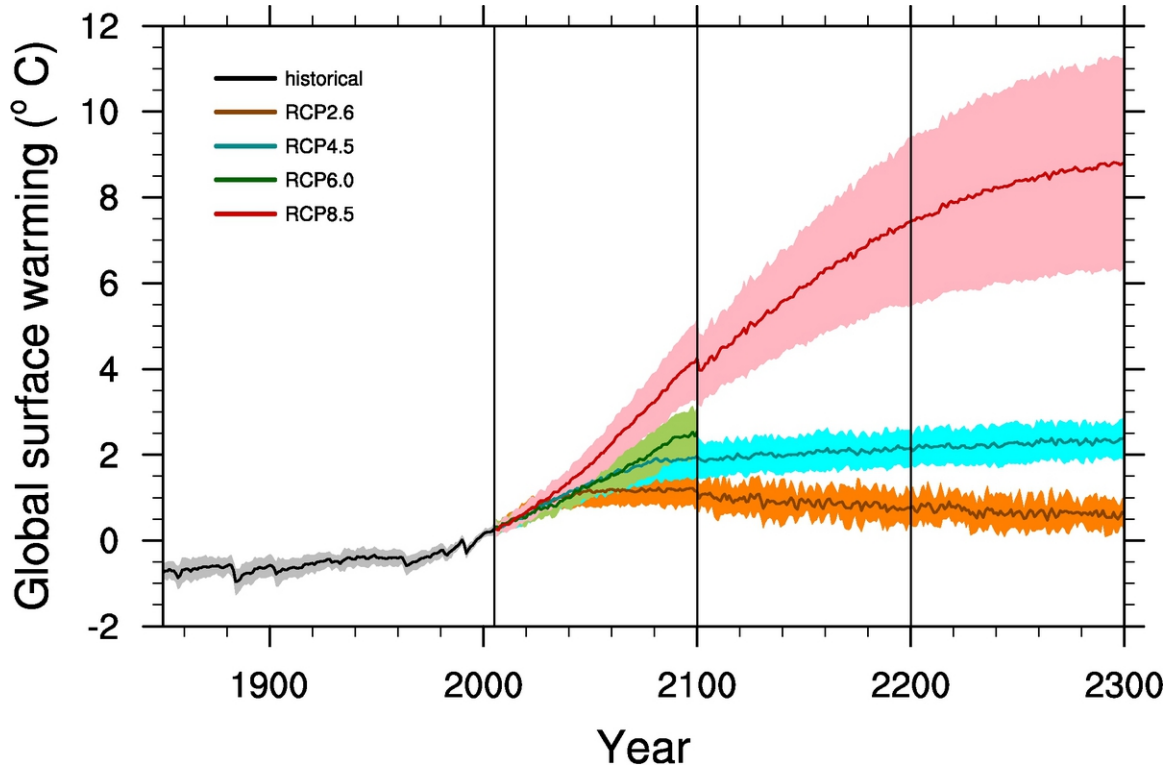
12

13

14

Figure 12.3: [PLACEHOLDER FOR SECOND ORDER DRAFT: Global mean climate forcings (W m^{-2}) realised in the CMIP5 simulations diagnosed for four RCP scenarios. Thin green and orange lines correspond to net all-sky and longwave clear-sky climate forcings respectively. Climate forcing has been computed using the methodology of Forster and Taylor (2006), which includes rapid adjustment in the forcing term and further assumes each model has an invariant climate feedback parameter, which here has been calculated from the abrupt $4\times\text{CO}_2$ experiments using the method of Gregory et al. (2004). Climate forcings are referenced to the equivalent period (2005–2100 average) of the model's preindustrial control integration. Each of these lines represents a single CMIP5 model result averaged over all available ensemble members. Thick lines show the multi-model averaged climate forcing. Grey lines on the RCP6.0 panel show the net climate forcings diagnosed from 21 CMIP3 models for the SRES A1B scenario, taken from Forster and Taylor (2006).]

1



2

3

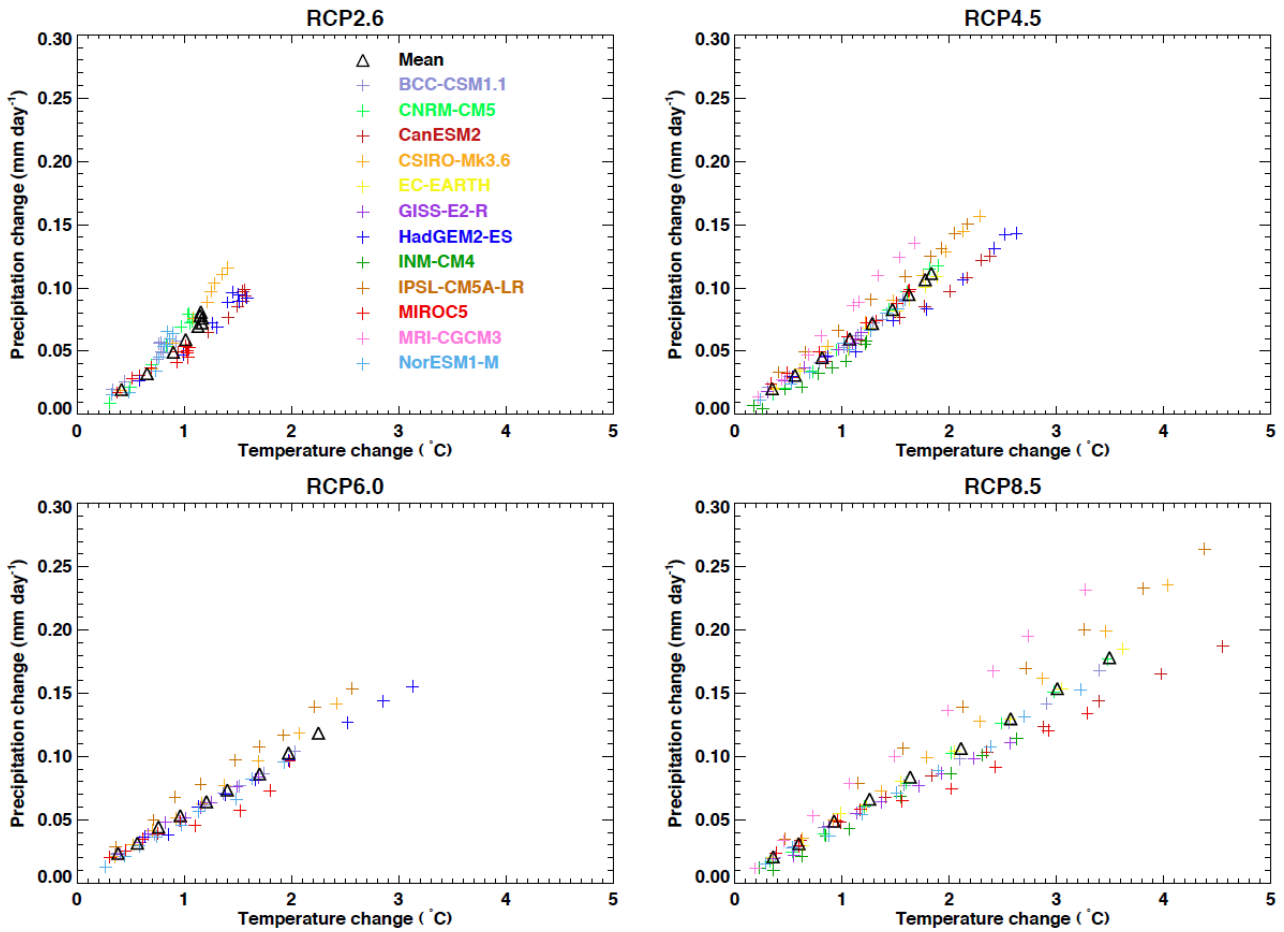
4

5

6

Figure 12.4: Time series of global mean surface air temperature anomalies (relative to 1986–2005) from concentration-driven experiments from CMIP5. Projections are shown for each representative concentration pathway (RCP) for the multimodel mean (solid lines) and ± 1 standard deviation across the distribution of individual models (shading).

1



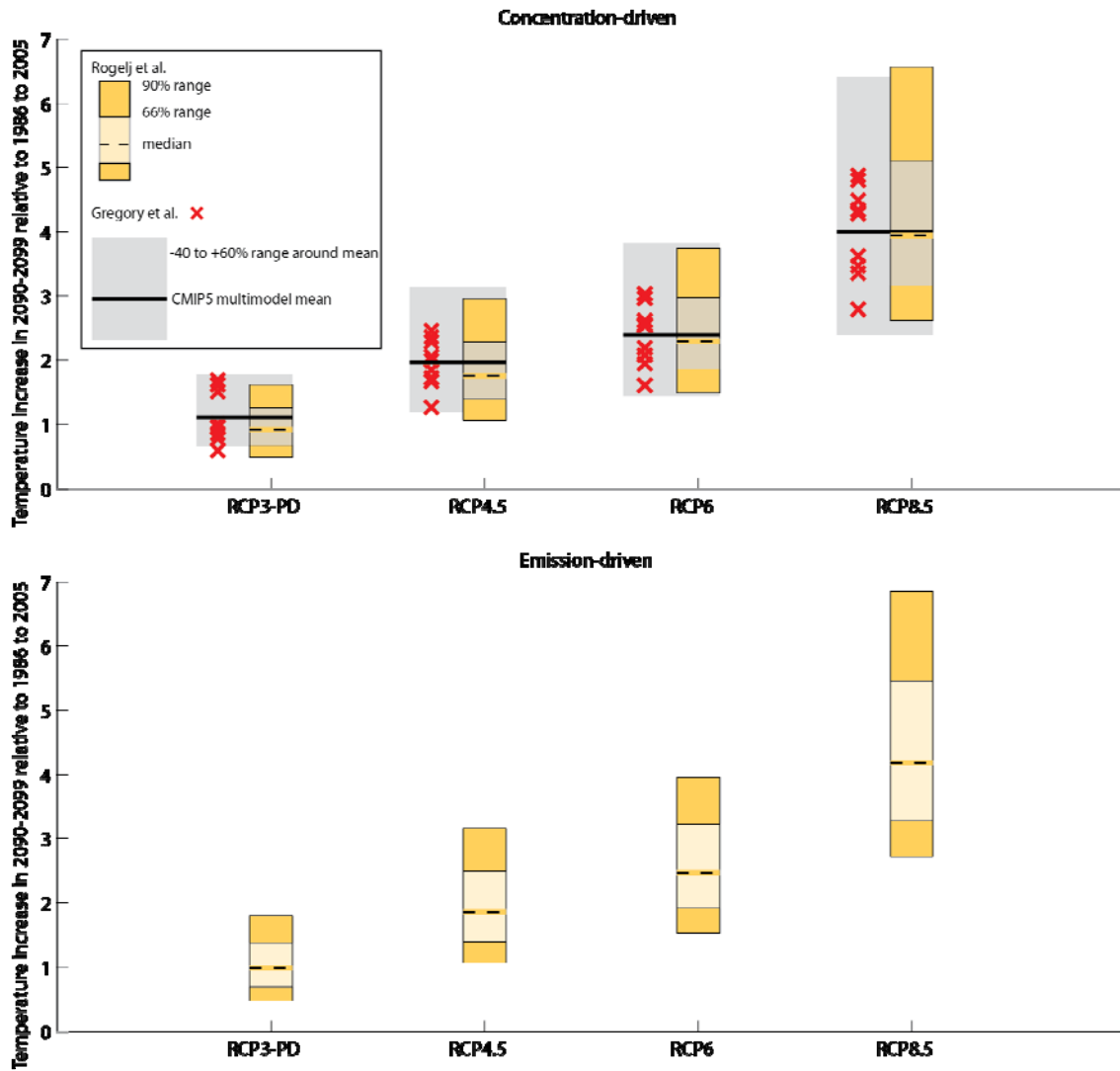
2

3

Figure 12.5: Global mean precipitation (mm/day) versus temperature (°C) changes relative to 1986 to 2005 for CMIP5 model projections for RCPs. Each coloured symbol represents the ensemble mean for a single model averaged over successive decadal periods (2006 to 2015 up to 2086 to 2095). The black triangles are multi-model means.

7

1

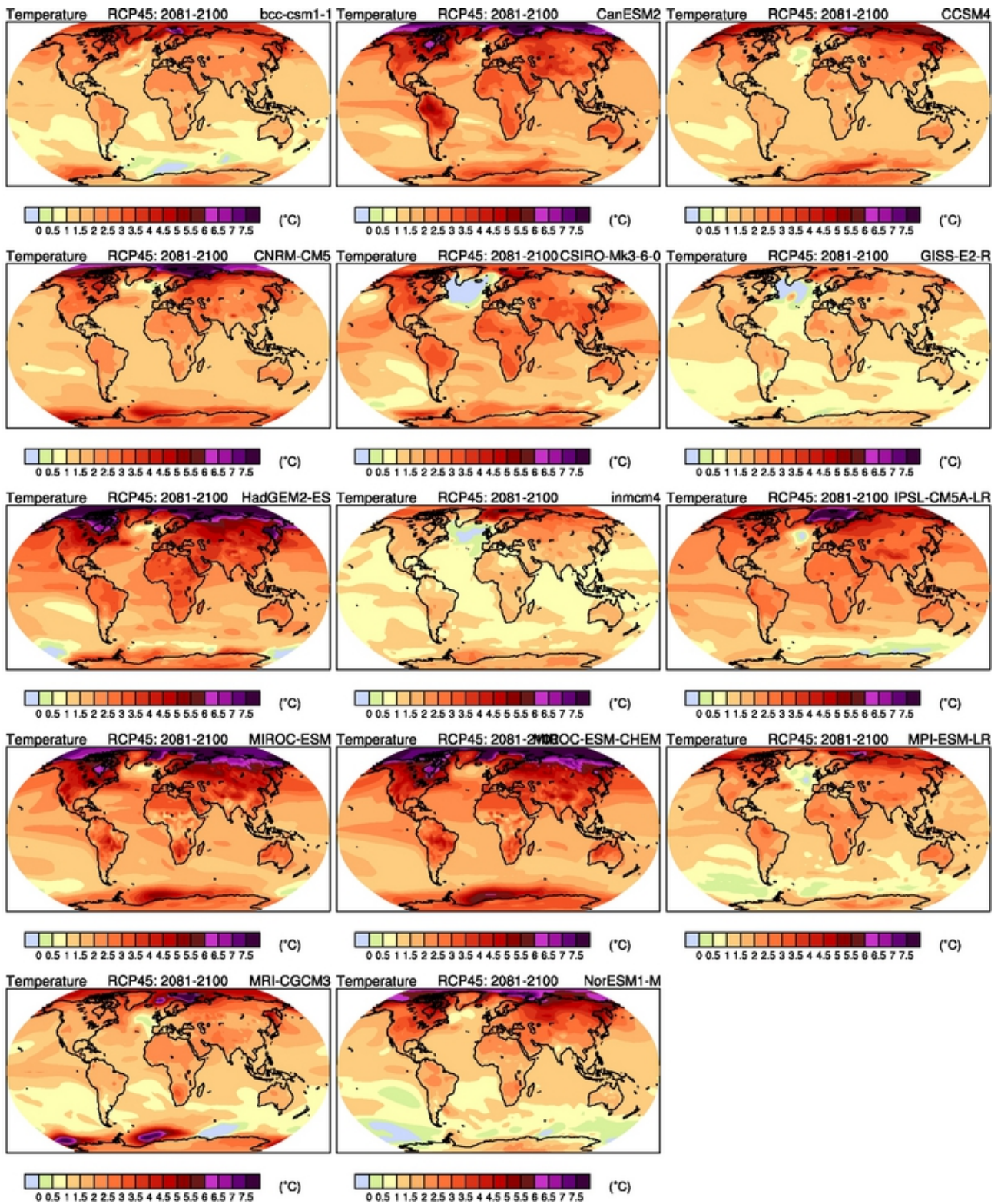


2

3

4 **Figure 12.6:** Uncertainty estimates for global mean temperature change with respect to 1986–2005 using different
 5 techniques. The yellow bars show the median, 33–66% range and 10–90% range based on (Rogelj et al., 2011a). The
 6 solid black line indicates the CMIP5 ensemble mean and the grey bars show –40% and +60% of that mean.

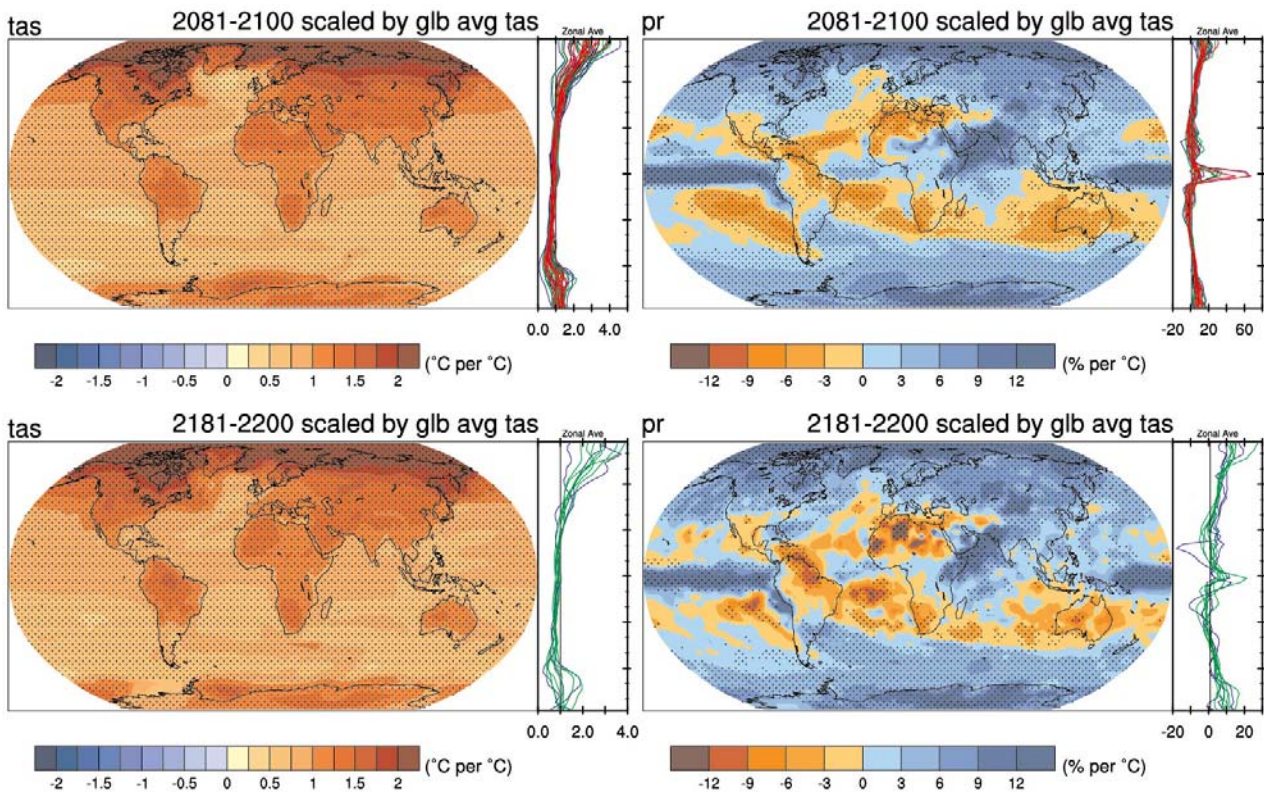
1



2
3
4
5
6

Figure 12.7: Surface air temperature change in 2081–2100 displayed as anomalies with respect to 1986–2005 for RCP4.5 from each of the concentration-driven models available in the CMIP5 archive.

1



2

3

4

5

6

7

8

9

10

11

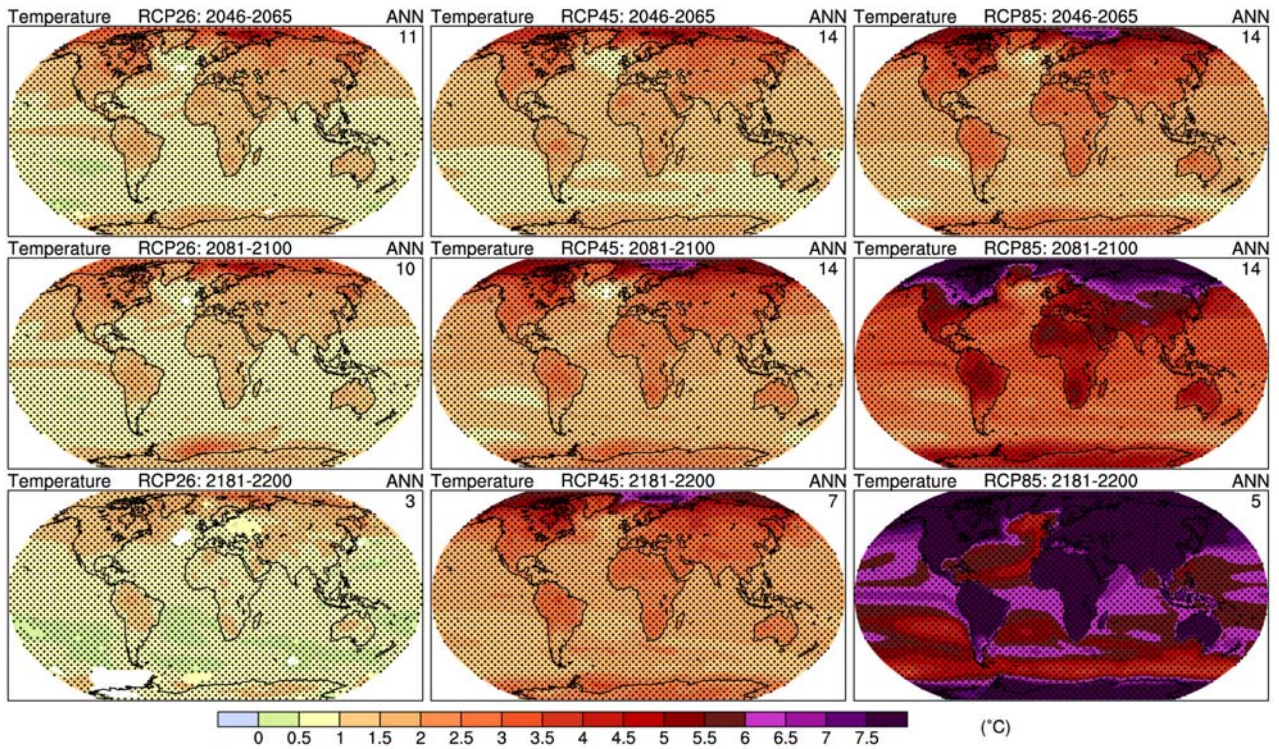
12

13

14

Figure 12.8: Temperature (left) and precipitation (right) change patterns derived from transient simulations from the CMIP5 ensembles, scaled to 1°C of global average warming. The patterns have been calculated by computing 20-year averages at the end of the 21st (top) and 22nd (bottom) Century and over the period 1986–2005 for the available simulations under all RCPs, taking their difference (percentage difference in the case of precipitation) and normalizing it, grid-point by grid-point, by the corresponding value of global average temperature change for each model and scenario. The normalized patterns have then been averaged across models and scenarios. The colour scale represents °C (in the case of temperature) and % (in the case of precipitation) per 1°C of global average warming and stippling indicates the mean change averaged over all realisations is larger than the 95% percentile of the distribution. Zonal means of the geographical patterns are shown for each individual model for RCP2.6 (blue), 4.5 (green), 6.0 (black) and 8.5 (red). RCP8.5 is excluded from the stabilisation figures.

1



2

3

4

5

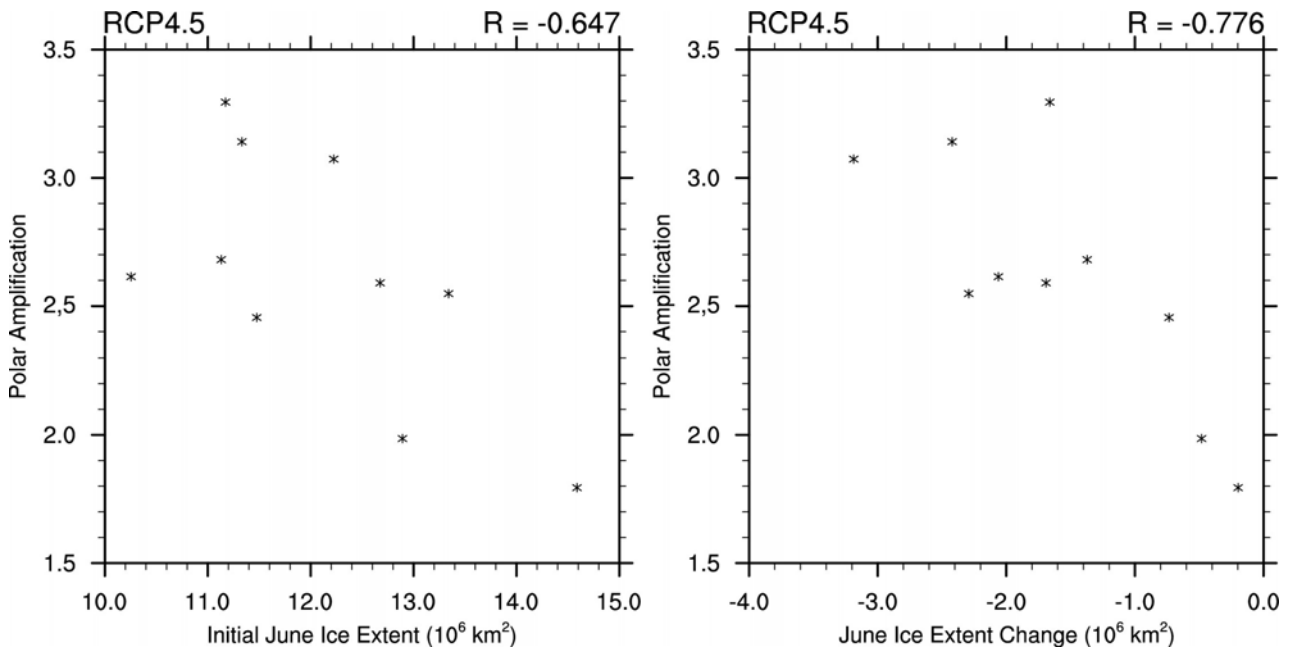
6

7

8

Figure 12.9: 9-panel figure of multimodel ensemble average of surface air temperature change (compared to 1986–2005 base period) for 2046–2065, 2081–2100, 2181–2200 for RCP 2.6, 4.5 and 8.5. Model agreement is assessed as in (Tebaldi et al., 2011). Grid points are stippled where at least half of the models show significant change and >80% of them agree on the sign, while white shading indicates at least half of the models show significant change but less than 80% of those agree on the sign.

1



2

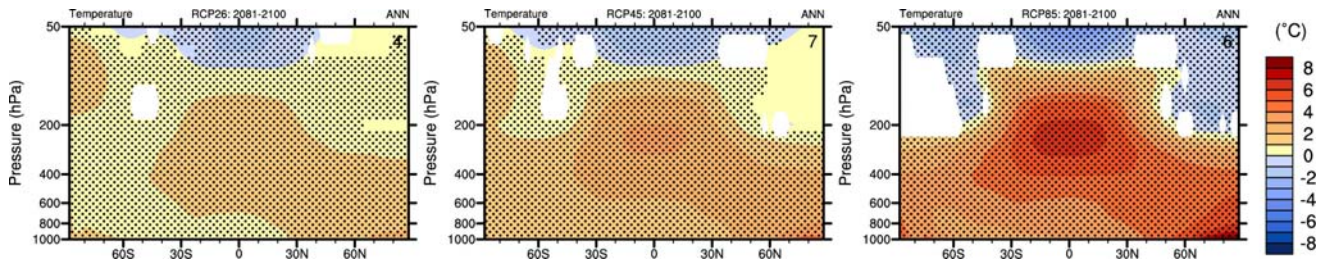
3

4

5

Figure 12.10: Scatter diagram of initial June sea-ice extent versus polar amplification factor from the available CMIP5 models under RCP4.5.

1



2

3

4

5

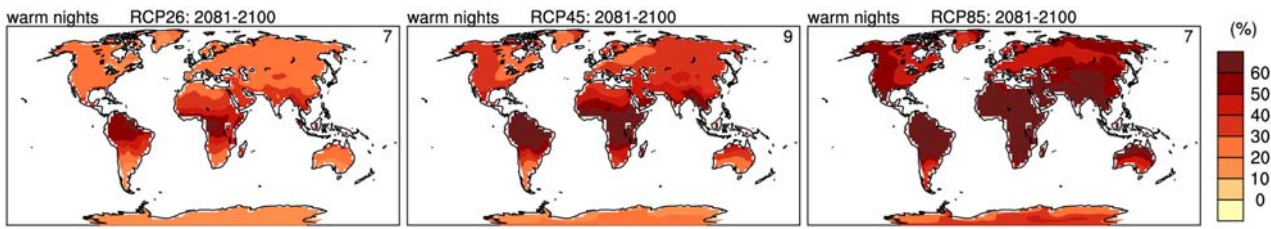
6

7

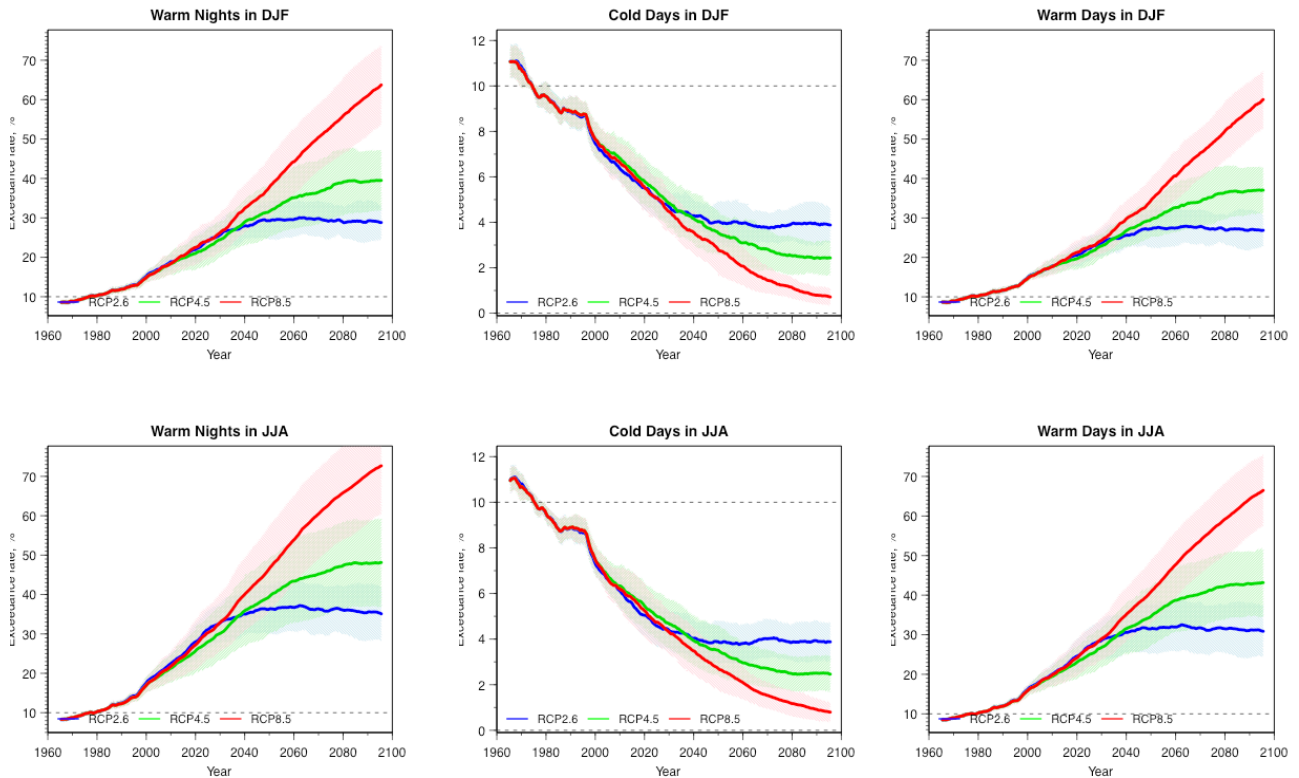
8

Figure 12.11: CMIP5 multi-model changes in annual, zonal mean temperature relative to 1986–2005 for 2081–2100 under the RCP2.6 (left), RCP4.5 (centre) and RCP8.5 (right) forcing scenarios. Model agreement is assessed as in (Tebaldi et al., 2011). Grid points are stippled where at least half of the models show significant change and >80% of them agree on the sign, while white shading indicates at least half of the models show significant change but less than 80% of those agree on the sign.

1



2



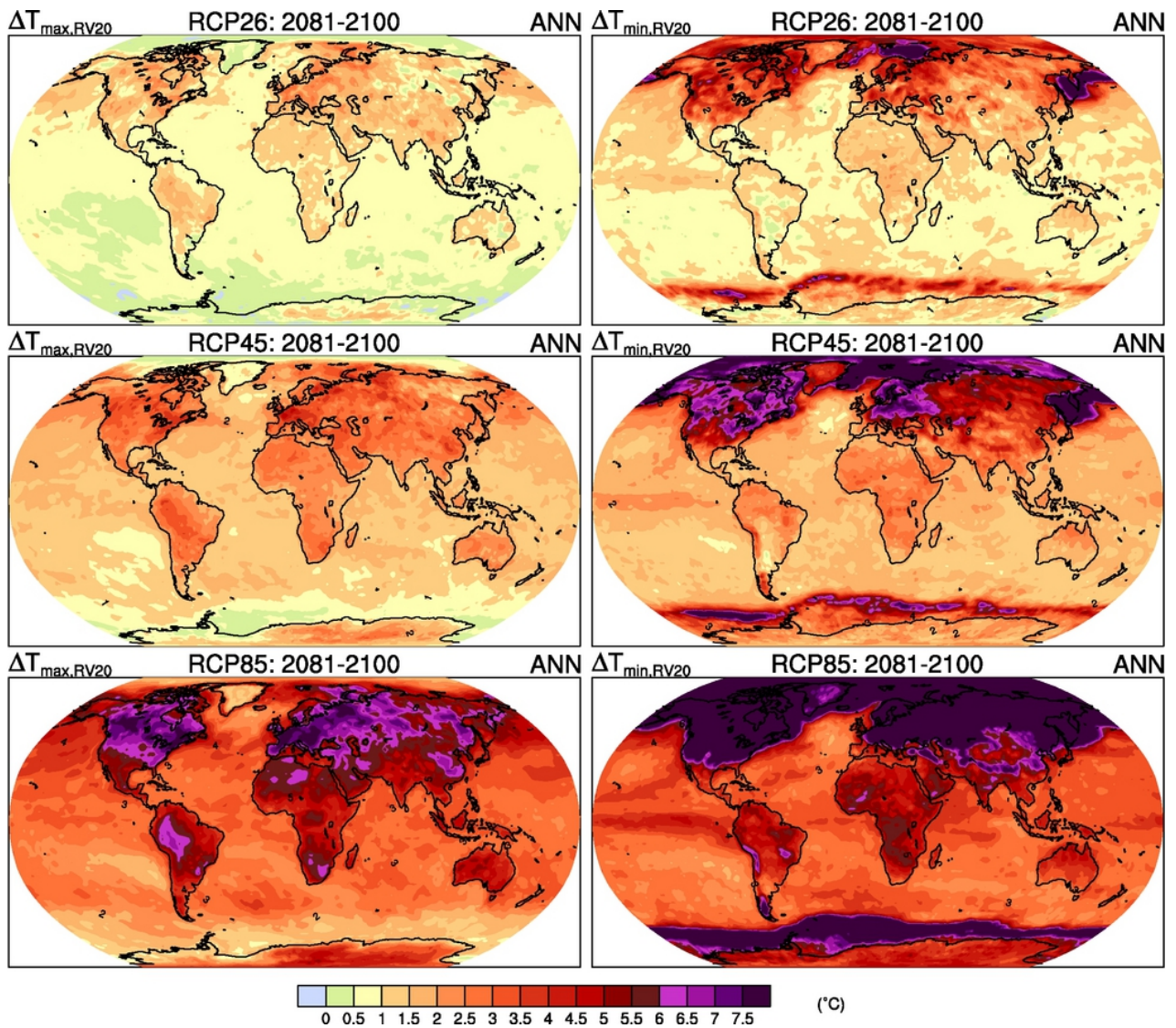
3

4

5 **Figure 12.12:** CMIP5 multimodel mean geographical changes in warm nights (the percentage of days when minimum
 6 temperatures are above the 90th percentile) at the end of the 21st century (top row) and 20-year smoothed timeseries
 7 (middle and bottom row) of globally averaged seasonal warm nights, cold days (the percentage of days when maximum
 8 temperatures are below the 10th percentile) and warm days (the percentage of days when maximum temperatures are
 9 above the 90th percentile) for RCP2.6, 4.5 and 8.5 based on available CMIP5 models. Shading in the timeseries
 10 represents the ± 1 standard deviation across the individual models. Units are absolute values relative to the 1961–1990
 11 base period.

12

1

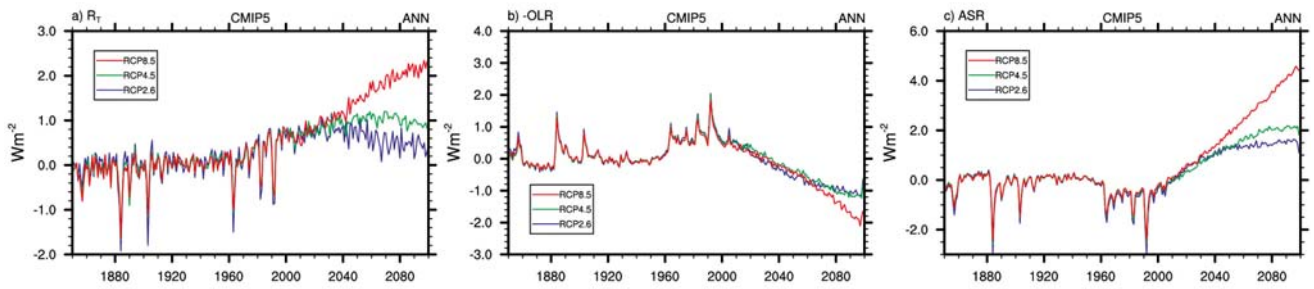


2

3

4 **Figure 12.13:** The CMIP5 multi-model median change in 20-yr return values of annual warm temperature extremes
 5 (left hand panels) and cold temperature extremes (right hand panels) as simulated by CMIP5 models in 2081–2100
 6 relative to 1986–2005 in the RCP2.6 (top panels), RCP4.5 (middle panels), and RCP8.5 (bottom panels) experiments.
 7 Global averages of changes are indicated in the titles.

1



2

3

4

5

6

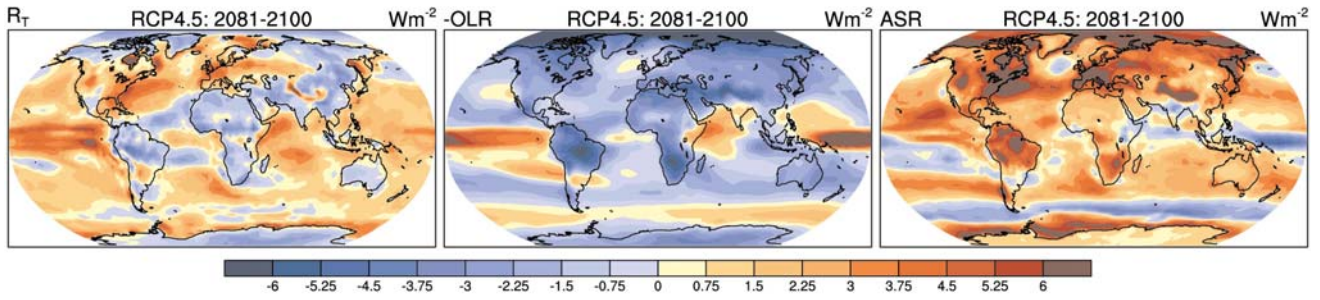
7

8

9

Figure 12.14: Time evolution of the global mean (a) net total radiation anomaly at the TOA, (b) net longwave radiation anomaly at the TOA and (c) net shortwave radiation anomaly at the TOA for the historical period and three RCP scenarios from available models. All the fluxes are positive downward and units are $W m^{-2}$. The anomalies are computed with respect to the 1900–1950 base period. [PLACEHOLDER FOR SECOND ORDER DRAFT: include RCP6.0 and compute anomalies with respect to the control simulation].

1



2

3

4

5

6

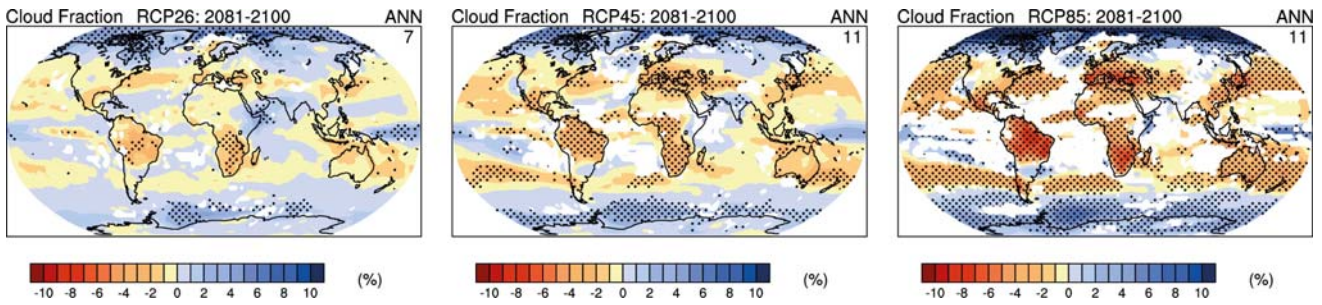
7

8

9

Figure 12.15: CMIP multi-model changes in annual net radiation (R_T , left) net longwave radiation ($-OLR$, centre) and absorbed solar radiation (ASR , bottom) at the TOA for the RCP4.5 scenario from available models. All fluxes are positive downward, units are $W m^{-2}$ and $R_T = ASR - OLR$. The net radiation anomalies are computed with respect to the 1900–1950 base period. [PLACEHOLDER FOR SECOND ORDER DRAFT: the anomalies will be computed with respect to the control simulation]

1



2

3

4

5

6

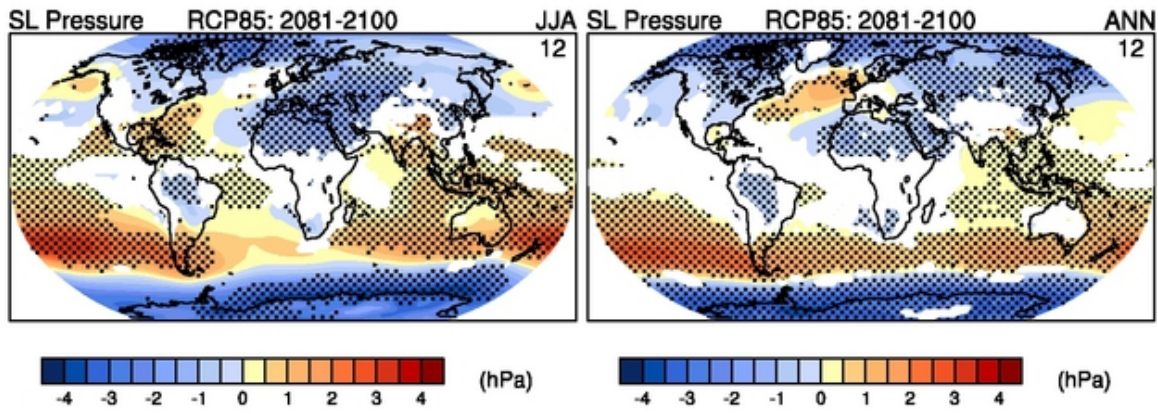
7

8

9

Figure 12.16: CMIP5 multi-model changes in annual total cloud amount relative to 1986–2005 for 2081–2100 under the RCP2.6 (left), RCP4.5 (centre) and RCP8.5 (right) forcing scenarios. Model agreement is assessed as in (Tebaldi et al., 2011). Grid points are stippled where at least half of the models show significant change and >80% of them agree on the sign, while white shading indicates at least half of the models show significant change but less than 80% of those agree on the sign.

1



2

3

4

5

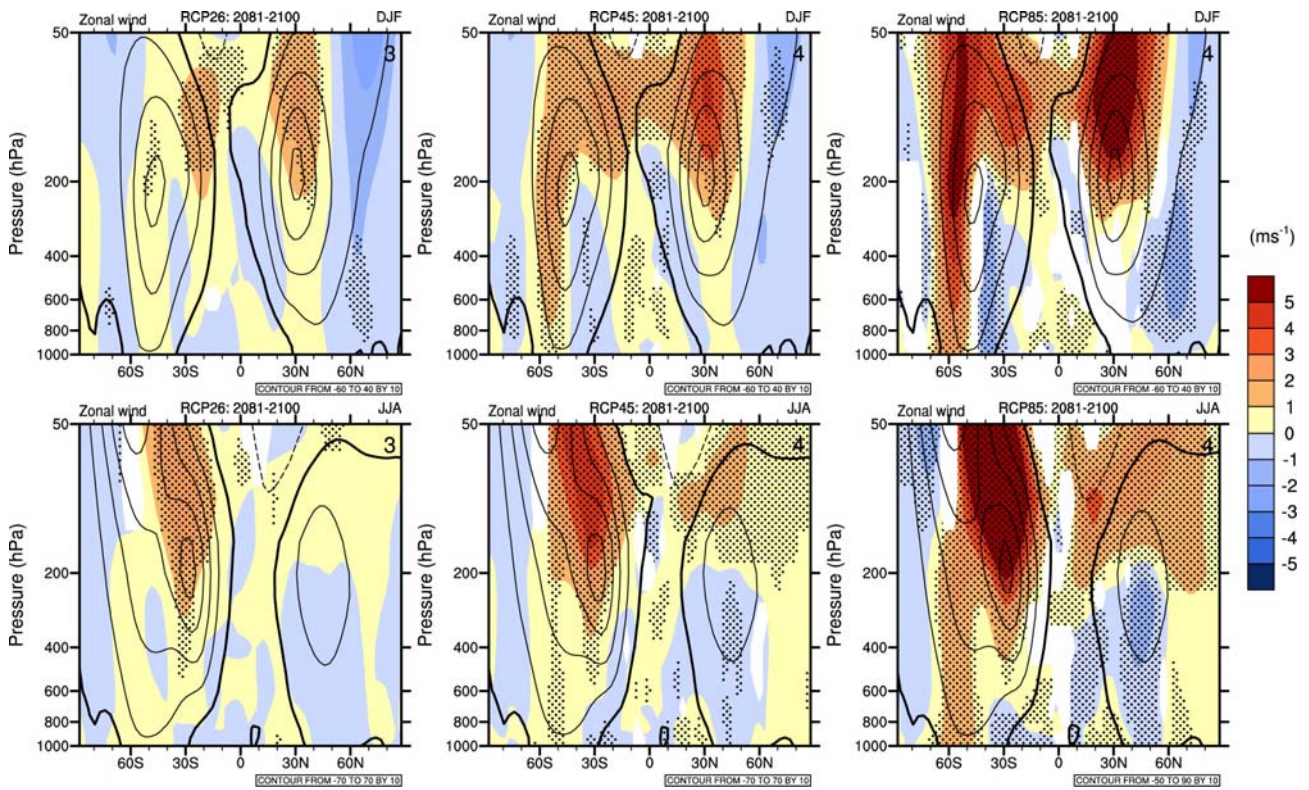
6

7

8

Figure 12.17: CMIP5 multimodel ensemble average of sea level pressure change (2081–2100 minus 1986–2005) for RCP2.6, 4.5 and 8.5 for DJF and JJA seasons. Model agreement is assessed as in (Tebaldi et al., 2011). Grid points are stippled where at least half of the models show significant change and >80% of those agree on the sign, while white shading indicates at least half of the models show significant change but less than 80% of those agree on the sign.

1



2

3

4

5

6

7

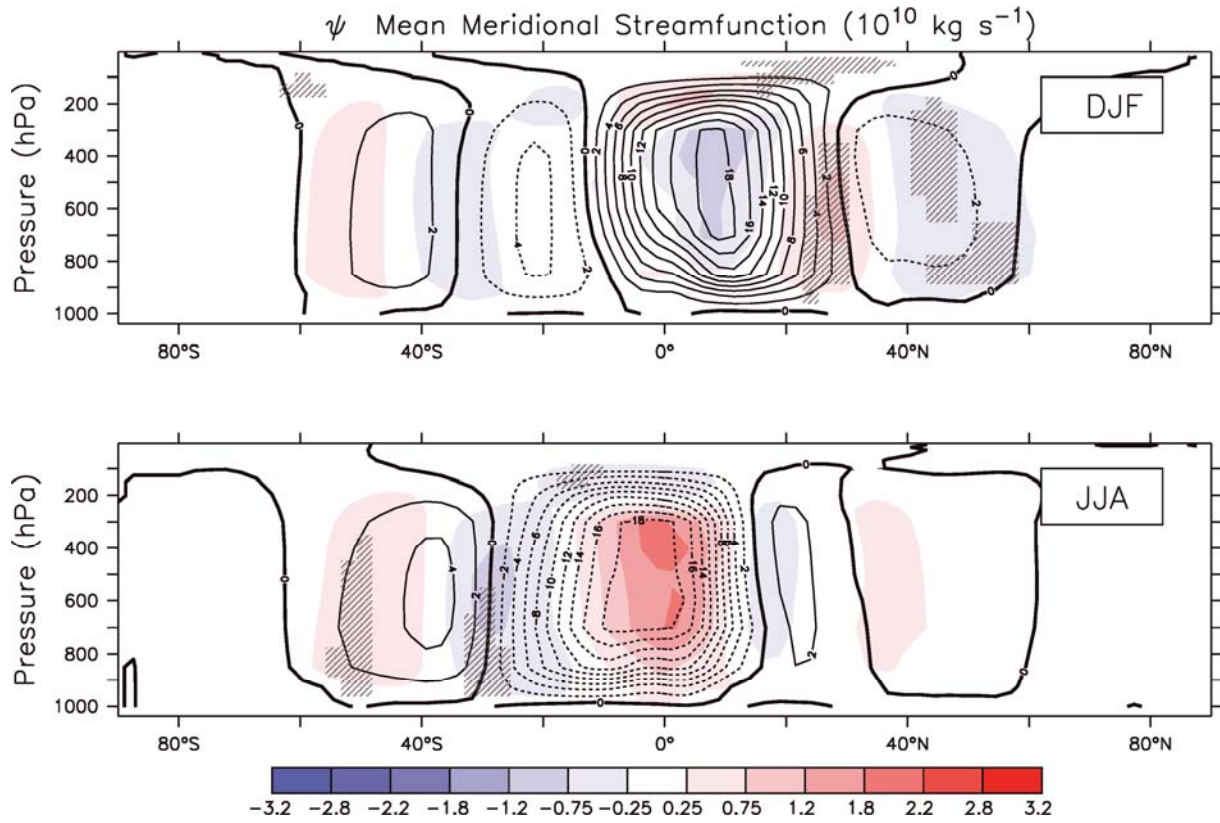
8

9

10

Figure 12.18: CMIP5 multimodel ensemble average of zonal wind change (2081–2100 minus 1986–2005) for RCP2.6, 4.5 and 8.5. Changes are shown for DJF and JJA. Black contours represent the multimodel mean average for the 1986–2005 base period. Model agreement is assessed as in (Tebaldi et al., 2011). Grid points are stippled where at least half of the models show significant change and >80% of them agree on the sign, while white shading indicates at least half of the models show significant change but less than 80% of those agree on the sign. [PLACEHOLDER FOR SECOND ORDER DRAFT: If chemistry-climate models show substantially different results from the standard CMIP5 models, highlighting that in additional panels needs to be considered.]

1



2

3

4

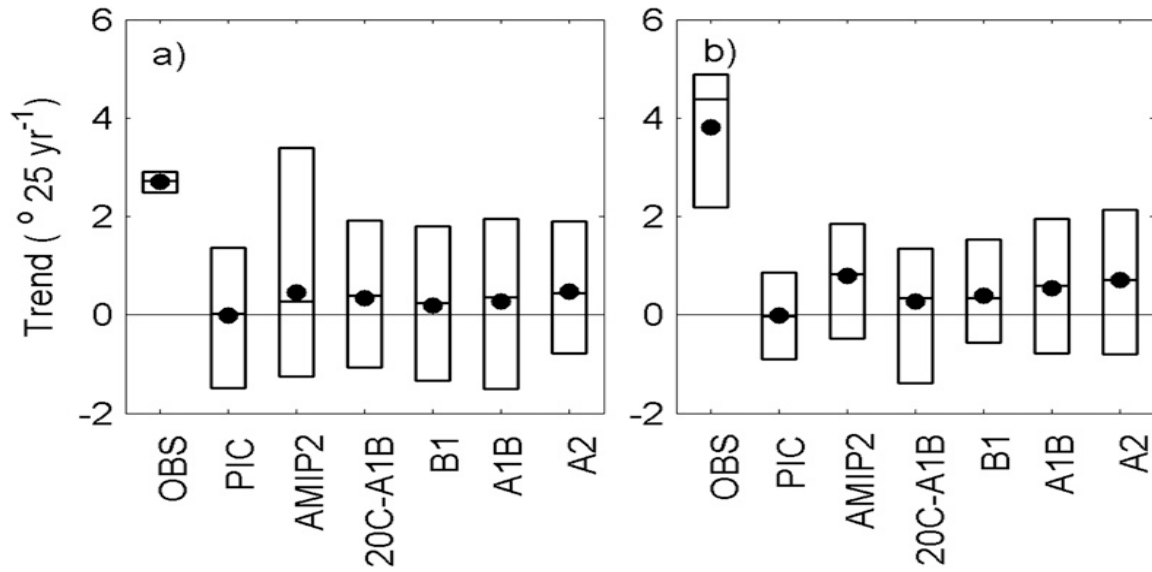
5

6

7

Figure 12.19: [PLACEHOLDER FOR THE SECOND ORDER DRAFT: Boreal winter (DJF) and boreal summer (JJA) zonal-mean stream function ($10^{10} \text{ kg s}^{-1}$) from CMIP3 model experiments. Contours show the model simulations in an idealized 1%/year rise in CO_2 concentration. Shading displays the changes in the strength of the meridional overturning circulation. The placeholder diagram is obtained from (Gastineau et al., 2008).]

1



2

3

4

5

6

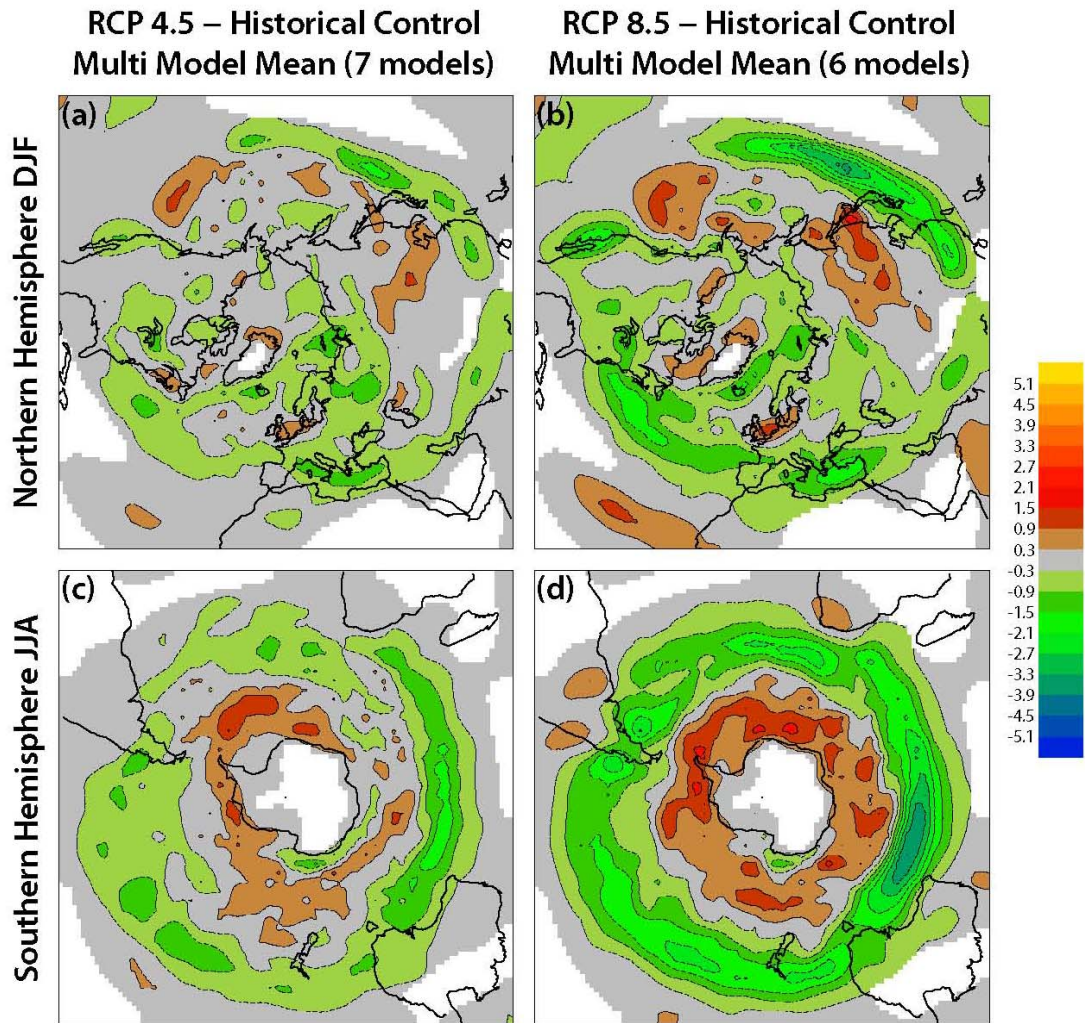
7

8

9

Figure 12.20: [PLACEHOLDER FOR THE SECOND ORDER DRAFT: Trends in Hadley cell width from observations and GCM realizations under different GHG forcings. Trends show Hadley cell widening identified by a) 500hPa streamfunction (ψ_{500}) and b) outgoing long-wave radiation (OLR). In the models (observations), the boxes show the 95% confidence interval (entire range) of the trends. The mean and median of each distribution are represented by the circle and the horizontal bar, respectively. Figure from (Johanson and Fu, 2009)]

1



2

3

4

5

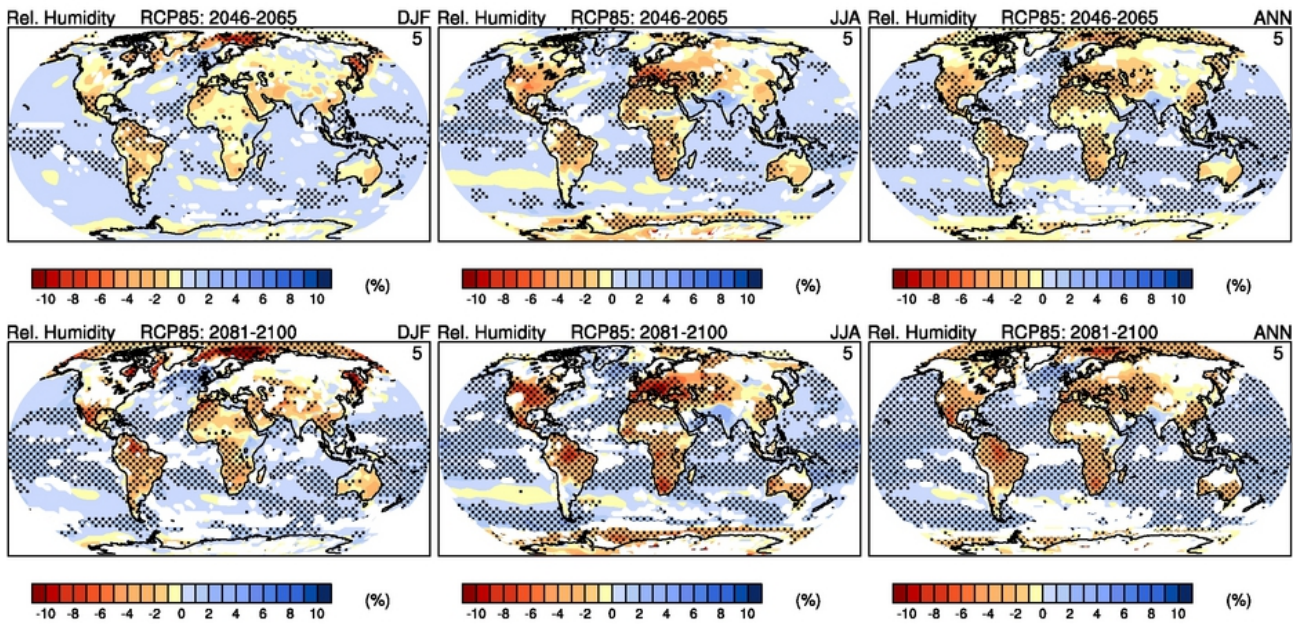
6

7

8

Figure 12.21: Change in winter, extratropical storm track density for (2081–2100) – Historical Control (1986–2005) for CMIP5 multi-model ensembles: (a) RCP 4.5 Northern Hemisphere DJF and (b) RCP 8.5 Northern Hemisphere DJF (c) RCP 4.5 Southern Hemisphere JJA and (d) RCP 8.5 Southern Hemisphere JJA. Storm-track computation uses the method of Bengtsson et al. (2006, their Figure 13a) applied to 850 hPa vorticity. Densities have units (number density/month/unit area), where the unit area is equivalent to a 5° spherical cap (~10⁶ km²).

1



2

3

4

5

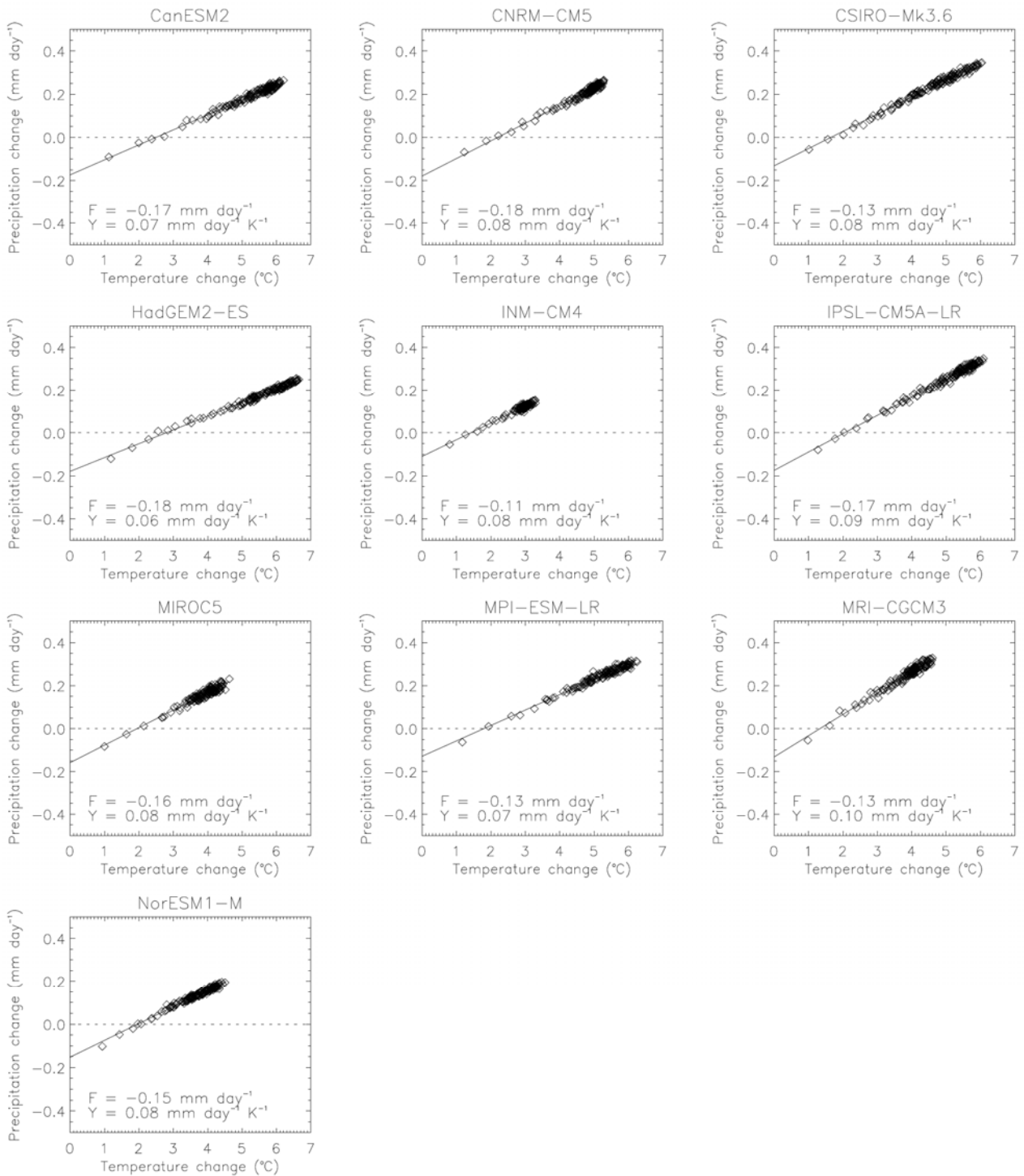
6

7

8

Figure 12.22: Changes in near-surface relative humidity under RCP 8.5 for the seasons DJF (left) and JJA (right) relative to 1986–2005 for the periods 2046–2065 (top row), 2081–2100 (middle row) and 2181–2200 (bottom row). Model agreement is assessed as in (Tebaldi et al., 2011). Grid points are stippled where at least half of the models show significant change and >80% of them agree on the sign, while white shading indicates at least half of the models show significant change but less than 80% of those agree on the sign.

1

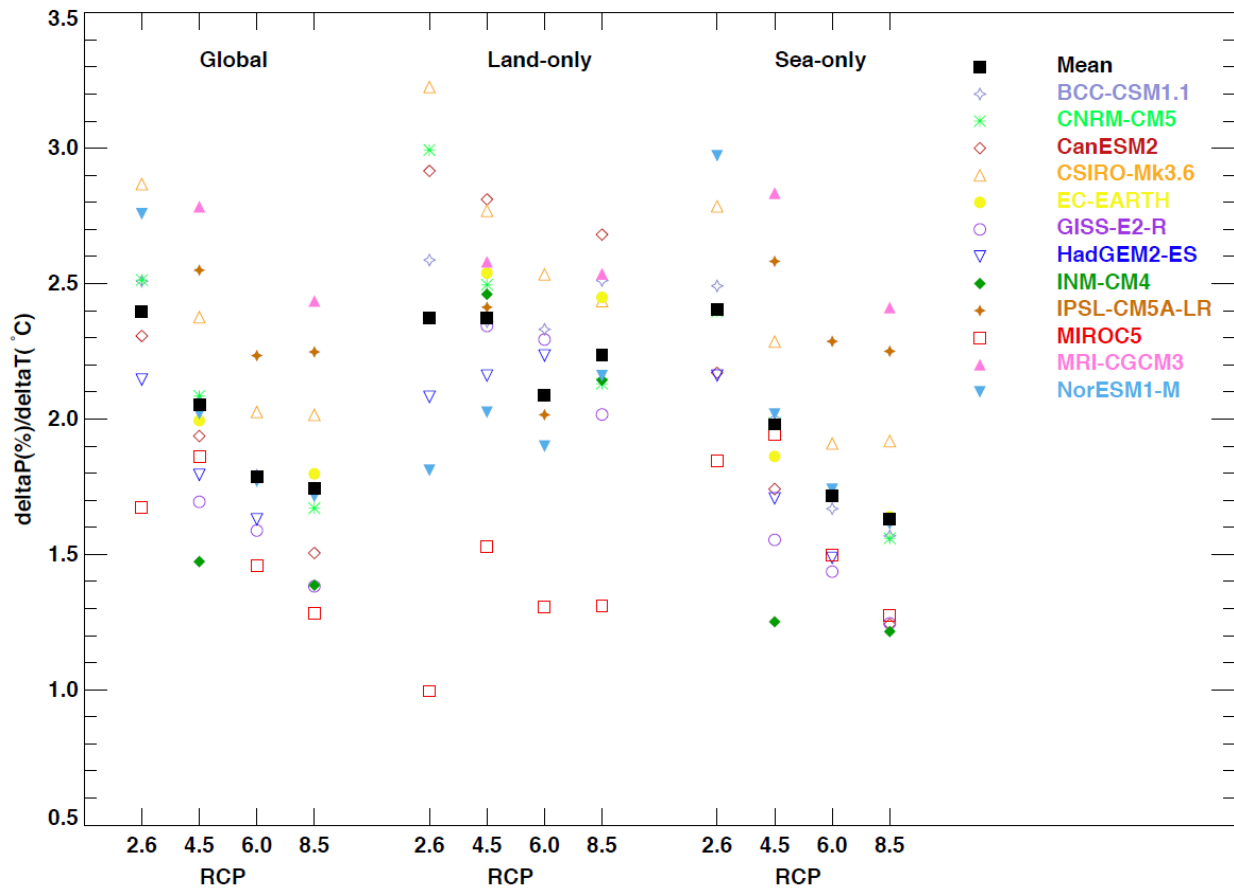


2

3

4 **Figure 12.23:** Global mean annual mean precipitation (mm/day) versus temperature changes for CMIP5 instantaneous
 5 4 x CO₂ step experiments relative to the mean of their control simulations. Ordinary least squares regression linear fits
 6 of global mean precipitation against global mean temperature changes over the first 150 years of the 4 x CO₂
 7 experiments, computed relative to the mean of the control experiment over the corresponding 150 years, are plotted.
 8 The fitted intercept at zero temperature change (F) and slope (Y) are also listed for each model.

1



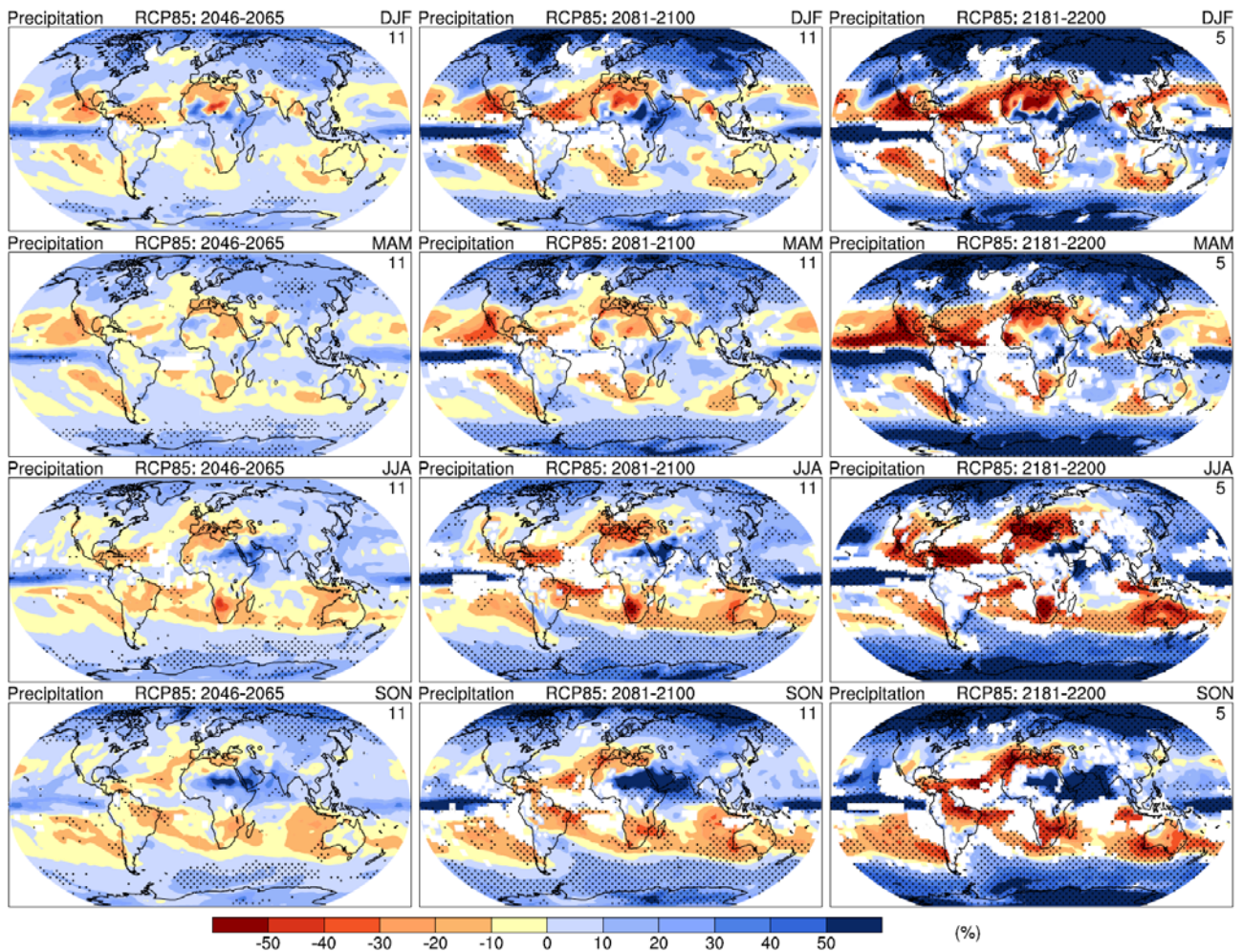
2

3

4 **Figure 12.24:** Percentage changes per °C of global warming in global, land and sea precipitation for CMIP5 model
 5 projections for the four RCPs in the period 2079 to 2098 relative to 1986 to 2005. Land and sea values use global mean
 6 temperature in the denominator. Each coloured symbol represents the ensemble mean for a single model. The black
 7 squares are multi-model means.

8

1

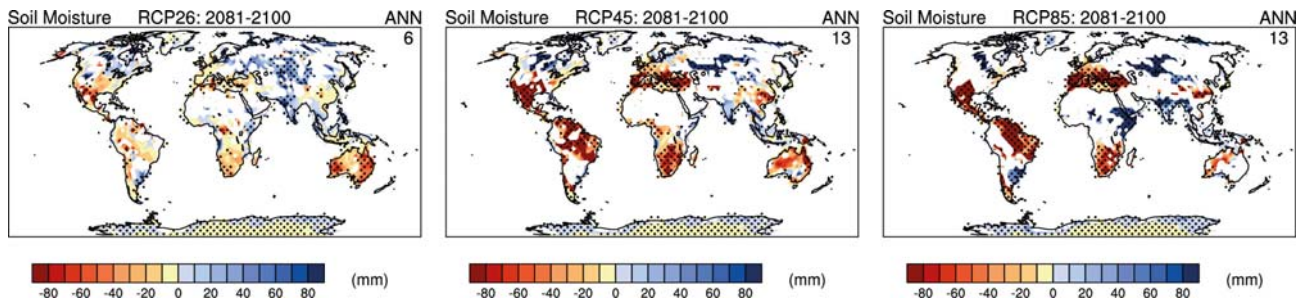


2

3

4 **Figure 12.25:** Multi-model CMIP5 average percent change in seasonal mean precipitation averaged over the periods
 5 2045–2065, 2081–2100 and 2181–2200 under the RCP8.5 forcing scenarios. Model agreement is assessed as in
 6 (Tebaldi et al., 2011). Grid points are stippled where at least half of the models show significant change and >80% of
 7 them agree on the sign, while white shading indicates at least half of the models show significant change but less than
 8 80% of those agree on the sign.

1

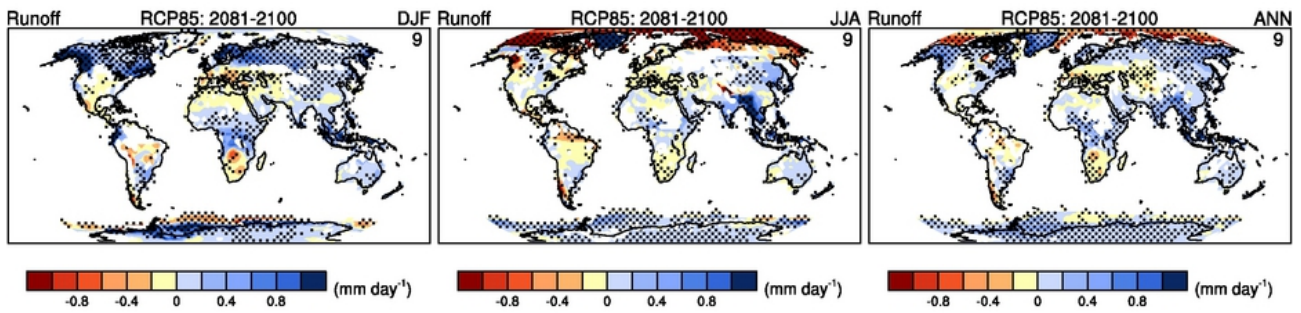


2

3

4 **Figure 12.26:** Percent change in annual soil moisture projected for 2081–2100 from a six-member CMIP5 ensemble for
 5 (a) RCP 2.6, (b) RCP 4.5, and (c) RCP 8.5. Model agreement is assessed as in (Tebaldi et al., 2011). Grid points are
 6 stippled where at least half of the models show significant change and >80% of them agree on the sign, while white
 7 shading indicates at least half of the models show significant change but less than 80% of those agree on the sign.

1



2

3

4

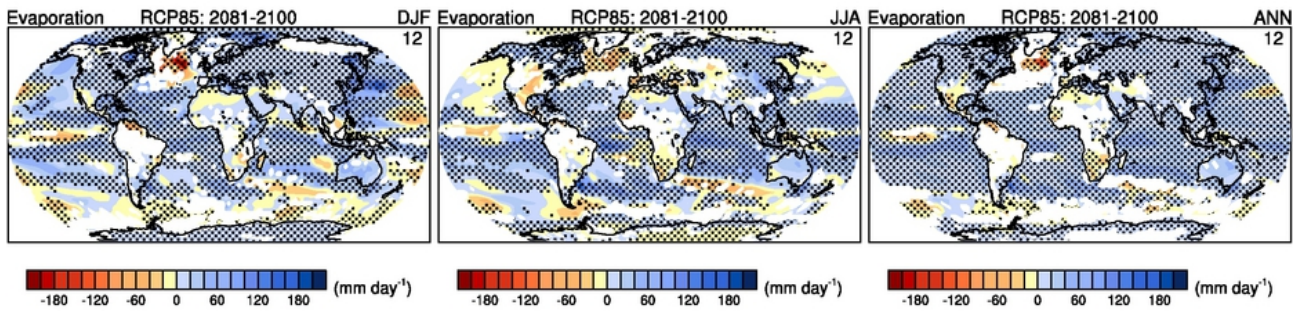
5

6

7

Figure 12.27: Percent change in annual runoff projected for 2081–2100 from a six-member CMIP5 ensemble for (a) RCP 2.6, (b) RCP 4.5, and (c) RCP 8.5. Model agreement is assessed as in (Tebaldi et al., 2011). Grid points are stippled where at least half of the models show significant change and >80% of them agree on the sign, while white shading indicates at least half of the models show significant change but less than 80% of those agree on the sign.

1



2

3

4

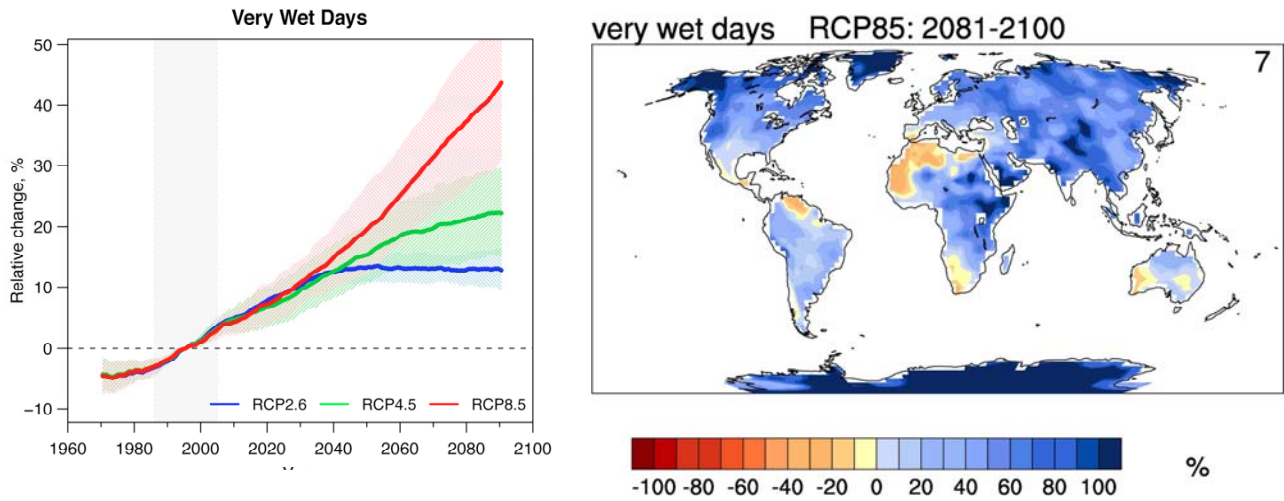
5

6

7

Figure 12.28: Percent change in annual evaporation projected for 2081–2100 from a multi-member CMIP5 ensemble for (a) RCP 2.6, (b) RCP 4.5, and (c) RCP 8.5. Model agreement is assessed as in (Tebaldi et al., 2011). Grid points are stippled where at least half of the models show significant change and >80% of them agree on the sign, while white shading indicates at least half of the models show significant change but less than 80% of those agree on the sign.

1



2

3

4

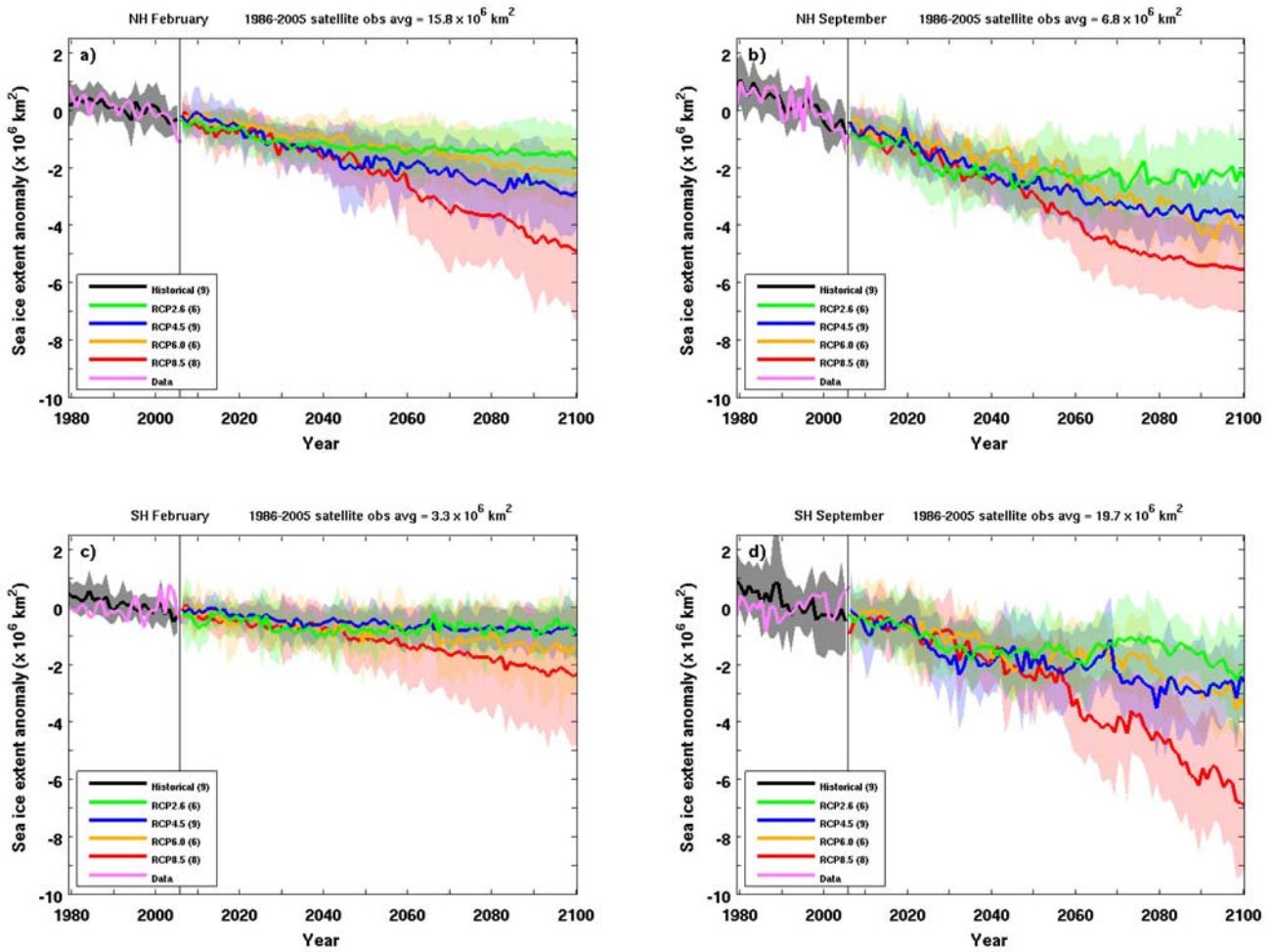
5

6

7

Figure 12.29: Projected changes (relative to the 1985–2005 baseline period) from the CMIP5 models in R95p, the annual total precipitation occurring on days when the daily precipitation is greater than the 95th percentile of the 1961–1990 period. a) Global average percent change over land regions for the RCP2.6, 4.5 and 8.5 scenarios. b) Percent change over the 2081–2100 period in the RCP8.5. Equal model weighting.

1

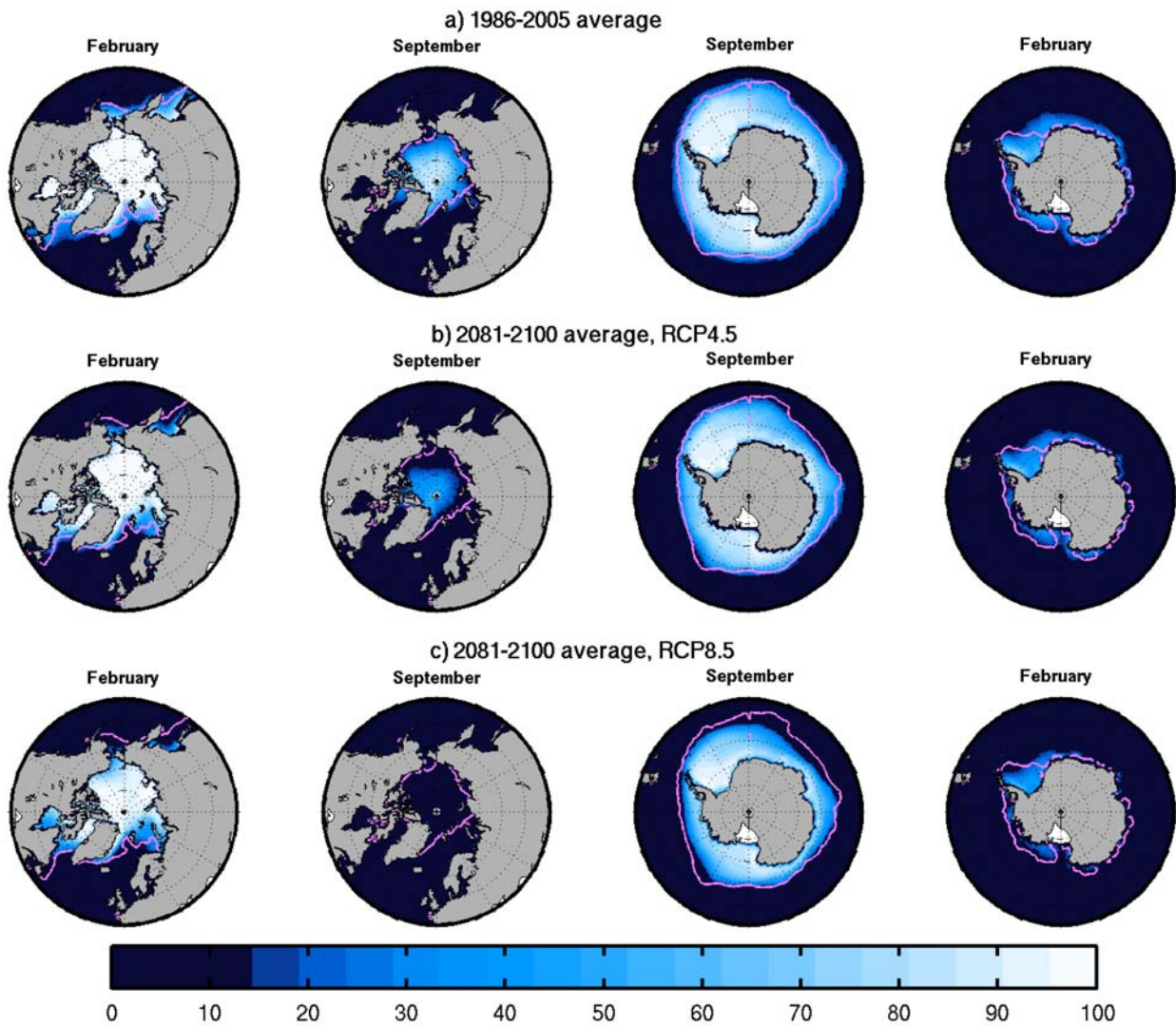


2

3

4 **Figure 12.30:** Anomalies in sea ice extent as simulated by CMIP5 models over the late 20th century and the whole 21st
 5 century using RCP2.6, RCP4.5, RCP6.0 and RCP8.5 for (a) Northern Hemisphere February, (b) Northern Hemisphere
 6 September, (c) Southern Hemisphere February and (d) Southern Hemisphere September. The solid curves show the
 7 multi-model means and the shading denotes the ± 1 standard deviation of the individual ensemble members. Sea ice
 8 extent is defined as the total area where sea ice concentration exceeds 15%. Anomalies are relative to the reference
 9 period 1986–2005. The number of models is given in the legend. Also plotted (solid pink curves) are the satellite data
 10 of Comiso (2008) over 1979–2005.

1

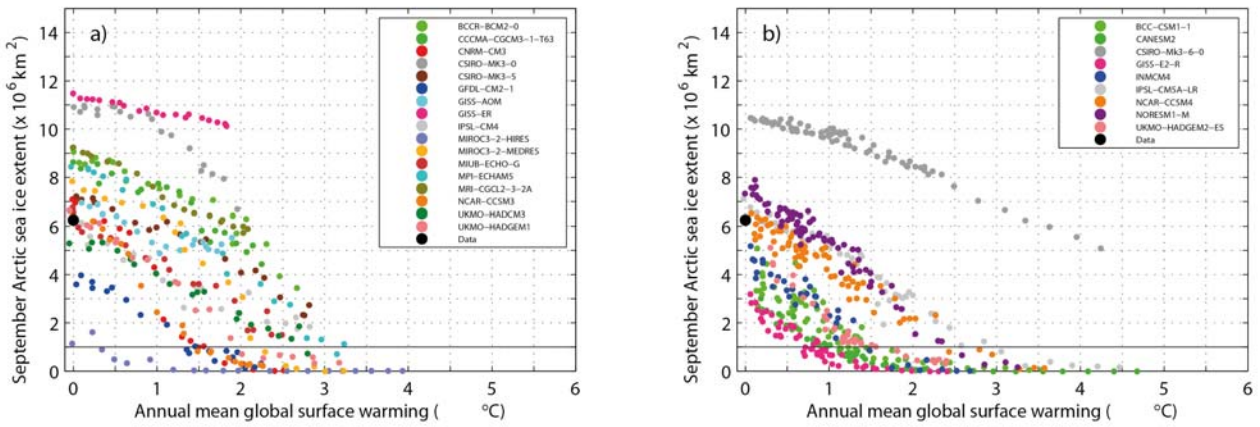


2

3

4 **Figure 12.31:** February and September CMIP5 multi-model mean sea ice concentrations (%) in the Northern and
 5 Southern Hemispheres for the periods (a) 1986–2005, (b) 2081–2100 under RCP4.5 and (c) 2081–2100 under RCP8.5.
 6 The pink lines show the observed 15% sea ice concentration limits averaged over 1986–2005 (Comiso, 2008).

1



2

3

4

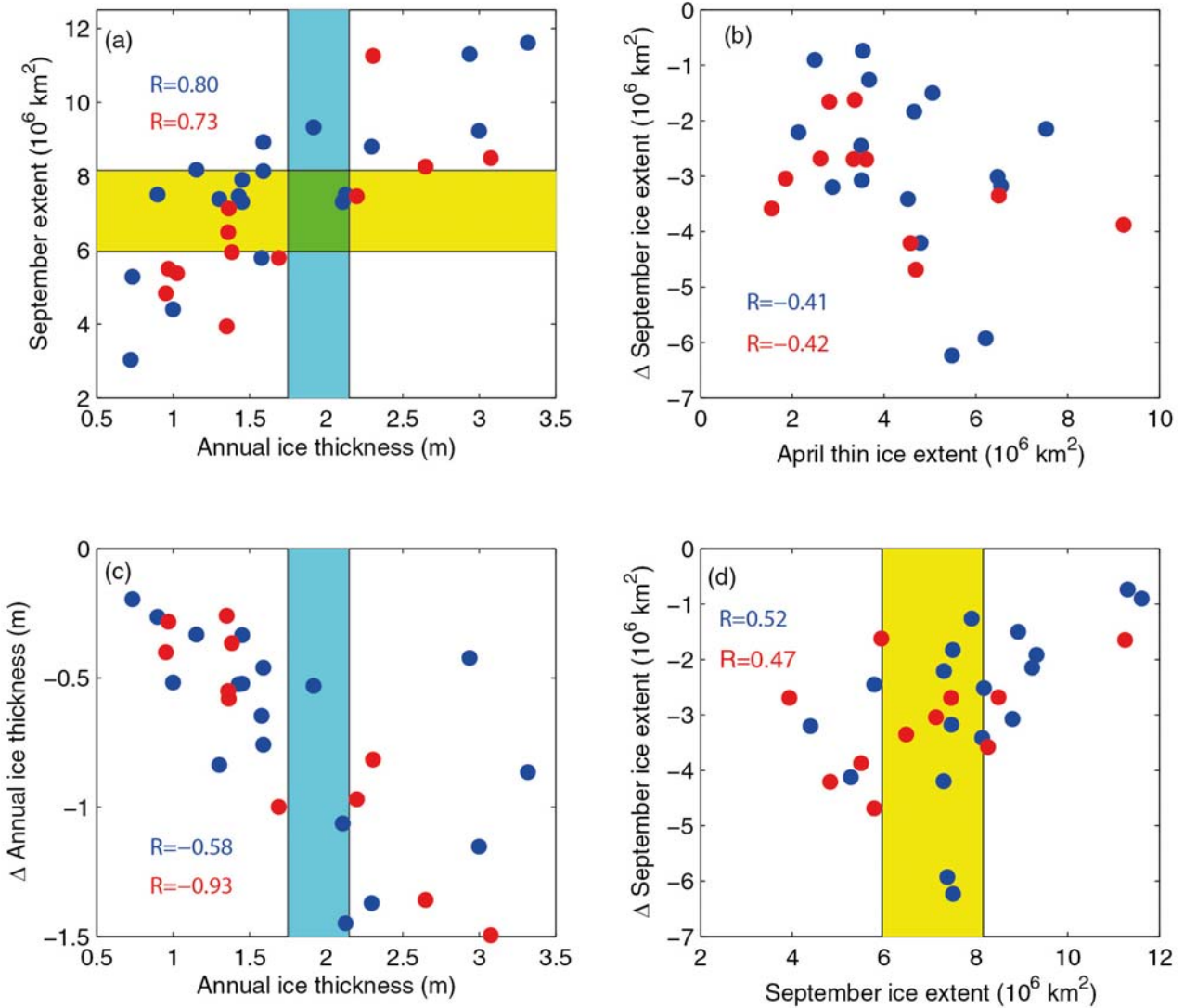
5

6

7

Figure 12.32: September Arctic sea ice extent versus annual mean global surface temperature change with respect to the period 2000–2005 for (a) CMIP3 models (SRES A1B scenario) and (b) CMIP5 models (all RCPs). Model outputs are averaged over five years. The black circle shows the mean observed September Arctic sea ice extent over 2000–2005 (Comiso, 2008).

1



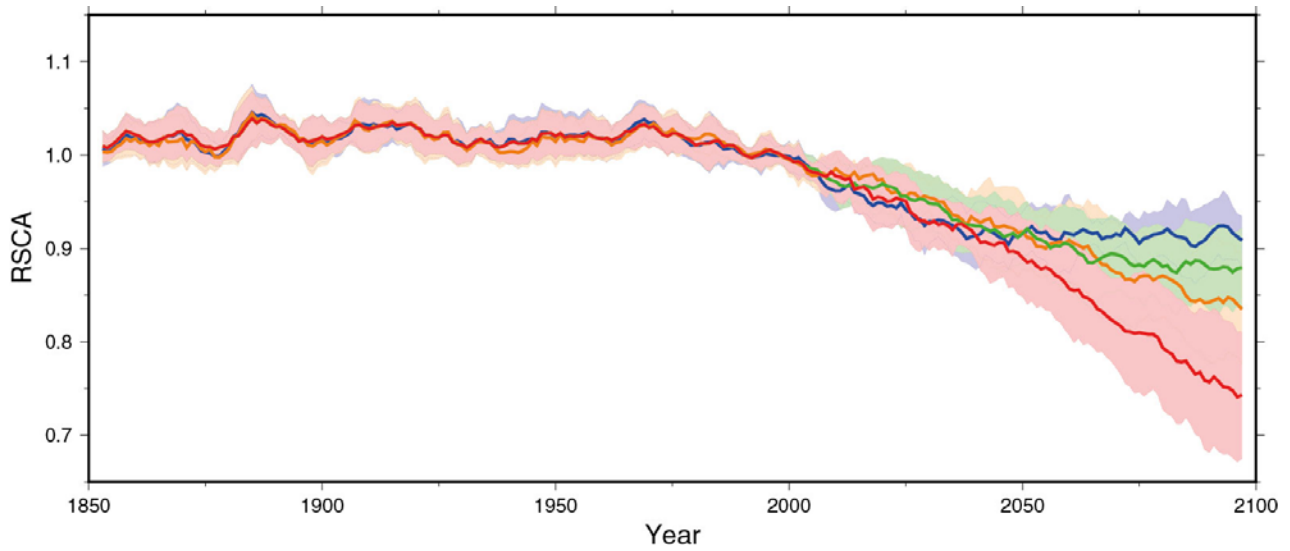
2

3

4 **Figure 12.33:** Scatter plots of Northern Hemisphere sea ice quantities averaged over 1980–1999 or changes in mean
 5 Northern Hemisphere sea ice quantities between 2040–2059 and 1980–1999. The ice thickness is averaged over the
 6 ocean surface north of 70°N . The thin ice extent is the extent of ice which is less than 1 m thick. Correlations (R) are
 7 shown in bold font if they are significant at the 95% confidence level. The blue and red circles correspond to CMIP3
 8 (SRES A1B scenario) and CMIP5 (RCP4.5) models, respectively. Shading denotes the observed range spanning the ± 1
 9 standard deviation about the mean value derived from Comiso (2008) satellite data for ice extent and about a bias
 10 corrected estimate obtained with the Pan-Arctic Ice-Ocean Modeling and Assimilation System (PIOMAS), in which sea
 11 ice concentration data were assimilated (Schweiger et al., 2011), for ice thickness. This bias correction is based on a
 12 comparison of PIOMAS outputs with U.S. submarines and ICESat-derived ice thickness data.

13

1

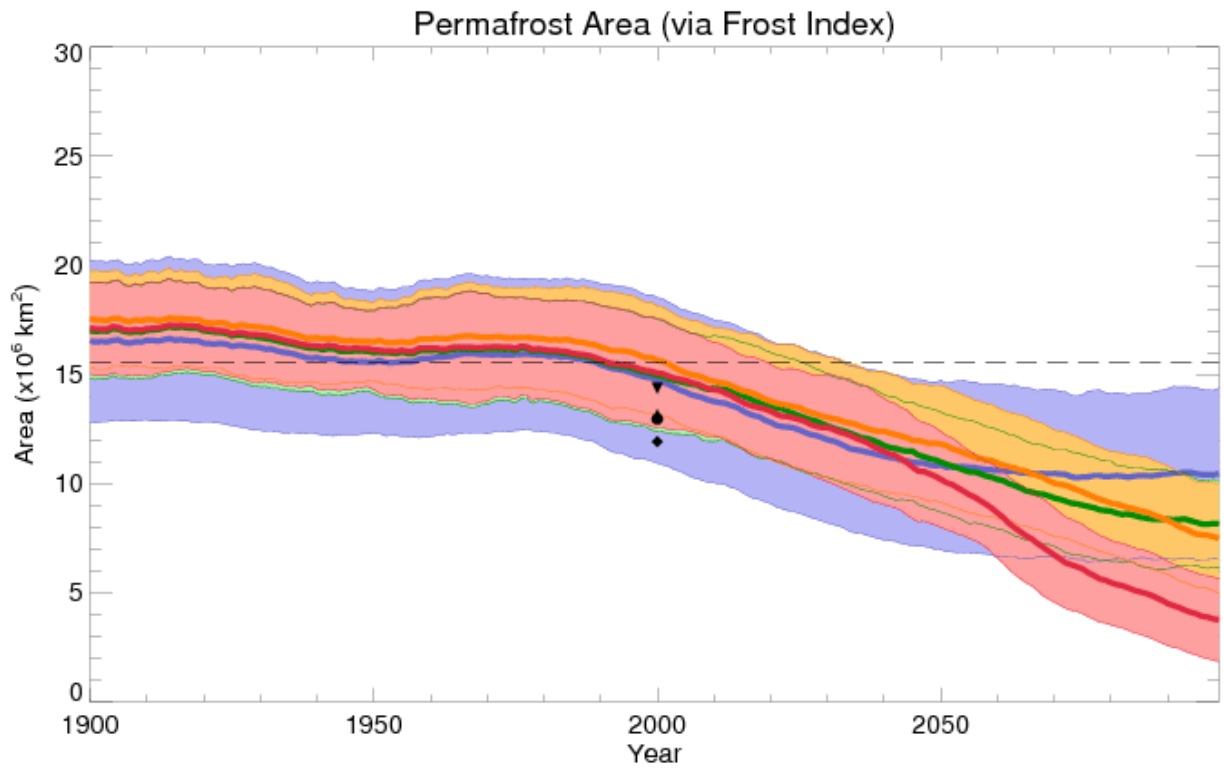


2

3

4 **Figure 12.34:** Northern Hemisphere spring (March to April average) relative snow covered area (RSCA) in the CMIP5
 5 MMD, obtained through dividing the simulated 5-year box smoothed spring snow covered area (SCA) by the simulated
 6 average spring SCA of 1986-2005 reference period. Blue: RCP2.6; Green: RCP4.5; Orange: RCP6.0; Red: RCP8.5.
 7 Thick lines: MMD average. Shading and thin dotted lines indicate the inter-model spread (one standard deviation).

1



2

3

4

5

6

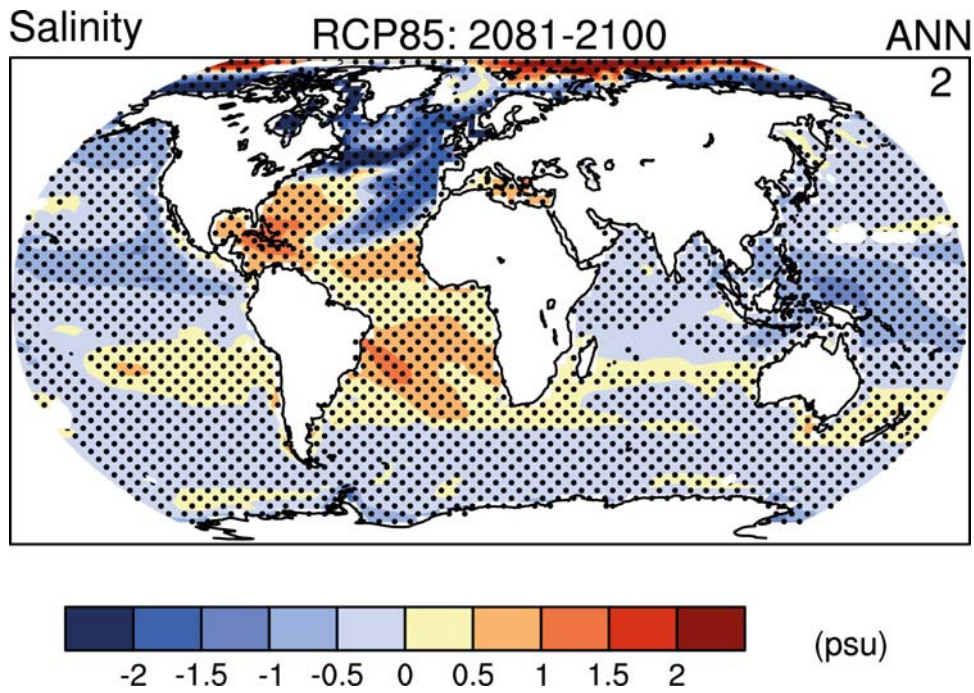
7

8

9

Figure 12.35: Northern Hemisphere diagnosed near-surface permafrost area in the CMIP5 MMD following Nelson and Outcalt (1987) and using 20-year average monthly surface air temperatures and snow depths. Blue: RCP2.6; Green: RCP4.5; Orange: RCP6.0; Red: RCP8.5. Thick lines: MMD average. Shading and thin lines indicate the inter-model spread (one standard deviation). Black symbols at the year 2000 represent the diagnosed near-surface permafrost extents using reanalysis data (circle = ERA-I, up triangle=MERRA, down triangle=JRA, diamond=CFSRR).

1



2

3

4

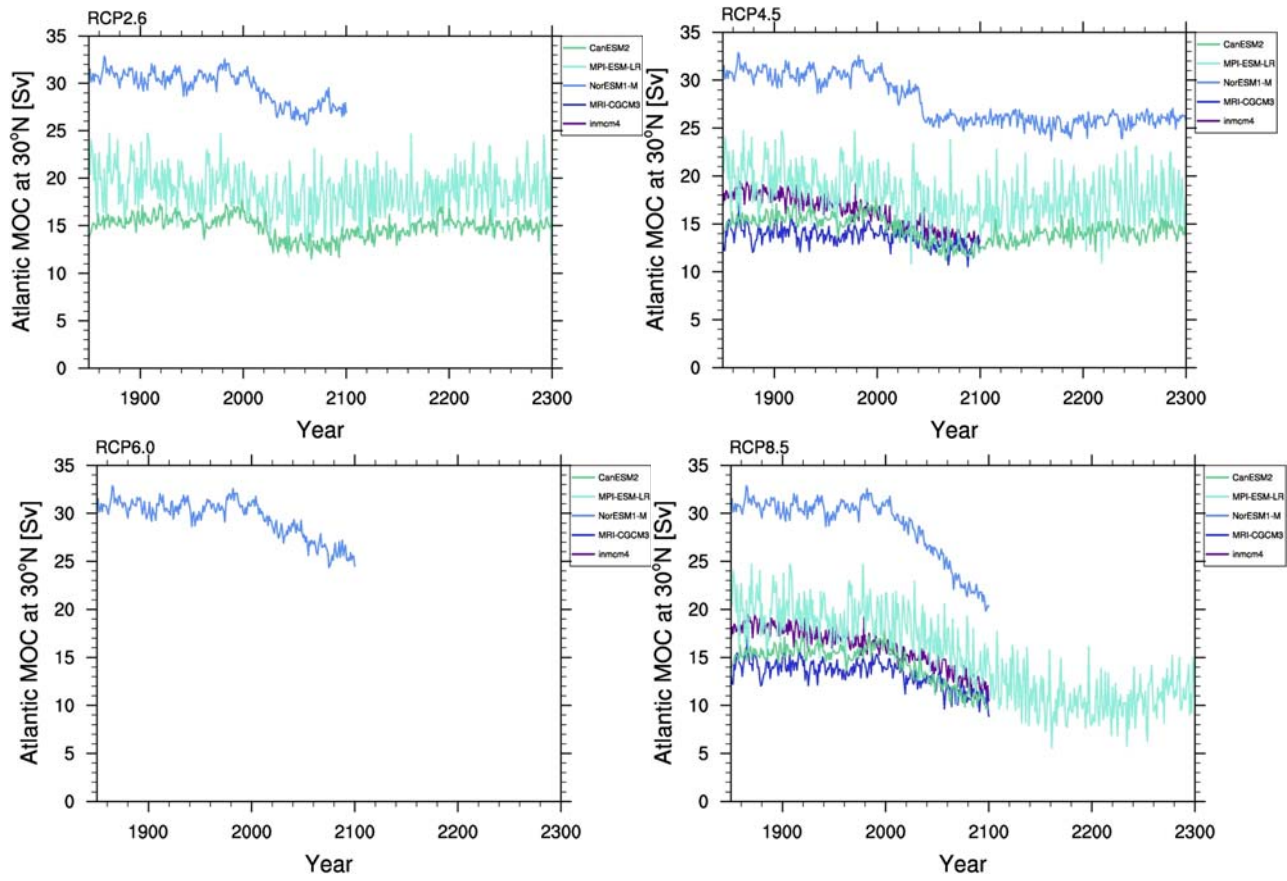
5

6

7

Figure 12.36: Projected sea surface salinity differences 2081–2100 for RCP8.5 relative to 1986–2005 from CMIP5 models. Model agreement is assessed as in (Tebaldi et al., 2011). Grid points are stippled where at least half of the models show significant change and >80% of them agree on the sign, while white shading indicates at least half of the models show significant change but less than 80% of those agree on the sign.

1



2

3

4

5

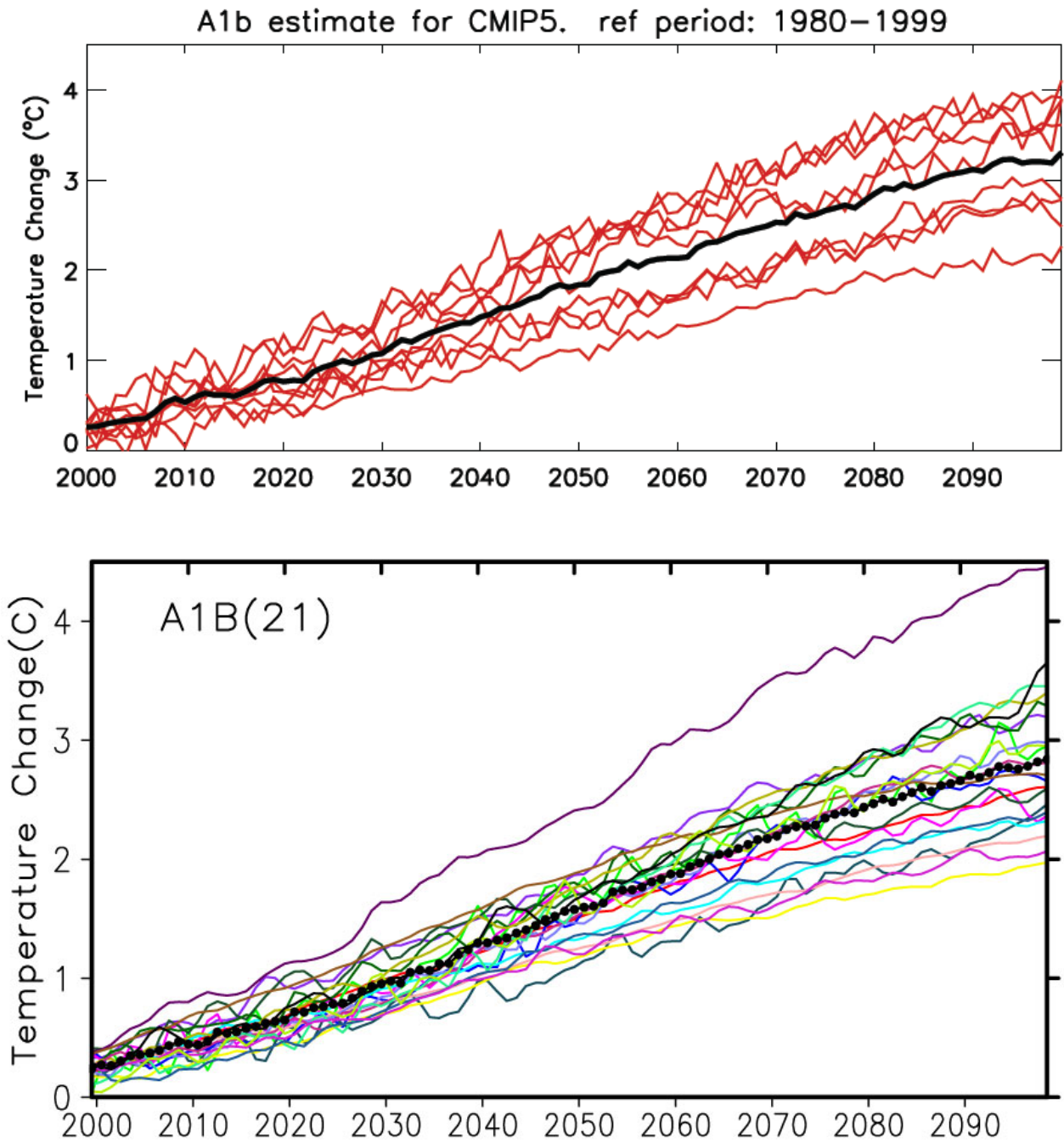
6

7

8

Figure 12.37: Multi model projections of Atlantic meridional overturning circulation (AMOC) strength at 30°N from 1850 through to the end of the RCP extensions. a) RCP2.6; b) RCP4.5; c) RCP6.0; d) RCP8.5. Results are based on a small number of CMIP5 models available. Curves show results from only the first member (r1i1p1) of the submitted ensemble of experiments.

1



2

3

4

5

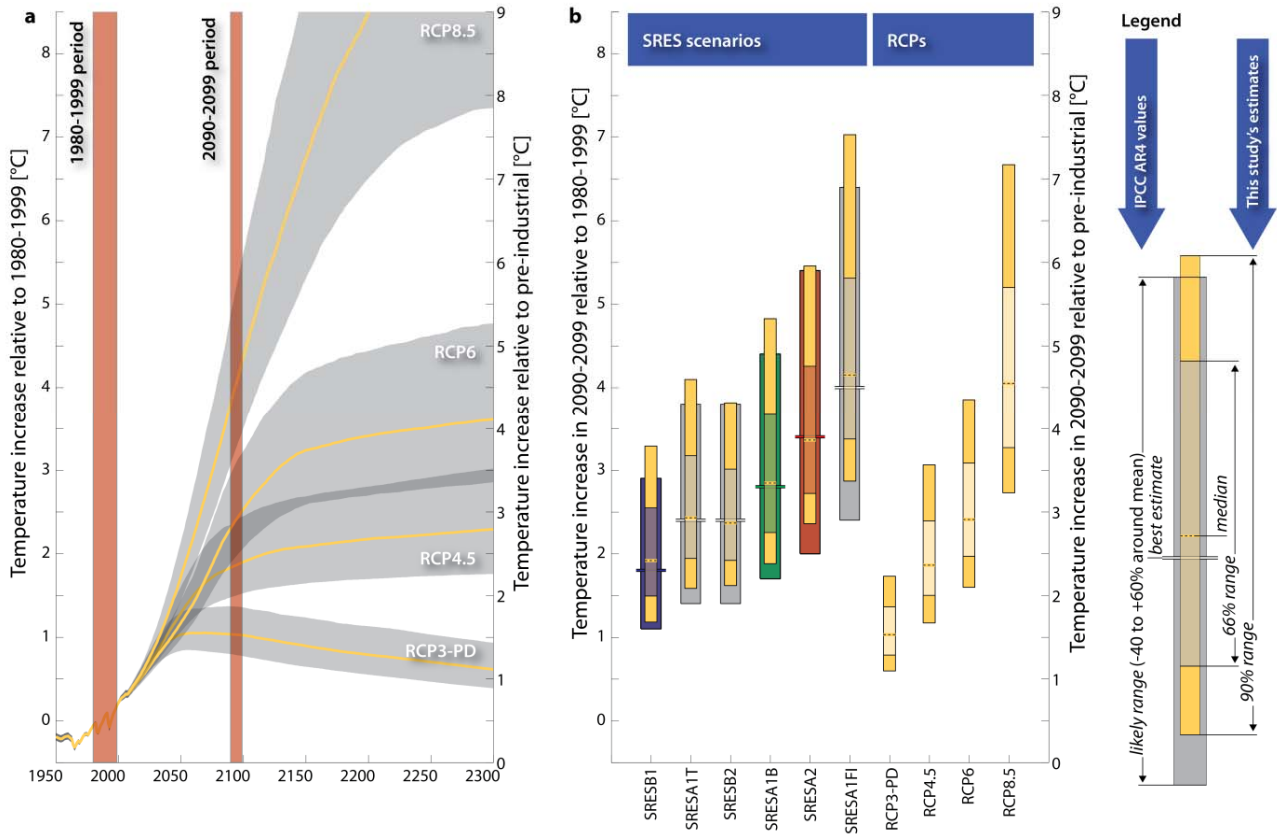
6

7

8

Figure 12.38: Upper panel, an emulation of the global mean temperature response of the CMIP5 models run under SRES A1B with anomalies computed with respect to 1980–1999. The emulation technique is described in (Good et al., 2011). Lower panel, reproduction of part of Figure 10.5 of AR5 showing the CMIP3 model responses under SRES A1B with the same anomaly period.

1



2

3

4

5

6

7

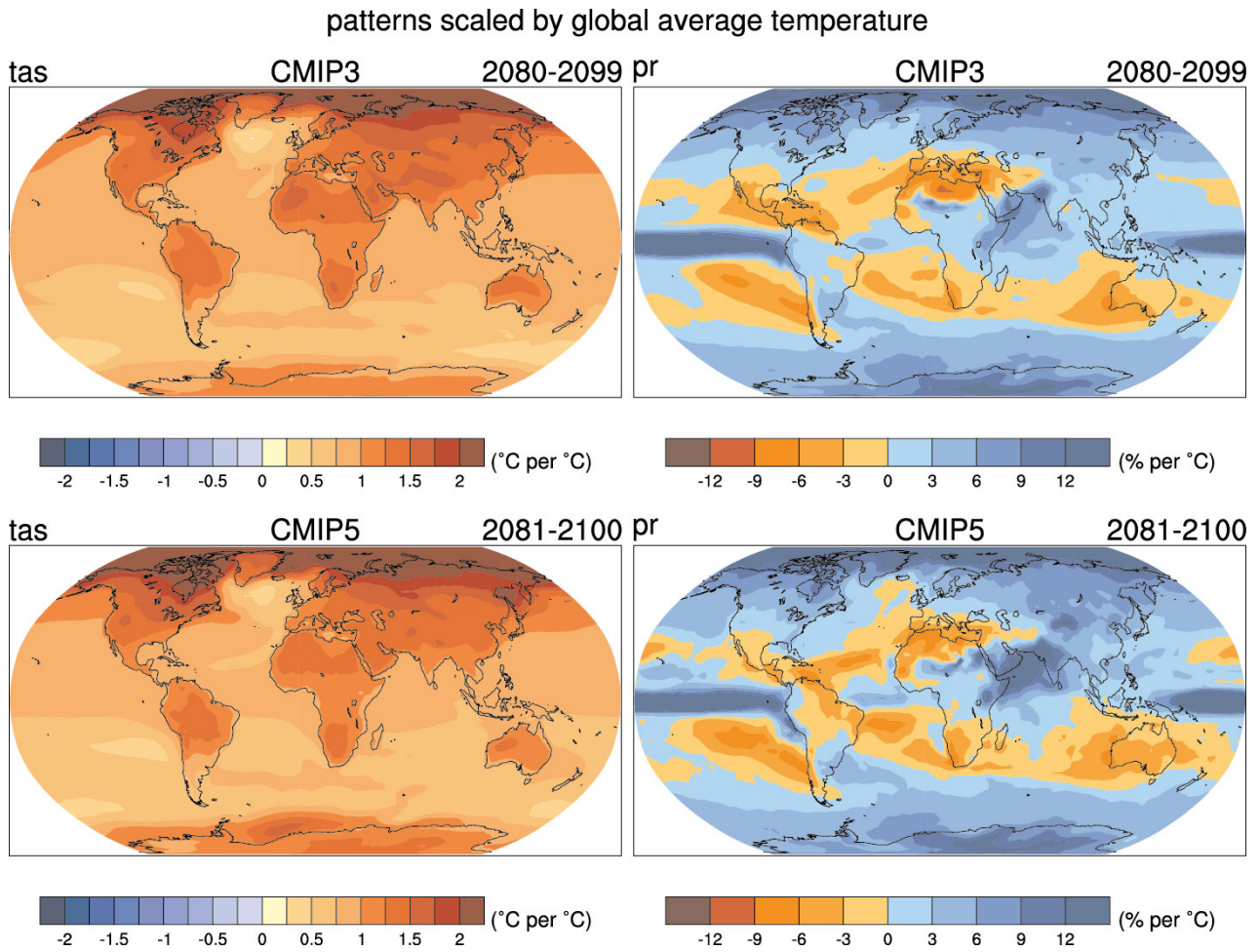
8

9

10

Figure 12.39: Temperature projections for SRES scenarios and the RCPs. (a) Time-evolving temperature distributions (66 per cent range) for the four RCPs computed with this study’s ECS distribution and a model setup representing closely the carbon-cycle and climate system uncertainty estimates of the AR4 (grey areas). Median paths are drawn in yellow. Red shaded areas indicate time periods referred to in panel b. (b) Ranges of estimated average temperature increase between 2090 and 2099 for SRES scenarios and the RCPs respectively. Note that results are given both relative to 1980–1999 (left scale) and relative to pre-industrial (right scale). Yellow ranges indicate results of this study; other ranges show the AR4 estimates. Colour-coding of AR4 ranges is chosen to be consistent with the AR4.

1

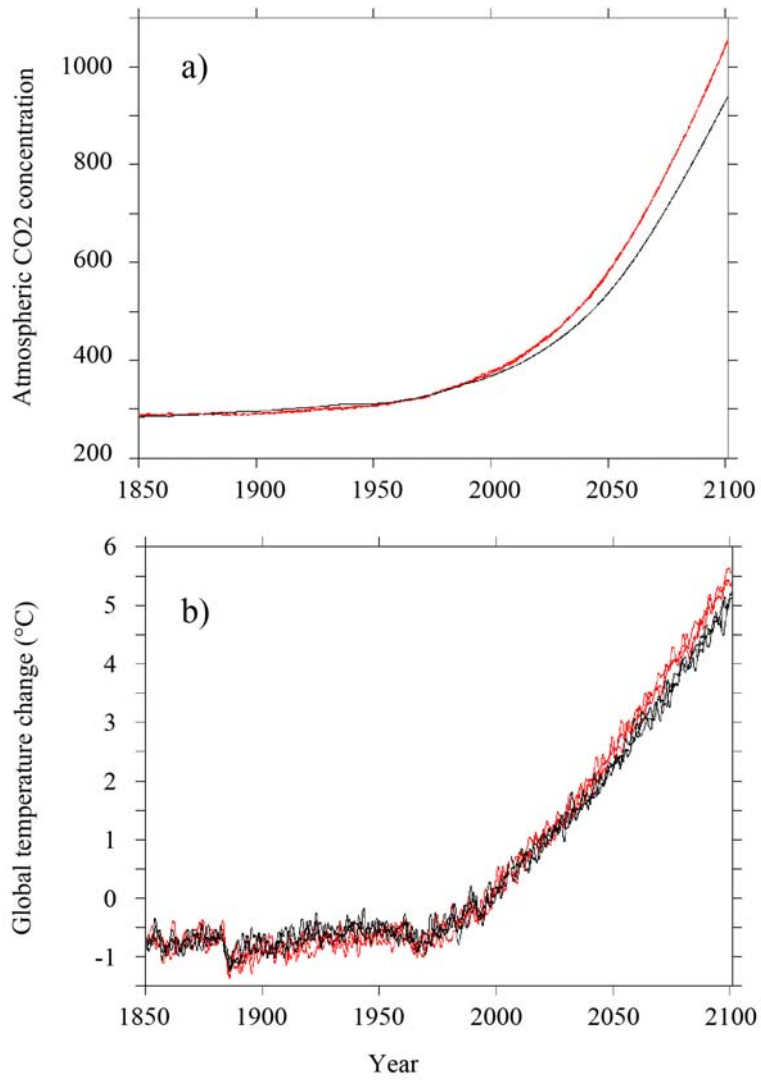


2

3

4 **Figure 12.40:** Patterns of temperature (left column) and percent precipitation change (right column) by the end of the
 5 21st century (2081–2100 vs 1986–2005), for the CMIP3 models average (first row) and CMIP5 models average (second
 6 row), scaled by the corresponding global average temperature changes.

1

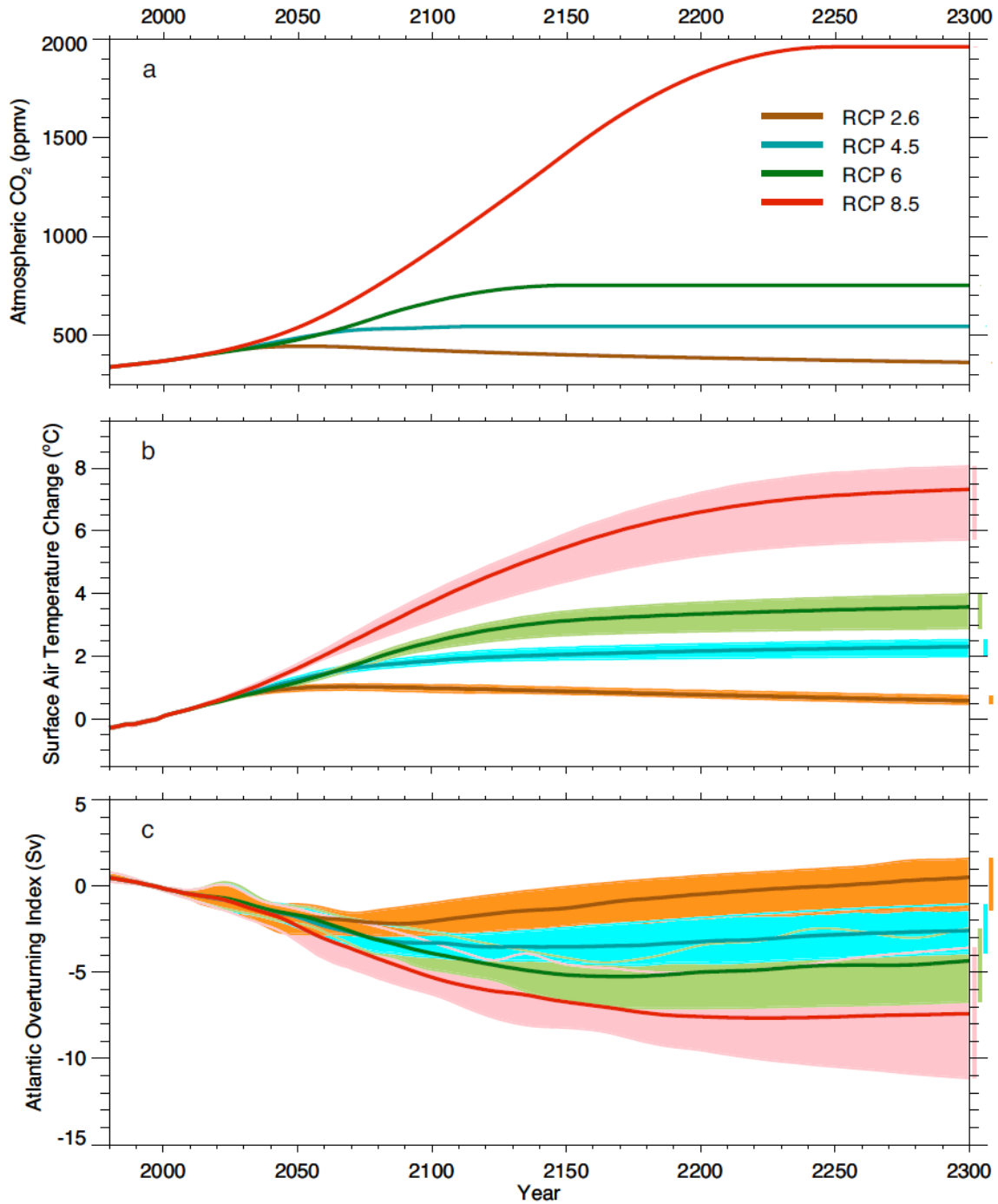


2

3

4 **Figure 12.41:** Comparison between ESM simulations with CO₂ emissions (red) or CO₂ concentration (black) as
 5 external forcing. a) atmospheric CO₂ concentration (ppm), b) global average surface air temperature difference (°C).

1



2

3

4

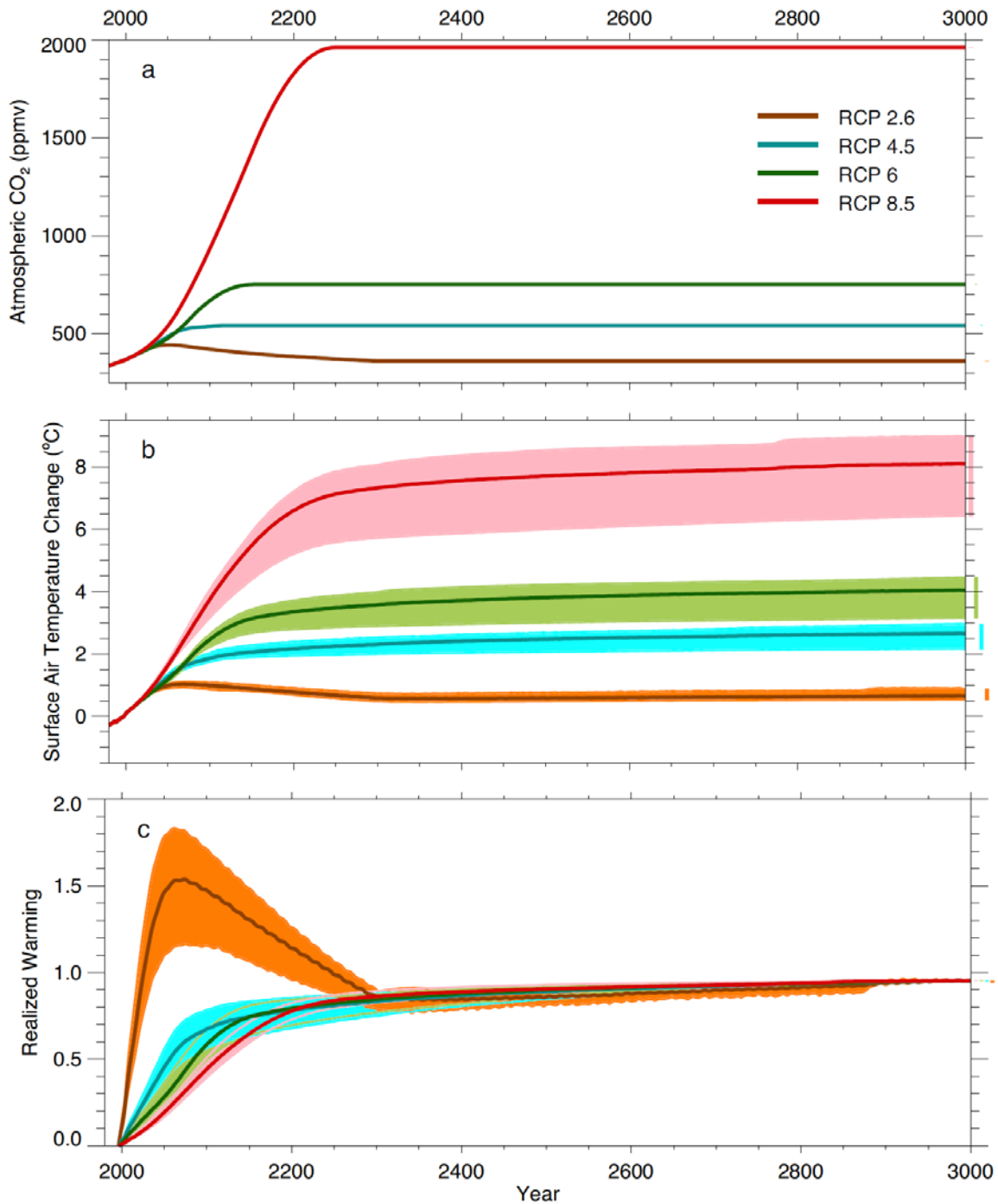
5

6

7

Figure 12.42: Atmospheric CO₂ forcing, b) projected global mean surface temperature warming and c) projected change in meridional overturning circulation, as simulated by 6 EMICs (Bern3D, CLIMBER 2, CLIMBER 3-alpha, DCESS, MESMO and UVic) for the 4 RCPs up to 2300. A ten-year smoothing was applied.

1



2

3

4

5

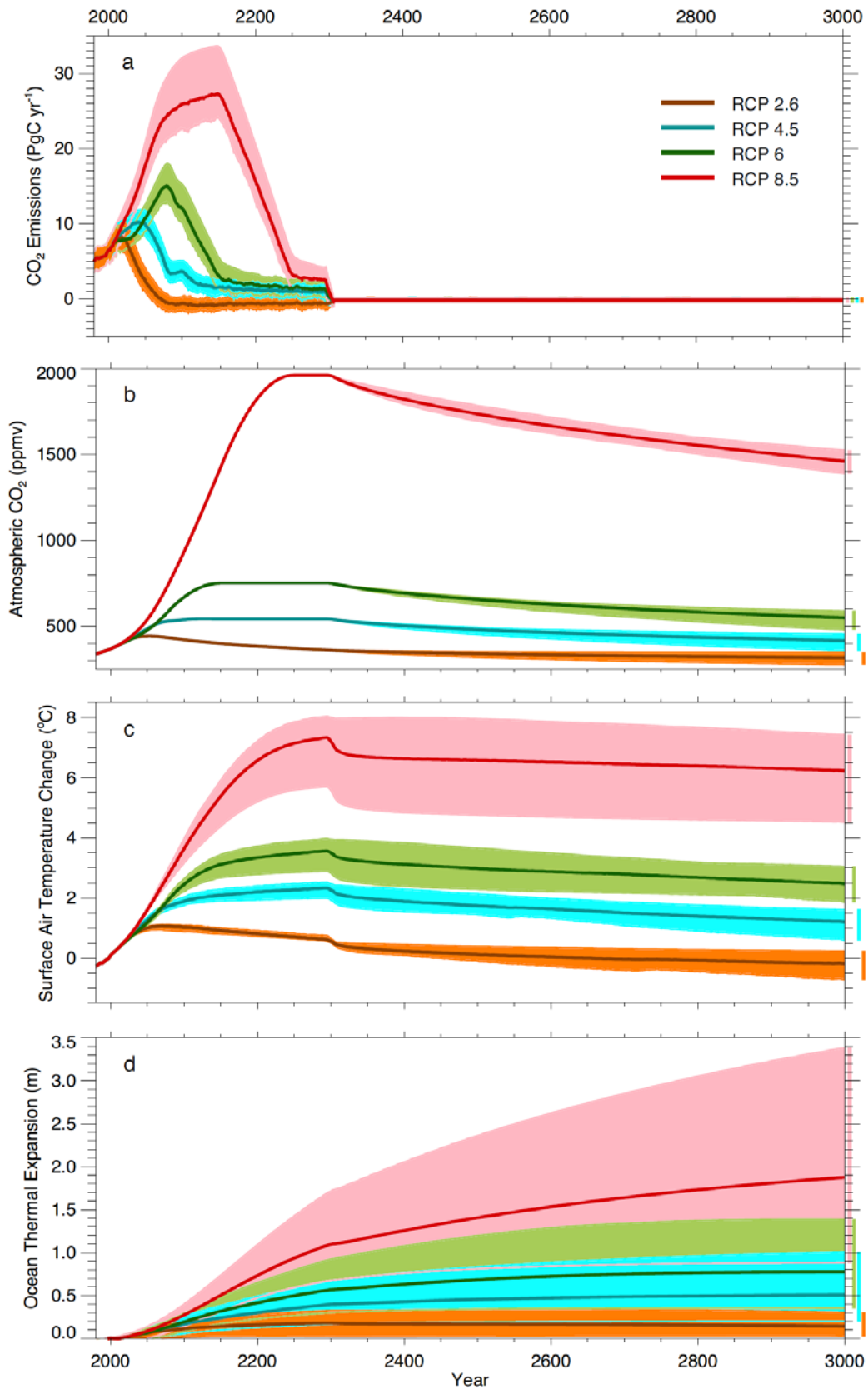
6

7

8

Figure 12.43: Atmospheric CO₂ forcing, b) projected global mean surface temperature warming and c) fraction of realized warming calculate as the ratio of global temperature change at a given time to the change averaged over the 2980–2999 time period, as simulated by 4 EMICs (Bern3D, DCESS , MESMO and UVic) for the 4 RCPs up to 2300 followed by a constant (2300 level) radiative forcing up to the year 3000. A ten-year smoothing was applied.

1

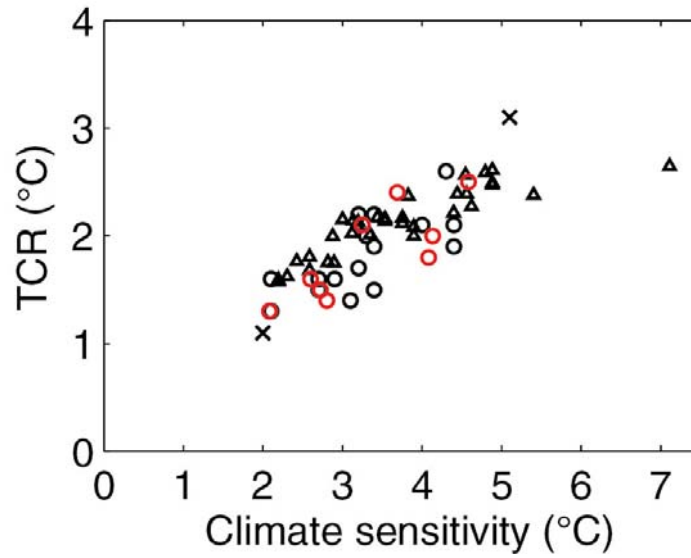


2

3

4 **Figure 12.44:** a) compatible anthropogenic CO₂ emissions, b) projected atmospheric CO₂ concentration, c) global mean
 5 surface temperature change and d) ocean thermal expansion, as simulated by 6 EMICs (Bern3D, CLIMBER
 6 2, CLIMBER 3-alpha, DCESS, MESMO and UVic) for the 4 RCPs, assuming zero anthropogenic emissions after 2300.
 7 A ten-year smoothing was applied.

1

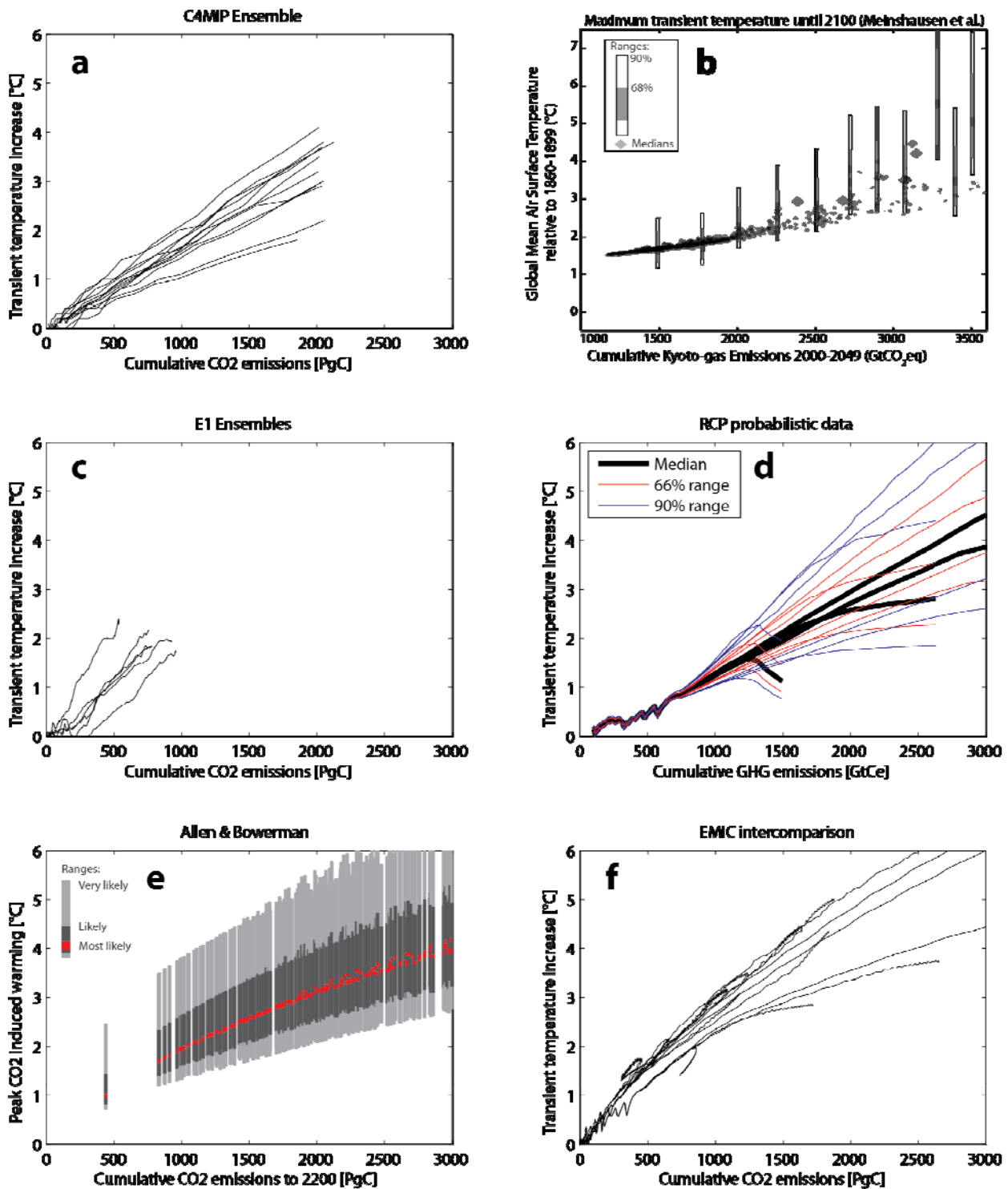


2

3

4 **Figure 12.45:** Transient climate response (TCR) versus equilibrium climate sensitivity for the CMIP5 AOGCMs (red
 5 circles). Results from Meehl et al. (2007b) Figure 10.25 are given for comparison in black: circles mark CMIP3 models,
 6 triangles mark a perturbed physics ensemble of the HadCM3 AOGCM, crosses mark ranges covered by the IPCC TAR
 7 AOGCMs for each quantity.

1



2

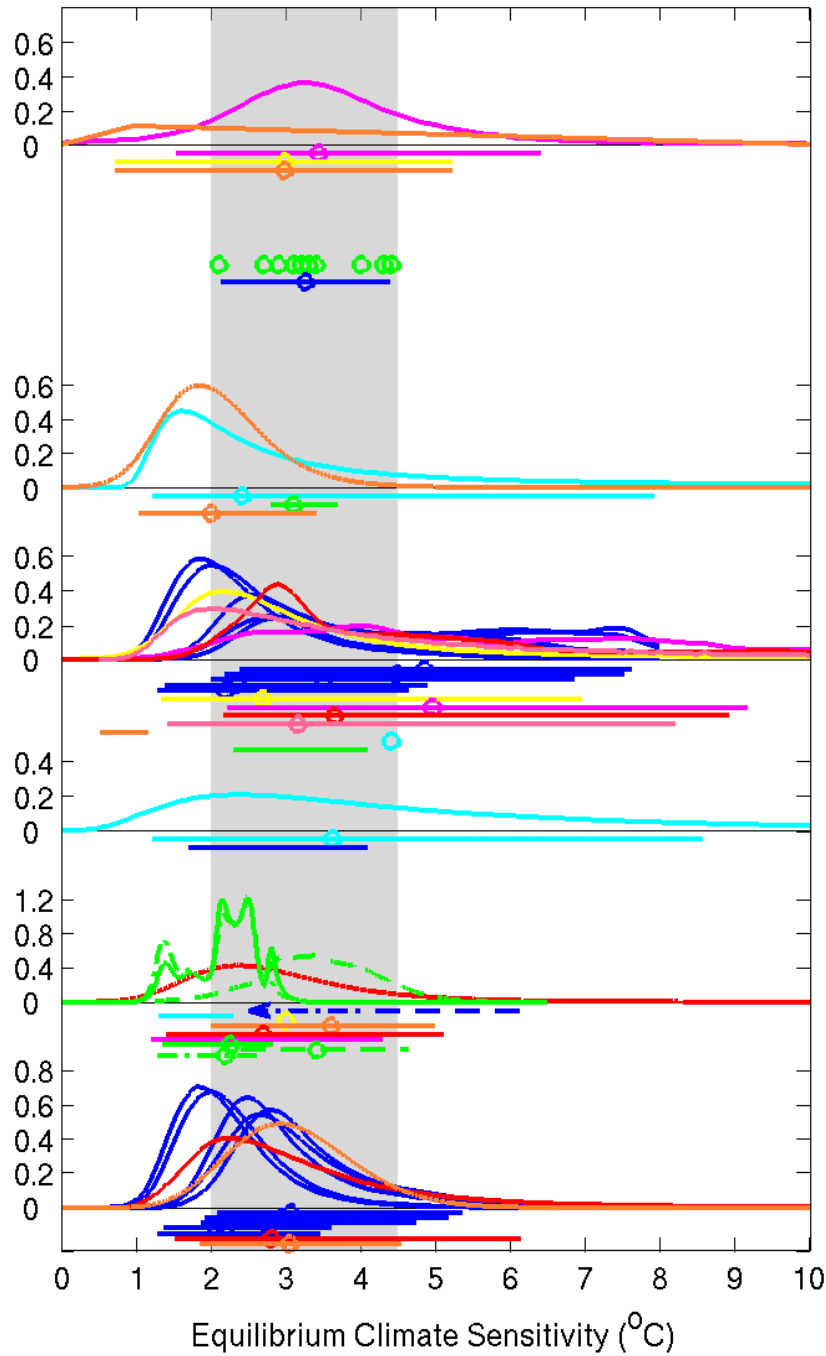
3

4

Figure 12.46: Global temperature change vs. cumulative emissions for different scenarios and models. a) Transient global temperature increase vs. cumulative carbon emissions for C4MIP (Matthews et al., 2009), b) maximum temperature increase until 2100 vs. cumulative Kyoto-gas emissions (CO₂ equivalent) (Meinshausen et al., 2009), c) as in panel a but for the ENSEMBLES E1 scenario (Johns et al., 2011), d) transient temperature increase for the RCP scenarios based on the MAGICC model constrained to C4MIP, observed warming, and the IPCC AR4 climate sensitivity range (Rogelj et al., 2011a), e) peak CO₂ induced warming vs. cumulative CO₂ emissions to 2200 (Allen et al., 2009; Bowerman et al., 2011), f) transient temperature increase from the new EMIC simulations (see Figure 12.44).

11

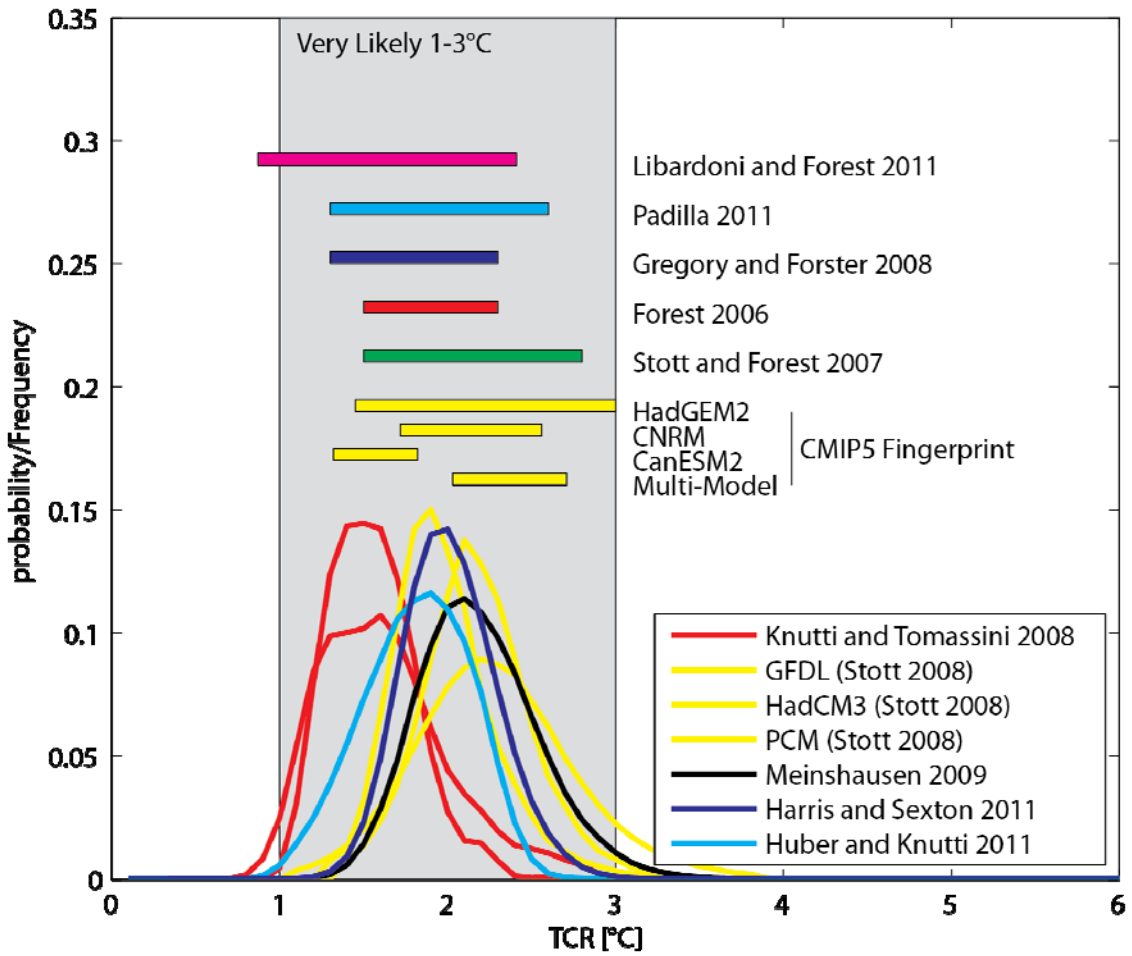
1



2
3
4
5
6

Box 12.1, Figure 1: Probability density functions, distributions and ranges for equilibrium climate sensitivity, based on Figure 10.20b plus climatological constraints shown in IPCC AR4 Box 12.2 Figure 1.

1



2

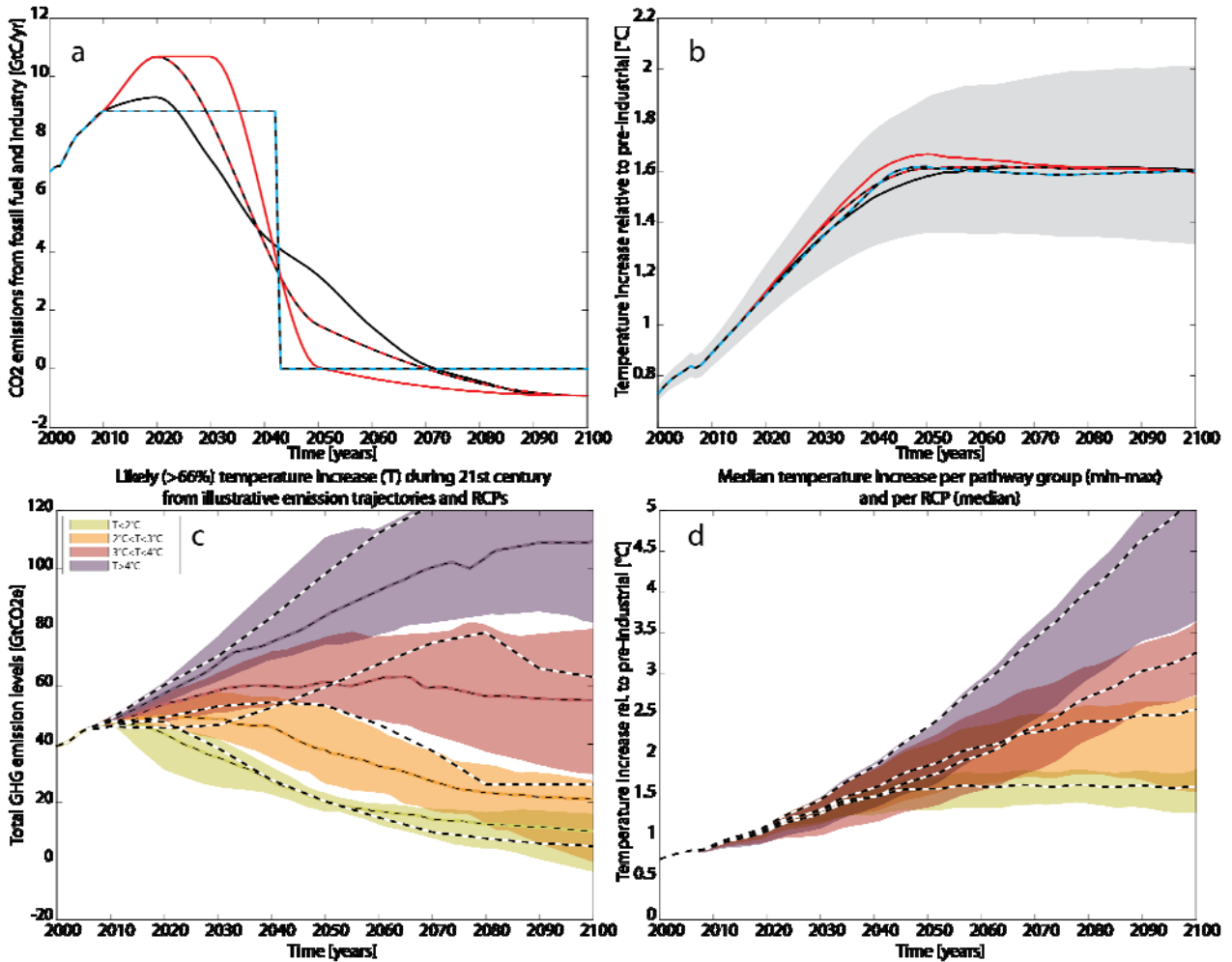
3

4

5

Box 12.1, Figure 2: Probability density functions, distributions and ranges (5–95%) for the transient climate response from different studies. See Figure 10.20a for details.

1



2

3

4

5

6

7

8

9

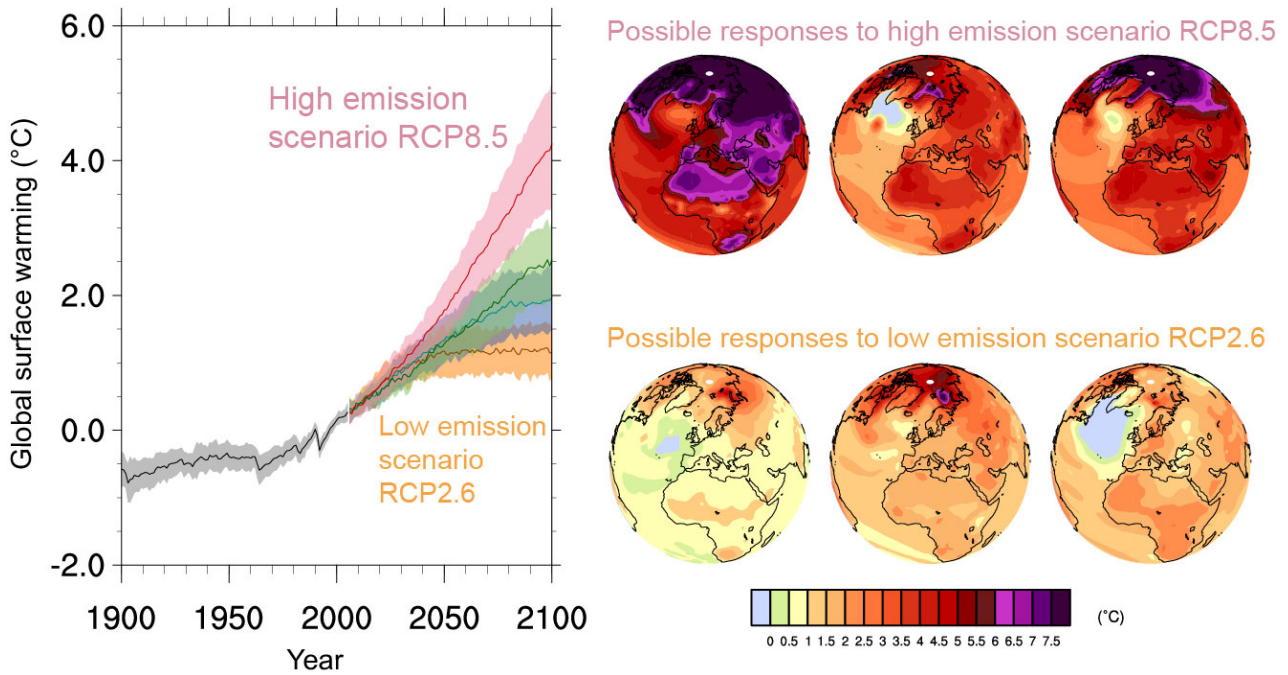
10

11

12

Figure 12.47: a) CO₂ emissions for the RCP3PD scenario (black) and three illustrative modified emission pathways leading to the same warming, b) global temperature change relative to preindustrial for the pathways shown in panel a. c) Coloured bands show IAM emission pathways over the twenty-first century. The pathways were grouped based on ranges of "likely" avoided temperature increase in the twenty-first century. Pathways in the yellow, orange and red bands likely stay below 2°C, 3°C, 4°C by 2100, respectively, while those in the purple band are higher than that. Emission corridors were defined by, at each year, identifying the 20th to 80th percentile range of emissions and drawing the corresponding coloured bands across the range. Individual scenarios that follow the upper edge of the bands early on tend to follow the lower edge of the band later on, d) global temperature relative to preindustrial for the pathways in panel a. Data in panels c,d based on Rogelj et al. (2011b).

1

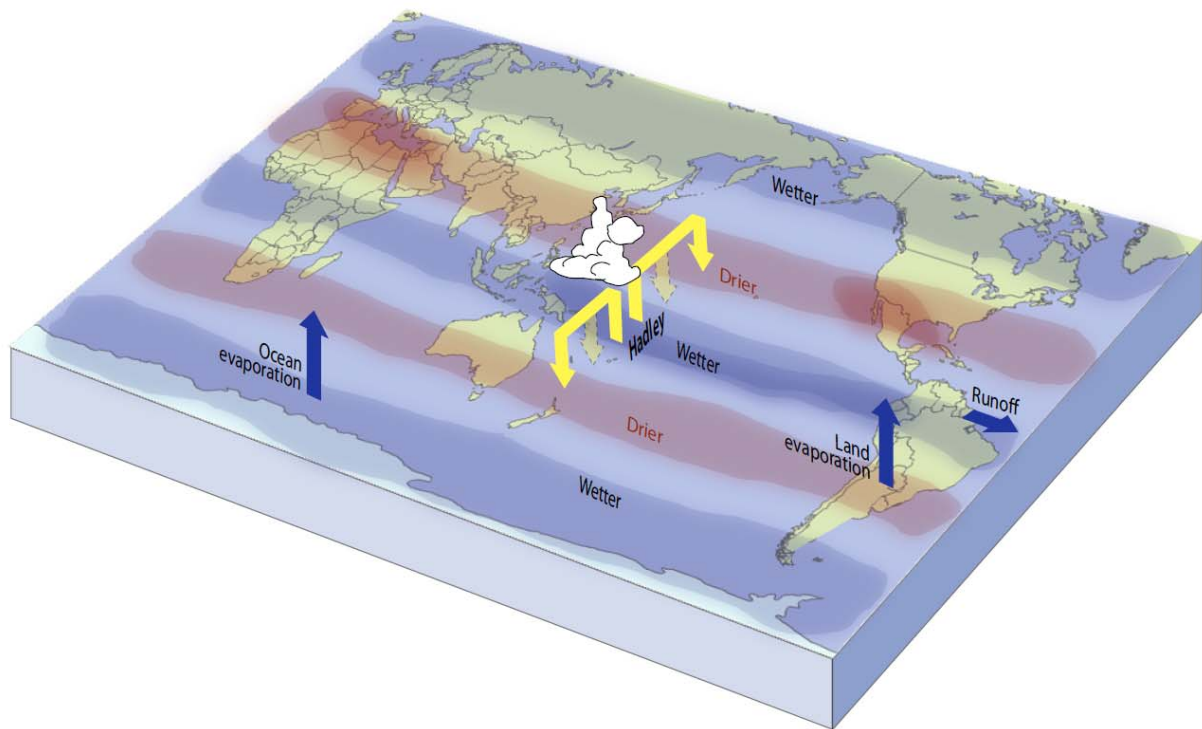


2

3

4 **FAQ 12.1, Figure 1:** Global mean temperature change (mean and one standard deviation, relative to 1986–2005) for
 5 the CMIP5 models and the four RCP scenarios. For the highest (RCP8.5) and lowest (RCP2.6) scenario, illustrative
 6 maps of surface temperature change at the end of the 21st century (relative to 1986–2005) are shown for three CMIP5
 7 models. These models are chosen to show a rather broad range of response but this particular set of models is not
 8 representative of any measure of model response uncertainty.

1

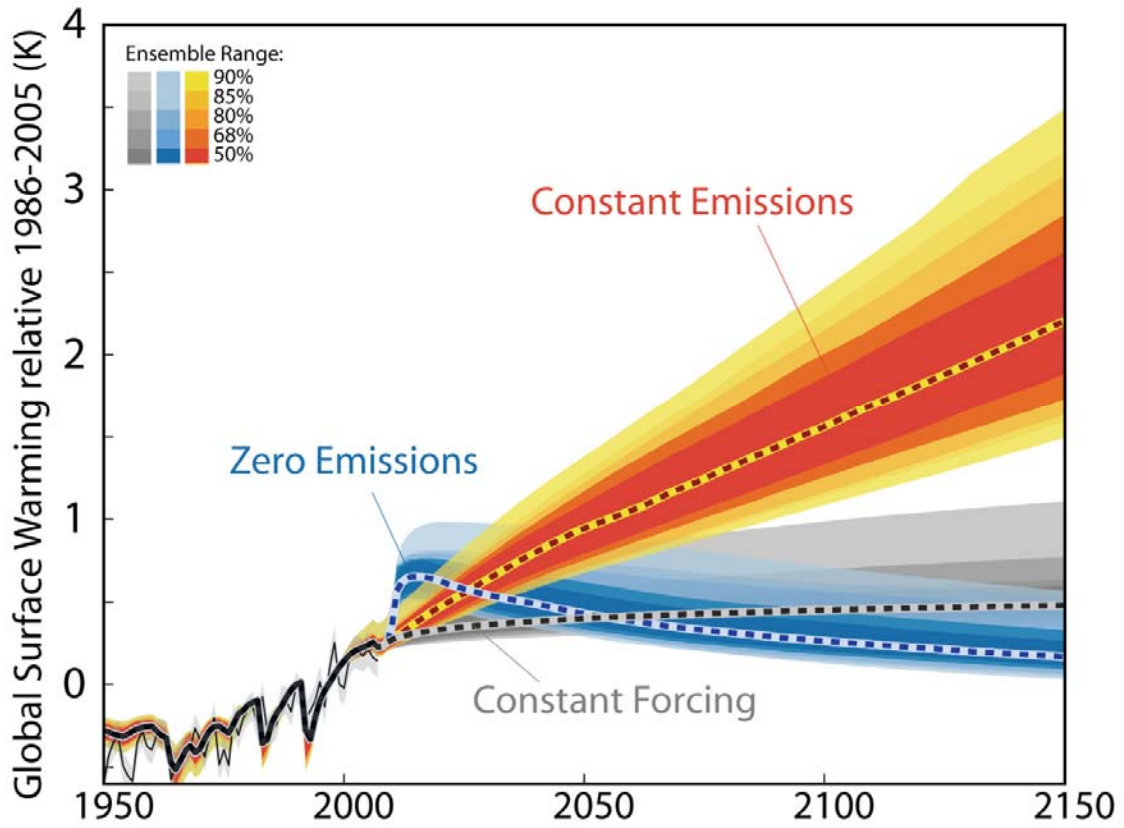


2

3

4 **FAQ 12.2, Figure 1:** Schematic diagram of the water cycle and projected changes. The blue arrows indicate major
 5 types of water movement through the Earth's climate system: precipitation from the atmosphere, evaporation from the
 6 surface and runoff from the land to the oceans. The shaded regions denoted as 'drier' and 'wetter' indicate areas with
 7 decrease and increased rainfall, respectively. Yellow arrows indicate an important atmospheric circulation, the Hadley
 8 circulation, whose upward motion promotes tropical rainfall while suppressing subtropical rainfall. Model projections
 9 indicate that this circulation will shift its downward branch poleward in both the Northern and Southern Hemispheres,
 10 with associated drying. Wetter conditions are projected at high latitudes because a warmer atmosphere will allow
 11 greater precipitation.

1



2

3

4

5

6

7

FAQ 12.3, Figure 1: Projections based on the energy balance carbon cycle model MAGICC for constant atmospheric composition (constant forcing, grey), constant emissions (red) and zero emissions (blue) starting in 2010, with probabilistic estimates of uncertainty. Figure adapted from Hare and Meinshausen (2006) based on the MAGICC calibration to all CMIP3 and C4MIP models (Meinshausen et al., 2011a; Meinshausen et al., 2011b).